Technical, Environmental and Economic Assessment of Medium Deep Borehole Thermal Energy Storage Systems

Dissertation

Doctoral thesis submitted in fulfillment of the requirements
for the degree of Doktor-Ingenieur (Dr.-Ing.)
at the
Department of Material and Earth Sciences,
Technische Universität Darmstadt

TECHNISCHE
UNIVERSITÄT
DARMSTADT

Graduate School of
Energy Science
and Engineering

Submitted by

Dipl.-Ing. Bastian Welsch
born on 13.06.1984 in Tübingen, Germany

First assessor: Prof. Dr. Ingo Sass
Second assessor: Prof. Dr. Liselotte Schebek

Darmstadt 2019

Board of examiners

Head:	Prof. Dr. Andreas Henk
First assessor:	Prof. Dr. Ingo Sass
Second assessor:	Prof. Dr. Liselotte Schebek
Examiner:	Prof. Dr. Eva Schill
Examiner:	Prof. Dr.-Ing. Jochen Hack

Declaration

I hereby declare that the presented dissertation is based on original research and is the result of my own work. I certify that this dissertation contains no material which has been accepted for the award of any other degree in my name, in any university or other tertiary institution and, to the best of my knowledge and belief, contains no material previously published or written by another person, except where due reference has been made in the text.

Darmstadt,   2nd November 2018

Abstract

In Germany, the reduction of greenhouse gas emissions has been stagnating for a couple of years now. As a consequence, the climate targets for 2020 are at a risk of being missed. The energy transformation has strongly focused on the electricity sector while mostly disregarding the heating sector. Solar thermal energy and industrial waste heat offer a considerable potential for the replacement of fossil fuels in the heating sector. However, their utilization is hampered by the asynchronous seasonal fluctuation of heat demand and heat supply. Thermal energy storage technologies are required, which are able to absorb large amounts of heat in summer, store it for several months and release it during winter with minimal losses.

Borehole thermal energy storage (BTES) is such a technology for seasonally storing heat on a district scale. A dense array of multiple borehole heat exchangers (BHE) exploits the natural subsurface as a heat storage medium. Conventional BTES systems usually do not exceed a depth of 200 m. Consequently, their operation implies a large thermal impact on shallow geologic formations. This, in combination with comparatively strict groundwater regulations in Germany, impedes the construction of such shallow systems.

The unprecedented, still unrealized concept of medium deep borehole thermal energy storage (MD-BTES) is expected to remedy these shortcomings. MD-BTES systems consist of much less, but appreciably deeper BHEs (up to 1000 m). Consequently, they require significantly less ground surface. Therefore, they are particularly advantageous in densely populated urban areas, which are characterized by large heat demands and scarcely available space. More importantly, a large portion of the thermal energy is stored into deeper geologic formations, reducing the thermal impact on shallow aquifer systems. However, the magnitude of this reduction has not been quantified yet. Furthermore, the general applicability of MD-BTES systems, as well as their economic and environmental implications remain unclear.

As part of this thesis, a large number of numerical simulations was analyzed in a parameter study to investigate the influence of various design and operation variables on the performance of MD-BTES systems. In total, 200 different MD-BTES geometries were compared. Moreover, the influence of subsurface conditions, operating temperatures and the interconnection scheme of BHEs was studied. The results demonstrate the excellent suitability of MD-BTES systems for large scale seasonal heat storage. With a proper dimensioning and in convenient geological and hydrogeological framework conditions, these systems can reach storage efficiencies of 80% or more, while maintaining relatively high supply temperatures of 30 °C. Further numerical simulations provide evidence for a significant mitigation of the thermal impact on shallow groundwater resources by the application of MD-BTES systems instead of their shallow counterparts.

In order to resolve the economic and environmental questions connected to MD-BTES, a *MATLAB* based assessment tool was developed. It is used for a comprehensive economic and environmental life cycle assessment study on the integration of MD-BTES into district heating concepts. The results reveal the dependency of the economic and environmental impacts on the assumed financial and economic boundary conditions. However, they also demonstrate the high economic competitiveness of MD-BTES in combination with solar thermal collector fields, when supposing a likely increase of energy prices in the future. Furthermore, the combination of a solar thermal collector field, an MD-BTES system and a small combined heat and power plant undercuts the emissions of system combinations without any seasonal storage by 32% and more, when assuming a probable decrease in the emission factor of the electricity grid mix.

Kurzfassung

Die Reduzierung der Treibhausgasemissionen in Deutschland stagniert seit einigen Jahren. Die Klimaziele für das Jahr 2020 sind gefährdet. Dies ist nicht zuletzt auch der starken Fokussierung der Energiewende auf den Strommarkt zuzuschreiben. Gerade im Wärmesektor liegt jedoch ein erhebliches Potenzial für die Nutzung erneuerbarer Energiequellen. Aufgrund deutlich ausgeprägter, gegenläufiger saisonaler Schwankungen des Wärmebedarfs und der Wärmebereitstellung z. B. aus solarthermischer Erzeugung, ergibt sich ein Wärmeüberschuss während der Sommermonate, der in der Regel ungenutzt bleibt. Dieser Wärmeüberschuss kann mittels geeigneter Technologien über mehrere Monate zwischengespeichert und zu Zeiten höheren Wärmeverbrauchs zur Gebäudebeheizung und Warmwasserbereitung bereitgestellt werden.

Erdwärmesondenspeicher sind eine vielsprechende Technologie zur saisonales Wärmespeicherung auf Quartiersebene. Zahlreiche, in einer kompakten Anordnung niedergebrachte Erdwärmesonden dienen als Wärmetauscher mit dem natürlichen geologischen Untergrund und machen diesen als Wärmespeichermedium nutzbar. Herkömmliche, oberflächennahe Erdwärmesondenspeicher, die eine Tiefe von 200 m in der Regel nicht überschreiten, verursachen eine erhebliche thermische Anomalie im oberflächennahen Untergrund. Der vergleichsweise strenge Grundwasserschutz in Deutschland steht einem verbreiteten Einsatz von Erdwärmesondenspeichern daher bislang entgegen.

Das innovative und baulich noch nicht umgesetzte Konzept der mitteltiefen Erdwärmesondenspeicherung umgeht dieses Problem. Mitteltiefe Speicher bestehen aus deutlich weniger, dafür bis zu 1000 m tiefen Erdwärmesonden. Dadurch benötigen mitteltiefe Speicher wesentlich weniger Baufläche. Dies ist insbesondere im dicht besiedelten urbanen Raum, wo sich der Wärmeverbrauch konzentriert, von großem Vorteil. Außerdem wird ein Großteil des Wärmeeintrages in den tieferen Untergrund verlagert, wodurch oberflächennahe Aquifere geschützt werden.

Im Rahmen dieser Arbeit wurden zahlreiche numerische Simulationen durchgeführt, um den Einfluss von Auslegungs- und Betriebsparametern auf das Betriebsverhalten mitteltiefer Erdwärmesondenspeicher zu untersuchen. Über 200 unterschiedliche Speichergeometrien wurden verglichen. Außerdem wurden Betriebstemperaturen variiert und der Einfluss der Sondenverschaltung auf die Leistungsfähigkeit mitteltiefer Speicher analysiert.

Die Simulationen belegen die hervorragende Eignung mitteltiefer Systeme zur saisonalen Wärmespeicherung. Bei vergleichsweise hohen Ausspeisetemperaturen von 30 °C und unter geeigneten geologischen und hydrogeologischen Randbedingungen können mitteltiefe Systeme Speichernutzungsgrade von über 80% erreichen. Weitere Simulationen zeigen zudem eine deutlich geringere thermische Beeinträchtigung oberflächennaher Grundwasservorkommen durch mitteltiefe Systeme als durch oberflächennahe Speichersysteme vergleichbarer Kapazität.

Um eine Aussage zu ökonomischen und ökologischen Folgen treffen zu können, die mit der Integration mitteltiefer Erdwärmesondenspeicher in Fernwärmesysteme verbunden sind, wurde ein *MATLAB* basiertes Bewertungsinstrument entwickelt. Mit dessen Hilfe wurde eine umfassende lebenszyklusbasierte ökonomische und ökologische Bewertungstudie verschiedener Fernwärmeerzeugungssysteme durchgeführt. Diese Studie verdeutlicht, dass bei steigenden Kosten für Strom und Gas und gleichzeitiger Steigerung des regenerativen Stromanteils im Strommix der Einsatz mitteltiefer Speicher ein erhebliches Einsparpotenzial an Treibhausgasen unter wettbewerbsfähigen Bedingungen birgt.

Acknowledgement

Foremost, I would like to thank my advisor Prof. Dr. Ingo Sass for his supervision and his valuable support. He gave me a lot of good advice, but he also allowed myself room for developing my own ideas and approaches. Furthermore, he enabled my association to the Darmstadt Graduate School of Excellence Energy Science and Engineering, which was a great opportunity for me to come into contact with many interesting personalities from highly diverse scientific fields. Without the resultant exchange of ideas, my work wouldn't have been that successful.

One of these scientists I came to know over the Graduate School is Prof. Dr. Liselotte Schebek. I want to thank her for being the co-supervisor of my dissertation. She was a huge help concerning the topic of life cycle assessment, which was outside my subject area. Prof. Schebek particularly contributed valuable suggestions to the manuscript of my second fist-author publication.

Furthermore, I would like to express my deep gratitude to Dr. Wolfram Rühaak. He was a huge support from the very beginning of my doctoral studies. He not only contributed decisive advice and engaged in numerous discussions on my research, but also was a good mentor regarding scientific working in general. Moreover, I significantly benefited from his programming experience. He provided source code, which enabled me to easily acquire and improve my own programming skills.

My special thanks go to Dr.-Ing. Daniel Schulte, whose dissertation project was strongly related to mine. We had countless constructive talks about our research. He supported and encouraged me wherever possible. Not least, his English language skills provided the basis for the success with our joint publications. Moreover, he is not only a loyal and obliging colleague but also turned out to be a dear friend of mine.

I also have to give cordial thanks to Laura Göllner-Völker and Julian Formhals, who also became trusted friends of mine in the course of my doctoral studies. Laura had a huge share in preparing and drafting our joint research paper. Julian, who is continuing my research, engaged in several discussions and made major contribution in developing our coupled simulation approach.

Furthermore, I would also like to thank Dr. Kristian Bär and Dr. Sebastian Homuth for the inspiring discussions and their thought-provoking impulses. I could benefit a lot of their wealth of experience in geothermal issues, but they were also a big help in other matters.

I also want to thank Simone Ross-Krichbaum, Dr. Tanja Drobek, Heide Rinnert, Vera Becker, Gabi Schubert and Rainer Seehaus for their administrative and technical support. They facilitated all the work and proceedings at the institute and the Graduate School.

Moreover, I would like to mention Frank Brettreich, Philipp Heiß, Sascha Michaelis, Sabrina Schmiedt, Sarah Steiner, Torben Treffeisen, Jan Weber and Tobias Zöller, who all contributed to my research as part of their bachelor or master theses or as student research assistants.

My research results were partly derived from the project "Simulation und Evaluierung von Kopplungs- und Speicherkonzepten regenerativer Energieformen zur Heizwärmeversorgung". This project (HA project no. 375/13-14) was funded within the framework of Hessen ModellProjekte, financed with funds of Energietechnologieoffensive Hessen – Projektförderung in den Bereichen Energieerzeugung, Energiespeicherung, Energietransport und Energieeffizienz. Furthermore, I am very grateful for the partial funding of my research by the Funding Initiative for

Preface

The herein presented cumulative doctoral thesis originated from my engagement as a research fellow in the working group Geothermal Science and Technology at the Institute of Applied Geosciences, TU Darmstadt. It focuses on the assessment of medium deep borehole thermal energy storage (MD-BTES) systems, which comprises the technical suitability of such systems for seasonal heat storage, as well as the environmental and economic implications of integrating this technology into district heating systems. Two simultaneous dissertation projects bear a thematic reference to MD-BTES systems as well (see Figure 1). However, they do not thematically overlap with my dissertation but rather complement it: my colleague Dr.-Ing. Daniel Otto Schulte developed a numerical tool for the simulation and optimization of MD-BTES systems, which I could apply in my work. He submitted his thesis with the title "Simulation and Optimization of Medium Deep Borehole Thermal Energy Storage Systems" (Schulte 2016) on the 2nd of November 2016 and defended it on the 19th of December 2016. Our colleague Julian Formhals continues the work of Daniel Schulte and me in his dissertation. His focus lies on holistic system considerations and the integration of borehole thermal energy storage (BTES) into district heating networks.


Figure 1: Research activities and dissertation projects at the research group Geothermal Energy and Technology, TU Darmstadt directly or indirectly linked to MD-BTES.

MD-BTES has been a key research topic at the working group for several years now. During that time, a number of directly or indirectly related research projects tried to examine the topic from different perspectives (for an overview see Figure 1).

Large parts of the results included in this dissertation originate from the research project "Simulation and evaluation of coupling and storage concepts for renewable forms of energy for heat supply" (denoted as ETOH-Project, original German title: "Simulation und Evaluierung von Kopplungs- und Speicherkonzepten regenerativer Energieformen zur Heizwärmeversorgung"), which was accomplished from June 2013 to February 2015. The project (HA project no. 375/13-14) was funded within the framework of Hessen ModellProjekte, financed with funds of Energietechnologieoffensive Hessen – Projektförderung in den Bereichen Energieerzeugung, Energiespeicherung, Energietransport und Energieeffizienz. It was a joint research project between the Department of Geothermal Science and Technology (TU Darmstadt) and the local energy producer ENTEGA (former known as HEAG Südhessische Energie AG).

Moreover, important advances were achieved in the research project "Reducing the building energy demand through geothermal storage systems – Development of an interacting simulation model" (denoted as FiF-Project, original German titel: "Reduzierung des Gebäudewärmebedarfs mittels geothermischer Speicher – Entwicklung eines interagierenden Simulationsmodells"), which was funded by the Forum Interdisziplinäre Forschung, TU Darmstadt. The project comprised the development of an approach to couple numerical simulations of BTES systems with simulations of the surface components of a heating system.

Furthermore, I have been an associated member of the Darmstadt Graduate School of Excellence Energy Science and Engineering (GSC 1070), which is financed by the Deutsche Forschungsgemeinschaft (DFG) in the framework of the Excellence Initiative. The associated membership included remarkable travel funds, which I could spent for the participation and presentation of my work on international conferences like the World Geothermal Congrass 2015 in Melbourne.

This cumulative dissertation comprises the eight publications that are listed in Section *Cumulative Dissertation* and that are annexed to the Appendix. They summarize my research activities during the last five years and reveal the progress of my scientific work. At this point, I want to mention, that the here presented synopsis contains literal text passages from my first-author publications without giving any reference. I want to clarify, that these self-quotations are present and that they do not denote any intent to deceive.

This enveloping manuscript constitutes a comprehensive overview of my research results. It also contains some unpublished, unprecedented studies, which are important for the overall assessment of MD-BTES systems. Moreover, one strong focus is laid on the description of the environmental and economic assessment tool, which has been developed during the last stage of my research. The tool comprises many details, which are at the risk of fading into obscurity as they are solely published in the digital supplement of the respective research paper (Appendix G).

Table of Contents

List of Figures

List of Tables

Index of Abbreviations and Symbols

Abbreviations

BAU	Business as usual scenario	FEM	Finite element method
BAU SUB	Business as usual scenario including subsidies	GB	Gas boiler
BHE	Borehole heat exchanger	GHG	Greenhouse gas
BTES	Borehole thermal energy storage	HP	Heat pump
CHP	Combined heat and power / co-generation power plant	HVAC	Heating, ventilation and air conditioning
CP	Circulating pump	ICE	Internal combustion engine
CXA	Coaxial BHE with inlet in the annulus	LCA	Life cycle assessment
CXC	Coaxial BHE with inlet in the center pipe	LCI	Life cycle inventory analysis
DH	District heating	LCIA	Life cycle impact assessment
DOC	Dissolved organic carbon	MD-BTES	Medium deep borehole thermal energy storage
ECO	Economic/environmental scenarios	SA/V-ratio	Surface-area-to-volume ratio
EU ETS	European Union Emissions Trading System	STC	Solar thermal collector
EVO	Evolution scenario	TES	Thermal energy storage
EVO SUB	Evolution scenario including subsidies	TRY	Test reference year
FE	Finite element		

Formula symbols

A_{STC}	[m²]	Solar collector area
CED	[TJ]	Cumulative energy demand
COP	[-]	Coefficient of performance of the HP
EF	[g CO_2eq kWh^{-1}]	Emission factor
F	[€]	Operation costs
GWP	[t CO2eq]	Global warming potential
I	[€]	Investment costs
L_{BHE}	[m]	Length of borehole heat exchangers
$LCOH$	[€ct kWh^{-1}]	Levelized cost of heat
M	[€]	Maintenance costs
N_{BHE}	[-]	Number of borehole heat exchangers
P	[kW]	Thermal power demand/supply
Q	[kWh]	Thermal energy demand/supply
R	[€]	Revenue
S	[€]	Salvage/residual value
T	[°C]	Temperature
ΔT	[K]	Temperature difference
V	[m³]	Volume
$\dot{V}$	[m³ s^{-1}]	Volume flow rate
a	[-]	Year of operation
c	[J kg^{-1} K^{-1}] / [€ unit^{-1}]	Specific heat capacity / Specific costs
f_{GB}	[-]	Correction factor for gas firing

p_{STC}	[kW m⁻²]	Specific power output of STC
r	[-]	Interest rate
t	[s]	Time
z	[m]	Depth
α_{CHP}	[-]	Coefficient of share of cogeneration in the peak load demand
γ_{CHP}	[-]	Partial load share of the CHP
η	[-]	Efficiency / storage utilization ratio
θ	[-]	Storage filling level
λ	W m⁻¹ K⁻¹)	Thermal conductivity
μ		Arithmetic mean
ρ	[kg m⁻³]	Density
σ	[-]	Standard deviation

Subscripts and superscripts

E	Extracted	$iso, 6°C$	6 °C-isosurface
L	Loss	max	Maximum
S	Stored	min	Minimum
$S\text{-}BTES$	Shallow BTES	mod	Module
$U1$	Unit 1	net	Net
a	Index for year of operation	nom	At nominal power
an	Annulus	op	Operation phase
chg	Charging	out	Outlet
dir	Direct	$peak$	At peak load
$dischg$	Discharging	per	Peripheral devices
dr	Drilling	pp	BHE pipes
el	Electrical/electricity	$prod$	Production phase
end	End, last entry in a matrix	r	Rock
f	Fluid	rel	Relocation of the drill rig
gas	Natural gas	res	Residual value
gr	Grouting/back filling	sc	Steel casing
$grid\ el$	Grid electricity	st	Drilling site
i	Index for a specific component	sup	Supply
in	Inlet	th	Thermal
ip	Inner pipe	tot	Total

Cumulative Dissertation

This cumulative dissertation comprises the following eight journal publications. The full papers can be found in the Appendix.

Appendix A: Bär K, Rühaak W, **Welsch B**, Schulte DO, Homuth S and Sass I (2015): Seasonal high temperature storage with medium deep borehole heat exchangers, Energy Procedia, v. 76, p. 351-360, doi:10.1016/j.egypro.2015.07.841.

Appendix B: **Welsch B**, Rühaak W, Schulte DO, Bär K and Sass I (2016): Characteristics of medium deep borehole thermal energy storage, International Journal of Energy Research, v. 40, no. 13, p. 1855-1868, doi: 10.1002/er.3570.

Appendix C: Rühaak W, Steiner S, **Welsch B**, Sass I (2015): Prognosefähigkeit numerischer Erdwärmesondenmodelle (Uncertainty in numerical models of borehole heat exchangers), Grundwasser, v. 20, no. 4, p. 243–251

Appendix D: Schulte DO, Rühaak W, **Welsch B** and Sass I (2016): BASIMO – borehole heat exchanger array simulation and optimization tool, Energy Procedia, v. 97, p. 210-217, doi:/10.1016/j.egypro.2016.10.057.

Appendix E: Schulte DO, Rühaak W, Oladyshkin S, **Welsch B** and Sass I (2016): Optimization of Medium-Deep Borehole Thermal Energy Storage Systems, Energy Technology, v. 4, p. 104-113, doi:10.1002/ente.201500254.

Appendix F: Schulte DO, **Welsch B**, Boockmeyer A, Rühaak W, Bär K, Bauer S and Sass I (2016) Modeling insulated borehole heat exchangers, Environmental Earth Sciences, v. 75, p. 1-12, doi:10.1007/s12665-016-5638-x.

Appendix G: **Welsch B**, Göllner-Völker L, Schulte DO, Bär K, Sass I and Schebek L (2018): Environmental and Economic Assessment of Borehole Thermal Energy Storage in District Heating Systems, Applied Energy, v. 216, p. 73–90, doi:10.1016/j.apenergy.2018.02.011.

Appendix H: **Welsch B**, Rühaak W, Schulte DO, Formhals J, Bär K and Sass I (2017): Co-Simulation of Geothermal Applications and HVAC Systems, Energy Procedia, v. 125, p. 345–352, doi:10.1016/j.egypro.2017.08.040.

Appendix A, which constitutes the initial publication within our research project "Simulation and evaluation of coupling and storage concepts for renewable forms of energy for heat supply", provides the basis for the subsequent publications. It presents technical and operational fundamentals of seasonal heat storage in medium deep borehole heat exchanger (BHE) arrays as well as their general operating characteristics. Furthermore, it debates the key advantages of MD-BTES over shallow BTES and aquifer storage. An essential component of *Appendix A* is a case study, regarding two different heat supply scenarios for a specific university building at the campus of TU Darmstadt integrating an MD-BTES: the first scenario considers the charging of the BTES with excess heat from a combined heat and power plant (CHP) during summer, in the second scenario, the heat from the CHP is partly substituted by solar thermal heat. Furthermore, the case study investigates the behavior of four BTES systems, differing in number and depth of the BHEs by means of numerical simulation. The study substantiates the significance of a thorough foreknowledge about the geological site conditions, the system design and the expected heat flows for an adequate dimensioning of MD-BTES systems. Moreover, the paper

underlines the importance of coupled numerical simulations of the overall system in conjunction with mathematical optimization approaches.

Kristian Bär was the coordinator of our project "Simulation and evaluation of coupling and storage concepts for renewable forms of energy for heat supply". He drafted the manuscript to this publication, ascertained the heat demand curve and considered the scenarios for the numeric simulations. As a co-author of the paper, I carried out field investigations as well as laboratory experiments in order to characterize the site of our case study. My further contributions to the paper were the set-up of the numerical simulations together with Daniel Schulte and the preparation and interpretation of the results. Furthermore, I was strongly involved in discussions with Kristian Bär, Wolfram Rühaak and Daniel Schulte about the operation scenarios as well as issues concerning the numerical simulation of MD-BTES. Moreover, I supported Daniel Schulte in the development of a concept for the mathematical optimization and coupled simulation of these systems. Wolfram Rühaak supervised the programming work and the set-up of the models. Furthermore, he assisted in the handling of the software tools. Sebastian Homuth contributed with his experience in the required drilling technology and wrote the respective paragraph of the manuscript. Ingo Sass supervised the project and the research. All authors of the manuscript were involved in fundamental discussions on the concept of MD-BTES. Furthermore, they were all engaged in the revision of the article.

Appendix B describes an extensive numerical modeling study on the operational behavior of MD-BTES. It investigates the influence of several design parameters like the BHE length, the number of BHEs and the BHE spacing, as well as geological parameters like the hydraulic and thermal conductivity and the heat capacity of the reservoir rocks on the long-term performance of MD-BTES systems. For this purpose, more than 250 different numerical BTES models were simulated with the commercial software *FEFLOW*. The storage efficiencies as well as the storage capacities of the modeled storage systems are determined, compared and discussed. Thereby, favorable storage configurations and geological boundary conditions are identified. The results reveal that that potential for seasonal heat storage significantly increases with the size of the BTES system. Storage efficiencies of more than 80% and heat capacities of around 20 GWh per year are reached by the largest BTES systems under consideration.

As the first author of this paper, I mainly developed the experimental design, set-up all the numerical models and executed their simulations. Furthermore, I evaluated and illustrated the results and drafted the manuscript. Wolfram Rühaak supervised the numerical modelling work and gave assistance in all numerical issues that arose during the implementation of the study. Daniel Schulte was strongly involved in the drafting of the manuscript. He further supported the design of the numerical experiments, the interpretation and evaluation of the simulation results. The study was conducted as a main part of the research project "Simulation and evaluation of coupling and storage concepts for renewable forms of energy for heat supply". Kristian Bär coordinated the research project and therefore participated together with Wolfram Rühaak and Daniel Schulte in basic debate on the concept of MD-BTES. Ingo Sass supervised the project and the research. All co-authors contributed to the revision of the manuscript.

Appendix C debates the question on the uncertainty of BHE simulations due to uncertainties in the geological input parameters thermal conductivity, heat capacity and the geothermal gradient. The study recommends the simulation of a model ensemble as it is already common practice in meteorological simulation studies. Ensemble models reflect the uncertainties of the input

parameters and can give an estimation on the uncertainties of the simulation results. A numerical model of the medium deep borehole heat exchanger Heubach, Germany is used to demonstrate the applicability of the approach to geothermal closed loop systems.

Wolfram Rühaak is the first author of the paper. He had the idea of applying ensemble models to BHE simulations, initiated the study and mainly drafted the manuscript. In the course of her master thesis, Sarah Steiner carried out the numerical modelling work, evaluated the results and provided figures to the manuscript. As a co-author, I provided a huge amount of data concerning the geological underground conditions at the case study site in Heubach. Furthermore, I was strongly involved in the development of the numerical experiments and the models, gave advice for the simulation and supervised the master thesis of Sarah Steiner. Ingo Sass supervised the research and contributed valuable ideas. All co-authors contributed to the revision of the manuscript.

Appendix D introduces the structure and the principal features of *BASIMO*. *BASIMO* is a *MATLAB* based in-house development, which facilitates the numerical simulation and optimization of BTES systems. However, it is not restricted to storage applications but can also be utilized to simulate and optimize conventional single BHE systems or BHE arrays.

Daniel Schulte was the first author of this paper. As part of his PhD research, he was mainly responsible for the development and the programming of *BASIMO*. He iteratively tested and improved the program code to ascertain its accurate functionality. Furthermore, he wrote the manuscript and created all figures. Wolfram Rühaak guided the overall development of *BASIMO* and gave assistance in programming issues. As a co-author, I supported the testing and troubleshooting of the code. Furthermore, I was engaged in early discussion on the functionality and capability of *BASIMO*. Ingo Sass supervised the research. All co-authors contributed to the revision of the manuscript.

Appendix E presents an approach for the optimization of MD-BTES systems. The optimization is based on a proxy model, which is trained by numerical simulations. It is readily adaptable to various design parameters of BTES systems such as the BHE length, the number of BHEs or the BHE spacing. Firstly, the paper contains a concise illustration of the numerical methods that are applied during the training simulations. Secondly, it comprises a short introduction to the arbitrary polynomial chaos expansion, which is used for the generation of the proxy model. Furthermore, the optimization algorithm employed on the proxy model is summarized. Finally, an application example is used to demonstrate the functionality and to discuss approximation errors of the approach.

Daniel Schulte is the first author of this paper. After developing and programming the numerical simulator, he carried out the proxy training simulations and the optimization runs. Furthermore, Daniel Schulte assessed the results, determined the approximation errors and finally drafted the manuscript. Wolfram Rühaak was the supervisor of the programming work. He was strongly involved in the programming process and in many discussions on programming issues. Sergey Oladyshkin developed a *MATLAB* script for the implementation of the arbitrary polynomial chaos expansion and provided the corresponding text passages. As the issue was very closely related to my own research, I was strongly involved in countless discussions on fundamental questions concerning MD-BTES. Furthermore, I handed out advice on the setup of the experimental design of the simulation experiments and created some of the figures in the paper. Ingo Sass supervised the research. All co-authors contributed to the revision of the manuscript.

Appendix F concerns an advanced analytical BHE model, which allows for the consideration of a partial insulation at the uppermost section of a BHE. Such an insulating grout section can reduce the heat input from MD-BTES systems into shallow aquifers and hence, reduce the risk for a potential temperature induced contamination of the groundwater body. Furthermore, these insulations can enhance the efficiency of medium deep BHEs, as it reduces heat losses to shallower, colder rock formations. The paper outlines the improved analytical solution, which allows for a consideration of two grout sections with different thermal conductivities and dimensions. The solution is implemented in *BASIMO*. A benchmark simulation is compared to a fully discretized BHE model in order to demonstrate the functionality and accuracy of our approach. Moreover, an application example is used to highlight the capability of the improved analytical BHE solution.

The improved analytical solution for partially insulated BHEs is a joint development of Daniel Schulte and me. I had the principle idea of how the partial insulation could be realized in the analytical BHE solution and programed a first prototype of it in *MATLAB*. Daniel Schulte strongly improved the *MATLAB* code and implemented it into *BASIMO*, ran the simulations and the optimization for the application example. Finally, he assessed the results and wrote the manuscript. I was in permanent communication with Daniel Schulte, provided valuable ideas on the improvement of the code, and gave advice concerning the development and the assessment of the application example. Furthermore, I provided a majority of the figures for the manuscript. Anke Boockmeyer carried out the benchmark simulations in a fully discretized Open-GeoSys model and provided the benchmark data. Wolfram Rühaak gave important advice for the implementation of the development into *BASIMO*. Together with Kristian Bär, he was also involved in permanent interchange of ideas concerning the demand for partially insulated BHEs and the capability of the improved analytical solution. Sebastian Bauer supervised the work of Anke Boockmeyer, while Ingo Sass supervised Daniel Schulte and me. All co-authors contributed to the revision of the manuscript.

Appendix G is a comprehensive study on the economic and environmental impact of integrating an MD-BTES system into different district heating concepts. The study is based on an energy balance model, which is connected to an economic model and a life-cycle assessment scheme. The resultant tool is capable to assess district heating supply concepts including different shares of the implemented heat sources (i.e. a combined heat and power plant, a solar thermal collector field, a conventional gas boiler and a heat pump assisted BTES system) in terms of levelized cost of the supplied heat (*LCOH*) and the global warming potential (*GWP*) including the production and the use phase of the system. More than 9000 different system designs were investigated, varying the composition of the heat supply system and the size of the system components. Additionally, four different economic/ecological scenarios were considered. Pareto efficient system designs were identified for the different system compositions and scenarios and compared to each other. Furthermore, *Appendix H* contains a one-at-a-time sensitivity analysis, which illustrates the impact of the change of the main cost factors on the *LCOH* of different system designs. The authors discuss the limitations and the results of the study.

As the first author of this paper, I developed the energy balance model and the economic model and assisted in the development of the LCA model as well as in the data acquisition for the economic and ecological scenarios. Furthermore, I programmed all three models in Matlab Simulink, developed the experimental design and carried out all the simulations. Moreover, I evaluated the results, created most of the figures and drafted the manuscript. Laura Göllner-

Völker was in charge for the development of the LCA model and the acquisition of the LCA data and assisted in gathering the economic data. She provided valuable figures and the LCA related text passages. Laura Göllner-Völker and Daniel Schulte engaged in numerous discussions on the experimental design, the overall concept and the results. Beyond that, Daniel Schulte was a big support in drafting the manuscript. Kristian Bär gave valuable advice for the realization of the assessment tool and provided data concerning the drilling process. Liselotte Schebek and Ingo Sass supervised Laura Göllner-Völker's and my own research, respectively. All authors were involved in the revision of the manuscript.

Appendix H introduces the approach of coupling two separate software tools, one for the simulation of heat transport processes in the subsurface and the geothermal installation (i.e. *FEFLOW*) and one for the simulation of components of the heating, ventilation and air conditioning (HVAC) system (i.e. Matlab-Simulink), using the TCP/IP protocol suite. Ordinarily, both systems are simulated separately, ignoring that they interact with each other. This mutual interaction originates from an exchange of fluid or thermal energy, resulting in an interference of the fluid temperatures and therefore directly influencing the efficiencies of the different system components. The coupling presented in *Appendix G* allows for a simultaneous execution of both models and a data interchange between the models at defined communication steps. Fluid temperatures and the volume flow rates are committed and update the simulation of the respective other system part. Thereby, the interaction of both system parts is included, which provides a much more precise simulation of the overall system. Furthermore, mathematical optimization algorithms can be applied. Thereby, a systematic optimization of an entire geothermal based heating system can be conducted automatically. In order to demonstrate the functionality of the approach, *Appendix G* comprises a simple optimization example. As the coupling is relatively lose (i.e. no iteration scheme is implemented in the communication process), the approach is subject to transmission errors, which are investigated as well.

I was the first author of this paper. I developed the coupling and optimization concept and implemented the communication routines into Matlab-Simulink and *FEFLOW*. Furthermore, I have tested the concept, carried out the simulations presented in the paper, evaluated the results, created all figures and drafted the manuscript. Wolfram Rühaak had the idea for using the TCP/IP protocol suite and supervised the programming work. Daniel Schulte assisted in drafting the manuscript and was engaged in developing the optimization routines. Julian Formhals gave advice on the development of the coupling concept. Kristian Bär and Ingo Sass were engaged in early discussion on the necessity of coupled simulations and supervised the research. All co-authors participated in the revision of the manuscript.

Further publications

In addition to the aforementioned publications, I presented my research on several conferences and exhibitions both, in oral presentations and poster sessions. Those conference presentations, which resulted in a contribution to the corresponding proceedings, are listed below in chronological order:

Rühaak W, Schulte DO, **Welsch B**, Chauhan S, Bär K, Homuth S and Sass I (2014): Optimierung eines mitteltiefen Erdwärmesondenspeichers, at *Tagung der Fachsektion Hydrogeologie in der Deutschen Gesellschaft für Geowissenschaften*, Bayreuth, Germany, 29–31 May 2014.

Schulte DO, Chauhan S, **Welsch B**, Rühaak W and Sass I (2014): A MATLAB Toolbox for Optimization of Deep Borehole Heat Exchanger Storage Systems, at *Computational Methods in Water Resources XX. International Conference*, Stuttgart, Germany, 10-13 June 2014.

Welsch B, Bär K, Rühaak W and Sass I (2014): An Outcrop Analogue Study on the Suitability of Crystalline Rocks as Heat Storage Media, at *GeoFrankfurt 2014*, Frankfurt, Germany, 21–24 September 2014. (Poster)

Welsch B, Rühaak W, Bär K, Homuth S and Sass I (2014): Numerische Modellierung mitteltiefer Erdwärmesondenspeicher, at *Der Geothermiekongress 2014*, Essen, Germany, 11–13 November 2014.

Steiner S, Lemes Z, **Welsch B**, Rühaak W and Sass I (2014): Tiefe Erdwärmesonde Heubach – Erfahrungen und Schlussfolgerungen, at *Der Geothermiekongress 2014*, Essen, Germany, 11–13 November 2014.

Welsch B, Rühaak W, Schulte DO, Bär K, Homuth S and Sass I (2015): Untersuchung des Leistungsvermögens mitteltiefer Erdwärmesondenspeicher mittels numerischer Modellierung, at *Geotherm 2015*, Offenburg, Germany, 5–6 March 2015.

Rühaak W, Steiner S, **Welsch B** and Sass I (2015): Usage of ensemble geothermal models to consider geological uncertainties, at *EGU General Assembly*, Vienna, Austria, 12–17 April 2015.

Rühaak W, Bär K, Schulte DO, **Welsch B**, Chauhan S, Homuth S and Sass I (2015): Medium Deep High Temperature Heat Storage, at *EGU General Assembly*, Vienna, Austria, 12–17 April 2015.

Welsch B, Rühaak W, Schulte DO, Bär K, Homuth S and Sass I (2015): A Comparative Study of Medium Deep Borehole Thermal Energy Storage Systems Using Numerical Modelling, in *Proceedings World Geothermal Congress*, Melbourne, Australia, 19–25 April 2015.

Schulte DO, Rühaak W, Chauhan S, **Welsch B** and Sass I (2015): A MATLAB Toolbox for Optimization of Deep Borehole Heat Exchanger Arrays, in *Proceedings World Geothermal Congress*, Melbourne, Australia, 19–25 April 2015.

Bär K, Homuth S, Rühaak W, Schulte DO, **Welsch B** and Sass I (2015): Coupled Renewable Energy systems for seasonal High Temperature Heat storage via Medium Deep Borehole Heat Exchangers, in *Proceedings World Geothermal Congress*, Melbourne, Australia, 19–25 April 2015.

Welsch B, Rühaak W, Schulte DO, Bär K and Sass I (2015): A Comparative Study of Medium Deep Borehole Thermal Energy Storage Systems Using Numerical Modelling, at *Energy, Science & Technology International Conference and Exhibition – EST 2015*, Karlsruhe, Germany, 20–22 May 2015. (Poster)

Bär K, **Welsch B**, Schulte DO, Rühaak W, Homuth S and Sass I (2015): Coupling of Renewable Energies with Medium Deep Borehole Heat Exchangers to Cover the Annual Heat Demand of Larger Buildings by Seasonal High Temperature Heat Storage, at *Energy, Science & Technology International Conference and Exhibition – EST 2015*, Karlsruhe, Germany, 20–22 May 2015.

Schulte DO, Rühaak W, Chauhan S, **Welsch B** and Sass I (2015): Simulation and Optimization of Deep Borehole Heat Exchanger Arrays, *at Energy, Science & Technology International Conference and Exhibition – EST 2015*, Karlsruhe, Germany, 20–22 May 2015.

Bär K, **Welsch B**, Schulte DO, Rühaak W and Sass I (2015): Medium Deep High Temperature Heat Storage, at *GeoEnergy 2015*, Bergen, Norway, 2–3 September 2015.

Welsch B, Schulte DO, Rühaak W, Bär K and Sass I (2015): Technical and Economical Evaluation of Medium Deep Borehole Thermal Energy Storages, at *FEFLOW 2015 Conference*, Berlin, Germany, 21–23 September 2015.

Steiner S, Lemes Z, **Welsch B**, Rühaak W, Bär K and Sass I (2015): Mitteltiefe Erdwärmesonde Heubach, eine Erfolgsgeschichte – Schlussfolgerungen aus der thermischen Modellierung des laufenden Betriebs, at *10. Tiefengeothermie-Forum*, Darmstadt, Germany, 22 September 2015.

Schulte DO, Rühaak W, **Welsch B** and Sass I (2015): BASIMO Borehole Heat Exchanger Array Simulation and Optimization Tool, at *Der Geothermiekongress 2015*, Essen, Germany, 2–4 November 2015.

Schulte DO, Rühaak W, **Welsch B** and Sass I (2015): Simulation unkonventioneller Erdwärmesonden-Anlagen, at *Der Geothermiekongress 2015*, Essen, Germany, 2–4 November 2015.

Sass I, **Welsch B** and Schulte DO (2016): Mitteltiefe Erdwärmesondenspeicher – Lösung für den Nutzungskonflikt Grundwasserschutz versus Geothermienutzung?, in *Proceedings 7. Bochumer Grundwassertag*, Bochum, Germany, 17 March 2016.

Welsch B, Rühaak W, Schulte DO, Bär K and Sass I (2016): Advanced Coupled Simulation of Borehole Thermal Energy Storage Systems and Above Ground Installations, at *European Geoscience Union General Assembly 2016*, Vienna, Austria, 17–22 April 2016.

Welsch B, Rühaak W, Schulte DO, Bär K and Sass I (2016): Sensitivity Analysis on the Performance of Medium Deep Borehole Thermal Energy Storage Systems, at *European Geoscience Union General Assembly 2016*, Vienna, Austria, 17–22 April 2016. (Poster)

Schulte DO, Rühaak W, **Welsch B**, Bär K and Sass, I (2016): BASIMO - Borehole Heat Exchanger Array Simulation and Optimization Tool, at *European Geoscience Union General Assembly 2016*, Vienna, Austria, 17–22 April 2016.

Schulte DO, Rühaak W, **Welsch B**, Oladyshkin S and Sass I (2016): Optimization of Borehole Heat Exchanger Arrays, at *European Geoscience Union General Assembly 2016*, Vienna, Austria, 17–22 April 2016.

Rühaak W, **Welsch B**, Schulte DO, Bär K and Sass I (2016): Coupled Modelling and Optimization of Borehole Thermal Energy Storage and Above Ground Installations, at *67. Berg- und Hüttenmännischer Tag*, Freiberg, Germany, 8–10 June 2016.

Bär K, Rühaak W, **Welsch B**, Schulte DO, Homuth S and Sass I (2016): Seasonal high temperature heat storage with medium deep borehole heat exchangers – a conceptual case study, at *European Geothermal Congress*, 20-22 September 2016, Strasbourg.

Welsch B, Weber J, Bär K, Rühaak W, Schulte DO, Fritsche J-G and Sass I (2016): Möglichkeiten der geothermischen Nutzung der Tiefbohrung „Herz- und Kreislaufzentrum Rotenburg" at *11. Tiefengeothermie-Forum*, 29 September 2016, Darmstadt

Sass I, Bär K, Schulte DO, **Welsch B**, Formhals J, Hornich W and Homuth S. (2016): SKEWS (Solargekoppelter kristalliner Erdwärmesondenspeicher): Wärmespeicherprojekt der TU Darmstadt am Campus Lichtwiese, at *11. Tiefengeothermie-Forum*, 29 September 2016, Darmstadt.

Welsch B, Rühaak W, Schulte DO, Bär K and Sass I (2016): Systemoptimierung durch gekoppelte Modellierung von Erdwärmesondenspeichern und obertägigen Heizsystemkomponenten, at *Der Geothermiekongress 2016*, Essen, Germany, 29 November–01 December 2016

Schulte DO, **Welsch B**, Rühaak W, Bär K and Sass I (2016): Simulation teil-isolierter mitteltiefer Erdwärmesonden, at *Der Geothermiekongress 2016*, Essen, Germany, 29 November–01 December 2016.

Bär K, Sass I, **Welsch B**, Schulte DO and Rühaak W (2017): Seasonal High Temperature Heat Storage with Middle Deep Borehole Heat Exchangers – a Coupled-Modelling Study, in *Proceedings 42nd Workshop on Geothermal Reservoir Engineering*, Stanford University, Stanford, California, 13–15 February 2017.

Welsch B, Rühaak W, Schulte DO, Formhals J, Bär K and Sass I (2017): Optimization of Borehole Thermal Energy Storage System Design Using Comprehensive Coupled Simulation Models, at *European Geoscience Union General Assembly 2017*, Vienna, Austria, 23–28 April 2017. (Poster)

Welsch B, Schulte DO, Rühaak W, Bär K and Sass I (2017): Thermal Impact of Medium Deep Borehole Thermal Energy Storage on the Shallow Subsurface, at *European Geoscience Union General Assembly 2017*, Vienna, Austria, 23–28 April 2017. (Poster)

Schulte DO, **Welsch B**, Rühaak W, Bär K and Sass I (2017): BASIMO - Borehole Heat Exchanger Array Simulation and Optimization Tool, at *European Geoscience Union General Assembly 2017*, Vienna, Austria, 23–28 April 2017. (Poster)

Formhals J, Schulte DO, **Welsch B** and Sass I (2017): Coupled Simulation of Borehole Thermal Energy Storages and Solar District Heating Systems, at *European Geoscience Union General Assembly 2017*, Vienna, Austria, 23–28 April 2017.

Formhals J, **Welsch B**, Schulte DO and Sass I (2017): Effects of the District Heating Supply Temperature on the Efficiency of Borehole Thermal Energy Storage Systems, at *3rd International Conference on Smart Energy Systems and 4th Generation District Heating*, Copenhagen, Denmark, 12–13 September 2017.

Göllner-Völker L, **Welsch B**, Schulte DO, Schebek L and Sass I (2018): Environmental and Economic Assessment of Seasonal Storage Systems in Domestic Heating Grids using the Example of Medium Deep Borehole Thermal Energy Storage, at *12th International Renewable Energy Storage Conference IRES 2018*, Düsseldorf, Germany, 13–15 March 2018.

1   Introduction

Unlike some famous climate change deniers often propagate, there is a strong scientific consensus that anthropogenic greenhouse gas (GHG) emissions make a major contribution to the contemporary global warming (Oreskes 2004). The Paris Agreement (UN 2015), which has been reached on the *2015 United Nations Climate Change Conference*, has meanwhile (status 4th October 2018) been ratified or acceded to by 180 states and the EU. It represents an important move to counteract the climate change. The tenor of the agreement is a limitation of the global warming to well below 2 °C and to make every effort in order to limit the global warming to 1.5 °C compared to the pre-industrial level. Furthermore, it demands zero net anthropogenic GHG emissions should be reached by the year 2100 at the latest.

Like all the countries that had ratified the Paris Agreement, Germany had to set its own GHG reduction targets. In the end of 2014, the German Government had already enacted the Climate Action Programme 2020 (Aktionsprogramm Klimaschutz 2020, BMUB 2014), which includes a reduction of the GHG emissions until 2020 by 40% compared to the level of 1990. The Climate Action Plan 2050 (Klimaschutzplan 2050, BMUB 2016), which was issued in 2016 as a direct reaction on the Paris Agreement, targets a reduction of the GHG emissions until 2030 by 55%, until 2040 by 70% and until 2050 by 80 to 95% referred to 1990 (Figure 2). While there was a promising progress during the 1990s and the first decade of the new century, the reduction of GHG emissions attenuated during the last years. Despite the coalition agreement from the 14th of March 2018, which states that the current German Government adheres to the measures and targets envisaged in the Climate Action Programme 2020 and the Climate Action Plan 2050, the climate target 2020 will be missed without any further measures by probably eight percentage points (BMU 2018).
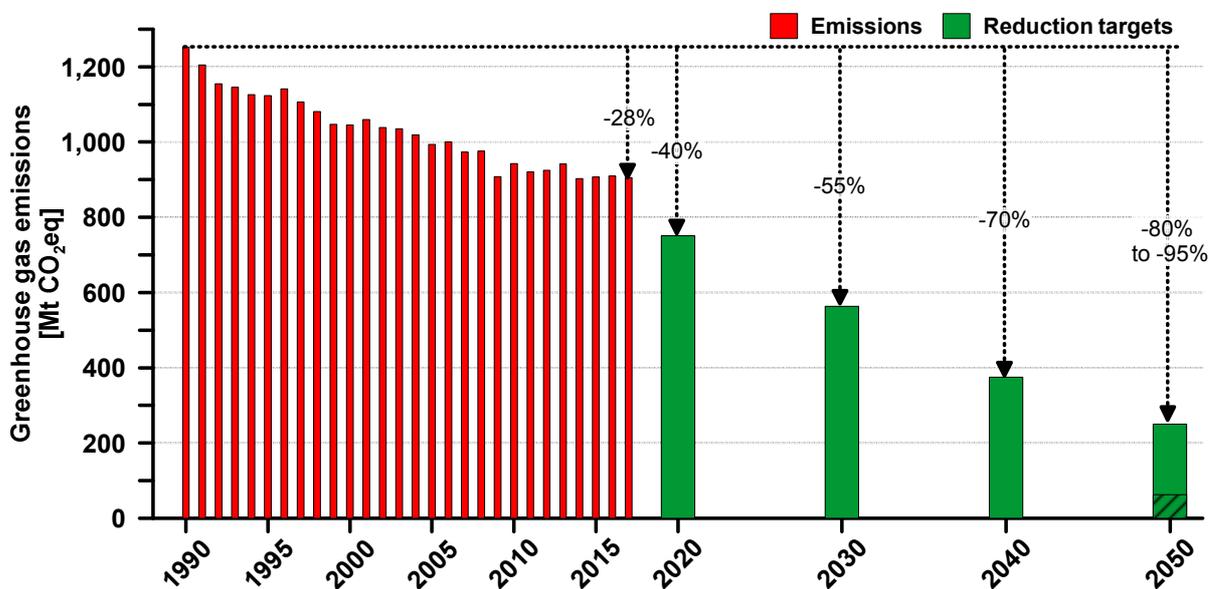
Figure 2: Temporal development of the total greenhouse gas emissions in Germany from 1990 to 2015 (without LULUCF–Land Use, Land-Use Change and Forestry, data source: UBA 2018, preliminary value for 2017) and reduction targets for Germany according to the Climate Action Programme 2020 (Aktionsprogramm Klimaschutz 2020, BMUB 2014) and the Climate Action Plan 2050 (Klimaschutzplan 2050, BMUB 2016).

Global efforts concerning the extension of renewable energy sources and the reduction of GHG emissions have mostly focused on the electricity sector (REN21 2018). This statement is also valid for Germany. The heating sector (i.e. space and tap water heating as well as process heat), which was responsible for approximately 53% of the final energy consumption in Germany in 2015 (AGEB 2016, Figure 3), has largely been neglected in the national attempts to reduce GHG emissions. Still, more than 70% of the final energy consumption in the heating sector (without process heat) are directly derived from fossil fuels (Figure 3), wherein the portions of fossil energy in district heating (DH) and in electric heating are not taken into account, yet. Thus, there is a huge potential for reducing GHG emissions in the heating sector. The question is, how to exploit this reduction potential best.
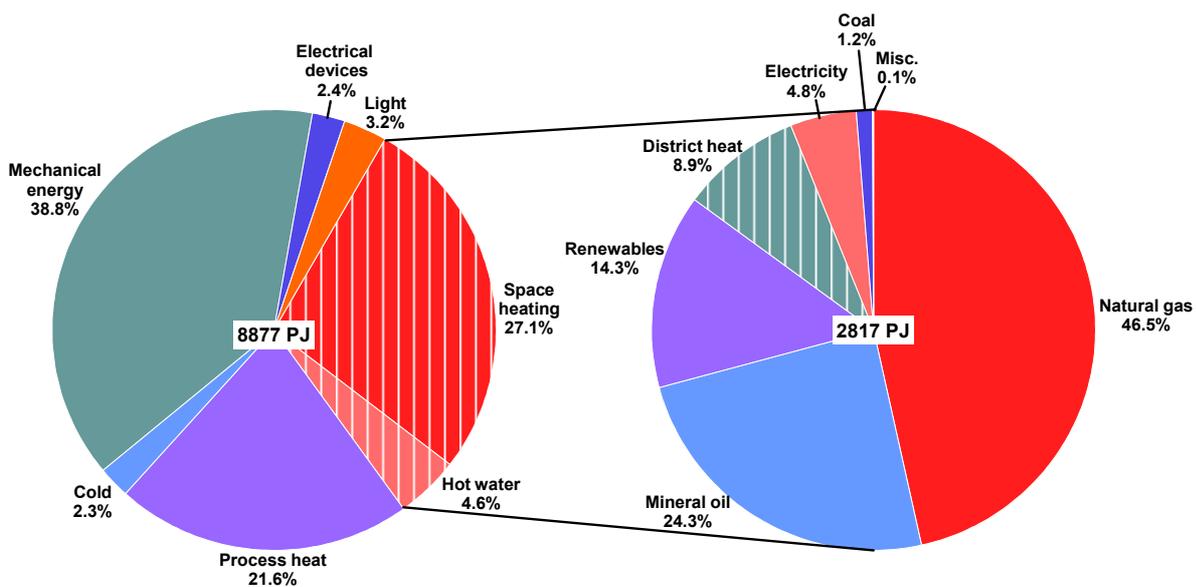
Figure 3: Final energy consumption in Germany 2015 (data source: AGEB (2016)).

DH is seen as an essential component in sustainable and decarbonized future energy systems (e.g. Lund et al. 2010; Connolly et al. 2014; Persson et al. 2014; Sass et al. 2015). It has several advantages compared to conventional decentralized heating options. A detailed list is for example given by Rezaie & Rosen (2012). Clear benefits for building owners and tenants are seen for example in reduced operation and maintenance costs and reduced space requirements. More importantly the overall fuel consumption is decreased due to the utilization of highly efficient combined heat and power (CHP) technology and thus, an abatement of GHG emissions can be achieved.

The application of DH is getting more and more attractive: an ever-growing portion of the world's population concentrates in urban settlements. According to the United Nations (UN 2014), today already 54% of mankind lives in urban areas. Until 2050, this number is expected to increase to 66%. In more developed regions, the ratio of urban to rural population is even higher. In Northern America, around 82% of the people already live in densely populated areas and about 69% of the Eastern Europeans (including Russians) and 80% of the Western and Northern Europeans live in urban agglomerations. Such populous areas are usually characterized by a high heat demand density (annual heat demand per unit area [TJ km^{-2}]) and are therefore particularly suitable for the implementation of DH grids.

In Germany, about 75% of the population lives in urban areas with an upward trend (UN 2014). Due to a lower average living area per capita in these areas, the heat consumption per capita is assumed to be around 10% lower than in rural areas (according to Kramer 2010). Taking this relation into account, still more than 70% of the final energy consumption for space and tap water heating can be apportioned to urban areas. This is in accordance with calculations given in Connolly et al. (2014), who calculated that approximately 70% of the heat demand in the EU27 are consumed in settlements with a heat demand density larger than 15 TJ km^{-2}. However, in Germany only about 9% of the final energy consumption for space heating and hot water supply is covered from DH (Figure 3). Provided that all DH systems are in urban areas, the share of DH in these areas lies at around 13%. Hence, there is still a huge potential for the expansion of DH systems in Germany. Certainly, there are some exceptions (e.g. Denmark) that already give more weight to DH, but comparable numbers to those from Germany can be expected for many other industrial countries.

However, future DH technologies face a couple of challenges that are associated with the transition of the current fossil fuel-based economy into a low-emission and sustainable energy system. On the one hand, the possible areas for DH are mostly situated in middle to high latitudes, where the heating demand shows a strong seasonality. On the other hand, a large amount of fluctuating renewable energy sources has to be integrated in future DH grids in order to decarbonize the heat production, while simultaneously guaranteeing the security of supply.

The concept of 4th generation DH (4GDH, Lund et al. 2014) describes, how future DH systems can cope with these tasks. The core of the concept comprises a significant reduction of grid temperatures. Supply temperatures are envisaged to be as low as 55 °C and return temperatures as low as 25 °C (Li & Svendsen 2012). Thereby, various advantages occur: first and foremost, lower grid temperatures lead to a significant reduction of heat losses and therefore to an improvement of the energy and exergy efficiency (Li & Svendsen 2012; Kauko et al. 2017). Moreover, lower grid temperatures increase the potential for exploiting low-carbon heat sources like geothermal energy or industrial waste heat, which are usually operated most efficiently when supplying low-temperature heat (e.g. Gadd & Werner 2014; Schmidt et al. 2017).
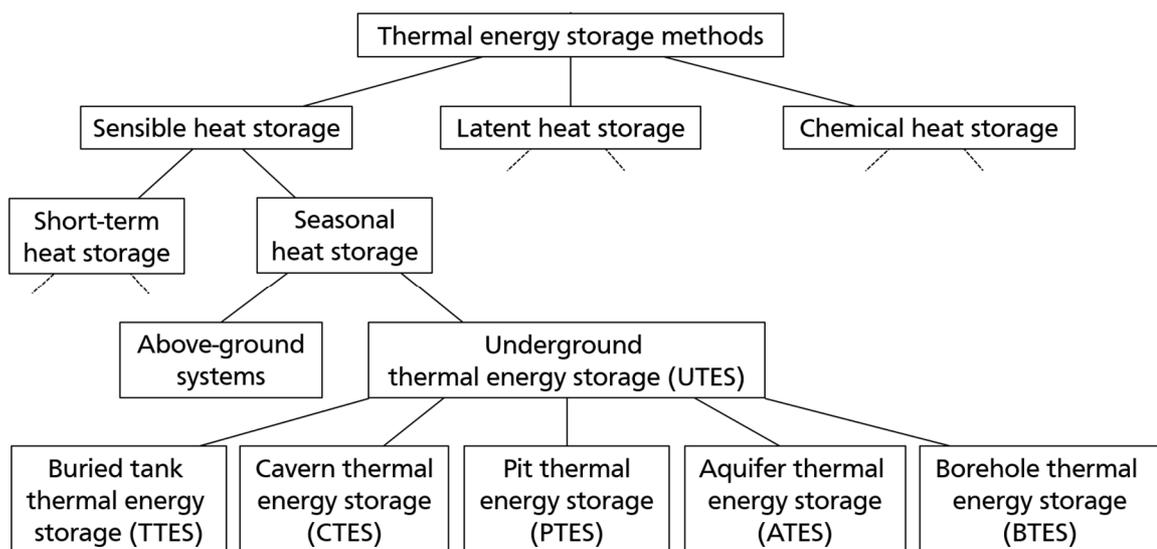
Figure 4: Categorization of thermal energy storage.

Another auspicious technology for substituting fossil heat sources in DH grids are large central solar heating plants (Schmidt et al. 2004; Bauer et al. 2010). However, solar energy is subject to seasonal fluctuations, which are contrary to the seasonal variation of the heat demand. In order to compensate the seasonal mismatch between supply and demand and thus to exploit the full potential of solar thermal energy, large-scale seasonal thermal energy storage (TES) systems are needed.

TES systems (Figure 4) in general can be subdivided by different aspects like the prevailing storage principle, the duration of a storage cycle, the placement of the storage system and the basic characteristic of the system. There are several seasonal TES technologies available (for an overview see for example Schmidt et al. 2004, Dincer & Rosen 2011, Pinel et al. 2011, Xu et al. 2014 and Hesaraki et al. 2015). However, their requirements are diametrically opposed: high storage capacities are desired, but the costs and the space required need to be minimized (Tian & Zhao 2013). With respect to heat storage on a district level, chemical and latent heat storage solutions are not competitive yet (Pinel et al. 2011). Only some sensible heat storage technologies meet the requirements for large-scale TES. These can be differentiated into large above-ground water tanks and underground heat storage (UTES) systems. UTES can be further categorized into buried water tanks, water or gravel-water pit TES systems (Kübler et al. 1997; Novo et al. 2010), cavern or aquifer storage (Thomsen & Overbye 2016; Lizana et al. 2017). As illustrated in Figure 5, the specific investment costs for such large scale sensible TES systems differ significantly depending on the storage technology as well as on the storage volume.
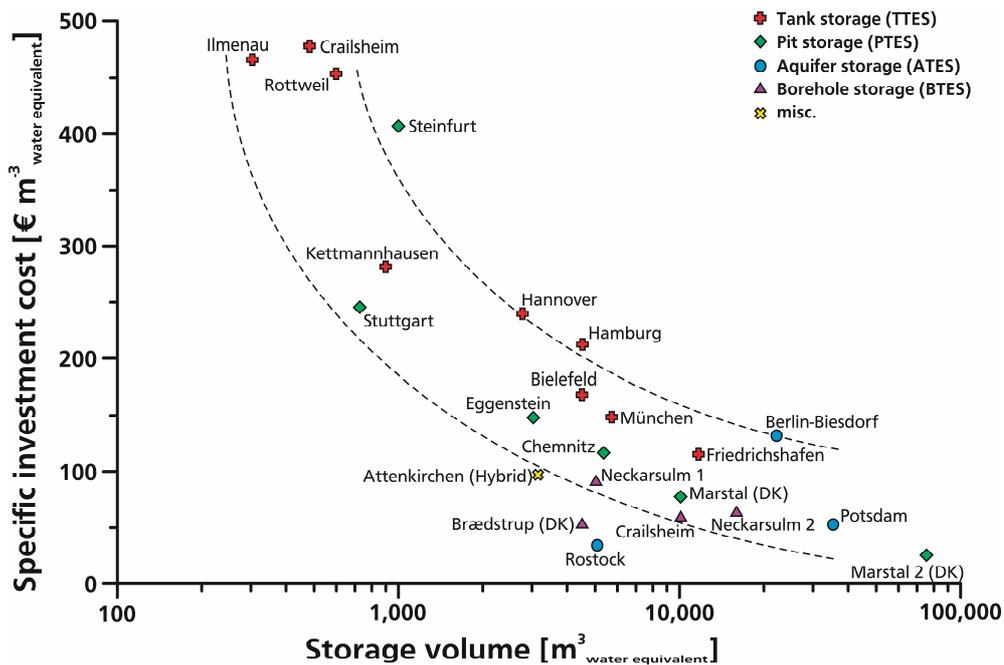
Figure 5: Specific cost of different seasonal TES systems as a function of their storage volume (after Mangold et al. 2012).

Another promising type of UTES are borehole thermal energy storage (BTES) systems (Givoni 1977; Hellström 1991; Nordell 1994; Reuss 2015; Gehlin 2016; Lizana et al. 2018). BTES usually utilizes the shallow subsurface up to a depth of 200 m as a heat storage medium via a borehole heat exchanger (BHE) array. A general technological overview of BTES systems is given in the following subchapter. Even though initial costs are very high for BTES systems, specific costs in relation to the storage capacity are relatively low compared to other storage

technologies (Schmidt et al. 2004; Tveit et al. 2009, see also Figure 5). The functionality of shallow BTES has already been demonstrated in several projects (e.g. Nordell 1988, 1990; Lundh & Dalenbäck 2008; Bauer et al. 2010; Sibbitt et al. 2012; Nordell et al. 2014; Rapantova et al. 2016). However, in most of the populated regions the shallow subsurface also comprises an important aquifer system often used for drinking water production. Thus, the operation of conventional BTES systems leads to a significant increase in groundwater temperature in the proximity of the BHE array. The magnitude of the impact on groundwater quality and microbiology is discussed controversially (see Chapter 1.2). Nevertheless, the protection of groundwater resources has a high priority. Accordingly, water authorities are encouraged (e.g. in UBA 2015) to follow restrictive permission policies for installing and operating such storage systems.

The herein presented novel concept of medium deep BTES (MD-BTES, Homuth et al. 2013; Bär et al. 2015; Schulte et al. 2015; Welsch et al. 2015; Bär et al. 2016; Schulte et al. 2016a; Schulte et al. 2016b; Schulte et al. 2016c; Welsch et al. 2016; Welsch et al. 2018), which aims for the employment of considerably deeper BHE arrays (up to 1000 m) for heat storage purposes, promises a reduction of the thermal impact on shallow aquifer systems and a much smaller surface area required. Furthermore, such systems could achieve higher supply temperatures and thereby higher efficiencies. Consequently, the utilization of MD-BTES would be more independent of the geological conditions and could lead to a more widespread application of seasonal heat storage. A detailed description of the concept of MD-BTES is given in Chapter 1.3.

1.1 Borehole Thermal Energy Storage

1.1.1 Differentiation and Definition

According to Sterner & Bauer (2017, translated from German) "an energy storage is a technological device for the storage of energy in the form of internal, potential or kinetic energy. An energy storage cycle comprises the three processes charging, storing and discharging. These processes are physically realized by the use of energy converters (charging/discharging), a storage unit and auxiliary devices. Accordingly, the whole device can be termed an energy storage system". Dincer & Rosen (2011) also define TES as "energy […] supplied to a storage system for removal and use at later time". They also emphasize that a storage process is made up by the three steps charging, storing and discharging.

However, there is no consistent definition for BTES systems in literature (Gehlin 2016). In fact, there are even some definitions that are not in line with the general definition for energy storage or TES as given above. Nordell (2000), for example, denotes all kinds of BHE applications as BTES systems. Even a single BHE for heat or cold extraction without any active recharge is termed a storage system.

In this thesis, the term BTES designates systems used for seasonal heat storage, consisting of multiple thermally interacting BHEs in a compact arrangement (Figure 6). The systems are charged actively and are discharged either with or without a heat pump (HP).

BTES belongs to the category of sensible heat storage. In such systems, excess heat is transferred to a storage medium, which thereby undergoes a temperature increase. The amount of stored heat Q_s is defined by the temperature difference ΔT, the density ρ, the specific heat capacity c and the volume V of the storage medium as given in Equation (1) (Dincer & Rosen 2011).

$$Q_s = \Delta T \cdot \rho \cdot c \cdot V \tag{1}$$

The heat is recovered by a reversion of the process. With regard to BTES systems the heat storage medium is basically rock or with increasing rock porosities also groundwater. Due to their high storage capacities and relatively low charging/discharging rates, BTES systems are best suited for seasonal heat storage.
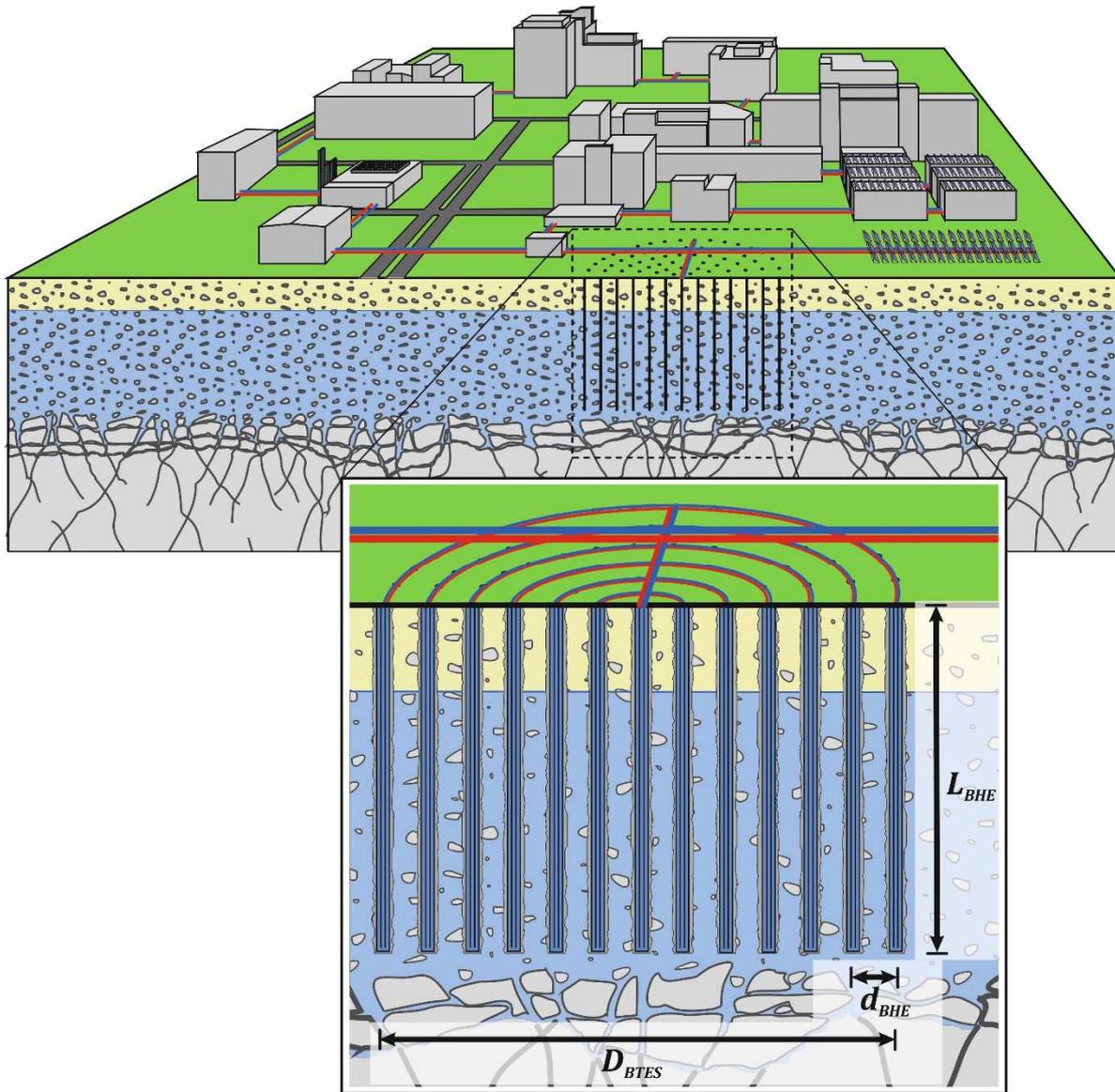
Figure 6: Schematic figure of a conventional, shallow BTES system in a local DH system.

1.1.2 Technical Description

As mentioned above, BTES systems consist of several BHEs that make up a BHE array. The geometry of a BTES system (Figure 6) is basically defined by the length of the BHEs (L_{BHE}), the BHE spacing (d_{BHE}), the number of BHEs as well as their positioning, which specifies the shape of the array. The array itself can be further specified by for example its diameter (D_{BTES}) in a circular arrangement or the edge lengths in a rectangular arrangement of the BHEs.

BHEs are vertical boreholes, equipped with a closed-loop pipe system. Commonly used types of pipe systems in shallow BHEs (see Figure 7) are U-pipes and double-U-pipes. With increasing depth of the BHEs, the market share of coaxial pipes increases. This has to do with the increased

robustness of such pipe configurations. Furthermore, the outer standpipe and the centered inner pipe can be mounted separately. Pipes in high-temperature storage systems must withstand fluid temperatures of up to 90 °C or even more. Therefore, as outer standpipe a steel casing is envisaged whereas the inner pipe should insure both, a high temperature resistance as well as a low thermal conductivity to reduce thermal short-circuiting. A composite pipe made up of a steel pipe coated with a polyethylene pipe could accomplish both requirements (Handke et al. 2015). The boreholes are usually backfilled with a cement-based grout material, which has the purpose to seal the borehole and to insure a good thermal connection between the pipes and surrounding geologic formation (exceptions are for example known from Sweden, where the pipe system is often placed in the water filled borehole, Andersson et al. 2013). A heat transfer medium (usually water or a monoethyleneglycol-water mixture) is circulated through the pipe system. The thermal gradient, which develops between the heat transfer medium and the surrounding subsurface, results in a heat flow between the fluid and the adjacent rock formation via conductive heat transport through the pipe and backfill material. Depending on the direction of the thermal gradient the heat transfer medium is either heated up or cooled down on its way through the BHE and the surrounding subsurface is cooled down or heated up, conversely.
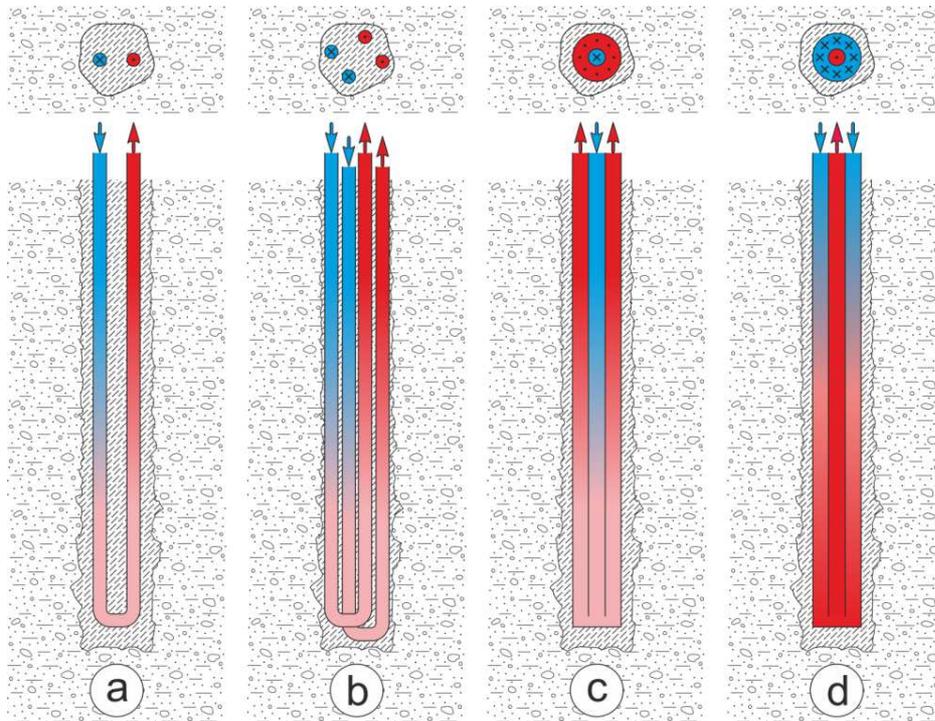
Figure 7: Types of borehole heat exchangers: a) U-Pipe, b) Double-U-Pipe, c) Coaxial BHE with centered inlet (CXC) and d) Coaxial BHE with annular inlet (CXA) (graphic by Sass and Mielke 2012 from Sass et al. 2016).

The seasonal operation of a BTES system is depicted in Figure 9 by the very simplified example of monthly constant heat rate conditions. During summertime (Figure 8a), excess heat, for example from solar thermal sources, industrial processes or power plants, is used to heat up a heat transfer fluid, which returns from the BTES system. The temperature increase ΔT can be calculated from the heat rate P, which describes, how much heat per time is exchanged with the fluid (Equation (2)).

$$\Delta T(t) = (T_{in}(t) - T_{out}(t)) = \frac{P(t)}{\rho_f \cdot c_f \cdot \dot{V}_f} \tag{2}$$

Where T_{out} is the temperature of the fluid returning from the BTES system, T_{in} is the temperature of the fluid going back to the storage system, $\dot{V}_f$ is the volume flow rate through the BHE array, ρ_f is the density and c_f the specific heat capacity of the fluid. Of course, ρ_f and c_f are both temperature dependent material parameters. However, for reasons of simplification they can be assumed to be constant over the considered temperature range. After the heating process, the fluid is split up again and recirculated through the different BHEs in parallel.

On its way through the BHE pipes, the fluid releases heat to the relatively colder subsurface. This is accompanied by a decrease in the fluid temperature. The circumjacent rock formation serves as sensible heat storage medium that is heated up continuously.

A heat plume develops in the subsurface, which is characterized by an elevated subsurface temperature (e.g. Mielke et al. 2014; Welsch et al. 2016). The temperature increase is highest around the BHEs and converges to the undisturbed subsurface temperature with increasing distance to the BTES system (e.g. Boockmeyer & Bauer 2016). Applying an average increase in the temperature $\Delta \bar{T}_r$ for the whole affected rock volume V_r, the total heat Q_S stored during the entire charging cycle can be expressed as Equation (3) by adapting Equation (1).

$$Q_S = \Delta \bar{T}_r \cdot \rho_r \cdot c_r \cdot V_r \tag{3}$$

By integrating the heat rate over a complete charging cycle, Q_S can be calculated according to Equation (4) (e.g. Dincer & Rosen 2011; Welsch et al. 2016).

$$Q_S = \int_{t_{S,0}}^{t_{S,end}} P(t)dt \tag{4}$$

During winter operation (Figure 8b), heat is extracted from the fluid in the BTES circuit with the heat rate P and transferred to a heating circuit or DH grid usually via a heat exchanger or an HP, in order to provide space heating and possibly tap water heating. Consequently, the BTES fluid temperature is reduced by ΔT according to Equation (2). The cooled down fluid is recirculated to the BHEs. Heat is transferred from the relatively warmer subsurface to the fluid. That in turn increases the fluid temperature and decreases the temperature of the storage formation – the storage system is discharged. By integrating the heat rate P over the whole discharging period, the total heat amount extracted from the storage Q_E can be calculated after Equation (5) (Dincer & Rosen 2011; Welsch et al. 2016).

$$Q_E = \int_{t_{E,0}}^{t_{E,end}} P(t)dt \tag{5}$$

The temperature of the fluid that returns from the BTES system (T_{out}) is a function of T_{in}, the volume flow rate $\dot{V}_f$ as well as the heat exchange rate with the subsurface P_{ground}. P_{ground} depends on the temperature in the storage formation and the mean fluid temperature $\bar{T}_f$ which can be calculated after Equation (6).

$$\bar{T}_f = \frac{T_{in} + T_{out}}{2} \tag{6}$$

Furthermore, T_{in} is linked to T_{out} by the heat rate P. According to the first law of thermodynamics, P and P_{ground} must be equal. Consequently, assuming a constant P and a constant $\dot{V}_f$, $\bar{T}_f$ must increase or decrease until the heat transport processes in the ground are in equilibrium.

By implication, this means that the charging or discharging heat rate P is restricted by the limits that are given for the fluid temperatures owing to material limits, etc.

a)

Flow of warm / cold fluid   Heat losses / gains

b)
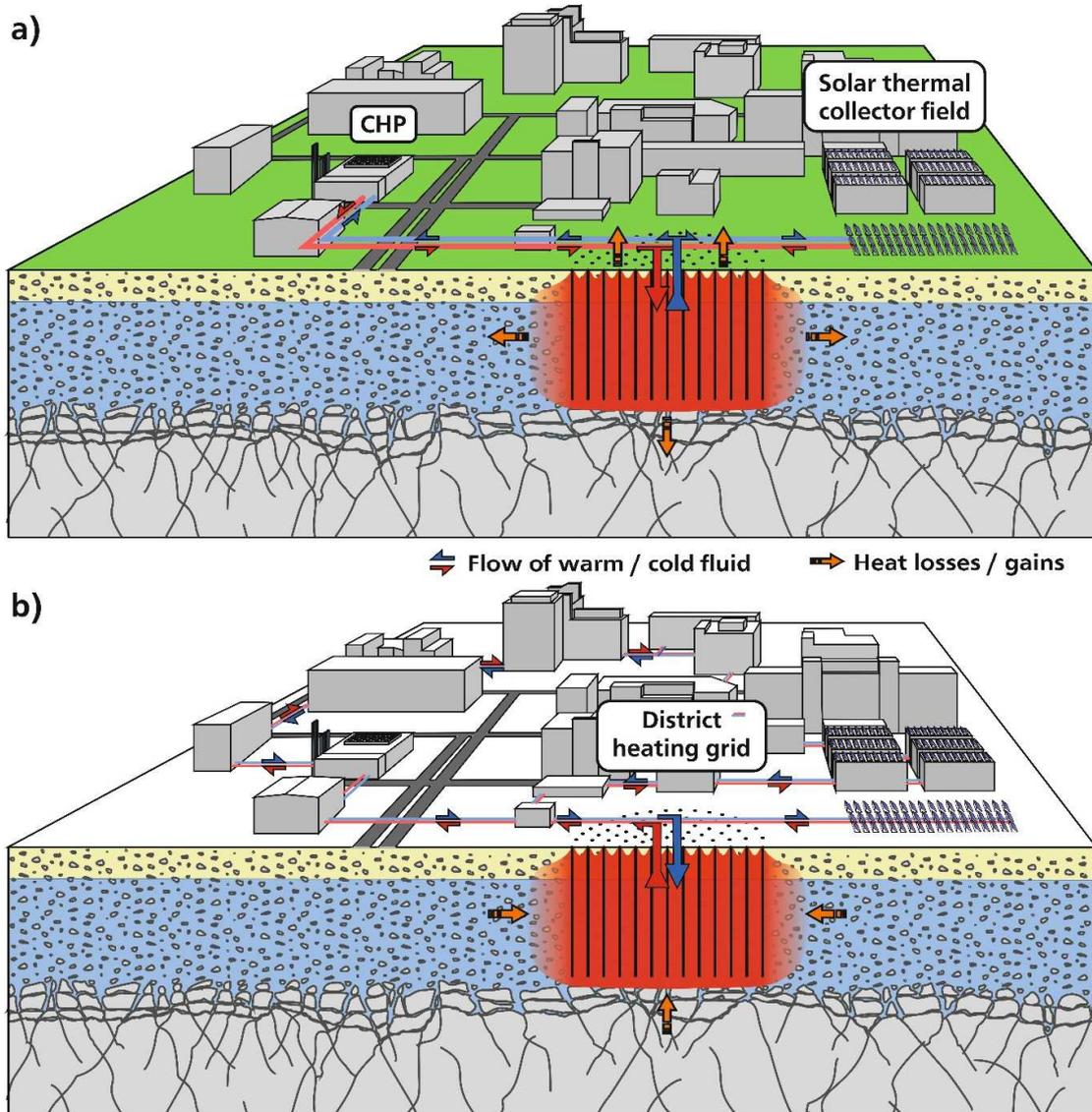
Figure 8: Schematic illustration of (a) summer and (b) winter operation of an exemplary BTES system.

Conduction is the prevailing heat transport process in the pipe walls, the grout and the storage formation. Hence, BTES is a rather inert storage technology that allows only for relatively low charging or discharging heat rates in the given temperature limits. Real storage operation is much more transient than depicted in the example above (Figure 9). Fluctuations in the heat demand as well as the intermittent nature of solar radiation or industrial processes lead to fluctuating heat rates with distinctive peaks that have to be transferred to or from the storage. To attenuate this fluctuations, BTES systems are usually coupled to one or more diurnal heat storage water tanks that are characterized by much higher charging or discharging rates and that are used to distribute the peaks to a larger time span, reducing the heat rates for the BTES system.
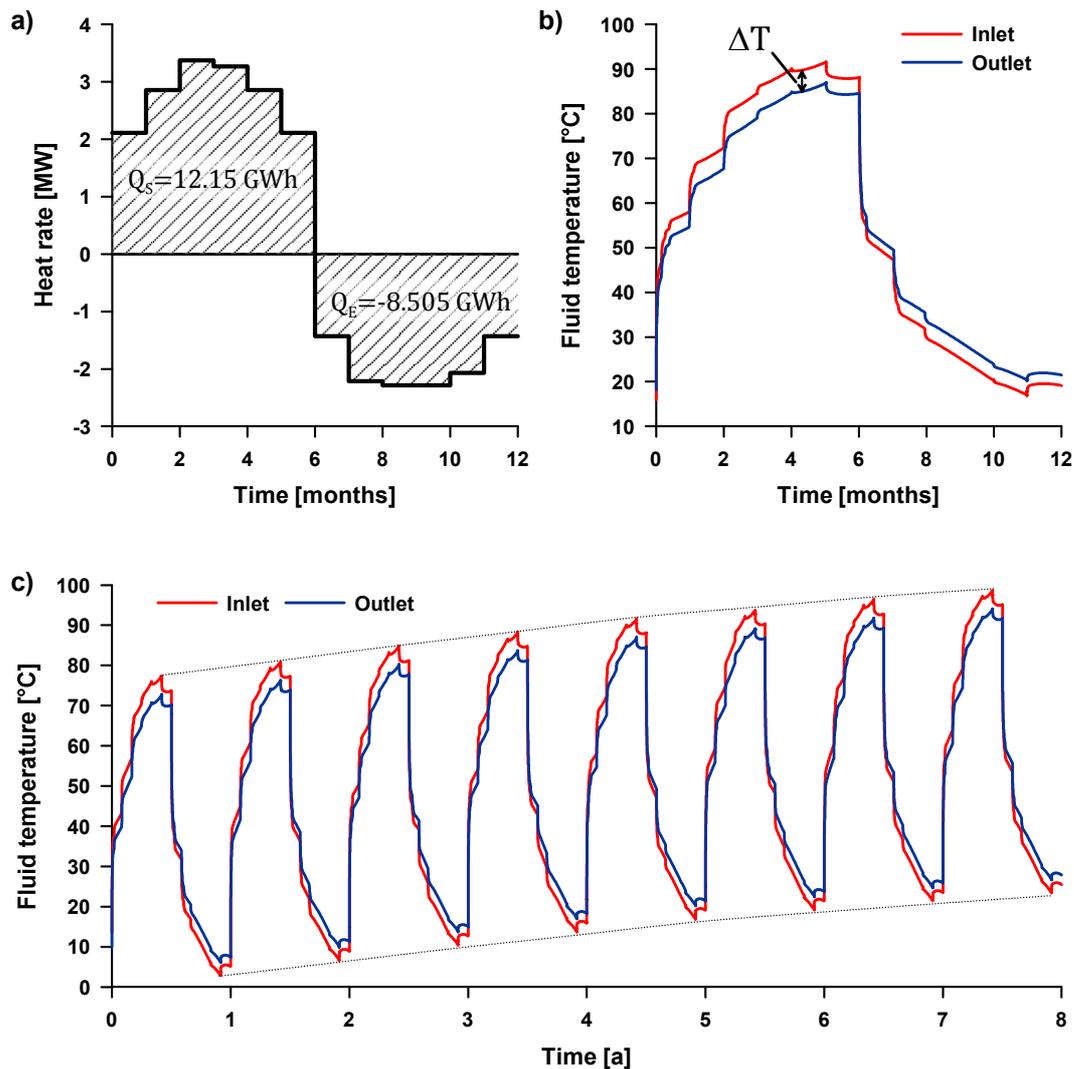
Figure 9: a) Default heat rate and the corresponding calculated fluid temperatures during b) the seventh year of operation and c) the complete simulated time span of eight years of a simplified MD-BTES system operation (37 BHEs with a length of 500 m and a spacing of 5 m). The hatched areas represent the total heat stored (Q_S) and the total heat extracted (Q_E) during the regarded time span.

Like any other sensible heat storage technology, BTES systems are subject to heat losses due to the dissipation of heat to the environment. They are, unlike for example a tank storage system, usually not insulated against the environment except for the ground surface at the top. Moreover, BTES systems do not contain any further system boundaries that allow for a spatial delimitation of the storage volume. It is solely defined by the range of the heat plume that develops in the ground. Whether a certain part of the stored heat is recovered during winter operation or not, depends to a large extend on the temperature gradient between the rock formation and the fluid in the BHEs (Boockmeyer & Bauer 2016). This temperature gradient in turn is basically determined by the discharging fluid temperature. Moreover, provided that the temperature gradient is large enough, the missing system boundaries also allow for a flow of natural geothermal heat from the surrounding rock formations into the storage region. Consequently, the transition from a BTES system to a usual BHE array for heat extraction is gradual and only defined by the system operation. By implication, a BTES could also be operated in an

unbalanced manner with more heat discharged than charged before, leading to storage efficiencies of more than 100%. This characteristic can be beneficial, as natural variations in the heat supply or demand can be compensated for to some extent. However, higher extraction rates entail lower supply temperatures to the heating system or the HP, impairing their efficiency.

The ratio of the absolute values of extracted and stored heat η (Equation (7)), commonly named the storage efficiency, is often used to evaluate the storage system's performance.

$$\eta = \left| \frac{Q_E}{Q_S} \right| \tag{7}$$

However, as the heat amounts Q_S and Q_E are predetermined by the operation of the system, η is only meaningful when the development of fluid temperatures as a consequence of a certain operation scheme are also taken into account. To illustrate that η is a control quantity, it should rather be named the storage utilization ratio.

1.1.3 History

The idea of using the ground as heat storage by shallow BHEs goes back to the 1970s/1980s (Givoni 1977; Andersson & Eriksson 1981; Beckmann & Gilli 1984). In the 1980s and early 1990s intensive research activities on shallow BTES were accomplished, particularly in Sweden and Finland: a first large-scale experimental and demonstration example was built in 1982/83 at Luleå University of Technology, Sweden, consisting of 120 BHEs with a length of 65 m each (Nordell 1987, 1990). Furthermore, the first numerical simulation models for BTES systems were developed (e.g. Lund & Östman 1985; Hellström 1989). Lund & Östman (1985) created a three-dimensional numerical model for BTES, which already accounted for convective heat flow in the storage region. They studied the behavior of different BTES models in conjunction with variable dimensioning factors of a solar DH system. Four different storage volumes were analyzed, which all had a cubic geometry and a uniform BHE spacing. The deepest system they considered had a BHE length of 75 m. They also examined the influence of groundwater flow on the storage behavior by simulating four different hydrogeological conditions. Nordell (1994) developed a model for the design optimization of shallow BTES, which also took into account economic aspects. He analyzed sensitivities of different design and operational parameters as well as cost data on the optimum design of a storage system.

Today, there are numerous BTES systems in operation. Table 1 gives a summary of systems reported in literature. However, especially in the Nordic countries, the number of existing BTES systems, which are not reported in literature is significant. Andersson et al. (2013) estimate the number of BTES in operation only in Sweden to approximately 400.

Table 1: Examples for present BTES systems (adapted from Gehlin 2016, slightly modified).

Country	City	System type	Year	Number of boreholes x borehole depth, further specifications	Heat/cold	References
Canada	Oshawa, Ontario	University campus	2004	384 x 213 m, limestone	Heat/cold	Dincer & Rosen (2007), Wong et al. (2006)
Canada	Okotoks, Drake Landing Solar Community	Residential	2007	144 x 35 m	Solar heat, high temp	Sibbitt et al. (2012), Wong et al. (2006)

Country	City	System type	Year	Number of boreholes x borehole depth, further specifications	Heat/cold	References
China	Tianjin	Business center	2011	3789 x 120 m	Heat/cold + ice storage	Yin et al. (2015)
China	China Academy of Building Research, Beijing	Office building, net zero energy	2014	20 x 100 m + 50 x 60 m	Solar + heat/cold	Yu et al. (2015), Li et al. (2015)
China	Zhungguancon International Center, Beijing	Office building	2008	1060 x 123 m	Heat/cold	Zhang & Xu (2014)
Denmark	Brædstrup	District heating	2012	48 x 45 m	Solar heat and district heating	Miedaner et al. (2015)
Finland	Sibbo	Logistics center	2012	150 x 300 m +159 in phase 2, rock	Heat/cold	Huusko & Valpola (2014)
Germany	Neckarsulm Solar district heating	Residential	1997 + 2001	528 x 30 m, clay	Solar district heating	Reuss (2015), Bauer et al. (2010), Bauer et al. (2013a)
Germany	Attenkirchen	Residential	2002	90 x 30 m	Hybrid solar district heating with central tank	Reuss et al. (2006)
Germany	Crailsheim	Residential + school	2007	80 x 55 m	Solar	Mangold (2007), Bauer et al. (2013a), Bauer et al. (2016)
Norway	Akershus	Hospital	2007	228 x 200 m, rock	Heat/cold	Midttømme et al. (2010), Bäcklund (2009)
Poland	Atrium 1	Office building	2014	50 x 200 m	Heat/cold without heat pump	
Romania	Bucharest	VW Bucharest Auto Showroom	2009	112 x 72 m	Heat/cold	Polizu & Hanganu-Cucu (2011)
Romania	Bucharest-Marguele	ELI-NP research center	2015	1080 x 125 m	Heat/cold	Bendea et al. (2015)
South Korea	Lotte World Tower, Seoul	Skyscraper	2015	720 x 200 m	Heat/cold	Viessmann (2012)
Sweden	Karlstad	Karlstad University campus	2015	204 x 240—250 m	Heat/cold	Olsson (2014), Gehlin et al. (2015)
Sweden	Entré, Lindhagen	Office building	2014	144 x 220 m	Heat/cold, without heat pump	Skanska AB (2018)
Sweden	Näsbypark	Historical building	2004	48 x 180 m	Heat/cold, recharge with lake water heat	Lund et al. (2004)
Sweden	Luleå	University building	1981 - 1989	120 x 60 m	Industrial high temp	Nordell (1994)
Sweden	Anneberg	Residential	2002	99 x 65 m	Solar high temp	Dalenbäck et al. (2000), Lundh & Dalenbäck (2008),

Country	City	System type	Year	Number of boreholes x borehole depth, further specifications	Heat/cold	References
						Nordell & Hellström (2000), Heier et al. (2011)
Sweden	Lund University	Astronomy House	2001	20 x 200 m, clayey soil and shale	Heat/cold	Andersson (2007)
Sweden	Emmaboda, Xy-lem	Industrial waste heat	2011	140 x 150 m, rock	Industrial high temp	Nordell et al. (2016)
Switzer-land	Därlingen, SERSO	Road heating	1994	91 x 65 m, rock	Heat from road	Eugster (2002), Eugster (2007)
United Kingdom	Croydon	Office and warehouse	2000	30 x 100 m, chalk	Heat/cold	Witte & Van Gelder (2007)
United Kingdom	DMU Leicester	Hugh Aston University building	2009	56 x 100 m	Heat/cold	Naiker & Rees (2011), Cullin et al. (2015)
United States	Richard Stockton College, Po-mona, New Jer-sey	Campus build-ings	1994	400 x 135 m, Sand/clay	Heat/cold	Stiles (1998)
United States	Oakland Univer-sity, Rochester, Michigan	Human Health building	2013	256 x 100 m	Heat/cold	Kistler & Karidis (2015)
United States	Ball State Uni-versity, Muncie, lndiana	University Campus	2013	1800 x 140—150 m + 1800 in phase 2	Heat/cold	Ball State University (2018)

1.2   Thermal Impact on Groundwater

All geothermal installations cause an increase or decrease of the subsurface temperature dependent on the heat amount exchanged with the subsurface and the delivery/removal of heat through the circumjacent geologic formations. Due to their usually high turnover of heat, seasonal TES systems are subject to considerable temperature differences of several tens degrees C between the charging and discharging periods. As BTES systems are not thermally insulated against the surrounding rock formations, heat losses occur, which cause a positive temperature anomaly around such storage systems. Accordingly, there are two different thermal cycles that have to be taken into consideration when referring to the thermal impact of heat storage on groundwater bodies: a relatively local but strong periodic change of groundwater temperature and a minor increase in the mean groundwater temperature. While the first one can be seen as a more or less reversing process, which cancels out on average, the irreversible heat loss process causes a persistent and cumulative temperature increase. The resulting heat aggregation can be displaced with flowing groundwater, resulting in a typical temperature plume in the direction of groundwater movement. The charging temperature of the storage represents the upper temperature limit. When storing heat from solar thermal collectors (STC) at a temperature of 90°C, groundwater temperatures of up to 80°C or even more are likely to occur in close proximity of conventional BTES systems. However, diffusion and mechanical dispersion cause a decrease of the temperatures with increasing distance to the storage system, mitigating the thermal impact to an insignificant limit in a certain distance. This distance usually lies in the range of several meters to some hundreds of meters, basically depending on the groundwater velocity and the time of operation.

It has been demonstrated in several studies that increasing groundwater temperatures can have various effects on the subsurface, which to some extend can also interact and interfere with each other. The following passages give only a partial overview on possible alterations. A broad overview on the topic can be found in UBA (2015), for example.

Increasing temperatures effect several geochemical reactions in the subsurface, leading to a change in the chemical constitution of the groundwater. This includes an increase in the carbonate saturation (e.g. Griffioen & Appelo 1993; Stumm & Morgan 1996) and an increased mobility of toxic substances like arsenic (Bonte et al. 2013b). Moreover, a temperature rise can lower the pH-value and oxygen concentrations (e.g. Brielmann et al. 2011; Jesußek et al. 2013) and increase the amount of dissolved organic carbon (DOC) by desorption and an increased mineralization of soil organic matter (Brons et al. 1991; Bonte et al. 2013b; Jesußek et al. 2013). Higher concentrations of DOC may necessitate an additional water treatment due to discoloration of the ground water (Bonte et al. 2013a; Bonte 2015). Desorption of organic carbon from the sediments can be accompanied by a release of organic pollutants into the groundwater (ten Hulscher & Cornelissen 1996; Jesußek et al. 2013). Additionally, the mineralization of soil organic matter can reduce the contaminant buffering capacity of the aquifer (Bonte et al. 2013a; Bonte 2015).

Apart from these hydrochemical effects, an increasing temperature can also cause considerable alterations in the microbial community composition (Brielmann et al. 2011; Bonte et al. 2013a) and abundance (Lienen et al. 2017). In particular, when there are increased concentrations of DOC and nutrients in combination with low oxygen concentrations, and especially in organically polluted aquifers, a temperature increase can cause massive alterations of the microbial species community and potentially encourage the reproduction of pathogenic micro-organisms (Brielmann et al. 2011).

The enhanced concentration of DOC as an electron donator together with microbial changes cause a shift in the redox conditions from iron reduction to sulfate reduction with increasing temperatures (Bonte et al. 2013a; Jesußek et al. 2013; Lienen et al. 2017). This in turn could have negative but in some cases also positive effects on the biodegradation potential of organic pollutants in the groundwater (Bonte et al. 2013a). Furthermore, the lowering of the redox potential might lead to a release of heavy metals from iron(III) oxides (Jesußek et al. 2013).

Negative effects on the groundwater quality must not necessarily be limited to the bounds of the thermal impact: an alteration of the chemical or biological composition of the groundwater, caused within the heat plume, might not regress to the initial state and linger on even outside the boundaries of the plume. On the contrary, the thermally induced alteration of the groundwater composition with its potentially negative impact on the groundwater quality is not necessarily tantamount to an impairment of drinking water quality: depending on the storage location, a potential contamination might never reach a drinking water production site in human time scales.

However, it is essential to minimize the thermal impact on shallow groundwater aquifers. This is the main reason for developing the new concept of MD-BTES, which is described in the following chapter.

1.3   The Concept of Medium Deep Borehole Thermal Energy Storage Systems

Conventional, shallow BTES systems are usually not deeper than 200 m (Table 1). In contrast, the new concept of MD-BTES intends to utilize the deeper subsurface as a heat storage reservoir up to a depth of 1000 m or even more. Systems with a comparable capacity would consist of fewer but appreciably deeper BHEs than their shallow counterparts (cf. Figure 10 against Figure 6). Thereby, the majority of the heat input into the subsurface could be shifted to deeper rock units, significantly diminishing the thermal impact on vulnerable shallow aquifer systems. A potential thermal insulation of the BHEs' topmost section (Appendix A) could amplify this protective effect.
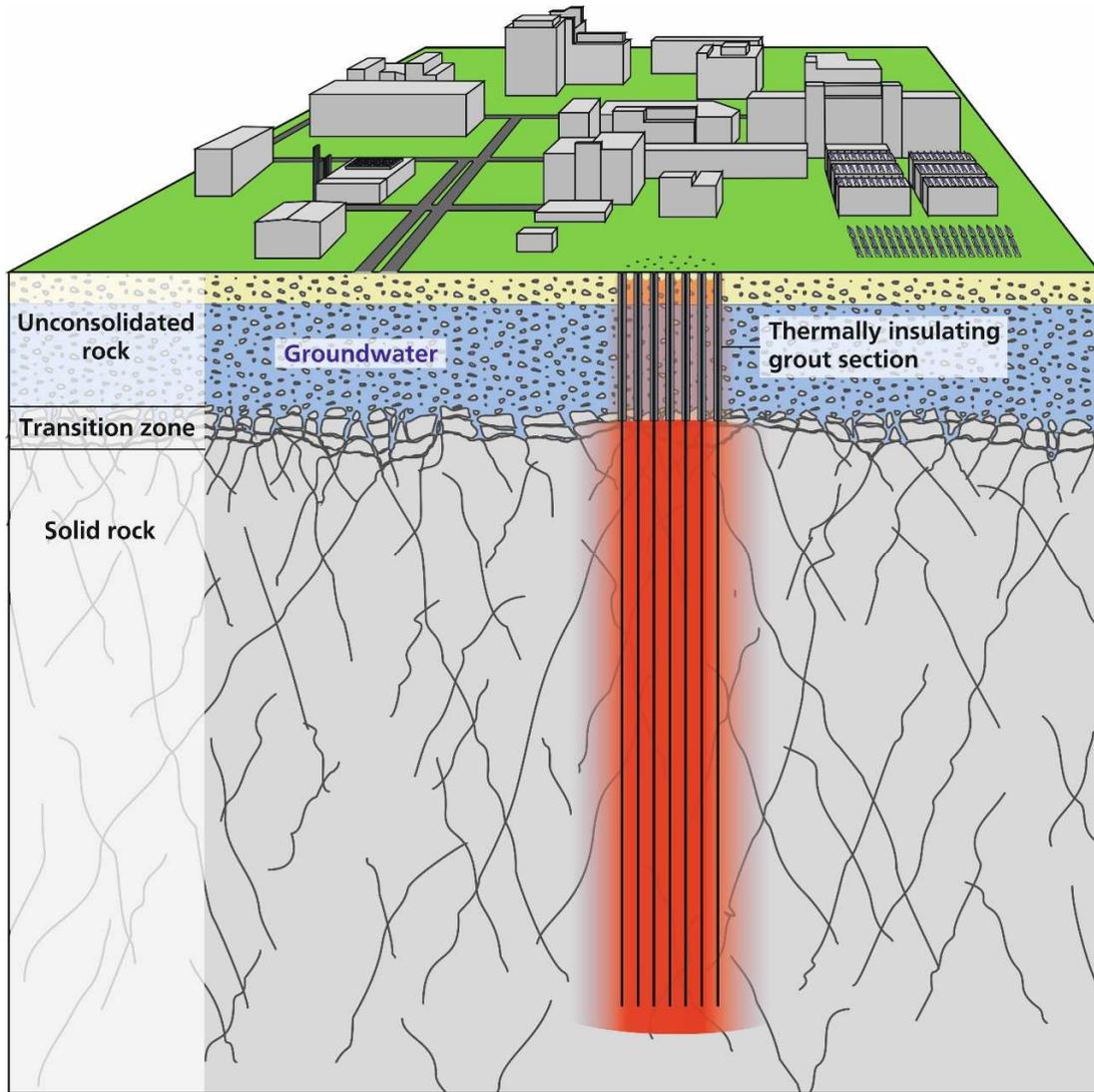
Figure 10: Schematic figure of an MD-BTES system.

A further advantage of MD-BTES originates from the increase of the undisturbed subsurface temperature with depth: assuming equal storage temperatures, the lateral temperature gradient decreases with depth, resulting in lower heat losses to the circumjacent rocks in deeper formations. This effect should at least partially compensate the loss of performance that goes along with the worse surface-area-to-volume ratio (SA/V-ratio) due to the elongated cylinder shape of an MD-BTES compared to the more compact cylinder shape of a shallow system with equal capacities.

Both the reduced thermal impact on shallow formations as well as the higher average natural subsurface temperature qualify MD-BTES systems for storing heat at high temperature levels of 90 °C or even more (Appendix A). This has a number of advantages compared to low-temperature energy storage: higher charging temperatures in the summer season result in higher discharging temperatures during the heating period in winter. Consequently, the coefficient of performance (*COP*) of a HP potentially increases and a higher exergy efficiency of the heating system can be achieved (Kizilkan & Dincer 2015). Low-temperature heating systems, which are characterized by supply temperatures of 25 to 35 °C, could even be supplied directly without the use of any HP (Reuss et al. 1997).

In addition to the aforementioned advantages, MD-BTES systems require less space at the surface. This is especially favorable in densely populated urban areas, where building plots are rare and expensive.

However, both their widely differing dimensions as well as their potential operation at higher temperature levels inevitably lead to a different behavior of MD-BTES systems compared to shallow ones. Hence, the results of former studies are not generally transferable to MD-BTES. As the concept has not been put into practice so far, there is no experience in operating an MD-BTES system. Consequently, numerical simulations are necessary to predict their performance and to estimate the influence of key parameters such as the dimensions of the storage system (e.g. the BHE length, the number of BHEs, the spacing between the boreholes), operational parameters like the fluid inlet temperature or thermal underground properties. Moreover, there are some measures that could further improve the performance of a BTES system. These include a thermal insulation at the top ground surface, a series connection of the BHEs and a reversal of the flow through coaxial BHEs. Several numerical simulations were carried out to address these issues. Chapter 3 gives an overview.

A certain contribution to groundwater protection as a consequence of the differing storage geometry of MD-BTES systems is indisputable. Yet, the magnitude of this effect is unknown, in particular, when a thermal insulation of the uppermost BHE sections is incorporated. For this reason, the available analytical BHE solution after Eskilson & Claesson (1988) has been refined so that a thermal insulation of BHE sections can be taken into account. Moreover, the improved analytical solution has been implemented into a numerical simulator. Chapter 4 summarizes a numerical simulation study, which was carried out in order to quantify the reduction of the thermal impact on shallow groundwater systems by MD-BTES. In addition, the effects of a thermal insulation of the uppermost BHE sections were investigated.

Further issues concern the economic and environmental implications integrating an MD-BTES system into DH networks. Evidently, resources and energy are spent for the production and implementation of any BTES system. Also, all BTES suffer from energy losses during operation. Both result in monetary costs and GHG emissions. However, financial and environmental effects of integrating MD-BTES systems to DH concepts have not been addressed so far. Thus, a dedicated economic and environmental life cycle analysis of DH concepts integrating BTES is part of this thesis. Therefore a *MATLAB* (The MathWorks Inc. 2016b) tool was developed (Chapter 1), which deploys a life cycle approach to assess the economic and environmental effects of such systems. Several BTES-assisted heat generation plant options for DH systems, including gas-fired boilers (GB), CHP, STCs and an HP were assessed with respect to their cost and their global warming potential (*GWP*), and compared against reference heat generation scenarios without seasonal heat storage (Chapter 6).

2 Methods

2.1 Numerical Simulation of Borehole Thermal Energy Storage Systems

BTES systems are complex energy systems. Their operational behavior and performance depend on many variables and boundary conditions and are therefore difficult to predict. Particularly with regard to MD-BTES systems, there are no real operating data or experience available that can be used as reference for upcoming projects, as such system types have not been put into practice so far. Numerical simulation is a well-established and imperative method to predict the behavior and optimize the performance of BTES systems. Therefore, it plays an important role in this dissertation to find answers to many of the emerging questions concerning MD-BTES. A summary of some popular numerical methods for BHE simulation is for example given by Yang et al. (2010). There are also some specialized approaches for the inspection of multi-BHE systems (i.e. BHE arrays and BTES systems) as for example introduced by Lazzarotto (2014).

One commercial simulation tool, which was standardly applied in the course of this dissertation, is *FEFLOW – Finite-Element Simulation System for Subsurface Flow and Transport Processes* (version 6.2, DHI-WASY 2014). *FEFLOW* is a powerful simulator for flow, mass and heat transport in porous and fractured media. The governing Equations are solved by a multi-dimensional finite element method (FEM). A profound introduction to the basics of the FEM is given for example by Zienkiewicz et al. (2013). *FEFLOW* allows for the consideration of complex geometries as well as some demanding problems like variable fluid density, variable saturation, unconfined aquifers, multispecies reaction kinetics, non-isothermal flow and multi-diffusive (thermohaline) effects (Diersch 2014).

More importantly, one of *FEFLOW's* standard features is the simulation of BHEs in a dual-continuum approach: while groundwater flow and heat transport processes in the subsurface are solved in the finite element (FE) mesh, the heat transport processes in a BHE are computed on the basis of simplified numerical (Al-Khoury et al. 2005; Al-Khoury & Bonnier 2006) or analytical (Eskilson & Claesson 1988) solutions, which are coupled to the FE mesh as one-dimensional representations (Bauer 2011; Diersch et al. 2011a). Compared to a fully discretized BHE model, the dual-continuum approach is much less expensive in terms of computational effort (see also Chapter 4.1).

Nevertheless, *FEFLOW* has also some crucial drawbacks, when it comes to the mathematical optimization of BTES systems (Chapter 2.2): a design optimization necessitates an adaption of the model's mesh geometry. Certainly, *FEFLOW* allows for the generation of highly sophisticated mesh geometries. However, the mesh generation has to be done manually, which is time-consuming and makes it unsuitable for an automated optimization. Furthermore, *FEFLOW* does not include any algorithm for the optimization of BHE systems.

For this reason, the *Borehole Heat Exchanger Array Simulation Tool – BASIMO –* has been developed (Appendix D). It is an FEM based program especially tailored to the simulation of BTES systems. A comprehensive description of the tool is given by Schulte (2016). It is programmed in *MATLAB* (The MathWorks Inc. 2016b). Accordingly, it can be easily coupled to the *MATLAB Global Optimization Toolbox* (The MathWorks Inc. 2016a), which includes a variety of user-friendly optimization algorithms (Schulte 2016). Moreover, it includes an automated mesh generation, which renders a mathematical optimization of the BTES geometry possible.

2.2 Optimization of Borehole Thermal Energy Storage Systems

Optimization plays an important role when regarding all types of energy systems. With respect to MD-BTES systems, numerous optimization issues arise, which are a matter of where the system boundaries are drawn. The following list is not intended to be exhaustive:

- BHE types, materials and geometries
- Working fluid
- BTES design (i.e. arrangement of BHEs, BHE length, number of BHEs and spacing)
- Operational parameters (e.g. flow rate, fluid temperatures)
- System combinations
- Design of the overall system including e.g. heat generation technologies, DH grid, HPs, consumers etc.

The term optimization is often misused to describe any improvement of a process, system or product compared to an initial state (Schellong 2016). From a mathematical point of view, optimization means to identify the optimal solution of an objective function (Pieper 2017), i.e. all other possible solutions within the parameter space are worse with respect to the resulting objective function value. Consequently, it describes the search for the best possible solution instead of achieving just an improvement. An objective function can for instance be a simple analytic function but it can also be the response of a numerical model on different input variables (Schulte 2016).

Mathematical optimization can be divided into several sub-disciplines. A distinction can for example be made between continuous and discrete problems depending on the nature of the input variables.

A standard constrained continuous optimization problem has the form as given in Equation (8).

$$
\begin{aligned}
\min_{x \in \mathbb{R}^n} \quad & f(x_i), && i = 1, \dots, n \in \mathbb{N} \\
\text{subject to} \quad & g_j(x_i) \leq 0, && j = 1, \dots, m \in \mathbb{N} \\
& h_k(x_i) = 0, && k = 1, \dots, p \in \mathbb{N} \\
& b_{l,i} \leq x_i \leq b_{u,i}
\end{aligned}
\tag{8}
$$

Where f is the objective function that has to be minimized and x are the input variables of f with the upper and lower bounds b_u and b_l. g and h are referred to as inequality and equality constraints, respectively. If neither g nor h exists, it is called an unconstraint optimization problem.

Usually, optimization problems are expressed as minimization problems. For the consideration of a maximization problem the correlation given in Equation (9) applies (Pieper 2017).

$$
\max_{x \in \mathbb{R}^n} f(x_i) \qquad \Longleftrightarrow \qquad \min_{x \in \mathbb{R}^n} -f(x_i)
\tag{9}
$$

Besides a global optimum, an optimization problem may have several local optima. According to Pieper (2017) a local minimum at $x_i^* \in \mathbb{R}^n$ is present, if in a close neighborhood $U_{x_i^*}$ around x_i^* Equation (10) is valid.

$$
f(x_i^*) \leq f(x_i) \qquad \text{for all } x_i \in U_{x_i^*}.
\tag{10}
$$

However, a local minimum at $x_i^* \in \mathbb{R}^n$ is only also a global minimum if Equation (11) applies.

$$f(x_i^*) \leq f(x_i) \qquad \text{for all } x_i \in \mathbb{R}^n. \tag{11}$$

Consequently, any global minimum also represents a local minimum.

Many optimization algorithms try to find a local optimum solution in an iterative approach. By varying the input parameters in an advanced way, in order to reduce the number of iterations, and evaluating the function response, they are intended to converge to a solution until a certain termination criterion is satisfied. However, these algorithms are not able to distinguish between local and global optima. One approach to determine the global optimum is to find all local optima. The local optimum with the best solution represents the global solution (Pieper 2017).

If an optimization problem has two or more objectives, for example the reduction of GHG emissions and the cost reduction of an energetic system, it is termed a multi-objective optimization problem, which can be express as shown in Equation (12).

$$\min_{x \in \mathbb{R}^n} \quad f(x_i), \qquad f(x_i) = (f_1(x_i), \dots, f_q(x_i))^T \tag{12}$$

As these objectives usually compete against each other, there is not one single optimal solution. Using the aforementioned example, this means, that the most economic system is normally not the system with the lowest emissions. Instead, several so-called Pareto efficient solutions exist. Each of them represents a parameter set (Pareto set), for which no objective can be improved without impairing any other. All the existing Pareto optimal solutions in the space of objectives constitute the so-called Pareto front (Pardalos et al. 2017).

With respect to MD-BTES based heating systems, the objectives can be diverse, for example:

- High fluid outlet temperatures of the BHEs
- High efficiencies of single components or the overall system
- Low costs
- Large solar fraction
- High level of self-sufficiency
- Low environmental impact (global warming potential, cumulative energy demand, etc.)

2.3 Life Cycle Assessment

The environmental impact of an energy system is not only composed of GHG emissions during its operation, but also of related environmental effects during the production and the implementation of the system components as well as their disposal at the end of the system's lifetime. For this reason, a life cycle approach is chosen to integrate an environmental consideration into the herein developed assessment tool.

Life Cycle Assessment (LCA), as described in detail in the standards DIN EN ISO 14040 (2009) and DIN EN ISO 14044 (2006), is a systematic method to assess environmental aspects and impacts of product systems from raw material acquisition to final disposal.

An LCA is subdivided into the four steps

- goal and scope definition,
- life cycle inventory analysis (LCI),
- life cycle impact assessment (LCIA) and
- interpretation of results.

In some cases, the goal of the study can be reached without conducting an LCIA, which is then called an LCI study. The four steps of an LCA are specified in the following paragraphs according to DIN EN ISO 14040 (2009) and DIN EN ISO 14044 (2006):

The goal definition should contain the intended application of the LCA as well as the potential target group and a statement about the reasons for conducting the study. The scope should include the system boundary and the level of detail of the LCA. It should define the regarded system and its purpose. Moreover, a reference unit should be specified that is used to standardize the LCA results, the so-called functional unit and it has to be specified, which impact categories, impact indicators and characterization models shall be taken into account. Furthermore, the scope should include without limitation data requirements and information about allocation procedures.

The LCI comprises the acquisition and quantification of input and output flows of the considered system during the whole life cycle. The collection of data includes for example energy or raw material inputs, or products and co-products, which can also be energy outputs. Data processing, which is also part of the LCI, involves data validation, the normalization of data to unit processes and the functional unit.

As the third phase of an LCA, the LCIA entails the selection of relevant impact categories, category indicators and characterization models with regard to the respective research question. There are commonly used impact categories, for which well-established impact indicators and characterization models exist such as global warming, depletion of stratospheric ozone or acidification. However, there are also environmental impacts that are more difficult to assess since for instance inventory data is missing, suitable characterization methods are lacking or their magnitude is very site-specific. Noise, smell or ionizing radiation are examples for impact categories, which require additional research and methodology development (Bauman & Tillman 2004). Following the selection step, the classification step comprises the attribution of LCI results to impact categories and impact indicators. Last but not least, the calculation of category indicator results represents another mandatory element in an LCIA. Optional elements are normalization, grouping and weighting of the indicator results. The aim of the LCIA is to gain further information that support the comprehension and the evaluation of the significance of potential environmental impacts.

The final phase of an LCA is the life cycle interpretation, in which the results of the LCI and the LCIA are consolidated and discussed. It shall provide condensed results, which allow for the derivation of conclusions, recommendations or the support of decision-making processes. They should be in line with the definition of the goal and scope.

3   Performance of Medium Deep Borehole Thermal Energy Storage Systems

3.1   Influence of Storage Geometry

An ideal sensible heat storage system has a spherical shape: spheres have the smallest SA/V-ratio, which to a large extend controls the relative heat losses from such a storage system. However, spherically shaped BTES systems are not realizable. Consequently, the optimal shape of a BTES system is obtained with a circular alignment of the BHEs. Nevertheless, many BTES systems with a quadratic or slightly rectangular base also perform well, as these geometries reach relatively small SA/V-ratios, too (Dincer & Rosen 2011).

Besides the general shape, the structure of a BTES system is mainly defined by the length of the BHEs, the number of the BHEs and the BHE spacing. Appendix B contains a comprehensive survey on the influence of these three design parameters on the performance of BTES systems. For this purpose, 200 different BTES configurations were compared, using the numerical simulation environment *FEFLOW 6.2* (DHI-WASY 2014; Diersch 2014) for modelling the heat transport processes in the BHEs and the subsurface. The BHE length, the number of BHEs and the spacing between the BHEs were varied in a full factorial experimental design. In order to reduce confounding effects, very simple geologic conditions were assumed.

Furthermore, a very simplified operation scenario was applied to the storage system models. In order to simulate the alternating storage operation while also ensuring the comparability of the results, the fluid inlet temperatures were kept constant during the charging and the discharging cycles, respectively (see Figure 11). During the charging periods, the inlet temperature was set to 90 °C, as this temperature can easily be supplied by solar thermal collectors but also describes the upper limit of the temperature resistance of the PE-X pipes. During heat extraction, the inlet temperature was set to 30 °C. This ensures, that low-temperature heating systems can be supplied without the use of a heat pump. The BHEs were connected to each other in a parallel arrangement, so that all BHEs were supplied with the same inlet temperature. The flow rate for each BHE was set to $4\,l\,s^{-1}$ for the whole simulation time. This value displays a reasonable compromise between a high heat exchange rate and a comparatively low pressure drop in the BHEs.
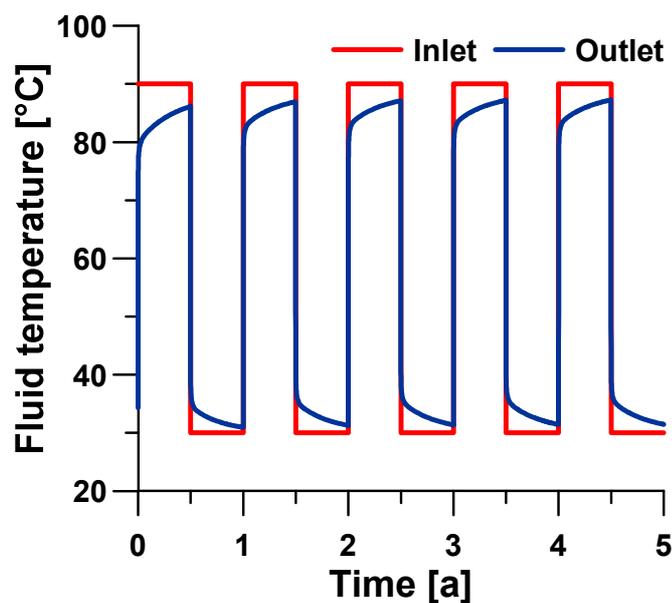
Figure 11: Applied operation scenario, which was repeated for the whole period under consideration.
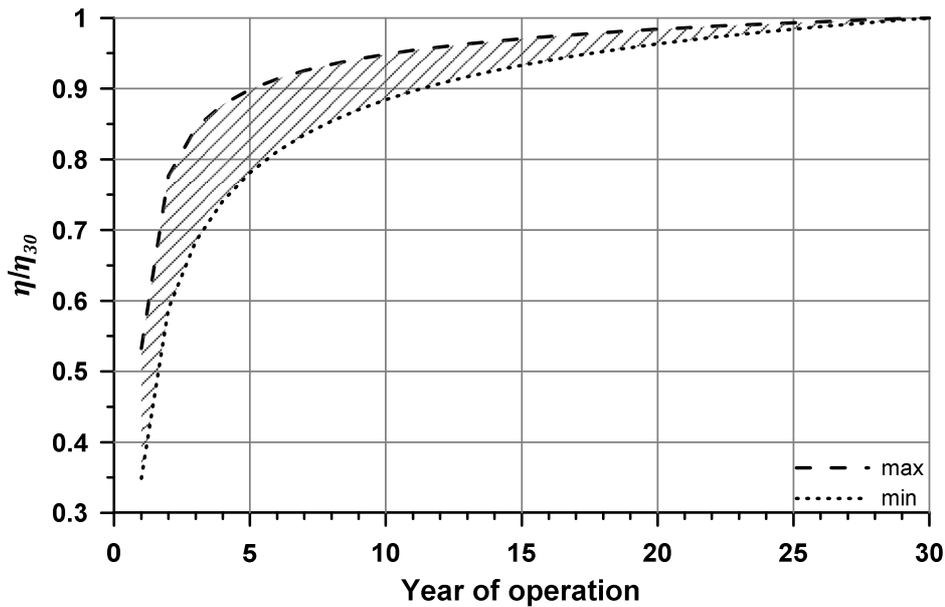
Figure 12: Development of the storage efficiency normalized to the final value in the 30th year of operation for systems with the optimal BHE spacing of 5 m (Welsch et al. 2016).

The performance of all storage systems improved significantly with time. Depending on the system design, the development took three to six years until 80% of the final efficiency (i.e. the efficiency after 30 years of operation) were reached (Figure 12). Accordingly, this has to be taken into account, when planning such a system. Depending on the storage development, further heat consumers could be connected to the BTES system gradually. That might for instance necessitate the utilization of mobile auxiliary heat units, which would support the BTES system during the first years of operation and afterwards be relocated to another site.

All three design parameters (length, spacing and number of BHEs) had an influence on the storage capacity and its efficiency. There was an optimal BHE spacing of approximately 5 m, where a maximum in storage efficiency and specific heat extraction rate was reached. This optimal spacing is of course dependent on the thermal properties of the subsurface. Consequently, it has to be determined for each specific storage site. Taking into account only the optimally spaced system variations, the amounts of stored (Figure 13a) and extracted heat (Figure 13b) in the 30th your of operation varied from 0.43 GWh a^{-1} to 22.4 GWh a^{-1} and from 0.14 GWh a^{-1} to 16.5 GWh a^{-1}, respectively. Larger systems performed much better than smaller systems. A lengthening of the BHEs as well as an increase in the BHE number lead to significant enhancements in the storage efficiency. In the best cases storage efficiencies of more than 80% were reached (Figure 13c) and the mean specific heat extraction rate exceeded 110 W m^{-1} (Figure 13d). However, an increase in the BHE number was more favorable than an increase in the BHE length (Figure 13c & d). Consequently, shallow BTES systems with a larger number of BHEs are – from a thermodynamic point of view – preferable to systems with an increased BHE length. Nevertheless, the results prompt the conclusion, that MD-BTES systems are very well suited for the seasonal storage of thermal energy on temperature levels up 90 °C or more.
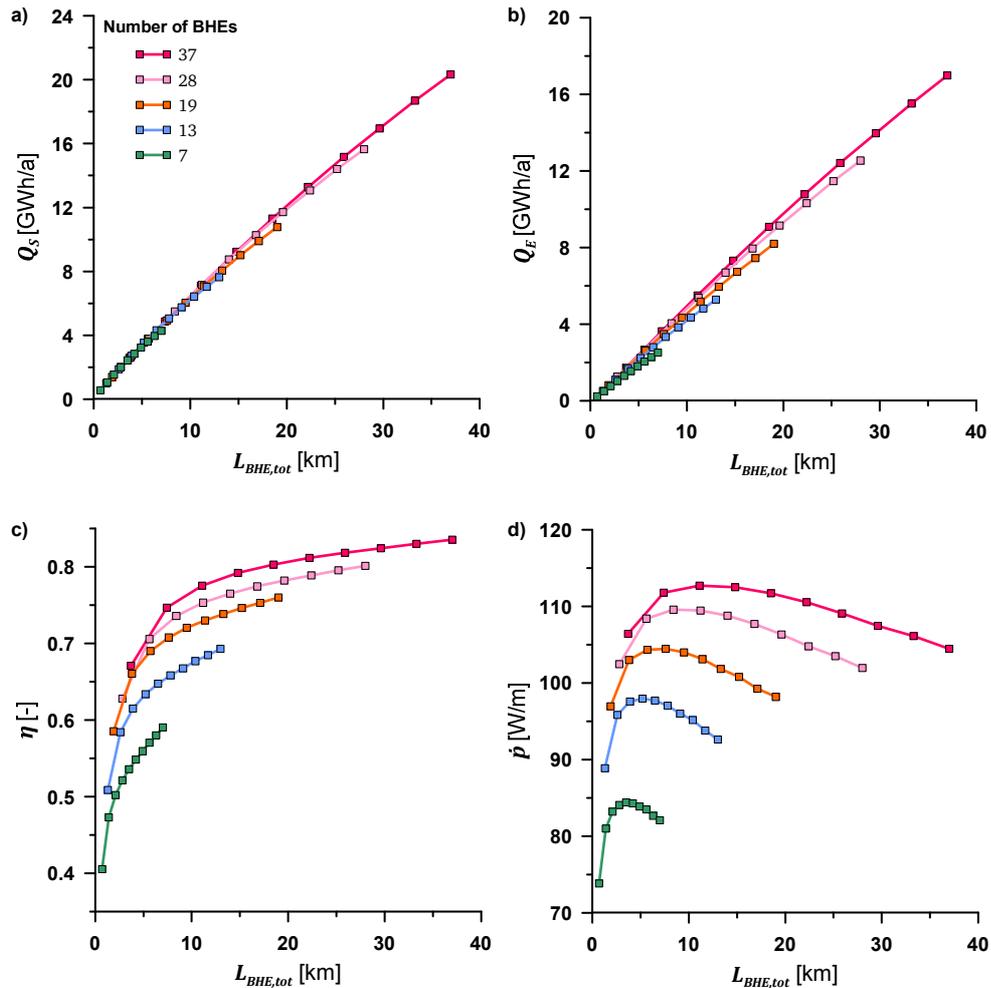
Figure 13: a) The amount of stored heat, b) the amount of extracted heat, c) the storage efficiency and d) the specific heat extraction rate in the 30th year of operation as a function of the total BHE length of a system design (for systems with a BHE spacing of 5 m). The total BHE length is the product of the BHE number and the length of the individual BHEs. For every bundle of the same BHE number the BHE length increases from 100 m to 1000 m in 100 m-steps from left to right (data from Welsch et al. 2016).

3.2 Influence of Geologic Properties

The thermal and hydraulic properties of the subsurface as well as boundary conditions like the hydraulic or geothermal gradient can have a significant impact on the performance of BTES systems. Besides the consideration of the design parameters, Appendix B contains a sensitivity study, which covers the variation of the rock thermal conductivity, rock heat capacity as well as the hydraulic conductivity of the storage rock under fixed hydraulic and geothermal gradients.

Under the very steady operational conditions applied in the study, the following general conclusions can be drawn:

- High rock thermal conductivities increase storage capacities but also conductive heat losses.
- The rock heat capacity has almost no influence on the storage performance.
- Groundwater flow can significantly impair the storage performance as convective heat losses increase.

It is expected that the influence of the heat capacity increases with a more transient operation of the storage system.

3.2.1 Parameter Uncertainties

The parametrization of underground properties in numerical models is subject to uncertainties; not only because of uncertainties in the prediction of the underground's structure but also due to variabilities in the rock properties as well. These uncertainties directly propagate to modeling results.

Appendix C addresses the handling of parameter uncertainties in geothermal modeling. It suggests the adoption of so-called ensemble models, which are commonly used for example in meteorology (e.g. Krishnamurti et al. 2000). Ensemble modeling means the auxiliary generation of several simplified models under the variation of input parameters within the range of uncertainty. Instead of performing a single prediction of the most probable system behavior, an ensemble of models can provide information on the range of possible results and give an estimate on their probability of occurrence. Consequently, ensemble modeling can be a useful tool to gather valuable additional information for the design of geothermal systems. Appendix C illustrates the approach by the example of a single medium deep BHE.

In the following example, an ensemble of models was used to consider uncertainties in the modeling of a hypothetical MD-BTES system, which were induced by uncertainties in the rock thermal conductivity. The assumed storage system site was located at TU Darmstadt campus Botanischer Garten. It was expected that the subsurface at the potential site was made up of Granodiorite only. As part of a case study on this storage site (Appendix A), an outcrop analogue study was carried out earlier. Its purpose was to collect rock samples from several rock types that are found in the city area of Darmstadt and its periphery. Subsequently, different rock parameters like thermal conductivity λ, thermal diffusivity κ and density ρ were measured in the laboratory. The thermal conductivity measurements are illustrated in Figure 14. They reveal a relatively large spread of values even for individual rock types.
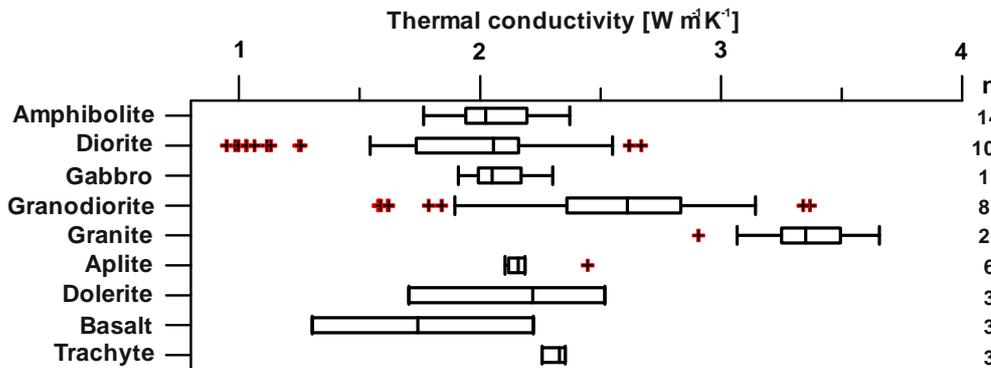
Figure 14: Box-and-whisker plot of thermal conductivities of different rock samples found in the area of Darmstadt.

The granodiorite dataset for the thermal conductivity contained 85 samples. A one-sample Kolmogorov-Smirnov test (Kolmogorov 1933; Smirnov 1948; Massey 1951) confirmed the hypothesis that the data came from a standard normal distribution with an arithmetic mean μ of $2.54\,\mathrm{W\,m^{-1}\,K^{-1}}$ and a standard deviation σ of $0.43\,\mathrm{W\,m^{-1}\,K^{-1}}$.

An ensemble of five models was created. All models included an MD-BTES system composed of 37 BHEs with a length of 500 m each, in a circular arrangement. The general model setup was based on the setup introduced in Appendix B. Solely the thermal conductivity of the subsurface was varied around the mean by one and two standard deviations (see Table 2). The operation scenario equaled the scenario with a varying default heat load as introduced in Chapter 1.1.2.

Table 2: Variation of thermal conductivity.

Model		$\mu - 2\sigma$	$\mu - \sigma$	μ	$\mu + \sigma$	$\mu + 2\sigma$
Thermal conductivity	[W m^{-1} K^{-1}]	1.67	2.11	2.54	2.97	3.40

Figure 15 illustrates the deviation of the outlet temperature of the different ensemble models from the outlet temperature of the model representing the arithmetic mean of the rock thermal conductivity (μ-model). Expectedly, lower thermal conductivities lead to higher fluid temperatures during the charging period and lower fluid temperatures during the discharging period. This was due to higher temperature gradients, which were necessary to achieve the default heat transfer rates. Higher thermal conductivities caused the opposite.
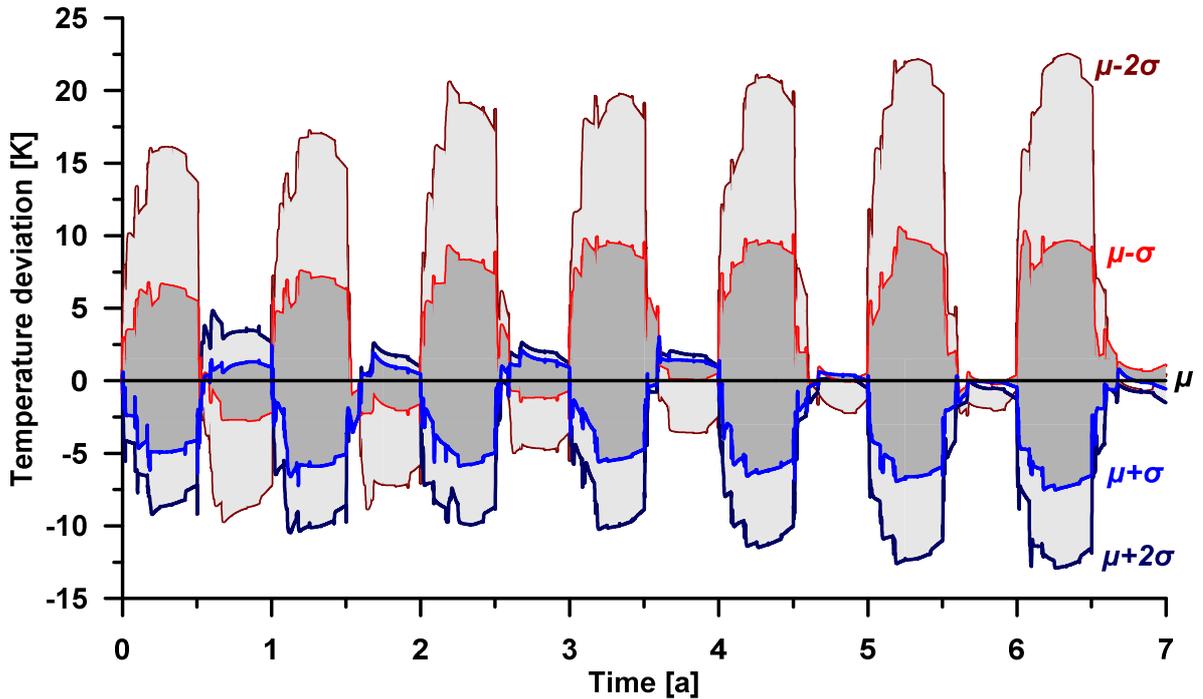
Figure 15: Deviation of the model ensemble's outlet temperature from the outlet temperature of the μ-model during the first 7 years of operation.

Furthermore, negative deviations from the mean thermal conductivity caused generally higher differences in the outlet temperature than positive deviations. During the first charging cycle the maximum absolute values of the temperature deviation lay at approximately 5 K and 6 K for the $\mu + \sigma$-model and the $\mu - \sigma$-model, respectively, and at around 9 K and 16 K for the $\mu + 2\sigma$-model and the $\mu - 2\sigma$-model. They even increased in the subsequent charging cycles by a few Kelvin. In contrast, the outlet temperatures during the discharging periods only differed by 1 to 2.5 K for the $\mu \pm \sigma$-models and by 5 to 10 K in case of the $\mu \pm 2\sigma$-models. Moreover, they seemed to converge with time. At a first glance, a misjudgment of the rock thermal conductivity has only minor impacts on the discharging process in the long-term operation. However, high positive fluid temperature deviations during the charging period are unfavorable, as they impair the efficiency of the heat generation units (e.g. STCs) and they can involve the risk of exceeding the permissible maximum temperature of the BHE pipes or other components. As a consequence, this could entail a reduction of the thermal loads during the charging period, which would also restrain heat extraction.

Accordingly, it is absolutely necessary to minimize the uncertainties in the rock properties by suitable exploration and prediction methods. The most accurate information about the storage reservoir will be gathered from an exploratory drilling at the project site. Thus, it is recommendable to conduct the drilling of the first BHE in a storage system as an exploratory drilling, which is used to improve the availability of data. These additional data can be used to enhance the accuracy of the storage model results and, if necessary, to adjust the BTES system design.

3.3 Influence of Temperature Levels

In order to quantify the effect of different charging and discharging fluid temperatures, they were varied for an exemplary storage set-up in a numerical simulation study (Appendix B). The results confirmed a strong dependency of the heat storage rate and extraction rate (Figure 16a) on both the charging and discharging temperature. Furthermore, the storage efficiency generally increased with higher charging temperatures and lower discharging temperatures (Figure 16b). However, reducing the discharging temperature lead to a stronger improvement of the storage efficiency than increasing the charging temperature by the same ΔT. In the latter case, the generally higher temperature level caused higher heat losses, which cushioned the efficiency improvement. Thus, the temperature levels, on which a BTES system is charged and discharged, have a significant impact on the system performance. They have a determining influence on the thermal gradient between the storage formation and fluid in the BHE pipes, which controls the heat exchange rate between the storage volume and the fluid.
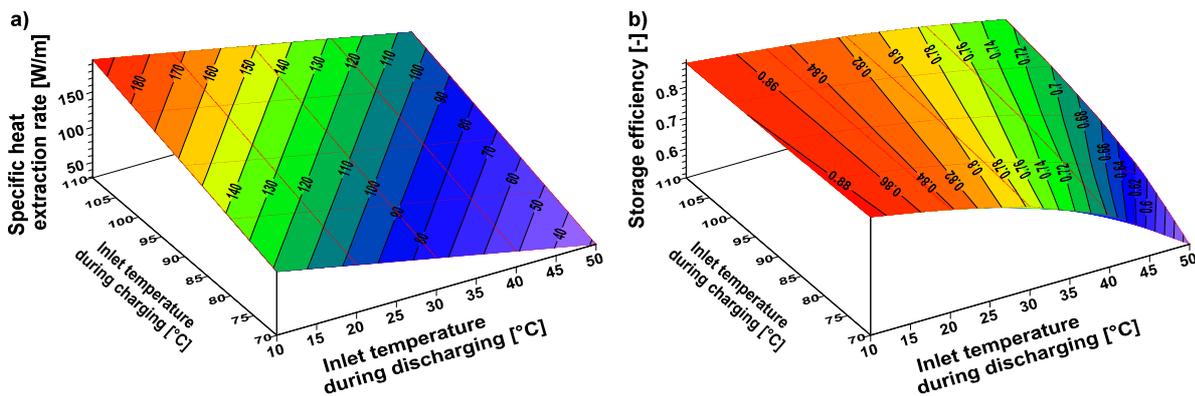
Figure 16: a) Mean specific heat extraction rate and b) storage efficiency as a function of the charging and discharging inlet temperatures in the 30th year of operation for an exemplary storage system design consisting of 37 BHEs, 500 m each with a spacing of 5 m (data from Welsch et al. 2016).

3.4 Design Optimization

A BTES design is basically characterized by the arrangement of the BHEs, their length and number as well as the spacing between neighboring BHEs. It affects to a large amount the investment costs for the system as well as its operational behavior. Consequently, the optimization of the BTES design is of utmost interest.

A convenient approach is the optimization of such systems on the basis of 3D numerical models. However, a design variation also necessitates an adaption of the model's mesh geometry. But therein lies one essential drawback of using *FEFLOW* as the numerical simulation environment (Chapter 2.1). In contrast, *BASIMO* is well suited for a mathematical optimization of the BTES design, as it allows for an automated mesh generation and the *MATLAB Global Optimization Toolbox* (The MathWorks Inc. 2016a) can easily be employed. Unfortunately, even when using

BASIMO models as objective functions, a direct optimization of the BTES design is very time consuming (Schulte 2016): firstly, iterative optimization algorithms can require a large number of objective function calls until they converge to the optimum solution and secondly, the simulation of a BTES system should cover at least a few years of operation to be meaningful. This, however, can take several hours to days, depending on the complexity of the model and the operation conditions.

Appendix E introduces a proxy-based optimization approach as a time-saving alternative to a direct optimization of the BTES design: first of all, a certain number of so-called training simulations are carried out with *BASIMO*, which should cover the variable space of interest. The input variables and responses of these training simulations display sampling points, which are used to generate a high-dimensional polynomial fit by applying the arbitrary polynomial chaos expansion technique (Oladyshkin & Nowak 2012). Finally, the received approximation is used as the new objective function in a direct optimization problem. Besides a general introduction to the approach, Appendix E also comprises a fictional example for the optimization of a BTES design: the total borehole length of a system was minimized while guaranteeing the provision of a specified amount of heat. The example demonstrates the general applicability of the proxy-based optimization approach. However, it also emphasizes the importance of a careful definition of the problem and a proper selection of input variables and their boundaries. A more detailed description of the proxy-based optimization procedure is also given by Schulte (2016).

3.5 Improvement Measures

Apart from the choice of the BHE type and geometries and the general BTES design, there are some more measures that could improve the performance of a BTES system. Three of these measures are considered in more detail in the following subchapters.

3.5.1 Thermal Insulation at the Top Ground Surface

A thermal insulation at the top surface shall restrain the heat losses to the atmosphere. Such a thermal insulation can be for example simply an additional mound of soil material, which is constructed at the top of the BTES system, or it could also be an installation of dedicated thermal insulating material like plastic-foams, concrete-foams, rock-, or glass-wool.

Appendix B contains a numerical comparison of BTES systems with and without an insulating layer at the top of the systems. The study further examines the role of the depth of theses storage systems on the importance of such a thermal insulation. It comes to the conclusion that a thermal insulation at the top ground level is only necessary for shallow BTES systems. The reason for that is the decreasing share of the top surface area in the total enveloping surface with increasing depth of the BTES system. Consequently the portion of heat losses through the top surface becomes more and more marginal.

3.5.2 Series Connection of Borehole Heat Exchangers

The operation of a BTES system can be implemented either with a parallel flow connection of all BHEs or with a series connection of different BHEs. In the first case, the total inlet flow volume is divided up into equal parts among all BHEs. Consequently, all BHEs are supplied with the same fluid temperature. In a series connection, the flow through the BHEs or through different BHE subassemblies happens consecutively. By connecting BHE in series from the storage center to the storage fringe, a lateral temperature zoning of the storage can be achieved. During

charging of the storage, the warm fluid firstly passes through the inner BHEs. The slightly cooled BHE fluid is then passed to the next BHEs in the series and so on. As a result, the temperature is warmest in the storage center and it decreases to its fringe. Therefore, the lateral temperature gradient from the storage periphery to the undisturbed subsurface is lowered, what diminishes the heat losses to the surrounding. During the discharging period, the process operation is reversed. This method is already established in shallow BTES systems (e.g. in Crailsheim, Bauer et al. 2013a; Mielke et al. 2014; Bauer et al. 2016). However, the value of a series connection for MD-BTES systems is not clear, as these systems usually do not have the lateral extent of a shallow BTES system.

In order to get a first insight into this, a numerical simulation of an exemplary MD-BTES system (37 BHEs, 500 m each, 5 m BHE spacing) was carried out. The arrangement of the BHEs, the model specifications and the operation scenario equaled those in Appendix B (see also Chapter 3.1). Three BHE subassemblies were defined. One inner assembly, consisting of 19 BHEs and one outer BHE ring consisting of 18 BHEs. The flow rate through a single BHE was maintained at 4 l s^{-1} to keep the pressure drop through the BHEs equivalent to that in the parallel connected system from Appendix B. Accordingly, the total flow rate had to be reduced. A period of ten years of operation was simulated.
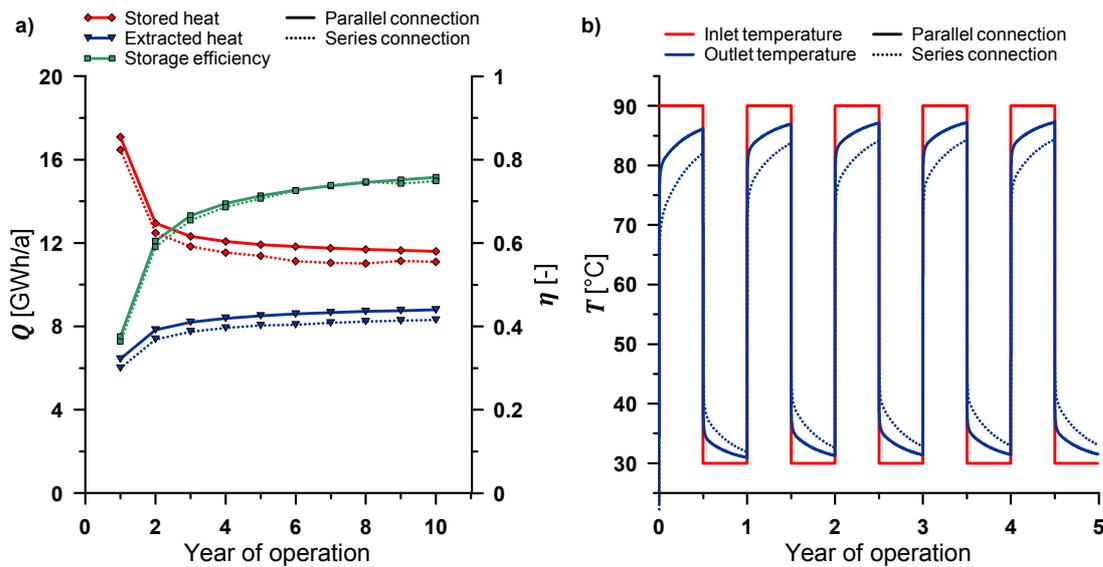
Figure 17: Comparison of a) amounts of stored heat and extracted heat and storage efficiency and b) fluid outlet temperatures of an exemplary MD-BTES system (37 BHEs, 500 m each, 5 m BHE spacing) in parallel and in series BHE connection.

The conversion to series connection entailed a slight diminishment of the storage capacity by approximately 4% to 6% (Figure 17a). This can be attributed to the on average decreased temperature gradient between the fluid and the rock. Even so, the storage efficiency was almost unaffected. On the contrary, the series connection implicated a higher overall temperature difference between the inlet and outlet of the storage systems (Figure 17b). As a result, on average around 3 °C higher outlet temperatures were achieved during the extraction periods. Consequently, this implies an increase in the *COP* of an HP, which is used to boost the temperatures on the required supply temperature of the heating system. A shift in the outlet temperature from 33 °C to 36 °C would cause an enhancement of an HP's *COP* from 7.46 to 8.64 by approximately 16% assuming a supply temperature of 55 °C and taking account of the assumptions concerning the *COP* calculation as introduced later in Chapter 5.1.5.

3.5.3 Alternation of Flow Direction in Coaxial Borehole Heat Exchangers

A further measure, which is debated to entail some improvements at basically no extra cost, is the reversal of the flow direction through the coaxial BHEs as part of the transition from charging to discharging operation and vice versa: during the charging operation, the heated up fluid is pumped down in the center pipe (CXC operation), where it is thermally insulated against the subsurface by the center pipe and the fluid in the annulus. Consequently, it only experiences a minor temperature decrease in the downstream section and the heat exchange with the subsurface principally starts at the bottom of the borehole, when the fluid enters the annulus (see Figure 18a). On its way up the annulus, it considerably cools down while it releases heat to the subsurface. Consequently, the fluid in the annulus is warmest at the bottom of the BHE, increasing the heat input there, and it is lowest in the uppermost part of the BHE, which in turn reduces the heat release in this region. During discharging, the relatively cold fluid is pumped down the annulus (CXA operation), where its temperature increases due to heat gains from the subsurface (see Figure 18b). The heated fluid flows up in the center pipe, where it is thermally insulated from the colder overlaying rock units, which is expected to cushion heat losses. However, these processes seem to have no effect in the long run. Figure 18 shows the difference between sheer CXA and sheer CXC operation after 90 days of charging a BTES system with 90 °C warm water and after 90 days of discharging a previously charged system with 30 °C cold water (results from a numerical modeling study). Although the temperature profiles of CXC and CXA operation differed significantly, the temperature difference and thus the exchanged heat with the subsurface were almost equivalent. Consequently, an alternation between CXC and CXA operation would imply only insignificant enhancements in the storage performance.
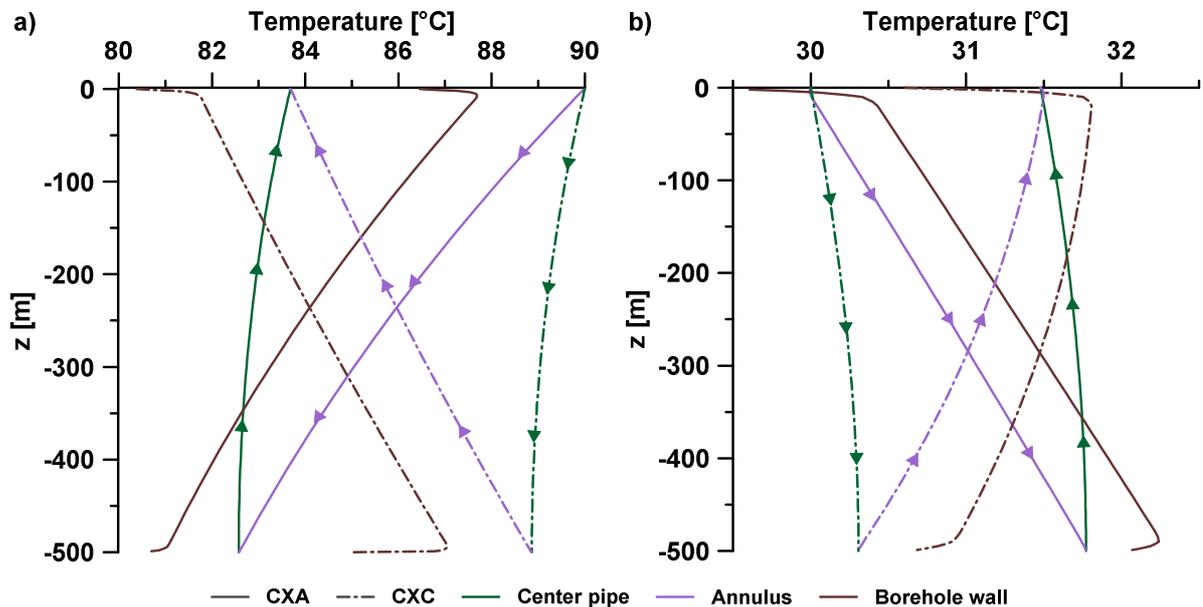
Figure 18: Comparison of temperature profiles of sheer CXA and sheer CXC operation in a BHE from the outer BHE ring of an exemplary MD-BTES (37 BHEs, 500 m each, 5 m spacing), (a) after 90 days of charging and (b) after 90 days of discharging the storage system.

Further numerical simulations confirm this assumption: a relatively small BTES system consisting of 7 BHEs, 100 m each and a large one consisting of 37 BHEs, 500 m each, were simulated in *BASIMO* and *FEFLOW*, respectively. For both storage designs, a sheer CXA operation and an alternation of CXC- & CXA-operation were compared (Figure 19), taking as a basis a very simplified operation scenario with constant inlet temperatures of 90 °C during 6 months of charging and 30 °C during 6 months of discharging (see also Chapter 3.1; the operation scenario, the model specifications as well as the BHE arrangements were identical to those introduced in Appendix B). The results reveal that in both system designs the alternating operation resulted in only marginal improvements in the storage capacity as well as in the storage efficiency. In case of the small BTES system, the amounts of extracted heat and the storage efficiency were enhanced by only around 0.05%, whereas in the large BTES system slightly higher improvements in the range from 0.2 to 0.6% were achieved. Hence, the assumption that seasonally alternating flow directions could be beneficial (as formulated in e.g. Appendix A) must be revised.
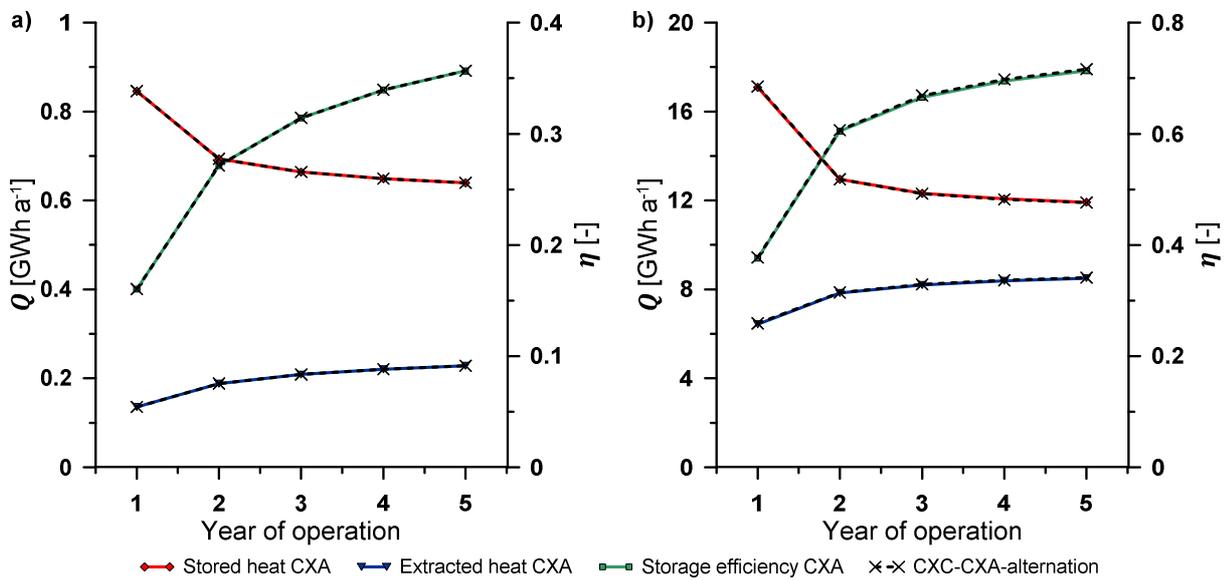
Figure 19: Comparison of sheer CXA operation to an alternating CXC-CXA operation of (a) a BTES system consisting of 7 BHEs, 100 m each, simulated in *BASIMO* and (b) a BTES system consisting of 37 BHEs, 500 m each, simulated in *FEFLOW*. Both systems had a BHE spacing of 5 m.

4 Reduction of the Thermal Impact on Shallow Aquifer Systems by Medium Deep Borehole Thermal Energy Storage

There are generally two reasons, why MD-BTES systems are considered to have a much lower thermal impact on shallow groundwater aquifers than shallow storage systems: firstly, the geometric proportions by itself lead to a decreased release of heat to the shallow subsurface in a medium deep system. Obviously, in a shallow system the whole heat storage is accomplished in the shallow subsurface, whereas in a comparably sized medium deep system the majority of heat is stored into deeper geologic formations. Secondly, medium deep systems allow for the implementation of a thermal insulation in the uppermost section of the boreholes, which further reduces the heat input into the groundwater body along the respective borehole section.

However, the magnitude of these effects has not been quantified so far. Numerical simulations are a convenient method to compare an MD-BTES system to a shallow system. But, besides the capability of considering groundwater flow, the numerical simulation must be able to take into account a thermal insulation of the upper section of a BHE.

4.1 Simulation of Partly Insulated Borehole Heat Exchangers

A suitable method to simulate a BHE with a partial thermal insulation in the uppermost section of the borehole is the development of a fully discretized BHE model. In such a model, all relevant BHE geometries like pipes, the grout zone and the borehole wall are represented in the FE mesh (Figure 20 shows the example of a fully discretized coaxial BHE).
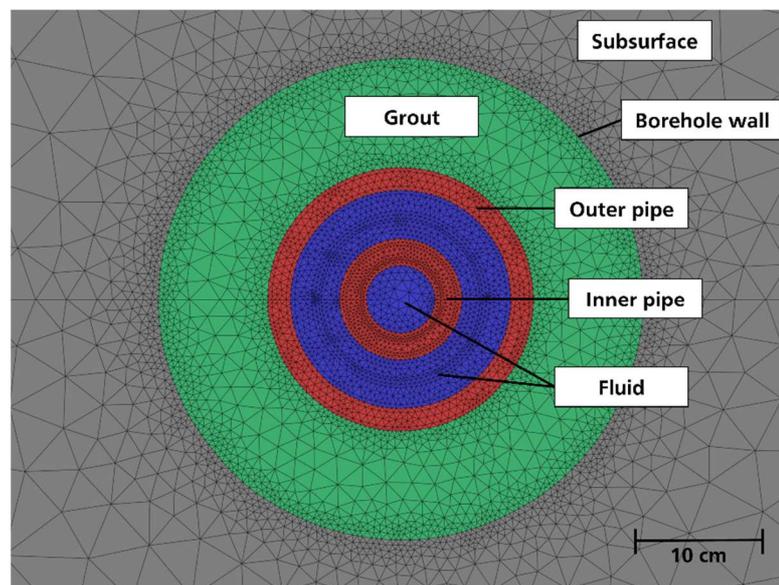
Figure 20: Horizontal cross-section through a fully discretized finite element model of a coaxial BHE.

However, such a fully discretized BHE model results in a FE mesh with a vast number of nodes, especially when considering more than a single BHE. Besides the much higher effort needed to design and generate the mesh, the node number significantly affects the computational effort to solve the simulation task. Therefore, the application of a fully discretized BHE model is often ineffective and only valuable for very specific issues. On the contrary, the analytical BHE solution after Eskilson & Claesson (1988), which is standardly included in *FEFLOW* (Diersch et al. 2011a, b; Diersch 2014), allows for a reduced node number and a comparatively fast computation of BHE systems. But, it is not able to consider more BHE sections with different borehole

diameters and grout parameters. For this reason, the existing analytical solution has been improved (Appendix F). The resulting solution can differentiate two BHE sections. Consequently, it allows for a fast and accurate simulation of partially insulated BHEs.

The advanced analytical BHE solution has been implemented in *BASIMO* (Appendix D) and successfully validated against a fully discretized BHE model. Yet, *BASIMO* is not qualified to quantify the thermal impact on groundwater resources, as it lacks the inclusion of advective heat transport. Therefore, the groundwater flow simulation environment *FEFLOW*, which combines conductive and advective heat transport in the subsurface, is chosen for the considerations. For this purpose, a *FEFLOW* plug-in has been programmed in C++ code, which contains the improved analytic BHE solution introduced in Appendix F and couples it to the 3D FE mesh in *FEFLOW* as described by Diersch et al. (2011a). A nodal reference distribution is used to indicate the BHE positions in the FE mesh. Borehole and pipe geometries are imported from a text file. Moreover, the plug-in reads *FEFLOW* different time series. Two of them define the volume flow through the BHEs and the inlet temperatures. Another time series determines the BHE type. Thus, the plug-in also allows for a change of the flow direction through a coaxial BHE from CXC to CXA and vice versa. This constitutes a further enhancement to the standard BHE solution in *FEFLOW*. The plug-in is attached to the digital supplement (Appendix J) of the thesis and a short instruction manual for the plug-in is given in Appendix I.

4.2 Comparison of Shallow and Medium Deep Borehole Thermal Energy Storage

A fictional simulation example was carried out in *FEFLOW* in order to demonstrate the capability of the developed solution as well as to exemplary illustrate the reduction of the thermal impact on shallow groundwater bodies in one specific case.

4.2.1 Model Set-up

The following simple geologic situation was assumed (Figure 21): crystalline basement was overlain by a 100 m thick overburden of unconsolidated rock material, which acted as groundwater aquifer. The assumed hydraulic and thermal properties for each of the two formations are given in Figure 21. The hydraulic gradient of 5% caused groundwater flow from east to west with a Darcy velocity in the aquifer layer of approximately 1.58 m a^{-1}.

Four different storage systems were compared (see Table 3): a shallow BTES system (217 BHEs, 85 m each), which only taped into the aquifer formation and three MD-BTES systems (37 BHEs, 500 m each), which to a large extend exploited the crystalline formation. To facilitate the comparability of the different systems, the total BHE lengths were equated. While one of the medium deep systems had a uniform BHE completion, the second MD-BTES system contained thermally insulating grout in the upper BHE sections, which were located in the groundwater body from 0 to 100 m below ground level. The insulating grout material had a thermal conductivity of 0.04 W m^{-1} K^{-1}. An increase of the borehole diameter in the insulating section was considered in the third MD-BTES model. This measure further increases the thermal resistance and consequently the insulating effect between the BHE fluid and the subsurface. All four systems had a coaxial BHE completion (comparable to that in Appendix B), a circular BHE arrangement and a borehole spacing of 5 m. A simplified operation scenario was applied to the storage systems (Chapter 3.1).
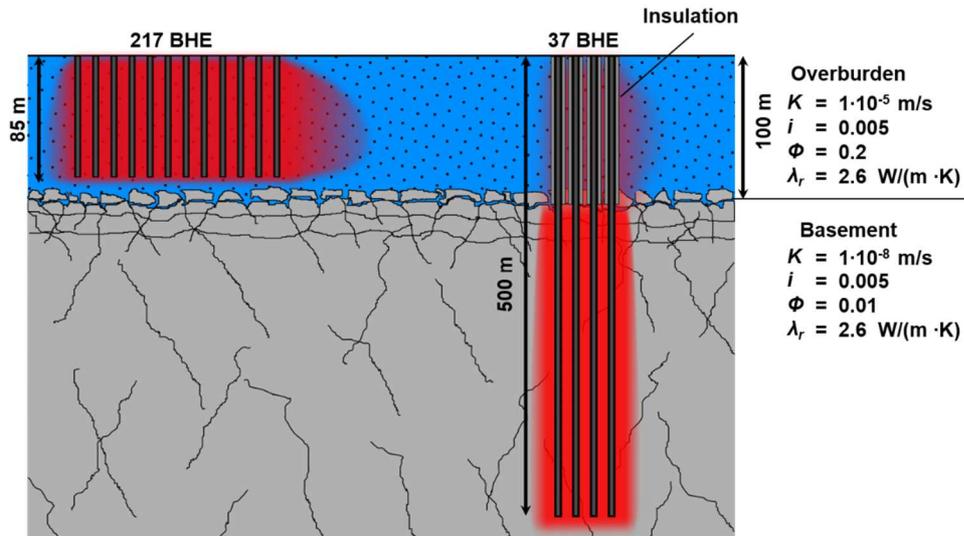
Figure 21: Schematic representation of the parametrization of the shallow BTES (left), the MD-BTES (right) and the underground properties in the numerical simulation study (not to scale).

Table 3: Model distinction for the comparison of shallow and MD-BTES systems.

		Model 1	Model 2	Model 3	Model 4
BTES type		Shallow	MD	MD	MD
Number of BHEs	[-]	217	37	37	37
BHE length	[m]	85	500	500	500
Total BHE length	[m]	18,445	18,500	18,500	18,500
BHE spacing	[m]	5	5	5	5
BHE completion	[-]	Coaxial	Coaxial	Coaxial	Coaxial
Borehole diameter of upper section (0–100 m)	[cm (in.)]	15.24 (6)	15.24 (6)	15.24 (6)	25.4 (10)
Borehole diameter of lower section (100–500 m)	[cm (in.)]	15.24 (6)	15.24 (6)	15.24 (6)	15.24 (6)
Thermal conductivity of grout in the upper section (0–100 m)	[W m^{-1} K^{-1}]	2	2	0.04	0.04
Thermal conductivity of grout in the lower section (100–500 m)	[W m^{-1} K^{-1}]	-	2	2	2

4.2.2 Results

Although all storage systems had a similar total borehole length, the storage capacities differed significantly (Figure 22a). In the shallow system on average 14.4 GWh of heat were stored per year. In contrast, the MD-BTES system without insulation only accumulated 12.3 GWh a^{-1}. This reduction can be attributed to the increased natural temperature of the deeper subsurface, which inhibited the heat transfer to the storage rock for the given operation scenario. With the integration of a thermal insulation, the respective sections could not contribute to the storage volume anymore. Consequently, the effective storage capacity was further reduced and the amounts of stored heat diminished to 10.0 GWh a^{-1} in case of the standard borehole diameter and 9.4 GWh a^{-1} in case of the widened insulation. The amounts of extracted heat Q_E showed an analogous trend.
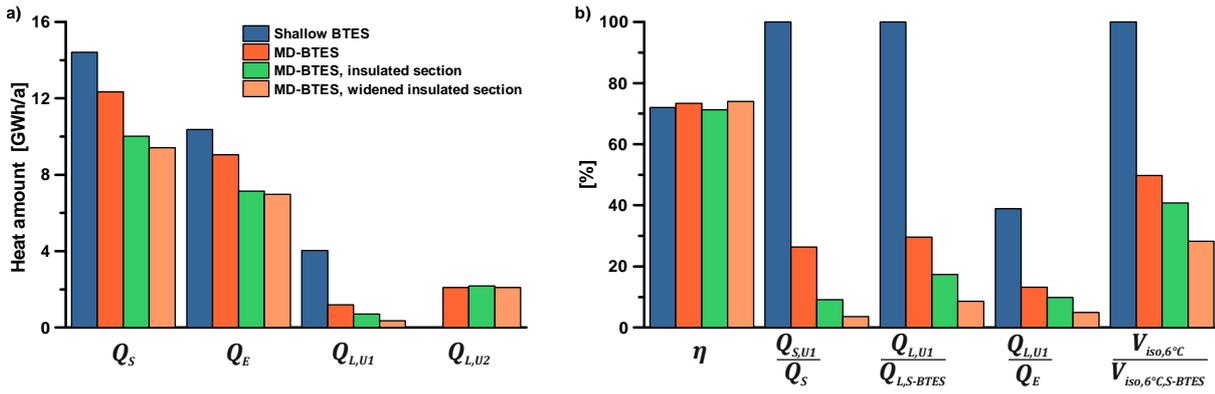
Figure 22: Comparison of a) absolute heat amounts and heat losses and b) storage efficiencies and relative heat losses. All values are averaged over 30 years of operation.

Despite the different system designs and storage capacities, all four BTES systems had a similar storage efficiency (Figure 22b). The second bar stack in Figure 22b reveals that in the shallow system 100% of the heat were stored in the aquifer unit (U1), while in the MD-BTES systems only a fraction of the heat was charged into U1. As a result, the unrecoverable fraction of the heat $Q_{L,U1}$, which is lost to U1, could also be reduced in the MD-BTES systems to approximately 30%, 17% and 9% of the heat losses to U1 in the shallow system. However, it has to be taken into account that the shallow system also had a much higher capacity. A more meaningful comparison is drawn when calculating relative heat losses by normalizing the heat loss values to the amount of discharged heat of the respective system (Figure 22b, fourth bar stack): in the shallow system the heat loss to U1 corresponded to 38.9% of the discharged heat, whereas in case of the medium deep systems it were only 13.2% without insulation, 9.8% and 5.0% with insulation and widened borehole diameter, respectively.
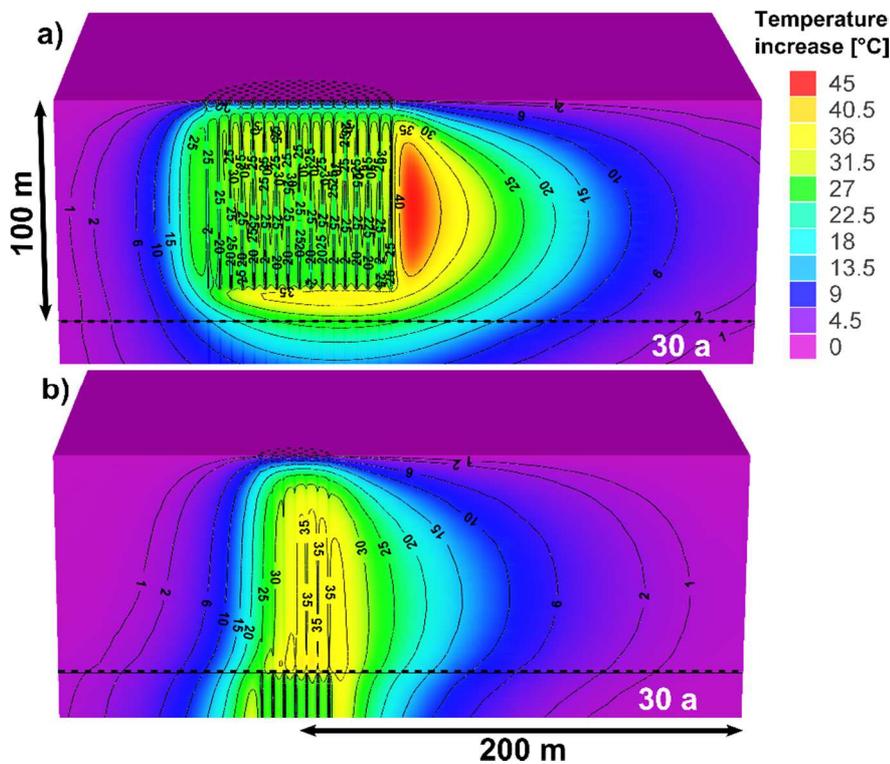
Figure 23: Increase of groundwater temperature in a shallow aquifer around a) a shallow BTES (217 BHE, 85 m each) and b) an MD-BTES (37 BHE, 500 m each) with a thermal insulation (standard diameter) in the respective section after 30 years of operation.

The unrecoverable heat that was continuously lost to the shallow subsurface during BTES operation lead to a persistent increase of groundwater temperature. In all four scenarios a heat plume developed, which was displaced in the direction of groundwater movement. After 30 years of operation, an elevated groundwater temperature could be observed up to a distance of several hundred meters from the storage center (Figure 23). The VDI guideline VDI 4640 part 4 (Verein Deutscher Ingenieure 2004) recommends a maximum change of the groundwater temperature of 6 K for direct thermal use of the subsurface. For this reason, the 6 K-isosurface is chosen in Figure 24 to illustrate the size of the heat plume in the critical aquifer unit U1. Compared to the shallow BTES system, the MD-BTES system without a thermal insulation could already halve the affected rock volume from approximately $2.71 \cdot 10^6$ m³ to $1.35 \cdot 10^6$ m³. Integrating a thermal insulation in the topmost sections of the BHEs depleted the volume by another 9 percentage points to about $1.11 \cdot 10^6$ m³. By enlarging the borehole diameter in the insulating grout section, the heat plume shrank to approximately $0.77 \cdot 10^6$ m³, which corresponds to only 28% of the size of the shallow system's heat plume.
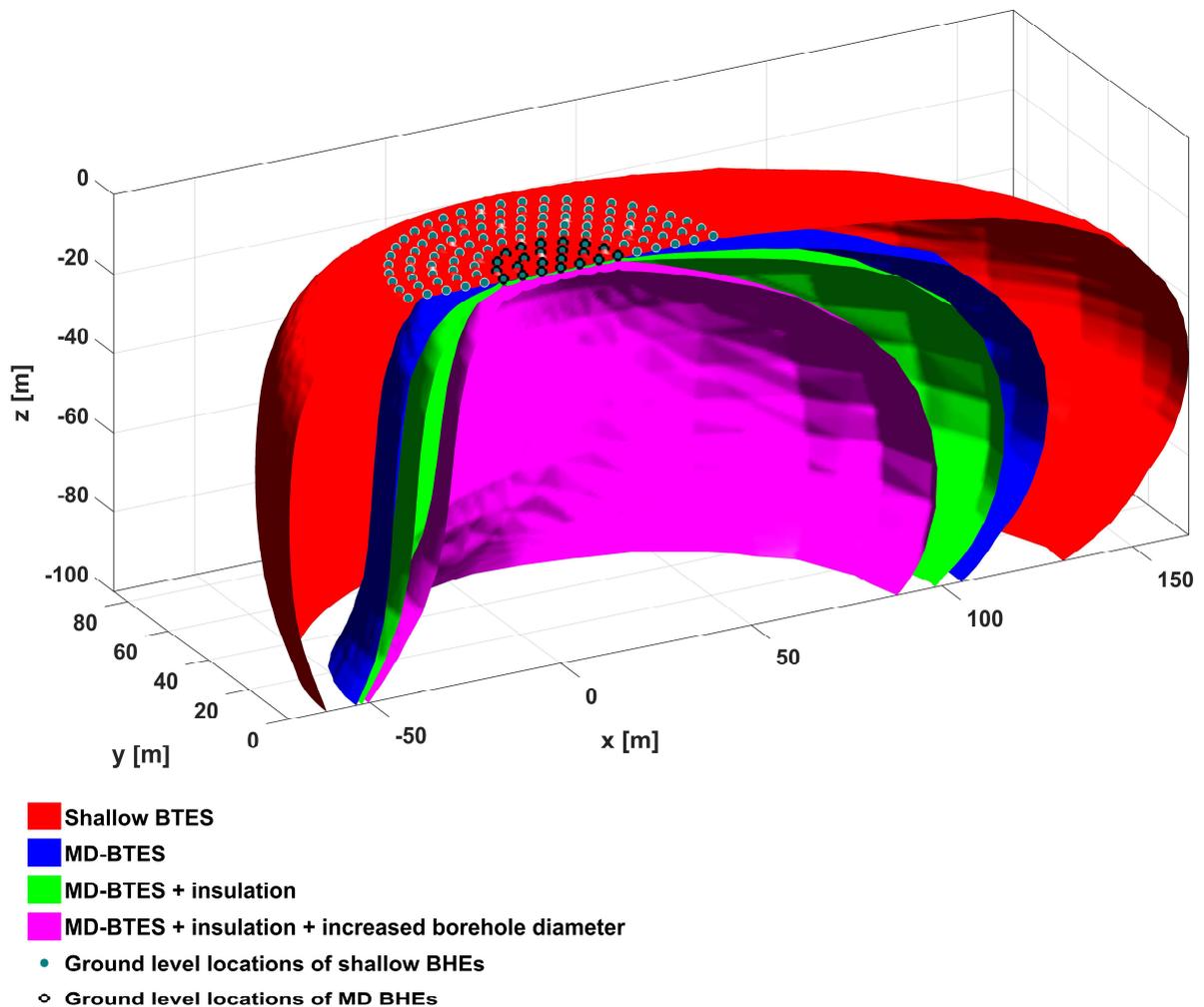
Figure 24: Temperature isosurfaces for 6 K-warming of the aquifer after 30 years of storage operation around a shallow BTES, an MD-BTES without insulation, an MD-BTES with insulation in the uppermost borehole section and an MD-BTES with insulation in the uppermost borehole section, which has additionally an increased borehole diameter. The isosurfaces are cut off along the plane of symmetry.

5 Economic and Environmental Assessment Tool

The evaluation of the integration of MD-BTES into DH concepts in terms of economic and environmental aspects necessitated the development of a convenient assessment tool with the following requirements:

- ability to consider different heat generation system configurations with and without MD-BTES storage
- ablility to quantify the energy and material flows connected to such a system during its lifetime and to rate these flows in terms of economy and environmental impact
- fast enough to allow for the assessment of a large number of system configurations in a short time
- ability of integrating mathematical optimization techniques
- opportunity to easily extend the tool by other heat generation technologies

The assessment tool has been developed in *MATLAB* (The MathWorks Inc. 2016b). It considers DH systems that include one or more of the following components: a GB, a CHP, an STC field and an HP-assisted BTES system (see Figure 25). A detailed description of the selected approach is given in the following sections.
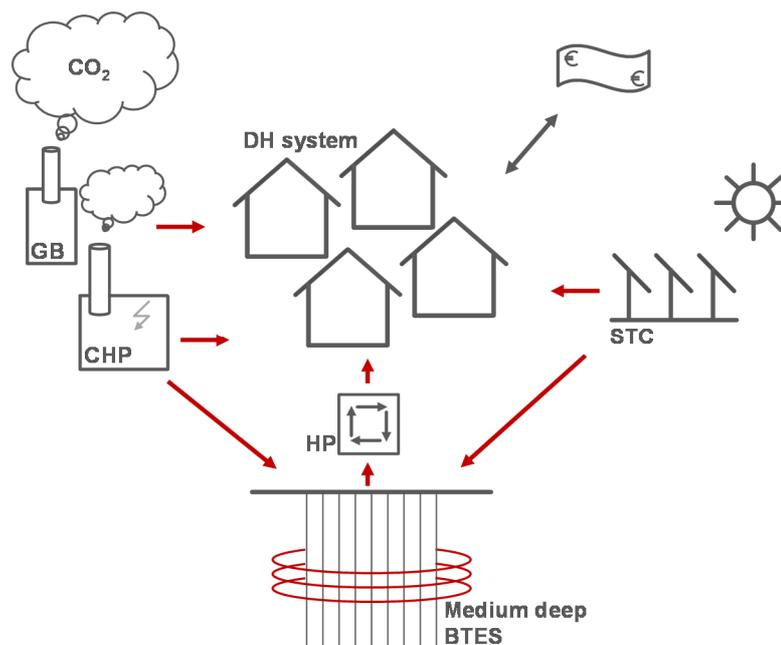
Figure 25: Schematic illustration of technologies, which are considered in the assessment tool (Welsch et al. 2018).

A specific system design is defined by the following parameters:

- size of the CHP, specified by the coefficient of share of cogeneration α_{CHP}
- size of the STC field, specified by the collector area A_{STC}
- size of the BTES, specified by the length L_{BHE} of the BHEs, while the number of BHEs N_{BHE} is kept constant at 37[1]

---

[1] The number of 37 BHEs originates from a circular alignment of the BHEs (see Welsch et al. 2016)

A GB is assumed in every system configuration to provide either the remaining capacity, which is not covered by the other technologies or at least back-up capacity to secure the supply. Accordingly, its capacity depends on the other three technologies and is calculated automatically. The size of the HP, which is needed to support the BTES system, is automatically determined as well, in accordance with the size of the storage system. Since the DH grid itself is assumed to be identical for all system designs, it is excluded from the assessment and only characterized by a synthetic load profile.

The assessment procedure for a specific system configuration can be divided into two substeps: Initially, based on the preset component sizes and the load profile of the DH gird, the simulation of the heating system is conducted. Subsequently, the energy flows and component sizes that are preset or derived from the simulation are used in a life cycle approach to calculate economic and environmental key figures (Figure 26). To this end, an economic and environmental scenario (ECO scenario) has to be defined, which determines the economic and environmental boundary conditions (e.g. heat and electricity prices, emission factors, technology subsidies etc.) and their supposed temporal change over the period of consideration.
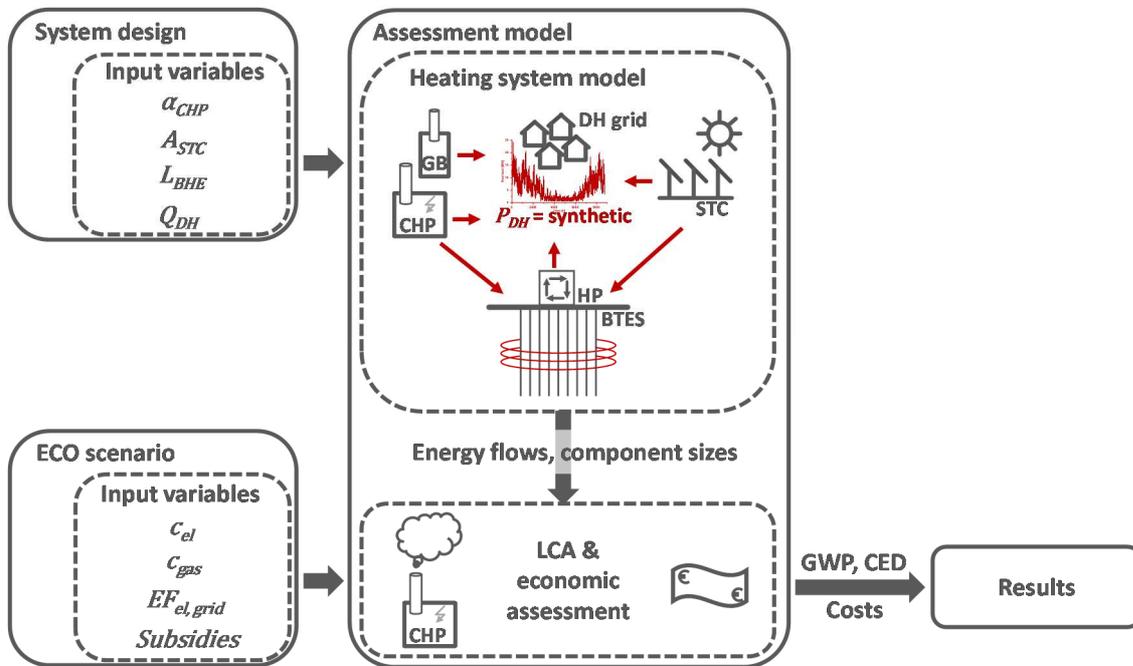
Figure 26: Schematic illustration of the assessment procedure (Welsch et al. 2018).

5.1   Heating System Model

The heating system is modeled by means of an energy balance calculation. First of all, the period under consideration a_{end} has to be defined (e.g. 30 years) and the annual heat demand of the grid must be set. On the basis of ambient temperature data, a load curve with an hourly resolution is generated. Furthermore, using the given collector size A_{STC} and a specific collector output curve p_{STC}, a profile for the heat supplied by the STC field is calculated. Moreover, the nominal thermal power of the CHP is determined according to the given share in the peak load demand α_{CHP}.

Subsequently, the heat balance is calculated according to the supply and demand curves, the nominal power of the CHP and the BTES charging and discharging behavior for every hour of the simulation period. The conditions given in Table 4 define, whether a component of the

system is producing heat or not and whether the seasonal storage system is charged or discharged. An explicit order of priority for the feed-in of the different heat sources into the DH grid is predefined: if available, solar thermal energy has priority over cogenerated heat. This ensures that the most environmentally friendly heat is utilized first. Then, cogenerated heat, which has a higher exergy, is favored over the low exergy heat from the storage system. Lastly, the difference between the heat demand and the heat supplied by the other technologies is compensated by the GB. In case the potential heat production from the CHP and/or the STC field outvalues the head demand, excess heat is transferred to the BTES system taking into account the storage system's current filling level. If not all of the heat from the CHP can be fed in the DH grid or the BTES system, the CHP has to operate at partial load, which is more inefficient than full load operation.

An example illustrates the approach: On a specific day, the heat demand P_{DH} is larger than the heat supply by the STCs P_{STC} (case 1, Table 4). All of the solar heat is fed directly into the DH grid. Furthermore, the heat demand P_{DH} is smaller than the sum of the supplied solar heat and the nominal heat supply by the CHP $P_{CHP,nom}$ (case 1.2, Table 4). Then, only a fraction of the CHP's nominal capacity $P_{CHP,dir}$ is needed to fully satisfy the heat demand of the DH grid. The GB as well as the BTES are not contributing to the provision of heat. The heat surplus from the CHP can be used to charge the BTES. However, if it exceeds the maximum possible heat storage rate $P_{BTES,chg,max}$ (case 1.2.2 Table 4), the potential of the CHP cannot be completely exhausted. It has to be operated in partial load.

The outcome of the energy balance model are hourly values of the thermal power P of each technology. These values are then used to determine the hourly natural gas consumption of the CHP and the GB as well as the electrical power output of the CHP. Furthermore, the auxiliary electricity for e.g. the operation of circulation pumps and the HP is determined according to either the components' size or the power values as well. The specific operational behavior of each system component, after which the energy supply and demand values are determined, is described in the Chapters 5.1.1 to 5.1.6 in more detail.

However, the cost analysis as well as the LCA are based on annual energy amounts. For this purpose, the sum of the respective hourly power values for each system component or energy source P provides the annual energy amounts Q_a (Equation (13)).

$$Q_a = \int P \, dt \tag{13}$$

For each energy quantity of interest, the output of the heating system model comprises a column vector Q from the size $(a_{end} + 1)$ as shown in Equation (14). The first row represents the year of operation zero, in which the system is assumed to be built. Any other rows contain an energy amount for each year of operation.

$$Q = \begin{bmatrix} 0 \\ Q_1 \\ Q_2 \\ \vdots \\ Q_{a_{end}} \end{bmatrix} \tag{14}$$

These energy vectors are passed to the economic and environmental assessment procedures.

Table 4: Conditions of heat supply operation.

1. $P_{DH} \geq P_{STC}$			$P_{STC,dir} = P_{STC}$
	1. $P_{DH} \geq P_{STC} + P_{CHP,nom}$		$P_{CHP} = P_{CHP,dir} = P_{CHP,nom}$
		1. $P_{DH} \geq P_{STC} + P_{CHP,nom} + P_{BTES,dischg,max}$	$P_{BTES,dischg} = P_{BTES,dischg,max}$ $P_{BTES,chg} = 0$ $P_{GB} = P_{DH} - \left(P_{STC} + P_{CHP,nom} + P_{BTES,dischg}\right)$
		2. $P_{DH} < P_{STC} + P_{CHP,nom} + P_{BTES,dischg,max}$	$P_{BTES,dischg} = P_{DH} - \left(P_{STC} + P_{CHP,nom}\right)$ $P_{BTES,chg} = 0$ $P_{GB} = 0$
	2. $P_{DH} < P_{STC} + P_{CHP,nom}$		$P_{CHP,dir} = P_{DH} - P_{STC}$ $P_{BTES,dischg} = 0$ $P_{GB} = 0$
		1. $P_{BTES,chg,max} \geq P_{CHP,nom} - P_{CHP,dir}$	$P_{CHP} = P_{CHP,nom}$ $P_{BTES,chg} = P_{CHP,nom} - P_{CHP,dir}$
		2. $P_{BTES,chg,max} < P_{CHP,nom} - P_{CHP,dir}$	$P_{CHP} = P_{CHP,dir} + P_{BTES,chg,max}$ $P_{BTES,chg} = P_{BTES,chg,max}$
2. $P_{DH} < P_{STC}$			$P_{STC,dir} = P_{DH}$ $P_{CHP,dir} = 0$ $P_{BTES,dischg} = 0$ $P_{GB} = 0$
	1. $P_{BTES,chg,max} \geq (P_{STC} - P_{STC,dir}) + P_{CHP,nom}$		$P_{CHP} = P_{CHP,nom}$ $P_{BTES,chg} = (P_{STC} - P_{STC,dir}) + P_{CHP,nom}$
	2. $P_{BTES,chg,max} < (P_{STC} - P_{STC,dir}) + P_{CHP,nom}$		$P_{BTES,chg} = P_{BTES,chg,max}$
		1. $P_{BTES,chg,max} \geq (P_{STC} - P_{STC,dir})$	$P_{CHP} = P_{BTES,chg,max} - (P_{STC} - P_{STC,dir})$
		2. $P_{BTES,chg,max} < (P_{STC} - P_{STC,dir})$	$P_{CHP} = 0$

5.1.1 Generation of Synthetic Load Profiles

The load profile is generated according to the approach after Hellwig (2003) as given in BDEW/VKU/GEODE (2013), which is normally used by gas providers in order to predict the gas demand of their gas grid as a function of the temperature forecast. However, it can also be used to estimate the heat demand of a certain consumer structure in dependence of an ambient temperature curve. Consequently, the tool needs ambient temperature data with hourly temperature values, for example from a test reference year (TRY) dataset as input parameter. Moreover, the consumer structure can be characterized in more detail by specifying the share of single family homes, multi-family homes and commercial buildings that are connected to the DH grid. The resulting hourly load curve (an example is given in Figure 27) is repeated for the whole period under consideration.
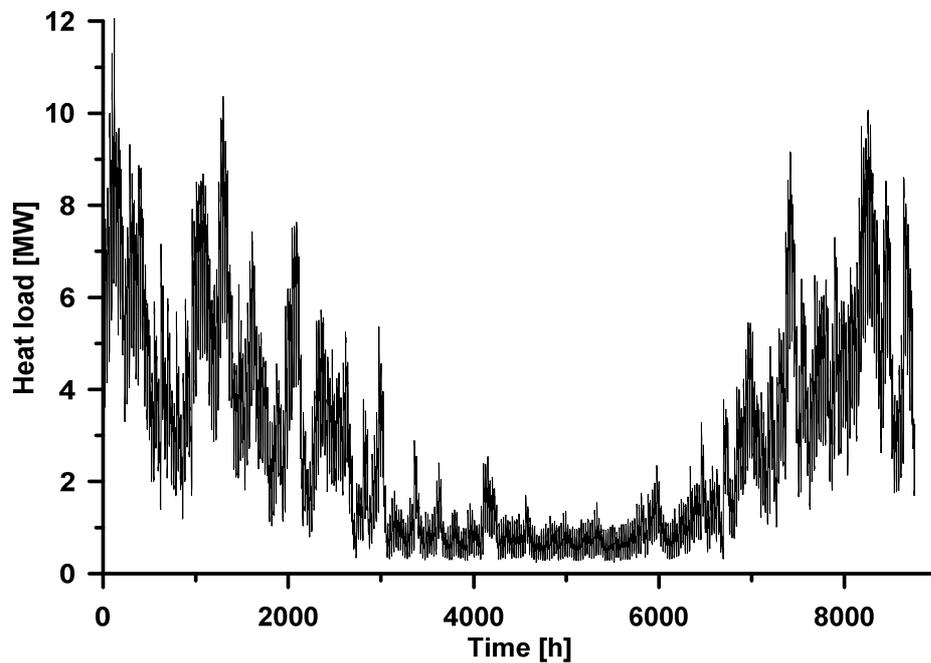
Figure 27: Exemplary synthetic hourly load profile for a DH grid in Germany with an annual heat demand of 25 GWh (Welsch et al. 2018, supplementary material).

5.1.2 Solar Thermal System

To describe the output of the STC field, first of all, a specific collector output curve p_{STC} was generated in advance. Therefore, a numeric simulation of a reference collector was carried out deploying the *Carnot-Toolbox* (Solar-Institute Jülich 2016) for *MATLAB Simulink* (The MathWorks Inc. 2016b). The simulation was based on solar radiation and ambient temperature values for the same year as the calculation of the DH grid's load demand. p_{STC} describes the thermal output of one square meter of STC for each hour of the year. However, the STC field is assumed to be equipped with an additional diurnal storage tank, in order to buffer peaks in the solar thermal energy production. To take this buffer effect into account, the thermal heat supplied by the STC is averaged to daily values. The total power output $P_{th,STC}$ of an STC field with a collector area A_{STC} is calculated by Equation (15).

$$P_{th,STC} = p_{STC} \cdot A_{STC} \qquad (15)$$

5.1.3 Combined Heat and Power Plant

The required nominal thermal power output $P_{th,CHP,nom}$ of the CHP is determined according to the input coefficient α_{CHP}, which describes the desired share of cogenerated heat in the peak load demand (Equation (16)).

$$P_{th,CHP,nom} = \alpha_{CHP} \cdot P_{DH,peak} \tag{16}$$

To account for scale effects, the thermal efficiency $\eta_{th,CHP,nom}$ and electrical efficiency $\eta_{el,CHP,nom}$ of the CHP modules at nominal power output depend on the size of the modules according to figures given in ASUE (2011). Both values are needed to relate the nominal electrical power output $P_{el,CHP,nom}$ to $P_{th,CHP,nom}$ according to Equation (17).

$$P_{el,CHP,nom} = P_{th,CHP,nom} \cdot \frac{\eta_{el,CHP,nom}}{\eta_{th,CHP,nom}} \tag{17}$$
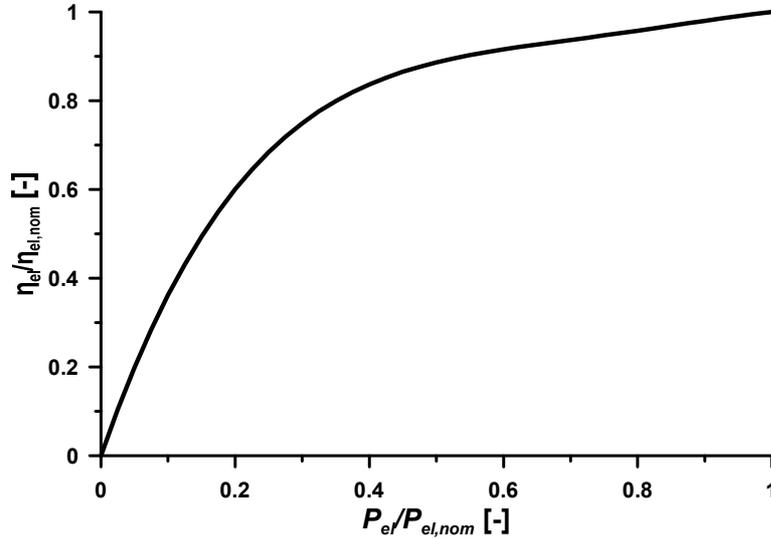
Figure 28: Assumed decrease of the relative electrical efficiency of a CHP module in partial load operation (Welsch et al. 2018, supplementary material).

Particular importance has to be ascribed to the part-load performance of the CHP. Both, the thermal efficiency $\eta_{th,CHP}$ and the electrical efficiency $\eta_{el,CHP}$ of a CHP module change in partial load operation. The electrical efficiency diminishes with decreasing load. Thus, a set of corresponding partial load share and efficiency values for a specific internal combustion engine ICE (EPA 2015) is normalized (Figure 28). A fourth order polynomial fit of these normalized values is given in Equation (18). It provides an algebraic expression of sufficient quality ($R^2 = 0.9976$) to calculate $\eta_{el,CHP}$ as a function of $\eta_{el,CHP,nom}$ and the partial load share γ_{CHP}, which is calculated after Equation (19).

$$\eta_{el,CHP} = \eta_{el,CHP,nom} \cdot (-2.2092 \cdot \gamma_{CHP}{}^4 + 6.9477 \cdot \gamma_{CHP}{}^3 - 8.1005 \cdot \gamma_{CHP}{}^2 + 4.3625 \cdot \gamma_{CHP}) \tag{18}$$

$$\gamma_{CHP} = \frac{P_{th,CHP}}{P_{th,CHP,nom}} \tag{19}$$

However, the thermal efficiency increases with decreasing load. It is assumed that this increase compensates the electrical efficiency drop so that Equation (20) is valid. This in turn implicates, that the overall efficiency $\eta_{tot,CHP}$ of the CHP stays constant.

$$\eta_{tot,CHP} = \eta_{th,CHP,nom} + \eta_{el,CHP,nom} = const. \tag{20}$$

With this assumption, the thermal partial load efficiency is determined by Equation (21).

$$\eta_{th,CHP} = \eta_{tot,CHP} - \eta_{el,CHP} \tag{21}$$

Given the efficiencies in the partial load operation, the electrical output $P_{el,CHP}$ as well as the natural gas consumption $P_{gas,CHP}$ can be calculated for every operating point by Equation (22) and (23), respectively.

$$P_{el,CHP} = P_{th,CHP} \cdot \frac{\eta_{el,CHP}}{\eta_{th,CHP}} \tag{22}$$

$$P_{gas,CHP} = P_{th,CHP} \cdot \frac{1}{\eta_{th,CHP}} \tag{23}$$

The electricity consumption $P_{el,CHP,per}$ of peripheral devices like the air supply system, the fuel gas compressor etc. is estimated according to standard values given by Schaumann & Schmitz (2010). To receive the net electrical output $P_{el,CHP,net}$ of the CHP, which is fed into the electricity grid, $P_{el,CHP,per}$ has to be subtracted from the electrical output $P_{el,CHP}$ (Equation (24)).

$$P_{el,CHP,net} = P_{el,CHP} - P_{el,CHP,per} \tag{24}$$

5.1.4 Medium Deep Borehole Thermal Energy Storage System

The comprehensive dataset from the previously conducted numerical parameter study (Appendix B) provides all relevant input parameters to approximate the storage behavior during operation: the storage efficiency is derived according to the storage dimensions and year of operation, whereas the storage charging and discharging rate as well as the fluid outlet temperature during discharge operation are both calculated as a function of the storage dimensions and the respective storage filling level at each point in time. The approach shall be explained in the following.

Each numerical storage simulation provided a heat budget of the storage operation. An example is given in Figure 29 (upper graph). From this heat budget, the amount of stored $Q_{S,a}$ and extracted heat $Q_{E,a}$ were calculated for each year a of operation according to Equations (25) and (26).

$$Q_{S,a} = Q_{max,a} - Q_{min,a-1} \tag{25}$$

$$Q_{E,a} = Q_{min,a} - Q_{max,a} \tag{26}$$
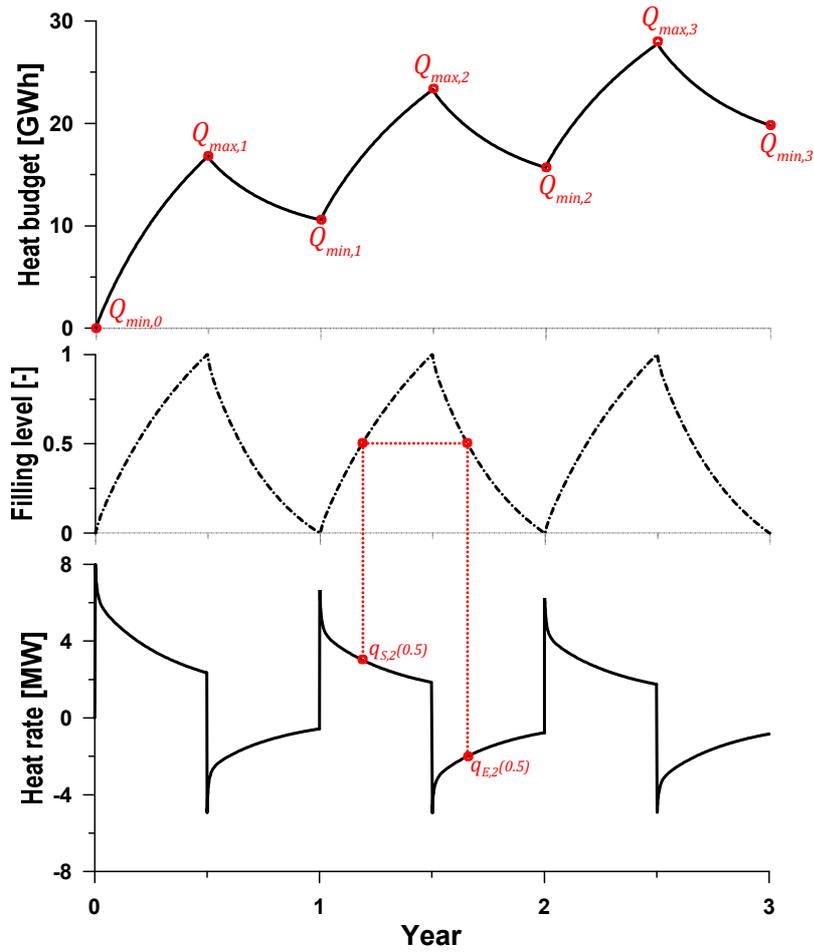
Figure 29: Heat budget, filling level and heat rate derived from the numerical simulation of an MD-BTES system (data from Welsch et al. 2016).

Indeed, the numerical simulations accomplished as part of Appendix B reflect very simple operational conditions. The BTES systems were operated in charging and discharging cycles of 6 months and under constant inlet temperatures. In order to deduce information from this very steady operation scenario about the storage behavior under more transient conditions, the storage filling level was introduced as an auxiliary quantity.

For this purpose, it is assumed that during each year of operation, the storage had been completely charged and completely discharged. Consequently, for each sample point in time t of a respective year of operation, the storage filling level θ (Figure 29, middle graph) could be calculated for the respective storage and extraction period according to Equations (27) and (28).

$$\theta_{S,a}(t) = \frac{(Q(t) - Q_{min,a-1})}{Q_{S,a}} \tag{27}$$

$$\theta_{E,a}(t) = \frac{(Q_{min,a} - Q(t))}{Q_{E,a}} \tag{28}$$

The numerical simulations of the BTES system also provided the heat rate $q(t)$, by which the storage system was charged or discharged (Figure 29, lower graph). Accordingly, datasets containing the filling level as well as the corresponding charging heat rate $q_{S,a}(\theta_{S,a})$ and the discharging rate $q_{E,a}(\theta_{E,a})$, respectively, could be compiled for each year of operation. These datasets were used as input parameters for the heating system model. During the heating system

simulation a storage filling level is calculated before each time step. To gain the corresponding charging and discharging rate, a linear interpolation between the available data points is conducted. The derived values for the charging and discharging heat rate restrict the storage operation in the subsequent time step. The fluid outlet temperature during discharge operation is approximated in the same manner. Values for borehole lengths, which were not represented in the experimental design of the numerical study, are interpolated linearly as well.

5.1.5 Heat Pump

The size of the HP is chosen depending on the desired storage discharge rate. Its electricity consumption is calculated with respect to the HP's COP. It is defined as the ratio of the HP's thermal power output to its electrical power input. Therefore, the electrical power input can be calculated from Equation (29).

$$P_{el,HP} = \frac{P_{th,HP}}{COP} \tag{29}$$

The COP is estimated using the simple Carnot model given in Equation (30) that can be found in several thermodynamic textbooks (e.g. Fischer & Madani 2017).

$$COP \approx \eta_{HP} \cdot \frac{T_{DH,supply}}{T_{DH,supply} - T_{BTES,out}} \tag{30}$$

All losses that lead to an impairment from the Carnot cycle efficiency are lumped together in the efficiency factor η_{HP}. It is set to the typical value of 0.5. While the fluid outlet temperature of the storage $T_{BTES,out}$ is variable according to the data set of Welsch et al. (2016, Appendix B), the supply temperature of the DH grid $T_{DH,sup}$ is kept constant at a default value.

5.1.6 Gas Boiler

Finally, the load supply of the natural gas boiler is computed. It is designed to cover the maximum difference between the heat demand and the sum of the thermal outputs of the CHP, the solar collectors as well as the HP assisted MD-BTES. In addition to that, it can be defined that the peak load boiler has to provide backup capacity to increase the reliability of the system. The natural gas consumption of the boiler $P_{gas,GB}$ is calculated by Equation (31).

$$P_{gas,GB} = P_{th,GB} \cdot \frac{1}{\eta_{th,GB}} \tag{31}$$

5.2 Cost Analysis

To value the economic output of a specific system design, the approach of levelized cost of heat ($LCOH$, Short et al. 1995; Moomaw et al. 2011) is applied. The $LCOH$ represents the financial mathematic average for the specific cost of the heat in Eurocent per Kilowatt-hour over the assumed period under consideration a_{end}. It is calculated according to Equation (32) from the net present value, which consists of the investment costs I, maintenance costs M, operation costs F (i.e. fuel/electricity costs), the revenue R of the system and the assumed interest rate r, and is divided by the system's discounted thermal energy output Q.

$$LCOH = \frac{\sum_{a=0}^{a_{end}}((I_a + M_a + F_a - R_a) \cdot (1+r)^{-a})}{\sum_{a=0}^{a_{end}}(Q_a \cdot (1+r)^{-a})} \cdot 100 \tag{32}$$

Evidently, investment costs arise at the beginning $a = 0$. However, if the period under consideration a_{end} exceeds a component´s lifetime l, the respective investment occurs again in the year after the lifetime is reached. In return, a salvage value S (residual value) is deducted at the end, if the period under consideration is exceeded by a component's lifetime. The respective column vector of the size $(a_{end} + 1)$ has form as shown in Equation (33).

$$I = \begin{bmatrix} I_0 \\ \vdots \\ I_{l+1} \\ \vdots \\ -S \end{bmatrix} \tag{33}$$

While investment costs for each component are estimated according to relationships between cost and component size, which were found in literature or developed from cost data, operation costs and revenues are calculated on the basis of the energy vectors provided by the heating system simulation. For this purpose, data with the assumed specific energy prices is stored in column vectors of the size $(a_{end} + 1)$ as shown in Equation (34), which contain a zero in the year of installation and an energy price c_a for each year a of operation in the subsequent rows:

$$c = \begin{bmatrix} 0 \\ c_1 \\ c_2 \\ \vdots \\ c_{a_{end}} \end{bmatrix} \tag{34}$$

Consequently, the element-wise multiplication of a c-vector with the dedicated Q-vector from the heating simulations gives the corresponding vectors for the energy costs F and revenues R, respectively (Equation (35)).

$$F = \begin{bmatrix} 0 \\ F_1 \\ F_2 \\ \vdots \\ F_{a_{end}} \end{bmatrix}, \qquad R = \begin{bmatrix} 0 \\ R_1 \\ R_2 \\ \vdots \\ R_{a_{end}} \end{bmatrix} \tag{35}$$

Maintenance costs are estimated as a percentage of the investment costs, except for the CHP, where they are estimated in dependence of the electric power and the produced electricity. As maintenance costs only apply during the operation of the system, the respective column vector has the form shown in Equation (36).

$$M = \begin{bmatrix} 0 \\ M_1 \\ M_2 \\ \vdots \\ M_{a_{end}} \end{bmatrix} \tag{36}$$

The following subchapters describe the appraisement of the different cost factors for each technology in detail.

5.2.1 Solar Thermal System

Investment Costs

The initial investment costs for the STCs are estimated using a formula (Equation (37)) for the specific costs of ground-mounted collectors given by Mauthner & Herkel (2016). This cost function includes the expenses for a diurnal heat storage.

$$I_{STC} = (598700 \cdot A_{STC}^{-1.021} + 190) \cdot A_{STC} \tag{37}$$

Maintenance and Operation Costs

Likewise, the annual maintenance and electricity costs for the circulation pump are estimated according to figures for ground-mounted solar thermal systems connected to DH grids (Equations (38) and (39)) also given by Mauthner & Herkel (2016).

$$M_{STC,a} = 0.0075 \cdot I_{STC} \tag{38}$$

$$F_{STC,a} = c_{el,a} \cdot 0.015 \cdot Q_{th,STC,a} \tag{39}$$

5.2.2 Combined Heat and Power Plant

Investment and Maintenance Costs

The specific investment and maintenance costs for a single CHP module are calculated according to ASUE (2011) and respectively multiplied by the total nominal power output and the amount of produced electricity according to Equations (40) and (41).

$$I_{CHP} = (9332.6 \cdot P_{el,CHP,mod}^{-0.4611}) \cdot P_{el,CHP,nom} \tag{40}$$

$$M_{CHP,a} = (2.3133 \cdot P_{el,CHP,mod}^{-0.141}) \cdot Q_{el,CHP,a} \tag{41}$$

Operation Costs and Revenues

The operation costs of the CHP plant are derived from the gas price and the equivalent energy amount of consumed gas, whereas the revenue is defined by the electricity price and the amount of sold electricity (Equations (42) and (43)).

$$F_{CHP.a} = c_{gas,a} \cdot Q_{gas,CHP,a} \tag{42}$$

$$R_{CHP,a} = c_{el,a} \cdot Q_{el,CHP,net,a} \tag{43}$$

According to the German Act on Combined Heat and Power Generation (KWKG 2016) , electricity produced by CHP plants has to be prioritized over conventionally produced electricity in feed-in, transfer and distribution. Thus, it is assumed that all the electricity produced by the CHP can be sold to the grid at any time.

5.2.3 Medium Deep Borehole Thermal Energy Storage System

Investment Costs

Since empirical cost data for MD-BTES systems was lacking, a profound cost estimation had to be carried out. The investment costs depend mainly on three factors: 1) costs for the drilling site facilities I_{st}, including the transport and erection of the derrick, 2) costs for the BHEs, which are composed of the drill costs I_{dr}, the pipe costs I_{pp} as well as the costs for the grouting I_{gr}

and 3) costs for relocating the derrick to the next drill position I_{rel}. Considering the number of BHEs N_{BHE}, this results in Equation (44).

$$I_{BTES} = I_{st} + N_{BHE} \cdot (I_{dr} + I_{pp} + I_{gr}) + (N_{BHE} - 1) \cdot I_{rel} \qquad (44)$$

Due to the straightness of the bore path and comparatively moderate prices for the targeted depths, the hydraulic down-the-hole hammer technology (e.g. Homuth et al. 2016) has been identified as the most suitable drilling method for the construction of MD-BTES systems (Schulte 2016).
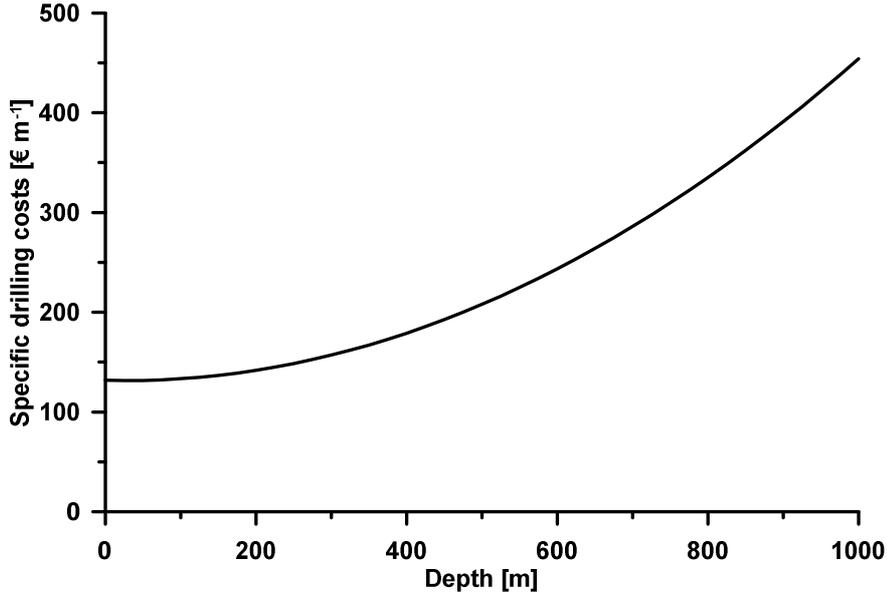
Figure 30: Assumed depth-dependency of the drilling costs (Welsch et al. 2018, supplementary material).

As this drilling technology is deployed only occasionally, the specific drill costs c_{drill} are estimated according to Equation (45), which is derived from confidential quote from an industrial partner and describes the increase of the specific costs with depth z of the borehole (Figure 30).

$$c_{dr}(z) = 0.00034 \cdot z^2 - 0.0176 \cdot z + 131.7 \qquad (45)$$

Using this correlation, the total costs for one borehole can be computed by Equation (46).

$$I_{dr} = \int_0^{L_{BHE}} c_{dr}(z) dz \qquad (46)$$

The costs for the steel casing (sc), the inner pipe (ip) and the grout as given in Equations (47) and (48) depend on the specific prices for the piping and grouting material, as well as the borehole length.

$$I_{pp} = (c_{sc} + c_{ip}) \cdot L_{BHE} \qquad (47)$$

$$I_{gr} = c_{gr} \cdot A_{an} \cdot L_{BHE} \qquad (48)$$

A_{an} in Equation (48) represents the cross sectional area of the annular space that has to be backfilled.

For I_{st} and I_{rel} lumped sums amounting to 40,000 € and 2,500 €, respectively, are used.

Maintenance and Operation Costs

BHE systems generally require very little maintenance during their design operational time. For this reason, it is assumed that the maintenance costs can be neglected. In addition to that, the operational costs are composed solely of the electricity costs for the operation of the circulating pumps according to Equation (49).

$$F_{BTES,a} = c_{el,a} \cdot Q_{el,CP,a} \tag{49}$$

The electricity consumption $Q_{el,CP,a}$ takes into account the pressure loss of the fluid in the BHE pipes, which is calculated for the according MD-BTES system.

5.2.4 Heat Pump

Investment Costs

The investment costs for the HP are estimated using the correlation given in Croteau & Gosselin (2015). Assuming the given reference *COP* and converting the figures into Euro (1 USD = 0.9°EUR), Equation (50) is obtained.

$$I_{HP} = (2053.8 \cdot P_{th,HP,nom}^{-0.348}) \cdot P_{th,HP,nom} \tag{50}$$

Maintenance and Operation Costs

Like for the STC, the HP's annual maintenance costs are expected to be 0.75% of its investment value and the operation costs depend on the electricity price and the amount of consumed electricity according to Equations (51) and (52).

$$M_{HP,a} = 0.0075 \cdot I_{HP} \tag{51}$$

$$F_{HP,a} = c_{el,a} \cdot Q_{el,HP,a} \tag{52}$$

5.2.5 Gas Boiler

Investment Costs

Finally, the investment costs for the boiler are estimated using cost figures (Equation (53)) for hot water boilers without exhaust gas heat exchangers (Gebhardt et al. 2002), where f_{GB} (Equation (54)) is the correction factor for gas firing:

$$I_{GB} = (11418.60 + 64.6115 \cdot P_{th,GB,nom}^{0.7978}) \cdot f_{GB} \tag{53}$$

$$f_{GB} = 1.0818 - 8.2898 \cdot 10^{-7} \cdot P_{th,GB,nom} \tag{54}$$

Maintenance and Operation Costs

While the annual maintenance costs as given in Equation (55) are expected to be 2% of the investment costs, the operation costs are calculated on the basis of the GB's annual gas consumption and the gas price according to Equation (56).

$$M_{GB,a} = 0.02 \cdot I_{GB} \tag{55}$$

$$F_{GB,a} = c_{gas,a} \cdot Q_{gas,GB,a} \tag{56}$$

5.3 Life Cycle Assessment

In the following, the substeps of an LCA study, as introduced in Chapter 2.3, are elucidated for the LCA procedure, which is integrated in the assessment tool. However, not all of the pre-scribed contents can be already defined, as they strongly depend on a specific study, which is conducted with the assessment tool (e.g. Appendix G). Instead, a focus is set to the implementation of the procedure in *MATLAB*. The strongly related LCI and LCIA steps are condensed to one subchapter.

5.3.1 Goal and Scope Definition

The LCA conducted within the assessment tool allows for an evaluation of the environmental burdens connected to the particular DH design. In this context, the functional unit is defined as the total heat amount delivered to the DH grid over the period under consideration. By default, it is assumed that the DH grid is located in Germany. However, by changing the respective input parameters, the assessment tool can easily be applied to other countries or regions as well.

Since the DH grid itself is not evaluated by the tool, the pipe production and installation steps concerning the construction of the grid are not analyzed. Moreover, transportation of goods is only considered in terms of raw material transport, which is already taken into account in the applied datasets. The transportation from production site to the system location is not included as it is expected to have just a minor effect on the overall results. Aside from that, the disposal phase (end-of-life) of the components is disregarded as well. This is a common practice in many LCA: first of all, it is assumed that the impact of the disposal phase is negligible compared to the production and use phase, and secondly, recycling processes may advance and are therefore difficult to predict. Another argument for this approach is that the subsurface installations of BTES systems have a much longer life time expectation than 30 years and reliable data about the dismantling of BTES is not available, yet. Besides, disregarding the end-of-life phase represents a conservative approach, as recycling usually leads to a reduction of an environmental impact of a system.

The main focus of the tool is to assess the impact of different DH systems on global warming. For this purpose, the midpoint impact category global warming potential (GWP) according to CML 2002 (Guinée 2002) is chosen: a specific GHG is characterized by the intensity to which a released unit mass of the gas absorbs infrared radiation in the atmosphere over a defined time interval (here 100 years) and thereby contributes to global warming (Bauman & Tillman 2004). To obtain the GWP of the GHG, this physical property is normalized to the respective value for CO_2. Consequently, the GWPs for different substances are comparable and can be added up to a comprehensive category indicator.

In addition to the global warming problematic, energy and resource efficiency are important characteristics of energy systems. When regarding DH systems, energy consumption is expected to play a much more important role than material resources. Therefore, the cumulative energy demand (CED) is used as an indicator in this context. In our case, it adds up all energy expenditures that are required to provide a certain amount (the functional unit) of heating energy.

Another major environmental impact of BTES systems is their potentially negative effect on the groundwater quality due to a rise in groundwater temperature (Chapter 1.2). As shown in Chapter 4, the temperature increase in the subsurface can be determined for example from

numerical simulations. However, the environmental impacts associated with a certain temperature increase are very difficult to quantify. There are no suitable characterization methods available, basically because the magnitude of the effects is strongly depend on site-specific conditions such as the present groundwater chemistry and the geology. Consequently, this impact category has to be omitted in the LCA approach.

5.3.2 Life Cycle Inventory and Impact Assessment

Initially, several datasets were compiled, which describe the environmental burdens connected to the production phase of the respective system components. To this end, the software OpenLCA (GreenDelta GmbH 2017) was employed, incorporating the following databases: *ecoinvent 3.1 cutoff* (Wernet et al. 2016), *GaBi 5* (Thinkstep AG 2011) and *Gemis 4.93* (IINAS 2016). The gathered data was evaluated with regard to its applicability. Finally, suitable datasets were adapted for our approach. They were normalized to either the nominal power (CHP, GB, HP) or the size (STC, MD-BTES) of the respective component in order to facilitate the inclusion of the LCA data into the assessment tool.

The environmental impact during the use phase basically results from the combustion of natural gas and electricity consumption. Furthermore, if cogenerated electricity replaces grid electricity, the system receives credits. Therefore, these burdens and credits are assessed on the basis of the gas consumption and electricity consumption or production of the respective system component.

For each component i of the system, the figures for the GWP and the CED are calculated separately according to Equations (57) and (58).

$$GWP_i = \sum_{a=0}^{a_{end}} (GWP_{i,prod,a} + GWP_{i,op,a}) \tag{57}$$

$$CED_i = \sum_{a=0}^{a_{end}} (CED_{i,prod,a} + CED_{i,op,a}) \tag{58}$$

$GWP_{prod,a}$ and $CED_{prod,a}$ are the values for the production phase, $GWP_{op,a}$ and $CED_{op,a}$ the values for each year a of operation (use phase).

The calculations in the *MATLAB* tool are accomplished in the same manner as in the calculation of the economic figures. They are based on column vectors of the size $(a_{end} + 1)$ for each technology, which contain the annual flows of the respective unit. For the production phase the vectors look as shown in Equation (59).

$$GWP_{i,prod} = \begin{bmatrix} GWP_{i,prod,0} \\ \vdots \\ GWP_{i,prod,l+1} \\ \vdots \\ -GWP_{i,res} \end{bmatrix}, \qquad CED_{i,prod} = \begin{bmatrix} CED_{i,prod,0} \\ \vdots \\ CED_{i,prod,l+1} \\ \vdots \\ -CED_{i,res} \end{bmatrix} \tag{59}$$

Where GWP_{res} and CED_{res} represent residual values, which are taken into account at the end, when a component's lifetime exceeds the period under consideration. Correspondingly, additional values for the production phase will be considered in certain years, if a component's lifetime is shorter than the period under consideration.

The impact figures for the operation phase are calculated taking into account the energy flow vectors for each component provided by the heating simulation. Therefore, time series of the emission factors for natural gas (EF_{gas}) and grid electricity (EF_{el}) as well as the cumulative energy demand for natural gas CED_{gas} and grid electricity CED_{el} are read in as column vectors as shown in Equations (60) and (61)[2].

$$EF_{gas} = \begin{bmatrix} 0 \\ EF_{gas,1} \\ EF_{gas,2} \\ \vdots \\ EF_{gas,a_{end}} \end{bmatrix}, \qquad EF_{el} = \begin{bmatrix} 0 \\ EF_{el,1} \\ EF_{el,2} \\ \vdots \\ EF_{el,a_{end}} \end{bmatrix}, \tag{60}$$

$$CED_{gas} = \begin{bmatrix} 0 \\ CED_{gas,1} \\ CED_{gas,2} \\ \vdots \\ CED_{gas,a_{end}} \end{bmatrix}, \qquad CED_{el} = \begin{bmatrix} 0 \\ CED_{el,1} \\ CED_{el,2} \\ \vdots \\ CED_{el,a_{end}} \end{bmatrix}, \tag{61}$$

These values represent specific values for the emissions and the cumulative energy demand, associated with the consumption, production and transportation of the energy carrier and refer to the deliverance of one kWh of energy. Consequently, their units are [kg CO_2eq kWh^{-1}] and [MJ kWh^{-1}], respectively. These vectors are multiplied element-wise with the energy flow vectors for each component to derive the respective flow vectors for the operation phase as shown in Equation (62).

$$GWP_{i,op} = \begin{bmatrix} 0 \\ GWP_{i,op,1} \\ GWP_{i,op,2} \\ \vdots \\ GWP_{i,op,a_{end}} \end{bmatrix}, \qquad CED_{i,op} = \begin{bmatrix} 0 \\ CED_{i,op,1} \\ CED_{i,op,2} \\ \vdots \\ CED_{i,op,a_{end}} \end{bmatrix} \tag{62}$$

Finally, the GWP and the CED of the overall system are then simply the sums of the components' individual impact over the n different components that make up the system according to Equation (63).

$$GWP = \sum_{i=1}^{n} GWP_i, \qquad CED = \sum_{i=1}^{n} CED_i \tag{63}$$

Besides the GWP and the CED, the emission factor (EF) for the produced heat is evaluated to allow for comparison with differently sized systems. It is defined as the ratio of summarized GWP values for production and operation of each component to the overall heat production of the according system as given in Equation (64) and has the unit [kg CO_2eq kWh^{-1}].

$$EF = \frac{GWP}{Q_{th,tot}} \tag{64}$$

---

[2] It should be noticed at this point that the EFs and $CEDs$ for gas and the grid electricity mix depend on the region or country that is considered in a specific study (e.g. Germany in Appendix G). Consequently, these are input parameters, which have to be defined and referenced in the specific study that is conducted with the assessment tool. Thus, these parameters and their data source cannot be specified here.

A more detailed description of data sources and data handling for each component as well as individual calculation rules are given in the following subchapters, separated into production and use phase. As already explained in the goal and scope definition (Chapter 5.3.1) the end-of-life phase is not taken into account.

5.3.2.1 Solar Thermal System

Production Phase

The production process of the solar thermal system is evaluated by using the *Ecoinvent* dataset *"solar collector system installation, Cu flat plate collector, one-family house, combined system"*. It includes all relevant parts and their assembly, and considers the installation of the collectors. The dataset also contains an HP and a storage system. Since both are assessed separately, these components are removed from the dataset.

Furthermore, all parameters are scaled according to a change of the functional unit from 12.5 m² to 1 m² in order to normalize the dataset. The resulting data is integrated into the evaluation process, assuming a linear correlation between collector size and environmental burdens. Consequently, the GWP and CED for the production results in Equations (65) and (66).

$$GWP_{prod,STC} = 176 \, \frac{kg \, CO_2 eq}{m^2} \cdot A_{STC} \tag{65}$$

$$CED_{prod,STC} = 2320 \, \frac{MJ}{m^2} \cdot A_{STC} \tag{66}$$

Considering that the applied dataset refers to relatively small systems, a linear parametrization neglects positive scaling effects. Consequently, the approach can be regarded as conservative.

Use Phase

The GWP and CED for the use phase is estimated following the simplified assumptions of Mauthner & Herkel (2016) including the emission factor for electricity as given in Equations (67) and (68).

$$GWP_{op,STC} = EF_{el,a} \cdot 0.015 \cdot Q_{th,STC,a} \tag{67}$$

$$CED_{op,STC} = CED_{el,a} \cdot 0.015 \cdot Q_{th,STC,a} \tag{68}$$

5.3.2.2 Combined Heat and Power Plant

Production Phase

The *Ecoinvent* database contains parameters for the production process of several differently sized CHP modules. However, in places the particular datasets differ significantly depending on whether the system includes a catalytic converter or not. Accordingly, the datasets have to be adjusted for comparability. Therefore, if missing a catalytic converter, it is added to the analyzed dataset.

When comparing the $GWPs$ and $CEDs$ of the adjusted CHP module datasets, a non-linear correlation between module size and specific GWP/CED for the production can be identified (Figure 31), which is described by Equations (69) and (70).

$$GWP_{prod,CHP,mod} = 4851 \frac{kg\ CO_2 eq}{kW} \cdot P_{th,CHP,mod}^{0.638} \tag{69}$$

$$CED_{prod,CHP,mod} = 59061 \frac{MJ}{kW} \cdot P_{th,CHP,mod}^{0.641} \tag{70}$$
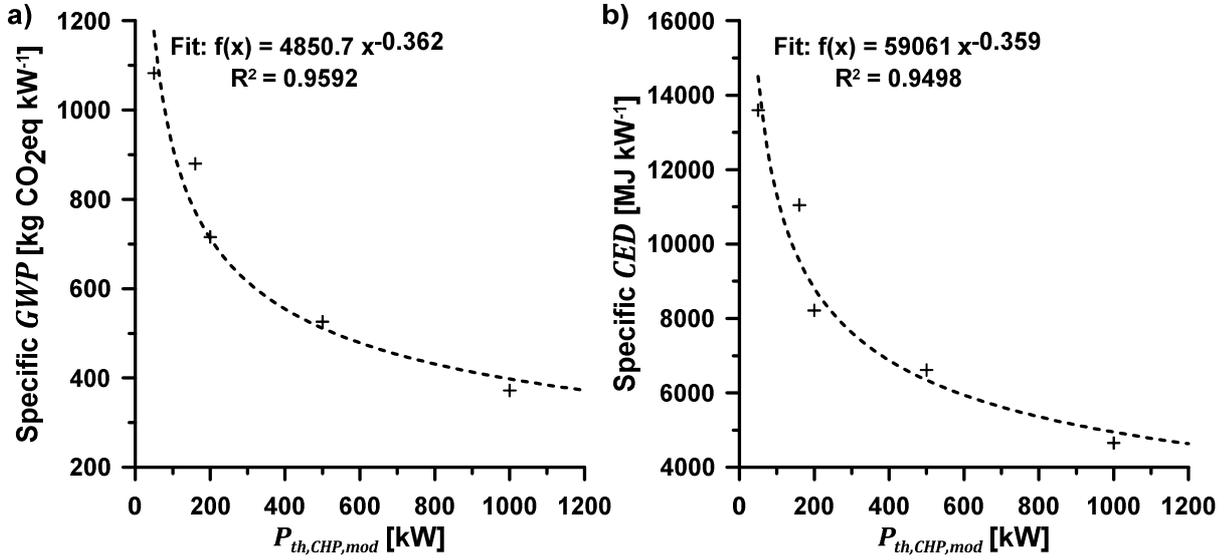
Figure 31: Specific GWP (a) and CED (b) from different CHP datasets dependent on the respective module size and the derived fitting function.

Use Phase

During the use phase, the CHP plant produces heat and electricity by burning gas. In order to avoid allocations of the environmental burden as described in the DIN EN ISO 14040/44 DIN EN ISO 14044 2006; DIN EN ISO 14040 2009, the CHP assessment is expanded by the evaluation of the electricity production. This implies that the CHP-produced electricity is fed into the electricity grid. Hence, two processes have to be evaluated – the gas burning and the replacement of grid electricity. The present grid electricity is rated with the GWP and CED of the assumed grid electricity mix. Combining both processes results in Equations (71) and (72) for the annual GWP and CED of the CHP plant's use phase.

$$GWP_{op,CHP,a} = EF_{gas,a} \cdot Q_{gas,CHP,a} - EF_{el,a} \cdot Q_{el,CHP,net,a} \tag{71}$$

$$CED_{op,CHP,a} = CED_{gas,a} \cdot Q_{gas,CHP,a} - CED_{el,a} \cdot Q_{el,CHP,net,a} \tag{72}$$

5.3.2.3 Medium Deep Borehole Thermal Energy Storage System

Production Phase

The construction of an MD-BTES comprises the drilling process as well as the production of the required materials for the BHEs. These include an outer steel pipe and an inner PE-X pipe (outer diameters: 0.127 m and 0.075 m), a cement based, thermally optimized grouting material and the heat transfer medium (water). Table 5 outlines the considered materials and corresponding *Ecoinvent* flows and processes as well as the materials, masses, the GWP and CED per BHE length.

Table 5: Environmental modeling of the MD-BTES.

BTES part	Material	*Ecoinvent* product flows/ processes	Mass [kg m⁻¹]	*GWP* [kg CO₂eq m⁻¹]	*CED* [MJ kWh⁻¹]
Outer pipe	Steel pipe	· Reinforcing steel · Drawing of pipe, steel	8.63	22.0	255.7
Inner pipe	PE-X pipe	· polyethylene pipe production, corrugated, DN 75	0.72	0.7	22.7
Grouting material	Thermally improved cement	· No standard flow; composition modeled individually[1]	9.2	3.3	17.5
Heat transfer medium	Water	· Water	10.81	0.02	0.3
Total				26.0	296.2

[1] The underlying material composition of the thermally improved cement cannot be particularized here, as it represents confidential information from an industrial partner. The rough composition is as follows: 50% cement, 25% highly thermally conductive additive, 25% filling material.

The fuel consumption of the envisaged hydraulic hammer drilling technology can be as low as one third of the consumption of conventional pneumatic hammer drilling (Homuth et al. 2016). In total terms, a hydraulic hammer drilling rig requires approximately 0.025 m³ h⁻¹ of diesel. Accordingly, the emission rate for the combustion amounts to 63.25 kg CO₂eq per hour. Based on the experience of a previous unpublished hydraulic hammer drilling project monitored by the Department of Geothermal Science and Technology at TU Darmstadt, the required drilling time t_{dr} for a borehole depth L_{BHE} can be estimated according to the empirical relation as given in Equation (73).

$$t_{dr} = 19.8 \cdot e^{0,0036 \cdot L_{BHE}} \tag{73}$$

Considering the number N_{BHE} and length L_{BHE} of the BHEs, the *GWP* and *CED* for the construction of the MD-BTES can be calculated according to Equations (74) and (75).

$$GWP_{prod,BTES} = N_{BHE} \cdot (26.03 \frac{kg\ CO_2\ eq}{m} \cdot L_{BHE} + 63.25 \frac{kg\ CO_2\ eq}{h} \cdot t_{dr}) \tag{74}$$

$$CED_{prod,BTES} = N_{BHE} \cdot (296 \frac{MJ}{m} \cdot L_{BHE} + 68 \frac{MJ}{h} \cdot t_{dr}) \tag{75}$$

Use Phase

The *GWP* and *CED* for the use phase results from the electricity consumption of the circulating pump taking into account the emission factor *EF* of the electricity mix as given in Equations (76) and (77).

$$GWP_{op,BTES,a} = EF_{el,a} \cdot Q_{el,CP,a} \tag{76}$$

$$CED_{op,BTES,a} = CED_{el,a} \cdot Q_{el,CP,a} \tag{77}$$

5.3.2.4 Heat Pump

Production Phase

A 10 kW HP dataset (Greening & Azapagic 2012) is selected from *Ecoinvent*, because it is the only available dataset that contains a detailed list of materials used in the production process. However, the HP is comparatively small and does not fit the size of the system under consideration. As a consequence, a linear correlation between size and GWP/CED as shown in Equations (78) and (79) is presumed, neglecting any positive scaling effects and thus constituting a conservative approach.

$$GWP_{prod,HP} = 58.5 \frac{kg\ CO_2eq}{kW} \cdot P_{el,HP,nom} \tag{78}$$

$$CED_{prod,HP} = 848 \frac{MJ}{kW} \cdot P_{el,HP,nom} \tag{79}$$

Use Phase

For the use phase, the GWP and CED is calculated from the electricity consumption for driving the HP and the EF for electricity according to Equations (80) and (81).

$$GWP_{op,HP,a} = EF_{el,a} \cdot Q_{el,HP,a} \tag{80}$$

$$CED_{op,HP,a} = CED_{el,a} \cdot Q_{el,HP,a} \tag{81}$$

5.3.2.5 Gas Boiler

Production Phase

The *Ecoinvent* dataset for a 10 kW gas boiler production equals a 10 kW oil boiler production. Therefore, it is assumed that the production phases of gas and oil boilers are similar. To develop parametrized datasets according to different possible sizes of the gas boiler, all datasets for gas and oil boilers have been analyzed. However, after the data evaluation only three data sets turn out to be adoptable. When comparing the GWPs and CEDs of these datasets, a non-linear correlation between GB nominal power and the specific GWP/CED for the production can be identified (Figure 32), which is reflected in Equations (82) and (83). Although the data base is very sparse, for lack of alternatives this relation is used in the assessment approach.

$$GWP_{prod,GB} = 78.1 \frac{kg\ CO_2eq}{kW} \cdot P_{th,GB,nom}^{0.729} \tag{82}$$

$$CED_{prod,GB} = 1017 \frac{kg\ CO_2eq}{kW} \cdot P_{th,GB,nom}^{0.727} \tag{83}$$

Use Phase

The EF for burning natural gas is used to determine the GWP and CED connected to the heat production during the use phase as given in Equations (84) and (85).

$$GWP_{op,GB,a} = EF_{gas,a} \cdot Q_{gas,GB,a} \tag{84}$$

$$CED_{op,GB,a} = CED_{gas,a} \cdot Q_{gas,GB,a} \tag{85}$$
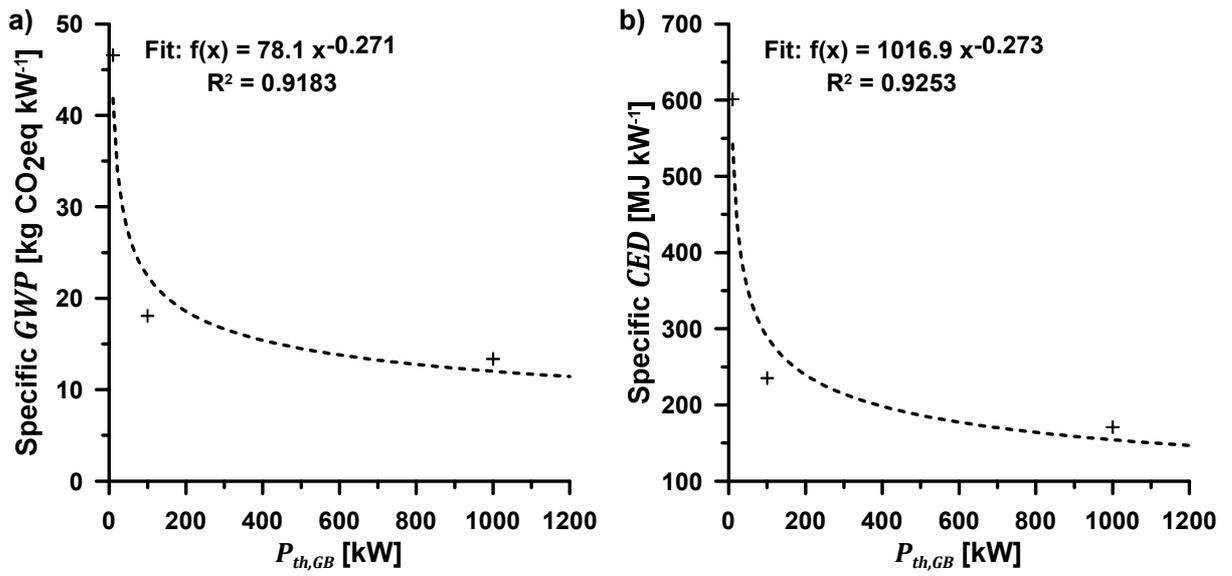
Figure 32: Specific GWP (a) and CED (b) from different gas and oil boiler datasets dependent on the respective boiler size and the derived fitting function.

6 Application of the Assessment Tool

6.1 Economic and Environmental Impact of Medium Deep Borehole Thermal Energy Storage in District Heating Systems

An extensive economic and environmental analysis of BTES-assisted DH systems under different variants of heat production applying the developed assessment tool is elaborated in Appendix G. The study analyzes the effect of integrating BTES systems into a hypothetical low-temperature DH grid under varying shares of STC-, CHP- and GB-capacity and under different economic and environmental scenarios (ECO scenarios). Even though the ECO scenarios under consideration are based on German boundary conditions and the results of this study are therefore only valid for Germany, the general conclusions concerning favorable conditions for BTES integration are transferable to other countries, as well.

It is shown that MD-BTES systems complement seasonally intermittent solar thermal energy. They can increase the share of solar thermal energy in the total heat production from approximately 21% to 76%. However, the most promising system designs combine a large STC field and a large BTES system with a small CHP to supply the HP and circulating pumps with cogenerated electricity.

Both the economic and environmental benefits of integrating BTES systems into district heat production are highly dependent on the underlying economic and environmental boundary conditions. Under the current conditions, considering German state subsidies for cogenerated electricity and for the investment costs of STC and thermal storage systems, the integration of an MD-BTES leads to a considerable increase in the heat cost and implies only a marginal reduction of GHG emissions. The combination of solar thermal energy with a seasonal storage system has to compete with highly efficient CHP technology, which has an eco-friendliness that results from replacing the electricity mix in the grid with higher *EF*s. Consequently, a decrease in the electricity mix *EF*, resulting from an increased share of renewables in electricity production, would induce a decline in the emission savings connected to the cogeneration of electricity and thus would diminish the current advantages of CHP. Under this very likely scenario, system combinations including STC and BTES could reduce the *GWP* of the DH system significantly. Furthermore, a potential increase in the natural gas price would lead to a distinct rise in the *LCOH* of CHP-based heating concepts. Compared with this, the combination of an STC and an MD-BTES is only marginally sensitive to changes in the natural gas price. Hence, it becomes the most favorable heating option when the average gas price passes a threshold of approximately 4 ct kWh^{-1}. A potential extension of the *European Union Emissions Trading System* (EU ETS) to the considered system size would also have comparatively smaller impacts on combined STC and BTES systems.

A trend scenario (EVO and EVO SUB scenarios in Appendix G) with a certain probability of occurrence is adduced to demonstrate the potential of MD-BTES systems. The gas price, electricity price and the emission factor of the grid electricity are varied according to a long-term prediction study (Schlesinger et al. 2014, see Figure 33). Under these assumptions, the integration of an MD-BTES system can reduce the *LCOH*. Depending on whether the currently valid German state subsidies are considered, the *LCOH* reduction can be as much as 7.4% (with subsidies) or 5.6% (without). Furthermore, MD-BTES systems are capable of reducing emissions by 42%, compared to the most favorable scenario without seasonal TES (compromise solutions in Figure 34). Consequently, when assuming a future rise in gas price and further expansion of

renewables in electricity production, MD-BTES systems are able to considerably reduce heat costs and significantly lower the *GWP* of DH systems.
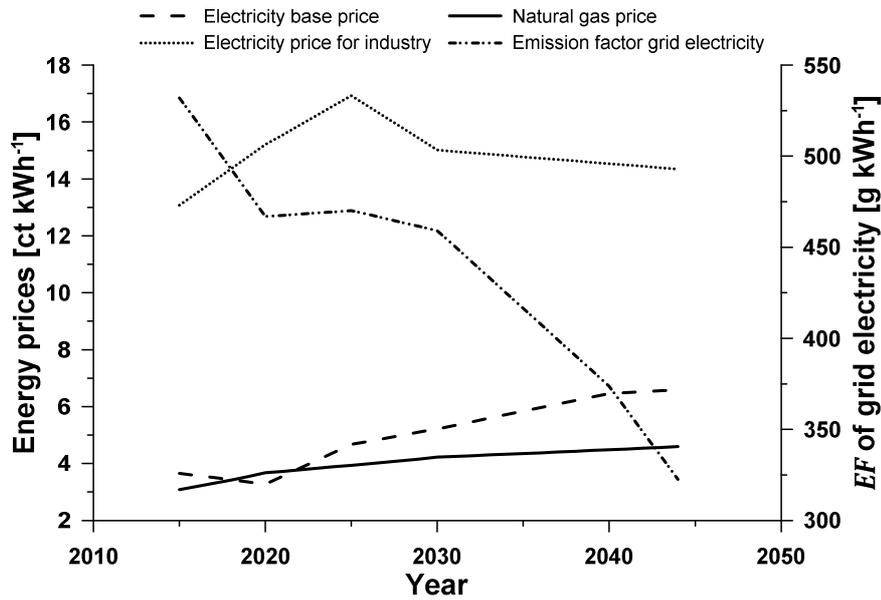
Figure 33: Assumed development of energy prices and the *EF* of the grid electricity in the applied prediction scenario (EVO and EVO SUB scenarios in Appendix G) referring to Schlesinger et al. (2014; figure adapted from Welsch et al. 2018, supplementary material).
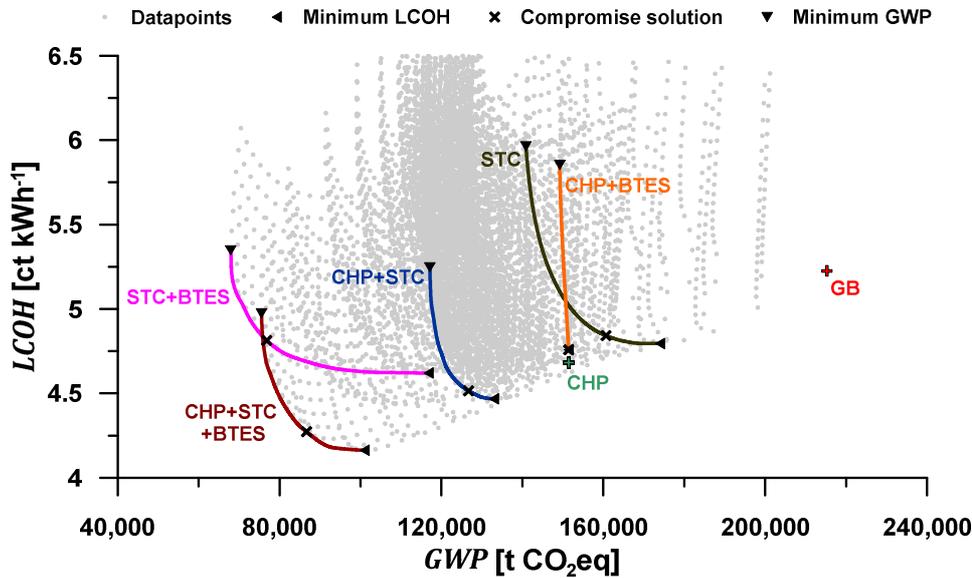
Figure 34: Pareto fronts for different district heat generation combinations in the very likely case (EVO SUB) of rising energy costs and an increasing share of renewables in the electricity grid mix under consideration of current German state subsidies (adapted from Welsch et al. 2018).

Another important finding reported in Appendix G is the limited compatibility of CHP technology and seasonal storage systems in the underlying mode of operation that follows the heat demand. BTES can possibly increase electricity sales, if the CHP operation is managed to obtain high prices instead. This fundamental change to the system boundary conditions was not considered and should be addressed in the future.

6.2 Example for a Mathematical Optimization

Although Appendix G gives a broad overview on the relationship between the system design, its costs as well as its GWP, the step size between the different sample points of the input variables is quite large. Presumably, there are system designs that are even better than the ones identified as Pareto efficient by the pattern search approach applied in Appendix G. This shall be elucidated in the following example.

Proceeding from the overall compromise solution in scenario EVO SUB (BHE length of 750 m, STC area of 50,000 m² and a CHP share of 5%, Appendix G), the system design with the lowest $LCOH$ should be identified. As a nonlinear constraint, the identified system had to achieve at least the same or even had to fall below the GWP of the compromise solution of 86,660 t CO_2eq. Consequently, the optimization problem reads as shown in Equation (86).

$$\min_{L_{BHE}, A_{STC}, \alpha_{CHP} \in \mathbb{R}^3} LCOH(L_{BHE}, A_{STC}, \alpha_{CHP})$$

$$\text{subject to} \quad GWP(L_{BHE}, A_{STC}, \alpha_{CHP}) \leq 86{,}660 \text{ t } CO_2 \text{eq}$$
$$0 \text{ m} \leq L_{BHE} \leq 1{,}000 \text{ m}$$
$$0 \text{ m}^2 \leq A_{STC} \leq 1{,}000 \text{ m}^2$$
$$0 \leq \alpha_{CHP} \leq 1$$

(86)

In order to solve the problem, the function *fmincon* from the *MATLAB Global Optimization Toolbox* (The MathWorks Inc. 2016a) was applied. *fmincon* comprises algorithms that are capable for solving constrained nonlinear multivariable optimization problems. For our purpose, the interior-point approach (Byrd et al. 1999; Byrd et al. 2000; Waltz et al. 2006) was selected from the available algorithms.

Under the preset termination criterions the algorithm needed 7 iterations to converge to a solution. The minimum was found at a system design with a BHE length of approximately 718 m, a STC area of 51,240 m² and a CHP share of only 1%. Compared to the compromise solution in Appendix G, the $LCOH$ was reduced from 4.27 to 3.96 ct kWh[-1] by another 9%. Moreover, the GWP could also be improved to 83,646 t CO_2eq by 3.5%.

The example demonstrates the general application of the assessment tool for a direct mathematical optimization. However, the solution surface seems to have several local minima. Hence, it is particularly advantageous to have an idea, in which region the global optimum is expected, in order to start the optimization at a convenient parameter set.

7   Estimation of the Greenhouse Gas Mitigation Potential in Germany

In Germany, approximately 70% of the final energy for space and water heating (~1972 PJ) is consumed in urban areas, where DH is a viable alternative to decentralized heating systems. However, only around 13% of this heat is actually supplied by DH (Chapter 1). Consequently, the GHG mitigation potential of the integration of MD-BTES systems depends largely on the expansion of DH in general. In order to estimate this potential, five different expansion scenarios were considered (Table 6). Scenario 1, with a share of DH of 13% equals the current state, while the other scenarios represent possible future expansion stages. The final energy consumption in urban areas was split up into DH and decentralized heat production according to the assumed shares in the particular scenario.

Table 6: Assumed expansion stages for district heating in urban areas.

Expansion scenario	Share of DH	Share of decentralized heat production	Final energy consumption in German urban areas	
			DH [PJ]	Decentralized heat [PJ]
1	13%	87%	256	1716
2	25%	75%	493	1479
3	50%	50%	986	986
4	75%	25%	1479	493
5	100%	0%	1972	0

Based on the obtained figures for final energy, the annual *GWP* of heat production in urban areas could be estimated using different *EF*s for DH and for decentralized heat. The *EF* for decentralized heat was deduced from the share of the different heat sources in the final heat consumption and their specific *EF*s as illustrated in Table 7. Renewable and miscellaneous heat sources were not specified any further. Comparatively low *EF*s were set for these sources. Consequently, decentralized heat production is upvalued, which in this context represents a conservative approach.

The *EF* for centralized heating were obtained from several different DH system configurations. Apart from a current DH composition ("DH actual") as specified by IINAS (2017), four system combinations from Appendix G (compromise solutions, EVO SUB) were taken into consideration (Table 8). To attain better comparability to decentralized systems, heat losses were taken into account applying a simplified grid transmission efficiency factor of 85.6% (value derived from Li & Svendsen 2012).

Table 7: Calculation of the mean emission factor for decentralized heating systems.

Heat source	Final heat consumption in Germany[1] [PJ]	Share [%]	*EF* of energy source[2] [g kWh^{-1}]
Natural gas	1310.6	51.0	289
Mineral oil	684.1	26.6	374
Renewables	402.1	15.7	25[3]
Electricity	136.2	5.3	532
Coal	33.2	1.3	679
Misc.	1.6	0.1	0[3]
Decentralized heat	2567.8	100.0	289

[1] Without district heating, according to AGEB (2016).
[2] According to IINAS (2017), value for decentralized heat calculated as weighted mean.
[3] This energy source is not specified any further in the base data. The assumed EF represents a conservative approach.

Table 8: Emission factors assumed for the different DH system configurations.

System configuration	EF [g kWh^{-1}]	Data source	Factor for grid losses	Assumed EF [g kWh^{-1}]
DH actual	261	IINAS (2017)	*	261
CHP	202	Welsch et al. (2018)	1/0.856	236
CHP+STC	169	Welsch et al. (2018)	1/0.856	197
CHP+STC+BTES	116	Welsch et al. (2018)	1/0.856	135
STC+BTES	102	Welsch et al. (2018)	1/0.856	120

* Losses already taken into account in the base data.

Figure 35 illustrates the potential for mitigating GHG emissions in Germany by a general expansion of the DH grids and the application of advanced DH generation options. Unsurprisingly, the mitigation potential of different DH configurations increases with a growing centralized heat supply. Considering the DH scenario from IINAS (2017) ("DH actual"), an increase of the DH share in the German urban heat supply to 50% would result in a decrease of the GWP by about 6 Mt a^{-1}. Such an expansion of German DH grids is not unrealistic. In Denmark, for example, DH accounts for approximately 60% of the overall heat production (Dalla Rosa et al. 2013). However, the GWP mitigation could be increased even further by applying advanced DH configurations: when assuming the CHP+STC combination, the reduction already amounts to 23 Mt a^{-1}. Integrating an MD-BTES system (CHP+STC+BTES), which is according to Appendix G the most cost-effective system in scenario EVO SUB, could reduce the GWP by approximately 40 Mt a^{-1}. This corresponds to a decrease of the total GHG emissions in Germany by 3.2% with regard to the 1990 level. Assuming a completely centralized heat supply in urban areas, this combination could even achieve a reduction of 82 Mt a^{-1} (-6.6% compared to the level of 1990).

In this estimation, it is not considered that the share of renewables in the decentralized heat production will also increase. Furthermore, it can be expected that the heating demand will also significantly decrease due to building refurbishment measures. Consequently, the true GHG mitigation potential in the heating sector is markedly higher than the values presented here.
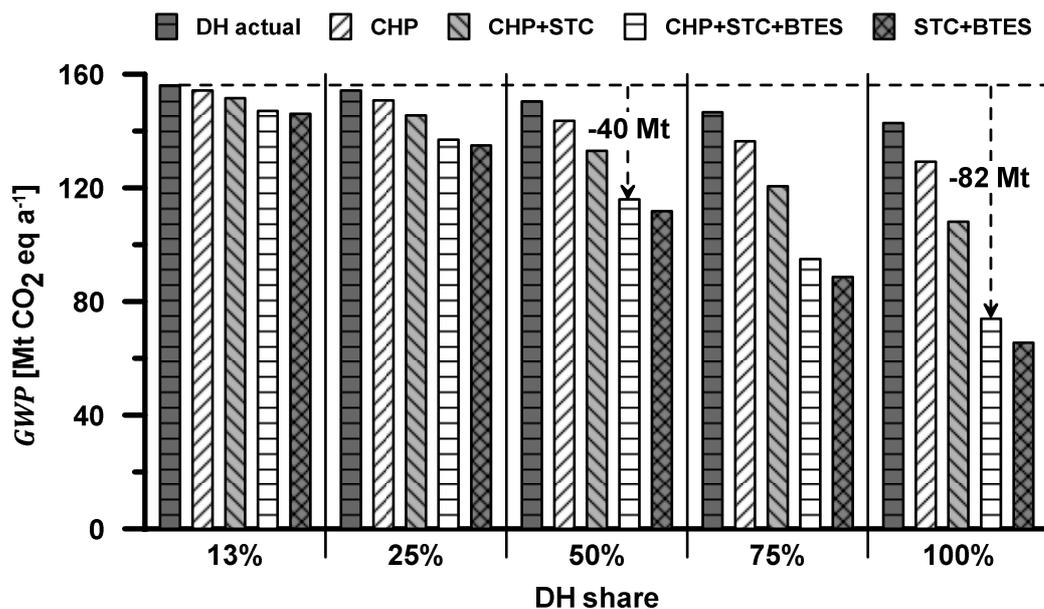
Figure 35: Annual GWP for the urban heat consumption in Germany depending on different DH system configurations and different shares of DH in the overall heat consumption.

8   Discussion and Conclusions

This dissertation contains a comprehensive evaluation of MD-BTES systems. Up until now, MD-BTES systems have not been put into practice. For this reason, numerical simulations were indispensable to gain a reliable insight into the operating characteristics of these systems. Various MD-BTES settings have been simulated. The effects of different storage configurations, fluid temperatures and subsurface properties were studied.

It has been demonstrated that despite their worse SA/V-ratio compared to shallow BHE arrays, MD-BTES systems were eminently suited for seasonal TES. With a proper dimensioning and in convenient geological and hydrogeological framework conditions these systems can reach storage utilization ratios of more than 80%, while supplying the heat on temperature levels of 30 °C or more. Consequently, HPs that are used to boost the temperature to the required supply level, can achieve high *COP*s. Heating systems with low supply temperatures of 35 °C or less could even be operated without the use of an HP. Accepting a reduction in the storage utilization ratio, even higher supply temperatures could be achieved. MD-BTES systems are large solutions, which are only efficient on a DH level. They are not suitable in single building heating systems compared to that presented e.g. in Appendix A.

It was shown that the BHE spacing has a significant impact on the storage performance. While a too low spacing reduces the exploited rock volume and thus constrains the storage capacity, a large BHE spacing diminishes the interaction of neighboring BHEs, which is the fundamental BTES mechanism. Consequently, there is an optimal BHE spacing, where the BTES performance has a maximum. It is dependent on the subsurface properties and in particular on the thermal conductivity. The high dependency of the storage performance on a proper BHE spacing implies very high demands on the drilling process: the deviation of the bore paths has to be as little as possible. With modern directional drilling technologies it is technically feasible to achieve the requested target. However, their application in BTES construction is economically not feasible. As already stated by Schulte (2016), the hydraulic down-the-hole hammer is envisaged to be a viable technology for drilling MD-BTES systems. It stands out due to its improved straightness of the bore path (Wittig et al. 2015) and comparatively moderate costs. Admittedly, the average deviation from the vertical line is still around 10% of the total vertical depth (Wittig et al. 2015). However, the main reason for the deviation of boreholes are inclined geologic joint faces. These can be for example bedding planes, fractures or faults. In a BHE array, all boreholes are usually drilled within a relatively close range. It can be expected that in most geologic settings (at least when folding tectonics are not an issue), the responsible joint faces have a similar orientation in all boreholes. As a result, a more or less parallel deviation of all holes should occur, leading to a preservation of the BHE spacing with depth.

Increasing the total BHE length generally improves the storage performance. This can either be achieved by increasing the length of all BHEs or by increasing the number of BHEs. However, the latter measure seems to be more efficient. Increasing the number of BHEs leads to a better SA/V-ratio than increasing the BHE's length. Consequently, a deeper system consisting of less BHEs will usually perform worse than a more shallow system with a similar capacity. Especially when the number of BHEs is below a critical value, a strong impairment of the storage performance can be observed: in the assumed case of a circular arrangement of BHEs, the critical number, which was necessary to achieve storage efficiencies of more than 70%, corresponded to a system with a center BHE surrounded by two entire BHE rings (in total 19 BHEs). However, the positive effect of increasing the BHE number also levels out with higher numbers.

More importantly in this context, MD-BTES systems should be thermally insulated in the top-most section of the BHEs, in order to reduce the thermal impact on shallow aquifer systems. Such a thermal insulation, however, not only reduces the heat losses to the aquifer unit, but also impairs the effective heat exchanger surface and thus the storage capacity. It becomes evident – the larger the number of BHEs in a system, the larger the ineffective BHE length. Accordingly, in an MD-BTES system the pros and cons for building less but deeper BHEs or vice versa have to be carefully balanced.

Concerning the subsurface properties, it was illustrated that the thermal conductivity has a major effect on the capacity of the storage system. Higher conductivities lead to increased charging and discharging rates. But, they also slightly impair the storage efficiency, as conductive heat losses intensify. Unexpectedly, the heat capacity of the subsurface had only a minor effect on the storage capacity. Two reasons come into question: firstly, as mentioned before, the capacity is principally constrained by the charging and discharging rates, which are determined to a large extend by the thermal conductivity of the subsurface. Secondly, a simplified relatively steady-state operation scenario has been applied. Under steady-state conditions, the heat capacity has no relevance. With a more transient storage operation, the influence of the rock heat capacity is expected to increase. By varying the hydraulic conductivities under a consistent hydraulic gradient, the impact of different groundwater flow velocities was studied. The results confirm that a slight groundwater flow is acceptable. But, flow velocities of more than approximately 1 m a^{-1} significantly affect the performance of MD-BTES by dissipating the stored heat out of the storage region. An elongated shape of the BHE arrangement in the direction of groundwater movement could reduce this effect to some extent.

Apart from all these general design aspects, also some specific improvement measures were regarded. While a thermal insulation at the ground surface level increases the performance of shallow BTES systems considerably, this positive effect dwindles with increasing storage depth. Likewise, a change in the fluid flow direction through the coaxial BHEs between charging and discharging has virtually no effect on the performance of MD-BTES systems. In contrast, a series connection of different BHE groups is favorable, as it increases the outlet temperatures of the system and thereby its exergetic efficiency.

The main reason for considering medium deep systems as an alternative to shallow BTES systems is the expected lower thermal impact on shallow groundwater aquifers and as a consequence thereof the wider applicability of this technology. Yet, recent studies promoting the application of MD-BTES (e.g. Appendix A, B, D, E, G & H) remain short on quantifying this crucial effect. For this reason, a numerical comparison study of an exemplary shallow BTES and exemplary MD-BTES systems with and without a thermally insulating grout section has been carried out. The results demonstrate that MD-BTES systems can significantly inhibit the thermal impact on near-surface groundwater bodies due to their prolonged shape, which leads to a shifting of the large portion of the thermal impact into deeper rock formations. An insulating grout section along vulnerable aquifer sections reduces the heat exchange length of the BHEs on the one hand and thereby impairs the storage capacity but, on the other hand, it further diminishes the thermal impact on the respective aquifer system. By increasing the diameter of the grout section, the protective effect of the insulation can be amplified. In the numerical simulation example an MD-BTES system with an enlarged insulating grout section reduced the relative heat losses to a near-surface aquifer by more than 87% compared to the shallow BTES system.

It also becomes evident, that even when insulating the BHEs in the concerning sections, a certain thermal impact is inevitable. However, as long as the opportunities of geothermal energy, or in particular of UTES, shall be exploited to some extent, not any change in groundwater temperature can be prohibited. Nevertheless, the precautionary principle has to apply. Accordingly, the risk of a negative impact by an UTES on surrounding drinking water production sites must be obviated by firstly, a proper selection of the storage site and secondly, a minimization of the thermal impact originating from the storage. Therefore, comprehensive subsurface-use planning, as proposed for example by Bauer et al. (2013b), UBA (2015) and Kabuth et al. (2016), is a basic prerequisite to identify suitable storage sites in intensively managed subsurface bodies. The magnitude and spatial distribution of the temperature rise, especially in shallow groundwater bodies, must be reduced by utilizing advanced storage approaches. MD-BTES displays such an advanced approach.

Besides the technical capability of MD-BTES systems for seasonal heat storage and their advantages concerning groundwater protection, another central contentious point remains: the economic feasibility and the environmental benefits that are associated with the implementation of MD-BTES into DH supply systems. In order to quantify the economic and environmental impacts of different DH system combinations, a *MATLAB* based assessment tool has been developed. It uses a simplified energy balance model in combination with a life cycle approach in order to determine the *GWP*, the *CED* and the *LCOH* of DH supply systems that can comprise a GB, a CHP, an STC field as well as a shallow to medium deep BTES unit, which is operated with the use of an HP. However, a comprehensive LCA should aim for the evaluation of all relevant environmental impacts connected to a system or product. In case of BTES systems, one major impact – the thermal impairment of groundwater – could not be incorporated and offset against the other impact categories. It had to be omitted as suitable characterization methods are lacking. Major reasons for that are seen in the strong site dependence of this issue, a still incomplete process understanding as well as the difficulty to quantify the harmfulness of thermally induced microbiological and chemical changes in the groundwater composition.

Anyhow, the applied LCA approach has proven itself valuable for the comparison of different DH system combinations in terms of *GWP*, *CED* and their cost efficiency. An extensive assessment study was carried out, taking account of all reasonable DH supply system combinations of the aforementioned technologies and varying the component sizes in a full factorial experimental design. Four different economic and environmental scenarios were applied, considering either constant or progressive input data (i.e. energy prices and the *EF* of the grid electricity mix in Germany) over the regarded time span and optionally incorporating current German subsidies on renewable technologies.

The study emphasizes the GHG reduction potential that goes along with the inclusion of MD-BTES systems into DH supply systems under favorable economic and environmental boundary conditions. It also reveals that such systems are economically competitive to common DH options like the combination of a CHP with conventional GBs for peak load supply. But, the assumed economic and environmental boundary conditions have a significant impact on the achieved GHG reductions and the profitability of MD-BTES systems. Under the current market conditions, CHP-technology is highly efficient, which hampers the application of BTES systems. By contrast, in a very likely economic and environmental scenario comprising progressive energy prices and a reduction in the *EF* of the grid electricity mix, the integration of an MD-BTES system lowered the GHG emissions by approximately 32% while also reducing the *LCOH* by 5.3% compared to the best system solution without any BTES.

The *EF* figures obtained in the assessment study were used to estimate the GHG mitigation potential for Germany associated with MD-BTES. The results reveal that an increase of the share of centralized heat in urban areas to 50% allows for DH grids in combination with CHP, STC fields and MD-BTES systems to reduce the GHG emissions in Germany by approximately 40 Mt a^{-1}. This amount equates a reduction of the total GHG emissions in Germany by 3.2% with regard to the 1990 level. Accordingly, MD-BTES systems in combination with an expansion of DH supply could make a perceptible contribution to reach the climate protection goals.

All in all, MD-BTES systems constitute a serious alternative to conventional seasonal TES systems. Moreover, a successful commercial launch of the technology would even broaden the range of seasonal TES application significantly, as these systems are more independent on the geologic conditions and the spatial structure while providing the high storage capacities that are required in large urban DH systems. Nevertheless, further research is required until MD-BTES systems achieve market maturity. A selection of important research topics shall be given in the following outlook section.

9 Outlook

Up to now, the MD-BTES system analysis was based on many simplifications: the technical assessment of MD-BTES was conducted, using very simple operation scenarios and subsurface conditions and singularly looking at the storage system. This was necessary to avoid noise in the simulation results that could have masked important findings concerning the variables of interest.

BTES-assisted DH supply systems usually consist of several subsystems like heat sources (e.g. STC, CHP), the BTES itself, heat consumers (i.e. the space heating system, the DH grid), diurnal storages (i.e. water tanks), additional heat sources for peak load coverage (e.g. GB) and an HP to boost the supply temperatures from the BTES system. The economic and environmental assessment of such overall systems, presented here, was based on a simple heat balance approach, which mostly disregards temperature levels and the mutual interference of the different components. In reality, the subsystems interact dynamically with each other. The fluid temperatures of the heat generation system, the heating system and the underground storage are interdependent and affect the performance of each component. Coupled simulation models, which co-simulate the subsystems, are required to take these interdependencies into account.

The first implementation of such a co-simulation is presented in Appendix H. A data exchange routine has been developed, which is based on the Transmission Control Protocol/Internet Protocol (TCP/IP). The routine couples the FE software *FEFLOW* (DHI-WASY 2014), which is used to simulate the heat transport processes in the BHEs and the subsurface, to *MATLAB-Simulink* (The MathWorks Inc. 2016b), which is deployed to model the system components on the surface using the *Carnot-Toolbox* (Solar-Institut Jülich 2016). A simple application example illustrates the approach and its capabilities in terms of mathematically optimizing integral systems. However, the approach must be applied to realistic BTES-assisted DH systems in future. A first attempt has already been made by Formhals et al. (2017), who used the coupling approach to investigate the influence of different DH supply temperatures on the performance of a BTES unit in a DH system. Future research has to focus on the design optimization of the overall system. This implies a fine adjustment of all components as well as the development of sufficient control strategies. In order to include economic and environmental objectives, the more sophisticated outcome of such coupled simulations can be used to replace the simplified energy balance based heating system model in the economic and environmental assessment tool.

A constructional realization of a pilot storage system is of particular importance: it is crucial to demonstrate that all the theoretical knowledge, which was gained during the past years and which is compiled in this dissertation, remains valid for all practical purposes. Furthermore, it is necessary to demonstrate that the drilling technology can meet the requirements. Moreover, an experimental test operation of such a pilot system would significantly extend our preliminary findings. The gathered data could be used to validate and improve the numerical models. Additionally, more detailed economic and environmental data, in particular concerning the drilling process, could be collected to further enhance the economic and environmental assessment of these systems.

A research proposal, which comprises the construction of a pilot MD-BTES system at the Campus Lichtwiese of the Technische Universität Darmstadt is in preparation. It intends for the completion of four BHEs with a depth of up to 750 m each. Obviously, an MD-BTES system consisting of such a little number of BHEs cannot be efficient nor economic. Though, all the

aforementioned demands on a pilot storage system can be met. Moreover, and that is an important advantage of BTES in general, the system can be easily extended to economic sizes, if the university administration decides to integrate the storage into their future heating concept.

Future research should focus on the LCA of BTES systems and geothermal applications in general: the assessment of the environmental impact of a temperature change in the subsurface caused by geothermal installations lacks a profound characterization method. However, suitable characterization methods should be developed in the future in order to objectify the discussion on the necessity and the extent of groundwater regulations concerning the utilization of geothermal energy.

References

AGEB (2016): Anwendungsbilanzen für die Endenergiesektoren in Deutschland in den Jahren 2013 bis 2015. Studie beauftragt vom Bundesministerium für Wirtschaft und Energie, Projektnummer: 072/15., Arbeitsgemeinschaft Energiebilanzen e.V.

Al-Khoury R and Bonnier PG (2006): Efficient finite element formulation for geothermal heating systems. Part II: transient, International Journal for Numerical Methods in Engineering, v. 67, no. 5, p. 725-745.

Al-Khoury R, Bonnier PG and Brinkgreve RBJ (2005): Efficient finite element formulation for geothermal heating systems. Part I: steady state, International Journal for Numerical Methods in Engineering, v. 63, no. 7, p. 988-1013.

Andersson O (2007): BTES for heating and cooling of the Aatronomy House in Lund, in Paksoy, HÖ, ed., Thermal Energy Storage for Sustainable Energy Consumption, Volume 234, Springer Netherlands, p. 229-233.

Andersson O, Ekkestubbe J and Ekdahl A (2013): UTES (Underground Thermal Energy Storage) - Applications and Market Development in Sweden, Journal of Energy and Power Engineering, v. 7, no. 4, p. 669-678.

Andersson S and Eriksson A (1981): Seasonal Storage in Hard Rock — Multiple Well System, in Ouden, C, ed., Thermal Storage of Solar Energy: Proceedings of an International TNO-Symposium Held in Amsterdam, The Netherlands, 5–6 November 1980, Dordrecht, Springer Netherlands, p. 249-258.

ASUE (2011): BHKW-Kenndaten 2011 - Module, Anbieter, Kosten, in Arbeitsgemeinschaft für sparsamen und umweltfreundlichen Energieverbrauch e.V., ed.

Bäcklund A-S (2009): Analys av en grundvärmebaserad värmcpumpsanläggning för uppvärmning och kylning av ett sjukhus (Analysis of a Ground Source Heat Based Heat Pump Facility for Heating and Cooling of a Hospital), Master thesis, NTNU Trondheim, Norway.

Ball State University (2018): Going Geothermal - Geothermal Energy System, https://www.bsu.edu/about/geothermal, Web Page, accessed 11 October 2018.

Bär K, Rühaak W, Welsch B, Schulte D, Homuth S and Sass I (2015): Seasonal High Temperature Heat Storage with Medium Deep Borehole Heat Exchangers, Energy Procedia, v. 76, p. 351-360.

Bär K, Rühaak W, Welsch B, Schulte D, Homuth S and Sass I (2016): Seasonal high temperature heat storage with medium deep borehole heat exchangers – a conceptual case study, in Proceedings European Geothermal Congress, Strasbourg, France, 19-24 Sept 2016.

Bauer D (2011): Zur thermischen Modellierung von Erdwärmesonden und Erdsonden-Wärmespeichern, Dissertation, Fakultät Energie-, Verfahrens- und Biotechnik, Universität Stuttgart, XIV + 121 p.

Bauer D, Drück H, Heidemann W, Marx R, Nußbicker-Lux J and Ochs F (2013a): Solarthermie2000plus: Wissenschaftlich-technische Begleitung des Förderprogramms Solarthermie2000plus zu solar unterstützter Nahwärme und Langzeit-Wärmespeicherung, Institute of Thermodynamics and Thermal Engineering (ITW), Universität Stuttgart, Research report to BMU-Project FKZ 0329607P

Bauer D, Drück H, Lang S, Marx R and Plaz T (2016): Weiterentwicklung innovativer Technologien zur solaren Nahwärme und saisonalen Wärmespeicherung - Akronym „WinterSun", Forschungs- und Testzentrum für Solaranlagen (TZS), Institut für Thermodynamik und Wärmetechnik (ITW), Universität Stuttgart, Research report to BMWi-Project FKZ 0325998A

Bauer D, Marx R, Nußbicker-Lux J, Ochs F, Heidemann W and Müller-Steinhagen H (2010): German central solar heating plants with seasonal heat storage, Solar Energy, v. 84, no. 4, p. 612-623.

Bauer S, Beyer C, Dethlefsen F, Dietrich P, Duttmann R, Ebert M, Feeser V, Görke U, Köber R, Kolditz O, Rabbel W, Schanz T, Schäfer D, Würdemann H and Dahmke A (2013b):

Impacts of the use of the geological subsurface for energy storage: an investigation concept, Environmental Earth Sciences, v. 70, no. 8, p. 3935-3943.

Bauman H and Tillman A-M (2004): The hitch hiker's guide to LCA: an orientation in life cycle assessment methodology and application, Lund, Sweden, Studentlitteratur, 543 p.

BDEW/VKU/GEODE (2013): Leitfaden Abwicklung von Standardlastprofilen Gas, *in* BDEW – Bundesverband der Energie- und Wasserwirtschaft e.V., VKU – Verband kommunaler Unternehmen e.V., and GEODE – Groupement Européen des entreprises et Organismes de Distribution d'Énergie, eds., Berlin.

Beckmann G and Gilli PV (1984): Thermal Energy Storage: Basics-Design-Applications to Power Generation and Heat Supply, Wien ; New York, Springer-Verlag, Topics in energy, xi, 230 p. p.

Bendea C, Antal C and Rosca M (2015): Geothermal energy in Romania: country update 2010-2014, *in* Proceedings World Geothermal Congress 2015, Melbourne, Australia, 19-25 April 2015.

BMU (2018): Klimaschutzbericht 2017, Bundesministerium für Umwelt, Naturschutz und nukleare Sicherheit, 142 p.

BMUB (2014): Aktionsprogramm Klimaschutz 2020Bundesministerium für Umwelt, Naturschutz, Bau und Reaktorsicherheit

BMUB (2016): Klimaschutzplan 2050 - Klimaschutzpolitische Grundsätze und Ziele der BundesregierungBundesministerium für Umwelt, Naturschutz, Bau und Reaktorsicherheit

Bonte M (2015): Impacts of Shallow Geothermal Energy on Groundwater Quality, London, IWA Publishing, KWR Watercycle Research Institute Series, VIII+135 p.

Bonte M, Röling WFM, Zaura E, van der Wielen PWJJ, Stuyfzand PJ and van Breukelen BM (2013a): Impacts of Shallow Geothermal Energy Production on Redox Processes and Microbial Communities, Environmental Science & Technology, v. 47, no. 24, p. 14476-14484.

Bonte M, van Breukelen BM and Stuyfzand PJ (2013b): Temperature-induced impacts on groundwater quality and arsenic mobility in anoxic aquifer sediments used for both drinking water and shallow geothermal energy production, Water Research, v. 47, no. 14, p. 5088-5100.

Boockmeyer A and Bauer S (2016): Efficient simulation of multiple borehole heat exchanger storage sites, Environmental Earth Sciences, v. 75, no. 12, p. 1021.

Brielmann H, Lueders T, Schreglmann K, Ferraro F, Avramov M, Hammerl V, Blum P, Bayer P and Griebler C (2011): Oberflächennahe Geothermie und ihre potenziellen Auswirkungen auf Grundwasserökosysteme, Grundwasser, v. 16, no. 2, p. 77.

Brons HJ, Griffioen J, Appelo CAJ and Zehnder AJB (1991): (Bio)geochemical reactions in aquifer material from a thermal energy storage site, Water Research, v. 25, no. 6, p. 729-736.

Byrd RH, Gilbert JC and Nocedal J (2000): A trust region method based on interior point techniques for nonlinear programming, Mathematical Programming, v. 89, no. 1, p. 149-185.

Byrd RH, Hribar ME and Nocedal J (1999): An Interior Point Algorithm for Large-Scale Nonlinear Programming, SIAM Journal on Optimization, v. 9, no. 4, p. 877-900.

Connolly D, Lund H, Mathiesen BV, Werner S, Möller B, Persson U, Boermans T, Trier D, Østergaard PA and Nielsen S (2014): Heat Roadmap Europe: Combining district heating with heat savings to decarbonise the EU energy system, Energy Policy, v. 65, p. 475-489.

Croteau R and Gosselin L (2015): Correlations for cost of ground-source heat pumps and for the effect of temperature on their performance, International Journal of Energy Research, v. 39, no. 3, p. 433-438.

Cullin JR, Spitler JD, Montagud C, Ruiz-Calvo F, Rees SJ, Naicker SS, Konečný P and Southard LE (2015): Validation of vertical ground heat exchanger design methodologies, Science and Technology for the Built Environment, v. 21, no. 2, p. 137-149.

Dalenbäck J-O, Hellström G, Lundin S-E, Nordell B and Dahm J (2000): Borehole heat storage for the anneberg solar heated residential district in Danderyd, Sweden, *in* Proceedings 8th International Conference on Thermal Energy Storage Terrastock 2000, Stuttgart, Germany, 28 August - 1 September 2000, p. 201-206.

Dalla Rosa A, Li H and Svendsen S (2013): Modeling Transient Heat Transfer in Small-Size Twin Pipes for End-User Connections to Low-Energy District Heating Networks, Heat Transfer Engineering, v. 34, no. 4, p. 372-384.

DHI-WASY (2014): FEFLOW finite element subsurface flow and transport simulation system - Release 6.2, Berlin, DHI-WASY GmbH.

Diersch H-JG (2014): Feflow - Finite Element Modeling of Flow, Mass and Heat Transport in Porous and Fractured Media, Springer Berlin Heidelberg.

Diersch H-JG, Bauer D, Heidemann W, Rühaak W and Schätzl P (2011a): Finite element modeling of borehole heat exchanger systems: Part 1. Fundamentals, Computers & Geosciences, v. 37, no. 8, p. 1122-1135.

Diersch H-JG, Bauer D, Heidemann W, Rühaak W and Schätzl P (2011b): Finite element modeling of borehole heat exchanger systems: Part 2. Numerical simulation, Computers & Geosciences, v. 37, no. 8, p. 1136-1147.

DIN EN ISO 14040 (2009): Environmental management - Life cycle assessment - Principles and framework (ISO 14040:2006); German and English version EN ISO 14040:2006, DIN EN ISO 14040:2009-11:,,

DIN EN ISO 14044 (2006): Environmental management - Life cycle assessment - Requirements and guidelines (ISO 14044:2006); German and English version EN ISO 14044:2006, DIN EN ISO 14044:2006-10,,

Dincer I and Rosen MA (2007): A Unique Borehole Thermal Storage System at University of Ontario Institute of Technology, *in* Paksoy, H, ed., Thermal Energy Storage for Sustainable Energy Consumption, Volume 234, Dordrecht, Springer Netherlands, p. 221-228.

Dincer I and Rosen MA (2011): Thermal Energy Storage: Systems and Applications, Hoboken, N.J., Wiley, XVIII, 599 p.

EPA (2015): Catalog of CHP Technologies, *in* U.S. Environmental Protection Agency Combined Heat and Power Partnership, ed.

Eskilson P and Claesson J (1988): Simulation model for thermally interacting heat extraction boreholes, Numerical Heat Transfer, v. 13, no. 2, p. 149-165.

Eugster WJ (2002): SERSO PLUS – Neue Wege in der Belagsheizung,, GtE . Mitteilungsblatt der Geothermischen Vereinigung e.V., v. 38-39/2002.

Eugster WJ (2007): Road and bridge heating using geothermal energy. Overview and examples, *in* Proceedings European Geothermal Congress 2007, Unterhaching, Germany, 30 May - 1 June 2007, Volume 2007.

Fischer D and Madani H (2017): On heat pumps in smart grids: A review, Renewable and Sustainable Energy Reviews, v. 70, p. 342-357.

Formhals J, Welsch B, Schulte D and Sass I (2017): Effects of the District Heating Supply Temperature on the Efficiency of Borehole Thermal Energy Storage Systems, *in* Proceedings 3rd International Conference on Smart Energy Systems and 4th Generation District Heating, Copenhagen, Denmark, 12–13 September 2017.

Gadd H and Werner S (2014): Achieving low return temperatures from district heating substations, Applied Energy, v. 136, no. Supplement C, p. 59-67.

Gebhardt M, Kohl H and Steinrötter T (2002): Preisatlas - Ableitung von Kostenfunktionen für Komponenten der rationellen Energienutzung, Institut für Energie und Umwelttechnik e.V. (IUTA)

Gehlin S (2016): Borehole thermal energy storage, *in* Rees, SJ, ed., Advances in Ground-Source Heat Pump Systems, Woodhead Publishing, p. 295-327.

Gehlin S, Andersson O, Bjelm L, Alm P-G and Rosberg J-E (2015): Country update for Sweden, *in* Proceedings World Geothermal Congress 2015, Melbourne, Australia, 19-25 April 2015.

Givoni B (1977): Underground longterm storage of solar energy—An overview, Solar Energy, v. 19, no. 6, p. 617-623.

GreenDelta GmbH (2017): openLCA – the Life Cycle and Sustainability Modeling Suite.

Greening B and Azapagic A (2012): Domestic heat pumps: Life cycle environmental impacts and potential implications for the UK, Energy, v. 39, no. 1, p. 205–217.

Griffioen J and Appelo CAJ (1993): Nature and extent of carbonate precipitation during aquifer thermal energy storage, Applied Geochemistry, v. 8, no. 2, p. 161-176.

Guinée JB (ed.) (2002): Handbook on life cycle assessment : operational guide to the ISO standards, Dordrecht, Kluwer Academic Publishers, Eco-efficiency in industry and science, v. 7, XI, 692 p.

Handke H, Reisig O, Düppre T, Zinke B and Schulz S (2015): Verrohrung für eine Erdwärmesonde zur Gewinnung geothermischer Energie, insbesondere tiefengeothermischer Energie, patent no. DE102015112892A1, Handke Brunnenbau GmbH, Wipotec Wiege & Positioniersysteme GmbH.

Heier J, Bales C, Sotnikov A and Ponomarova G (2011): Evaluation of a high temperature solar thermal seasonal borehole storage, *in* Proceedings ISES Solar World Congress, Kassel, Germany, 28 August - 2 September 2011.

Hellström G (1989): Duct Ground Heat Storage Model - Manual for Computer Code, Lund, Sweden, Department of Mathematical Physics, University of Lund.

Hellström G (1991): Ground Heat Storage: Thermal Analyses of Duct Storage Systems, Dissertation, Department of Mathematical Physics, University of Lund, 262 p.

Hellwig M (2003): Entwicklung und Anwendung parametrisierter Standard-Lastprofile, Dissertation, Institut für Energietechnik, Technische Universität München, VI + 145 p.

Hesaraki A, Holmberg S and Haghighat F (2015): Seasonal thermal energy storage with heat pumps and low temperatures in building projects—A comparative review, Renewable and Sustainable Energy Reviews, v. 43, p. 1199-1213.

Homuth S, Hornich W, Krenn H, Sass I and Spahn T (2016): Down-the-Hole Water-Powered Hammer Drilling Method for medium-deep Geothermal Energy Drilling, Oil Gas European Magazine, v. 132, no. 3, p. 39-41.

Homuth S, Rühaak W, Bär K and Sass I (2013): Medium Deep High Temperature Heat Storage, *in* Proceedings European Geothermal Congress 2013, Pisa, Italy.

Huusko A and Valpola SE (2014): lnsight into shallow geothermal energy research in Finland, The Newsletter of the ENeRG Network, v. 30, p. 3.

IINAS (2016): GEMIS - Globales Emissions-Modell Integrierter Systeme - model and database, version 4.93, *in* International Institute for Sustainability Analysis and Strategy, ed., Darmstadt.

IINAS (2017): GEMIS - Globales Emissions-Modell Integrierter Systeme - model and database, version 4.95, *in* International Institute for Sustainability Analysis and Strategy, ed., Darmstadt.

Jesußek A, Grandel S and Dahmke A (2013): Impacts of subsurface heat storage on aquifer hydrogeochemistry, Environmental Earth Sciences, v. 69, no. 6, p. 1999-2012.

Kabuth A, Dahmke A, Beyer C, Bilke L, Dethlefsen F, Dietrich P, Duttmann R, Ebert M, Feeser V, Görke U-J, Köber R, Rabbel W, Schanz T, Schäfer D, Würdemann H and Bauer S (2016): Energy storage in the geological subsurface: dimensioning, risk analysis and spatial planning: the ANGUS+ project, Environmental Earth Sciences, v. 76, no. 1, p. 23.

Kauko H, Kvalsvik KH, Rohde D, Hafner A and Nord N (2017): Dynamic modelling of local low-temperature heating grids: A case study for Norway, Energy.

Kistler D and Karidis G (2015): Oakland University Human Health Building - Flagship for Health, High Performing Buildings, v. Winter 2015, p. 6-15.

Kizilkan O and Dincer I (2015): Borehole thermal energy storage system for heating applications: Thermodynamic performance assessment, Energy Conversion and Management, v. 90, p. 53-61.

Kolmogorov A (1933): Sulla determinazione empirica di una lgge di distribuzione, Inst. Ital. Attuari, Giorn., v. 4, p. 83-91.

Kramer G (2010): Energieverbrauch der privaten Haushalte - Regionalisierte Ergebnisse, Statistische Monatshefte Rheinland-Pfalz, v. 05 2010, p. 362-374.

Krishnamurti TN, Kishtawal CM, Zhang Z, LaRow T, Bachiochi D, Williford E, Gadgil S and Surendran S (2000): Multimodel Ensemble Forecasts for Weather and Seasonal Climate, Journal of Climate, v. 13, no. 23, p. 4196-4216.

Kübler R, Fisch N and Hahne E (1997): High temperature water pit storage projects for the seasonal storage of solar energy, Solar Energy, v. 61, no. 2, p. 97-105.

KWKG (2016): German Act on Combined Heat and Power Generation of 2016 - Gesetz für die Erhaltung, die Modernisierung und den Ausbau der Kraft-Wärme-Kopplung. KWKG - Kraft-Wärme-Kopplungsgesetz vom 21. Dezember 2015 (BGBl. I S. 2498), das zuletzt durch Artikel 3 des Gesetzes vom 17. Juli 2017 (BGBl. I S. 2532) geändert worden ist.

Lazzarotto A (2014): A network-based methodology for the simulation of borehole heat storage systems, Renewable Energy, v. 62, no. 0, p. 265-275.

Li H and Svendsen S (2012): Energy and exergy analysis of low temperature district heating network, Energy, v. 45, no. 1, p. 237-246.

Li H, Yu Z, Wu J, Xu W and Zhang S (2015): Application of ground source heat pump system in a nearly zero energy building of China, in Proceedings Greenstock 2015, Beijing, China, 19-21 May 2015.

Lienen T, Lüders K, Halm H, Westphal A, Köber R and Würdemann H (2017): Effects of thermal energy storage on shallow aerobic aquifer systems: temporary increase in abundance and activity of sulfate-reducing and sulfur-oxidizing bacteria, Environmental Earth Sciences, v. 76, no. 6, p. 261.

Lizana J, Chacartegui R, Barrios-Padura A and Ortiz C (2018): Advanced low-carbon energy measures based on thermal energy storage in buildings: A review, Renewable and Sustainable Energy Reviews, v. 82, p. 3705-3749.

Lizana J, Chacartegui R, Barrios-Padura A and Valverde JM (2017): Advances in thermal energy storage materials and their applications towards zero energy buildings: A critical review, Applied Energy, v. 203, p. 219-239.

Lund H, Möller B, Mathiesen BV and Dyrelund A (2010): The role of district heating in future renewable energy systems, Energy, v. 35, no. 3, p. 1381-1390.

Lund H, Werner S, Wiltshire R, Svendsen S, Thorsen JE, Hvelplund F and Mathiesen BV (2014): 4th Generation District Heating (4GDH): Integrating smart thermal grids into future sustainable energy systems, Energy, v. 68, p. 1-11.

Lund J, Sanner B, Rybach L, Curtis R and Hellström G (2004): Geothermal (ground-source) heat pumps-a world overview, GHC BULLETIN, v. September 2004, p. 1-10.

Lund PD and Östman MB (1985): A numerical model for seasonal storage of solar heat in the ground by vertical pipes, Solar Energy, v. 34, no. 4, p. 351-366.

Lundh M and Dalenbäck JO (2008): Swedish solar heated residential area with seasonal storage in rock: Initial evaluation, Renewable Energy, v. 33, no. 4, p. 703-711.

Mangold D (2007): Seasonal storage - a German success story, Sun and Wind Energy, no. 1, p. 48-58.

Mangold D, Miedaner O, Tziggili EP, Schmidt T and Zeh B (2012): Technisch-wirtschaftliche Analyse und Weiterentwicklung der solaren Langzeit-Wärmespeicherung: Forschungsbericht zum BMU-Vorhaben 0329607N; wissenschaftlich-technische Programmbegleitung für Solarthermie2000plus, Steinbeis Forschungsinstitut für Solare und Zukunftsfähige Thermische Energiesysteme

Massey FJ (1951): The Kolmogorov-Smirnov Test for Goodness of Fit, Journal of the American Statistical Association, v. 46, no. 253, p. 68-78.

Mauthner F and Herkel S (2016): Classification and benchmarking of solar thermal systems in urban environments, Technology and Demonstrators: Technical Report Subtask C – Part C1

Midttømme K, Berre I, Hauge A, Musæus TE and Kristjansson BR (2010): Geothermal energy - country update for Norway, in Proceedings World Geothermal Congress 2010, Bali, Indonesia, 25-29 April 2010.

Miedaner O, Mangold D and Sørensen PA (2015): Borehole thermal energy storage systems in Germany and Denmark - construction and operation experiences, in Proceedings Greenstock 2015, Beijing, China, 19-21 May 2015.

Mielke P, Bauer D, Homuth S, Götz A and Sass I (2014): Thermal effect of a borehole thermal energy store on the subsurface, Geothermal Energy, v. 2, no. 1, p. 1-15.

Moomaw W, Burgherr P, Heath G, Lenzen M, Nyboer J and Verbruggen A (2011): Annex II: Methodology, in Edenhofer, O, Pichs-Madruga, R, Sokona, Y, Seyboth, K, Matschoss, P, Kadner, S, Zwickel, T, Eickemeier, P, Hansen, G, Schlömer, S, and von Stechow, C, eds., IPCC Special Report on Renewable Energy Sources and Climate Change Mitigation, Cambridge, United Kingdom and New York, NY, USA, Cambridge University Press.

Naiker SS and Rees SJ (2011): Monitoring and performance analysis of a large non-domestic ground source heat pump installation, in Proceedings CIBSE Technical Symposium, Leicester, UK, 6 - 7 Septermber 2011.

Nordell B (1987): The Borehole Heat Store in Rock at the Lulea University of Technology, Constructional and Operational Experience, The Lulevarme Project 1982-1985, Stockholm, Sweden, Swedish Council for Building Research, Document D6:1985.

Nordell B (1988): LARGE-SCALE SEASONAL HEAT STORAGE IN ROCK - Construction and operation experiences, Proceedings of the International Symposium on Engineering in Complex Rock Formations, Pergamon, p. 351-356.

Nordell B (1990): A Borehole Heat Store in Rock at the University of Lulea, The Lulevarme Project 1982-1988, Stockholm, Sweden, Swedish Council for Building Research, Document D12:1990, v. Accessed from http://nla.gov.au/nla.cat-vn1906055.

Nordell B (1994): Borehole Heat Store Design Optimization, Dissertation, Division of Water Resources Engineering, Luleå University of Technology, 196 p.

Nordell B (2000): Large-scale Thermal Energy Storage, in Proceedings WinterCities'2000, Energy and Environment,, Luleå, 14 February 2000.

Nordell B and Hellström G (2000): High temperature solar heated seasonal storage system for low temperature heating of buildings, Solar Energy, v. 69, no. 6, p. 511-523.

Nordell B, Scorpo AL, Andersson O and Rydell L (2014): The HT BTES plant in Emmaboda: Report from the first three years of operation 2010-2013, Luleå tekniska universitet.

Nordell B, Scorpo AL, Andersson O, Rydell L and Carlsson B (2016): Long-term Long Term Evaluation of Operation and Design of the Emmaboda BTES - Operation and Experiences 2010-2015, Luleå tekniska universitet, Research Report, Dnr: 2012-001272, Pnr: 35868-1, http://urn.kb.se/resolve?urn=urn:nbn:se:ltu:diva-22591, accessed 11 October 2018.

Novo AV, Bayon JR, Castro-Fresno D and Rodriguez-Hernandez J (2010): Review of seasonal heat storage in large basins: Water tanks and gravel–water pits, Applied Energy, v. 87, no. 2, p. 390-397.

Oladyshkin S and Nowak W (2012): Data-driven uncertainty quantification using the arbitrary polynomial chaos expansion, Reliability Engineering & System Safety, v. 106, p. 179-190.

Olsson J (2014): Rwkordstor anläggning i Karlstad, Svensk Geoenergi, v. 2014, no. 1, p. 12.

Oreskes N (2004): The Scientific Consensus on Climate Change, Science, v. 306, no. 5702, p. 1686-1686.

Pardalos PM, Žilinskas A and Žilinskas J (2017): Non-Convex Multi-Objective Optimization, Cham, Springer International Publishing, XII, 192 p.

Persson U, Möller B and Werner S (2014): Heat Roadmap Europe: Identifying strategic heat synergy regions, Energy Policy, v. 74, p. 663-681.

Pieper M (2017): Mathematische Optimierung: Eine Einführung in die kontinuierliche Optimierung mit Beispielen, Wiesbaden, Springer.

Pinel P, Cruickshank CA, Beausoleil-Morrison I and Wills A (2011): A review of available methods for seasonal storage of solar thermal energy in residential applications, Renewable and Sustainable Energy Reviews, v. 15, no. 7, p. 3341-3359.

Polizu R and Hanganu-Cucu R (2011): A case study or good practice in ground source heating/cooling: auto showroom, offices and workshop, VW Bucharest - Romania, in McCorry, M, and Jones, GL, eds., Geotrainet Training Manual for Designers of Shallow Geothermal Systems, Brussels, Belgium, Geotrainet, EFG, p. 128-132.

Rapantova N, Pospisil P, Koziorek J, Vojcinak P, Grycz D and Rozehnal Z (2016): Optimisation of experimental operation of borehole thermal energy storage, Applied Energy, v. 181, p. 464-476.

REN21 (2018): Renewables 2018 - Global Status Report, Renewable Energy Policy Network for the 21st Century

Reuss M (2015): 6 - The use of borehole thermal energy storage (BTES) systems, in Cabeza, LF, ed., Advances in Thermal Energy Storage Systems, Woodhead Publishing, p. 117-147.

Reuss M, Beck M and Müller JP (1997): Design of a seasonal thermal energy storage in the ground, Solar Energy, v. 59, no. 4–6, p. 247-257.

Reuss M, Beuth W, Schmidt M and Schoelkopf W (2006): Solar district heating with seasonal storage in Attenkirchen, in Proceedings 10th International Conference on Thermal Energy Storage Ecostock 2006, The Richard Stockton College of New Jersey, USA, 31 May - 2 June 2006, p. 193-200.

Rezaie B and Rosen MA (2012): District heating and cooling: Review of technology and potential enhancements, Applied Energy, v. 93, p. 2-10.

Rühaak W, Steiner S, Welsch B and Sass I (2015): Prognosefähigkeit numerischer Erdwärmesondenmodelle, Grundwasser, v. 20, no. 4, p. 243-251.

Sass I, Bracke R and Rühaak W (2015): Urban Heating, in Proceedings World Geothermal Congress, Melbourne, Australia, 19-25 April 2015, p. 5.

Sass I, Brehm D, Coldewey WG, Dietrich J, Klein R, Kellner T, Kirschbaum B, Lehr C, Marek A, Mielke P, Müller L, Panteleit B, Pohl S, Porada J, Schiessl S, Wedewardt M and Wesche D (2016): Shallow Geothermal Systems - Recommendations on Design, Construction, Operation and Monitoring, Wilhelm Ernst & Sohn, 312 p.

Schaumann G and Schmitz KW (eds.) (2010): Kraft-Wärme-Kopplung, Berlin [u.a.], Springer, XIII, 455 p.

Schellong W (2016): Analyse und Optimierung von Energieverbundsystemen, Berlin, Heidelberg, Springer Vieweg, XIII, 545 p.

Schlesinger M, Hofer P, Kemmler A, Kirchner A, Koziel S, Ley A, Piégsa A, Seefeldt F, Straßburg S, Weinert K, Lindenberger D, Knaut A, Malischek R, Nick S, Panke T, Paulus S, Tode C, Wagner J, Lutz C, Lehr U and Ulrich P (2014): Entwicklung der Energiemärkte – Energiereferenzprognose, Studie im Auftrag des Bundesministeriums für Wirtschaft und Technologie, Projekt Nr. 57/12, http://www.bmwi.de/Redaktion/DE/Publikationen/ Studien/entwicklung-der-energiemaerkte-energiereferenzprognose-endbericht.html, accessed 07.06.2017.

Schmidt D, Kallert A, Blesl M, Svendsen S, Li H, Nord N and Sipilä K (2017): Low Temperature District Heating for Future Energy Systems, Energy Procedia, v. 116, no. Supplement C, p. 26-38.

Schmidt T, Mangold D and Müller-Steinhagen H (2004): Central solar heating plants with seasonal storage in Germany, Solar Energy, v. 76, no. 1-3, p. 165-174.

Schulte DO (2016): Simulation and Optimization of Medium Deep Borehole Thermal Energy Storage Systems, Dissertation, Technische Universität Darmstadt, XXII, 132 p.

Schulte DO, Rühaak W, Chauhan S, Welsch B and Sass I (2015): A MATLAB Toolbox for Optimization of Deep Borehole Heat Exchanger Arrays, *in* Proceedings World Geothermal Congress 2015, Melbourne, Australia, 19-25 April 2015, p. 5.

Schulte DO, Rühaak W, Oladyshkin S, Welsch B and Sass I (2016a): Optimization of Medium-Deep Borehole Thermal Energy Storage Systems, Energy Technology, v. 4, no. 1, p. 104-113.

Schulte DO, Rühaak W, Welsch B and Sass I (2016b): BASIMO – Borehole Heat Exchanger Array Simulation and Optimization Tool, Energy Procedia, v. 97, p. 210-217.

Schulte DO, Welsch B, Boockmeyer A, Rühaak W, Bär K, Bauer S and Sass I (2016c): Modeling insulated borehole heat exchangers, Environmental Earth Sciences, v. 75, no. 10, p. 1-12.

Short W, Packey DJ and Holt T (1995): A Manual for the Economic Evaluation of Energy Efficiency and Renewable Energy Technologies, National Renewable Energy Laboratory

Sibbitt B, McClenahan D, Djebbar R, Thornton J, Wong B, Carriere J and Kokko J (2012): The Performance of a High Solar Fraction Seasonal Storage District Heating System – Five Years of Operation, Energy Procedia, v. 30, p. 856-865.

Skanska AB (2018): Entré Lindhagen, https://group.skanska.com/projects/57328/Entre-Lindhagen, Web Page, accessed 11 October 2018.

Smirnov N (1948): Table for Estimating the Goodness of Fit of Empirical Distributions, The Annals of Mathematical Statistics, v. 19, no. 2, p. 279-281.

Solar-Institute Jülich (2016): CARNOT 6.0 for MATLAB 2013b.

Sterner M and Bauer F (2017): Definition und Klassifizierung von Energiespeichern, *in* Sterner, M, and Stadler, I, eds., Energiespeicher - Bedarf, Technologien, Integration, Berlin, Heidelberg, Springer, p. 25-49.

Stiles L (1998): Underground thermal energy storage in the US, IEA Heat Pump Centre Newsletter, v. 16, no. 2, p. 22-23.

Stumm W and Morgan JJ (1996): Aquatic chemistry : chemical equilibria and rates in natural waters, New York, Wiley, Environmental science and technology, xvi, 1022 p. p.

ten Hulscher TEM and Cornelissen G (1996): Effect of temperature on sorption equilibrium and sorption kinetics of organic micropollutants - a review, Chemosphere, v. 32, no. 4, p. 609-626.

The MathWorks Inc. (2016a): Global Optimization Toolbox, Natick, MA.

The MathWorks Inc. (2016b): MATLAB 2016a, Natick, MA.

Thinkstep AG (2011): GaBi: Software and database contents for Life Cycle Engineering.

Thomsen PD and Overbye PM (2016): Energy storage for district energy systems, *in* Wiltshire, R, ed., Advanced District Heating and Cooling (DHC) Systems, Oxford, Woodhead Publishing, p. 145-166.

Tian Y and Zhao CY (2013): A review of solar collectors and thermal energy storage in solar thermal applications, Applied Energy, v. 104, no. Supplement C, p. 538-553.

Tveit T-M, Savola T, Gebremedhin A and Fogelholm C-J (2009): Multi-period MINLP model for optimising operation and structural changes to CHP plants in district heating networks with long-term thermal storage, Energy Conversion and Management, v. 50, no. 3, p. 639-647.

UBA (ed.) (2015): Auswirkungen thermischer Veränderungen infolge der Nutzung oberflächennaher Geothermie auf die Beschaffenheit des Grundwassers und seiner Lebensgemeinschaften – Empfehlungen für eine umweltverträgliche Nutzung, Dessau-Roßlau, Umweltbundesamt, TEXTE 54/2015, 159 p.

UBA (2018): National Trend Tables for the German Atmospheric Emission Reporting 1990-2016, Dessau, Umweltbundesamt.

UN (2014): World Urbanization Prospects: The 2014 Revision, CD-ROM Edition, United Nations, Department of Economic and Social Affairs, Population Division.

UN (2015): Paris AgreementUnited Nations Framework Convention on Climate Change, https://unfccc.int/sites/default/files/english_paris_agreement.pdf, accessed 4th October 2018.

Verein Deutscher Ingenieure (2004): VDI-4640 Teil 4: Thermische Nutzung des Untergrundes - Direkte Nutzung — VDI-4640 Part 4: Thermal use of the underground - direct uses.

Viessmann M (ed.) (2012): Umweltschonende Energieversorgung im zweithöchsten Gebäude der Welt - Zwölf Wärmepumpen für Super-Wolkenkratzer in Südkorea, Viessmann aktuell - Das Heiztechnik-Magazin, v. 44 (1), 22-23 p.

Waltz RA, Morales JL, Nocedal J and Orban D (2006): An interior algorithm for nonlinear optimization that combines line search and trust region steps, Mathematical Programming, v. 107, no. 3, p. 391-408.

Welsch B, Göllner-Völker L, Schulte DO, Bär K, Sass I and Schebek L (2018): Environmental and economic assessment of borehole thermal energy storage in district heating systems, Applied Energy, v. 216, p. 73-90.

Welsch B, Rühaak W, Schulte DO, Bär K, Homuth S and Sass I (2015): A Comparative Study of Medium Deep Borehole Thermal Energy Storage Systems Using Numerical Modelling, in Proceedings World Geothermal Congress 2015, Melbourne, Australia, 19-25 April 2015, p. 6.

Welsch B, Rühaak W, Schulte DO, Bär K and Sass I (2016): Characteristics of medium deep borehole thermal energy storage, International Journal of Energy Research, v. 40, no. 13, p. 1855-1868.

Welsch B, Rühaak W, Schulte DO, Formhals J, Bär K and Sass I (2017): Co-Simulation of Geothermal Applications and HVAC Systems, Energy Procedia, v. 125, p. 345-352.

Wernet G, Bauer C, Steubing B, Reinhard J, Moreno-Ruiz E and Weidema B (2016): The ecoinvent database version 3 (part I): overview and methodology, The International Journal of Life Cycle Assessment, v. 21, no. 9, p. 1218-1230.

Witte HJL and Van Gelder AJ (2007): Three years monitoring of a borehole thermal energy store of a UK office building, in Paksoy, HÖ, ed., Thermal Energy Storage for Sustainable Energy Consumption, Dordrecht, Springer Netherlands, p. 205-219.

Wittig V, Bracke R and Hyun-Ick Y (2015): Hydraulic DTH Fluid / Mud Hammers with Recirculation Capabilities to Improve ROP and Hole Cleaning for Deep, Hard Rock Geothermal Drilling, in Proceedings World Geothermal Congress, Melbourne, Australia, 19-25 April 2015.

Wong B, Snijders A and McClung L (2006): Recent lnter-seasonal underground thermal energy storage applications in Canada, at 2006 IEEE EIC Climate Change ConferenceMay 2006, p. 1-7.

Xu J, Wang RZ and Li Y (2014): A review of available technologies for seasonal thermal energy storage, Solar Energy, v. 103, p. 610-638.

Yang H, Cui P and Fang Z (2010): Vertical-borehole ground-coupled heat pumps: A review of models and systems, Applied Energy, v. 87, no. 1, p. 16-27.

Yin B, Wu X, Wang Y and Song C (2015): Performance analysis on a large scale borehole ground source heat pump combined with ice storage in Tianjin Cultural Center, in Proceedings Greenstock 2015, Beijing, China, 19-21 May 2015.

Yu Z, Li H, Wu J and Xu W (2015): Application of thermal energy storage in a nearly zero energy office building, in Proceedings Greenstock 2015, Beijing, China, 19-21 May 2015.

Zhang S and Xu W (2014): Research and development of large scale ground source heat pump system, Asian Heat Pump and Thermal Storage Technologies Network Newsletter 3, p. 4-11.

Zienkiewicz OC, Taylor RL and Zhu JZ (2013): The Finite Element Method: Its Basis and Fundamentals, Oxford, Waltham, Butterworth-Heinemann,, p. 756.

Appendix A – Seasonal high temperature storage with medium deep borehole heat exchangers

Published as:

Bär K, Rühaak W, **Welsch B**, Schulte DO, Homuth S and Sass I (2015): Seasonal high temperature storage with medium deep borehole heat exchangers, *Energy Procedia*, v. 76, p. 351-360, doi:10.1016/j.egypro.2015.07.841.

European Geosciences Union General Assembly 2015, EGU

Division Energy, Resources & Environment, ERE

Seasonal high temperature heat storage with medium deep borehole heat exchangers

Kristian Bär[a]*, Wolfram Rühaak[a,b], Bastian Welsch[a,b], Daniel Schulte[a,b], Sebastian Homuth[c], Ingo Sass[a,b]

[a]*Technische Universität Darmstadt, Institute of Applied Geosciences, Department of Geothermal Science and Technology, Schnittspahnstrasse 9, 64287 Darmstadt, Germany*
[b]*Darmstadt Graduate School of Excellence Energy Science and Engineering, Technische Universität Darmstadt, Jovanka-Bontschits-Straße 2, 64287 Darmstadt, Germany*
[c]*Züblin Spezialtiefbau GmbH Ground Engineering, Europa-Allee 50, 60327 Frankfurt a.M., Germany*

Abstract

Heating of buildings requires more than 25 % of the total end energy consumption in Germany. By storing excess heat from solar panels or thermal power stations of more than 110 °C in summer, a medium deep borehole thermal energy storage (MD-BTES) can be operated on temperature levels above 45 °C. Storage depths of 500 m to 1,500 m below surface avoid conflicts with groundwater use. Groundwater flow is decreasing with depth, making conduction the dominant heat transport process. Feasibility and design criteria of a coupled geothermal-solarthermal case study in crystalline bedrock for an office building are presented and discussed.

* Corresponding author. Tel.: +49-6151-16-70953; fax: +49-6151-16-6539.
  E-mail address: baer@geo.tu-darmstadt.de

1. Introduction

More than 50 % of the overall energy demand in Germany is due to heating and cooling purposes [1]. Therefore, groundbreaking techniques are needed to save energy and reduce greenhouse gas emissions especially in this low exergy sector. The combination of different renewable energy sources – solar thermal and geothermal – with already existing district heating systems fed by combined heat and power stations (CHP) is a promising new approach.

In summer, excess solar thermal energy is available, while in winter when thermal energy is needed for heating systems its quantity is usually not sufficient. There are different options to cope with the seasonal offset of thermal energy supply and demand. Besides traditional storage tanks at the surface, thermal storage in shallow aquifers and shallow borehole thermal energy storage (BTES, [2, 3]), geothermal heat storage in moderate depths is an innovative and yet barely tested concept. In difference to shallow heat storage systems, the proposed approach upgrades the naturally available geothermal energy in the subsurface by means of external heat input. This is done in summer when no space heating is required or at times when surplus energy from nearby sources is available. In winter when other sources of energy are not sufficiently and cheaply available, the thermal energy from the geothermal storage is used for heating purposes.

The focus of the presented study is the environmentally friendly and energy efficient redesigning of a more than 50 years old office and laboratory building. A BTES system [4] as well as an energy efficient building design will help to use sustainable energy sources for the next period of the building's lifetime.

2. High Temperature Borehole Thermal Energy Storage

The proposed system of a MD-BTES [5] consists of multiple boreholes with depths of 100 m – 1,000 m. Coaxial borehole heat exchangers (BHE) are implemented in the boreholes. The surrounding rock is utilized as a heat storage, the cementation and borehole wall function as heat exchanger. Typically, water (in some cases with refrigerant or other additives to prevent corrosion) is used as heat carrier fluid.

For the design of a MD-BTES two separate phases have to be considered. These phases are the charging phase and the extraction phase. During the charging phase hot water is injected into the BHE to heat up the reservoir. For heat extraction, cold water is pumped into the BHE in order to retrieve the stored thermal energy from the relatively hot formation. It is important to consider the two possible flow directions in a coaxial BHE. The inlet can be either the central pipe (CXC, Figure 1a) or the annulus (CXA, Figure 1b). Flow direction and inlet temperature influence the heat transfer between working fluid and subsurface. In the charging phase, the working fluid should reach the bottom of the wellbore in the insulated inner pipe before discharging the bulk of its heat into the surrounding rock at maximum depth. In the extraction phase, the cold fluid should be injected into the outer pipe to utilize the borehole wall as heat exchanger surface at full length. Furthermore, this reduces heat losses of the working fluid by circulating it back to the surface through the insulated central pipe after it reached its peak temperature at the bottom of the borehole. Consequently, seasonally alternating flow directions in the BHE are beneficial (Figure 1).

The advantage of BTES systems over open systems is the closed circulation system, which is not allowing a direct contact or mass transfer of heat carrier fluids with the groundwater or subsurface. Geochemical alteration processes and a direct hydrochemical or biological influence on the groundwater will be prevented. Furthermore, this protects auxiliaries like pumps, etc. on the surface against scaling and corrosion. This results in a higher lifetime expectancy of such systems and a more constant and therefore more economical operation.

Deep BHEs can be constructed almost everywhere, due to the fact that neither naturally occurring thermal aquifer systems nor special geological structures are needed. The only requirement for heat storage is a location with negligible groundwater flow at reservoir depth so that the induced thermal plume is not dissipated.

In contrast to conventional shallow BTES systems the mandatory heat pump is not necessarily needed due to the higher operation temperature levels [6]. Consequently, the electric power needed to run the system is reduced and thus the profitability of the system is increased. Additionally, deep BTES have a much smaller surface footprint than shallow BTES with the same capacity and are therefore a viable option in densely urbanized areas.
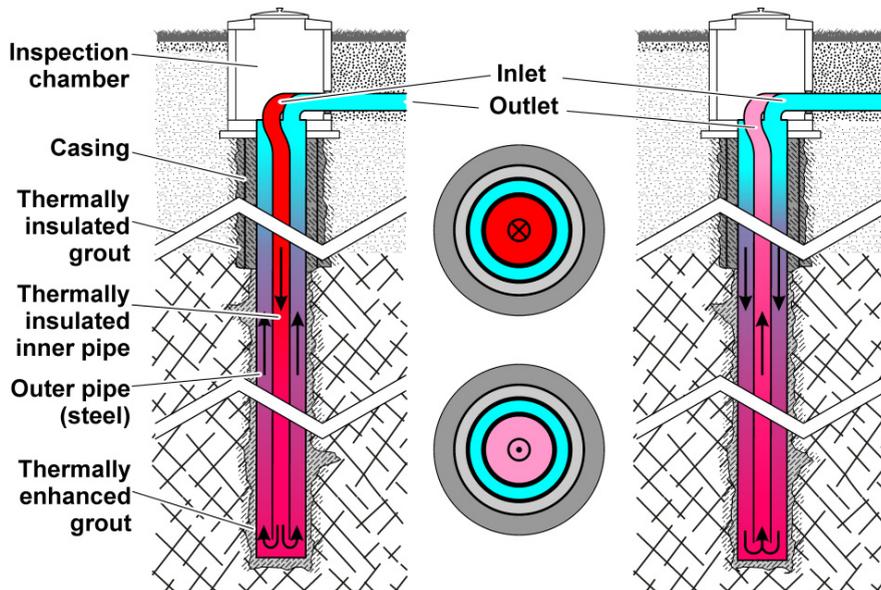
Fig. 1. Schematic horizontal and vertical cross sections of a deep coaxial borehole heat exchanger used as heat storage in summer (charge of the storage as CXC flow, left side and upper middle) and winter (discharge of the storage as CXA flow, right side and lower middle), respectively. Note that only the crystalline bedrock is used as heat storage while the caprock including possible aquifers are thermally insulated.

The completion depth of about 100 m – 1,000 m with higher underground temperatures compared to shallow systems results in a lower lateral temperature gradient between the heat carrier fluid and the surrounding rock. This means a notable decrease of heat losses, which additionally enhances system efficiency.

Charging the BTES with temperatures of up to 110 °C supplied by various heat sources in combination with greater depths can allow for return temperatures of the BTES of 45 °C – 75 °C after an initial charging phase of 3 to 5 years. This is highly depending on the setup of the storage and utilization scenarios [7]. The constant supply of such high heating temperatures allows for applications with conventional radiator-based high-temperature heating systems commonly installed in older buildings. This makes MD-BTES systems even an option for old buildings without low temperature heating systems not meeting the actual energy efficiency levels. Another option is to directly feed in to district heating systems and supply heat for multiple uses possibly even at cascading temperature levels.

For the dimensioning and operation of a BTES, good knowledge of the petrophysical (conductive heat transfer) and the hydraulic (convective heat transfer) properties as well as of the initial subsurface temperature regime is mandatory [8]. Additionally, important design parameters are the heat demand and the required temperature levels of the installed heating systems.

Different kinds of energy flows as well as different storage and utilization scenarios have to be assessed in the simulation and feasibility studies of such systems. Specific user profiles and economic frameworks have to be considered along with local heat sources and sinks.

3. Site Description

The planned drill site (Darmstadt, Germany) for the MD-BTES system is located next to the eastern master fault zone of the Upper Rhine Graben, which divides the urban area of Darmstadt in geological and hydrogeological terms (Figure 2a). A crystalline and Permian-Carboniferous fracture controlled aquifer of the Odenwald and Sprendlinger Horst is located in the eastern part of the city whereas the western part is dominated by a Quaternary porous aquifer of the sedimentary graben fill of the Upper Rhine Graben (Figure 2b).

The northern part of the Upper Rhine Graben fault system is characterized by steep faults in N-S to NNE-SSW direction, which show up to 2,000 m of cumulative vertical displacement. Especially in the inner city area a turn in strike direction to NE – SW results in a complex block mosaic structure [9, 10].

The lithology of the proposed MD-BTES site consists from top to bottom of a 4 - 5 m thick Quaternary soil layer, underlain by some 30 – 60 m thick intercalation of Permo-Carboniferous coarse to fine grained siliciclastic sediments, volcanoclastics and partly altered basaltic to andesitic volcanics [11]. Those unconformably overly the crystalline basement with an up to 30 m thick weathered zone at its top (Figure 2, [12]).
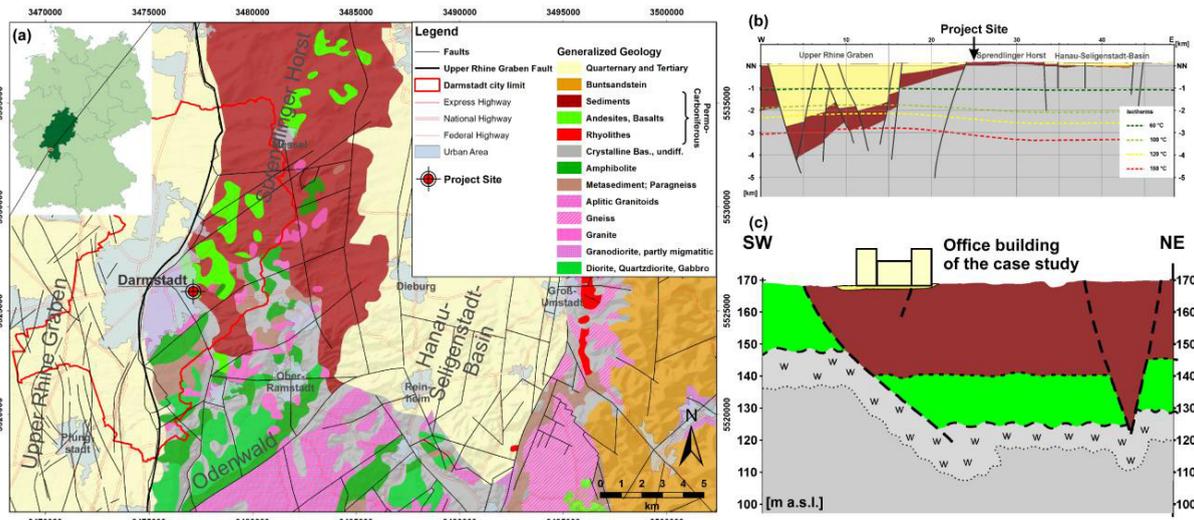
Fig. 2. (a) Simplified geological map of the project site at the eastern Upper Rhine Graben fault, after [13]. (b) Schematic W-E-cross section of the northern Upper Rhine Graben and accompanying graben shoulders including major isotherms [14]. (c) Schematic SW-NE-cross section of the project site, modified from [11], symbol w indicates weathered zone at the top of the crystalline bedrock.

The basement is mainly composed of granodiorite. Additionally, at this northern end of the Odenwald complex amphibolites, diabase, gneiss, granite, diorite, gabbro and hornfels occur [15, 16]. These varying, mostly NE-SW trending, formations are intruded by basic to acidic dyke rocks [17]. The basement is the target of the MD-BTES.

The upper 30 – 40 m of granodiorite are intensely weathered. This is due to its surface exposure during the Permian-Carboniferous, the Upper Cenozoic and the Lower Pleistocene. Near the fracture zone of the Upper Rhine Graben fault systems, weathering is most intensive and results in gravelly layers partially acting as porous aquifers. The hydraulic conductivity of these weathered and fresh rocks are in the range of $10^{-4} – 10^{-5}$ m/s and $10^{-6} – 10^{-7}$ m/s, respectively [12, 17, 18]. Dykes can be either permeable or impermeable [17]. Nonetheless, at depths of more than 100 m the permeability is supposed to be very low making it suitable for a MD-BTES system.

Information about the subsurface temperature result from the 3D geothermal model of Hesse, Germany [19]. Nearby deep drilling sites show that the geothermal gradient ranges between 2.6 and 3.9 °C/100 m.

4. Assessment of Different Heating Scenarios

For this case study two different heat supply scenarios (Figure 3 and 4) were assessed for the office building currently being redesigned in an environmentally friendly and energy efficient way compared to its current system:

1. The use of excess heat from a CHP to charge the MD-BTES system during summer and retrieving all required heat directly from the storage in winter,
2. The combination of scenario 1 with solar thermal collectors on the roof of the building charging the MD-BTES during summer and providing partial direct heat supply during winter. Additional heat demand for charging the MD-BTES is covered by the CHP.

The typical design of a project such as this would not include deep BHEs. Normally a multiple BHE array would be drilled and completed to a depth of not more than 100 – 200 m. At the project site, the boreholes will be placed in a parking lot next to the building. Because of space availability, an array of shallow BHEs large enough to cover the

heat demand is not possible due to the spatial restrictions. Therefore, a layout with a few deeper boreholes and a small surface footprint instead of a multiple borehole array is chosen.
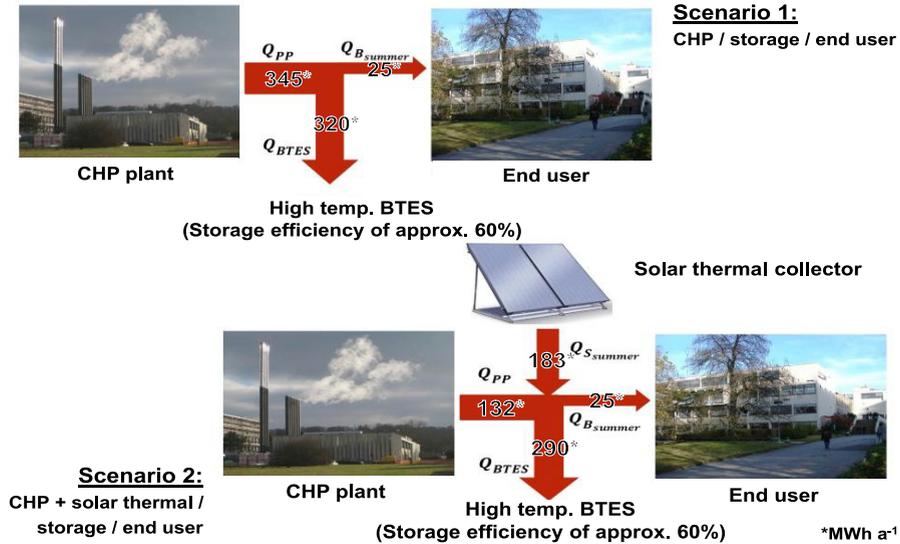
Fig. 3. (top): summer operation mode of scenario 1 with the combined heat and power (CHP) plant covering both the heat demand of the building and the MD-BTES. (bottom): summer operation mode of scenario 2 with the coupling of the CHP and solar thermal collectors to cover the heat demand of the building and the MD-BTES. Numbers are annual heat flows in MWh assuming a storage efficiency of 60%.
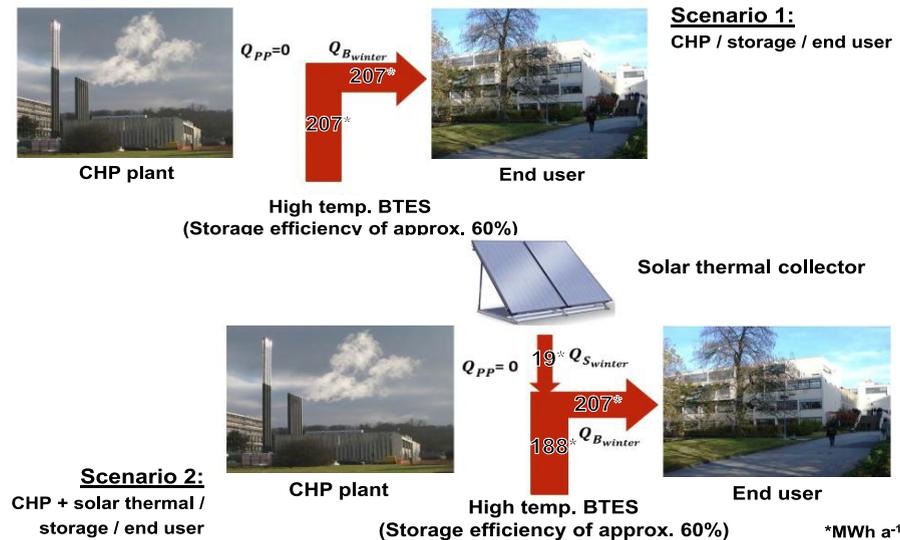
Fig. 4. Winter operation modes for scenarios (1) and (2) respectively with coupling of combined heat and power (CHP) plant, solar thermal collectors and MH-BTES. Numbers are annual heat flows in MWh assuming a storage efficiency of 60%.

In a first step, the building's heat demand and the heat gains of different solar installations were assessed according to national or international standards and requirements. Based on the results, the energy flow demand between the different heat sources and sinks of the three proposed scenarios were evaluated.

4.1. Heat Demand

The building's energy consumption was modelled using a standard software package for precise calculation of energy consumption of every single room inside a building considering the meteorological data of the Test Reference Years (TRY) provided by Germany's National Meteorological Service [20, 21]. All parameters influencing the energy use are defined in the software. The calculations of the required heating load are done according to the standards [22] and [23].
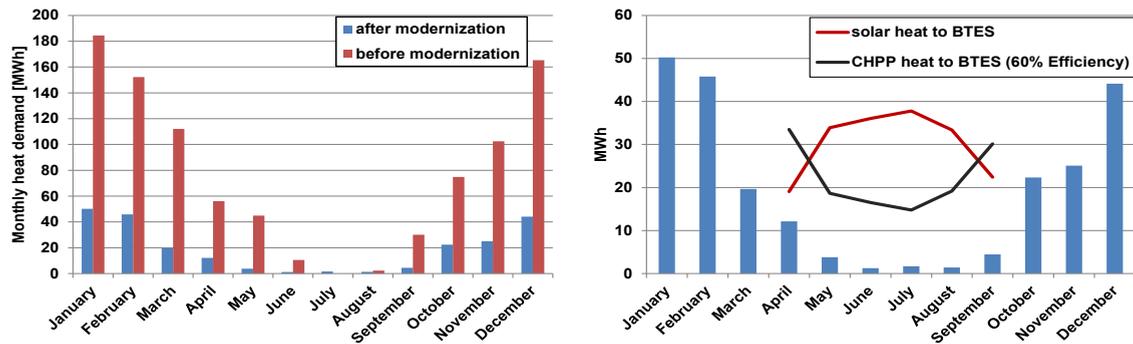
Fig. 5. (left): comparison of the modelled monthly heat demand of the project building before and after the modernization in 2012. (right): amount of solar heat available from the evacuated tube collectors which can be stored in summer and amount of heat needed from the CHP to cover the heat demand of the storage assuming a storage efficiency of 60%.

Both the heat demand of the building as build in the 1960's and after modernization in 2012 were calculated. Therefore, design construction parameters, the geometry, building service engineering and different space usage were considered. The model of the building was positively validated against measured energy usage in the building with its conditions before modernization. Unfortunately, the modernization is split into two phases. Therefore, a comparison of the actual to the modeled heat demand of the completely modernized building is not yet possible.

The results of the heat demand calculations show a significant reduction after modernization. The modeled value is 232 MWh/a, which represents a reduction of 75 % compared to the measured demand for 2009 of 935 MWh/a (modeled: 916 MWh/a) before the modernization (Figure 5). The calculated characteristic heating energy consumption of the modernized building is 37 kWh/(m²·a) compared to 148 kWh/(m²·a) before modernization, making it one of the most energy efficient buildings for teaching and research purposes of the University.

4.2. Solar Thermal Collectors

For scenario 2 the available roof top area for solar thermal collectors had to be assessed. The building has a flat roof (1,796 m²) easily adaptable for solar installations. The amount of energy produced varies depending on the location, manner of installation and type of the solar collectors. The solar heat gains of the solar thermal system were calculated after [24] for three different types of solar installations: flat plate collectors with an optimized inclination angle of 39°, flat plate collectors with seasonally changing optimized inclination angles of 21° and 57° and evacuated tube collectors situated flat on the roof with tubes tilted 25°. The design arrangement of the solar collectors was based on the limits set by [25] as well as the shading areas of existing construction elements (elevator shafts, ventilation systems) and the solar collectors itself [26].

The biggest amount of solar heat (422 MWh/a) of all considered installations was obtained in the installation with evacuated tube collectors. This is 72 % more than from flat plate collectors with inclination angles of 21° and 57° (114 MWh/a) and 75 % more than from those with an inclination angle of 39° (106 MWh/a). This large contrast between the systems is mainly caused by differences in efficiency of the collectors and in total collector surface area considering the required minimum spacing between collectors. The efficiency used for further calculations of the flat

plate collectors was 25 %, where the efficiency of the evacuated tube collectors was 62 %. The total surface area of evacuated tube collectors was 292 m², 181 m² for the flat plate collectors with 21°/57° inclination angle and 195 m² for those with an inclination angle of 39° (195 m²).

During the winter months, the only time when it's possible to obtain heat from the solar installation is from 12 to 3 pm. This means that the solar installation will be able to provide only a small fraction of a building's heat demand. The solar heat gains for minimum solar insulation (conservative approach) obtained for evacuated tube collectors were used for the calculations.

For the further calculations of the energy flow between the sources and sinks the year was divided into two parts. Charging of the MD-BTES in summer included the months April till September. Extracting heat in winter took place from October till March. The storage efficiency was assumed to be 60 % according to comparable projects [8].

4.3. Results

For scenario 1, the heat demand of the system resulting from the buildings summer heat demand (25 MWh/a) and the energy needed to charge the MD-BTES (345 MWh/a) to meet the buildings winter heating energy demand (207 MWh/a) amounts to 370 MWh/a. This is higher than the annual heat demand supplied by the CHP directly, but still 2.5 times less than what was delivered directly to the building before modernization.

For scenario 2, it was assumed that solar heat is able to meet only about 8 % (17 MWh/a) of the buildings winter heat demand directly because of its short availability and time lag in relation to the buildings heating energy demand. During summer the considered solar thermal installation was able to deliver all of the buildings summer heat demand (25 MWh/a) and supply the MD-BTES with 182 MWh/a of thermal energy. The additional amount of heat from the CHP, which is needed to charge the MD-BTES, was calculated to be 84 MWh/a.

These preliminary results, which do not consider any analytical or numerical analysis of the systems behavior, show that the solar thermal installation is able to deliver 68 % of the required heat of scenario 2. The rest of the heat (84 MWh/a) can be delivered by the CHP and amounts to only 58 % of the heat which was delivered to the building during summer months by the CHP (144 MWh) before its modernization and only 36 % of the total heat demand of the building. The proper design of the solar thermal installation combined with the MD-BTES should therefore be able to significantly reduce or exclude heat provided by the CHP to the project building and will therefore be responsible for a reduction in the CO_2 emissions compared to the current system.

4.4. Drilling Technology

Another important factor for the economic feasibility of MD-BTES systems are the drilling costs. Competitive and cheap drilling technologies are a prerequisite. Because of depth considerations and the geological setting the boreholes for the proposed MD-BTES (100 - 1,000 m b.g.s) shall be drilled with down the hole (DTH) hydraulic hammer drilling technology. Improved cutting transport, increased hole stability and enhanced deviation control (less than 5 to 10 % vertical deviation angle compared to 10 to 40 % with pneumatic hammer [27]) are reasons for the hydraulic hammer. Especially a minimized deviation from the vertical is a crucial prerequisite in BHE fields, where usually less than 10 m spacing between single BHEs is applied. Additionally, CO_2 emission reduction can be achieved since [28] showed that for an equivalent hole of 220 m a pneumatic drilling requires 2.9 l/m of diesel fuel in comparison to 0.7 l/m for the hydraulic hammer drilling process.

5. Design and Numerical Simulation of the System

The BHE completion design has an important influence on the thermal performance of the system. Stainless steel as outer casing material with a thermal conductivity of 54 W/m·K is used to ensure a higher efficiency of heat exchange between the subsurface and the heat carrier fluid in the outer pipe. For the inner pipe pre-insulated steel is recommended to reduce the effective thermal conductivity and thermal bypassing. A 10 mm thick PE foam insulator has a thermal conductivity of 0.026 W/m·K.

The deeper section of the granodiorite is suitable for heat storage whilst the caprock and the weathered zone locally and temporarily may act as an aquifer. Therefore, a thermally and hydraulically insulating backfill material for the shallow wellbore section is required as indicated in Figure 1.

In designing vertical BHEs, the determination of the necessary depth as well as array configuration and amount of boreholes is crucial. Typically, the depth is estimated based on the desired power extraction per unit depth by considering steady state heat transfer. Due to long term and peak power extraction during the operation time, the heat flow will change into transient behavior. In multi BHE systems the degree of geothermal heat enhancement by external heat input depends on various factors such as spacing of boreholes, depth of BHE and amount of heat and frequency of storage phases, etc. These factors affect the level of average output heat during heat extraction depending on the actual heat demand scenario. To find a best fit BHE scenario the consideration of those parameters is necessary but also results in more computation time. Here, best fit scenario means the BHE system with the highest efficiency and highest production capacity possible at minimum total BHE length and economical heat storage conditions.

5.1. Numerical Model

Numerical modeling of the MD-BTES was carried out using FEFLOW [29, 30] to describe the transient behavior of the subsurface and the production characteristics of the system with the set up given in Figure 6. It delivers information about the capacity and sustainability of the BHE system for a given size, depth, flow rate, heat extraction intervals and other factors.
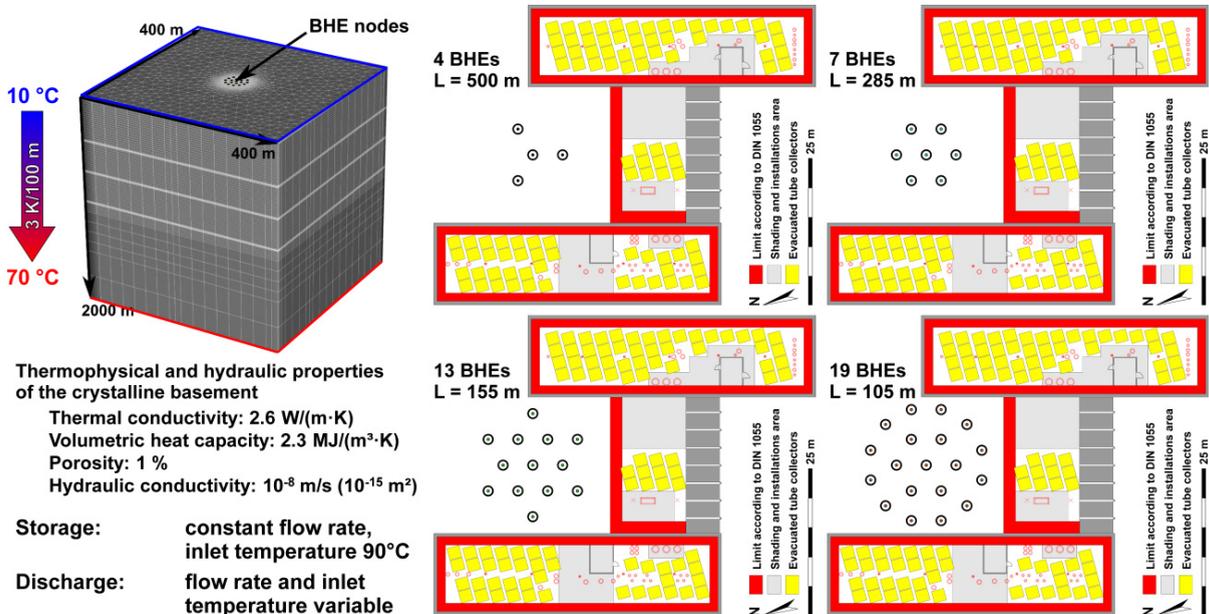
Fig. 6. (left): General set up, parameters, boundary conditions and flow rates and temperature during storage and extraction of the numerical FEFLOW models. (right): Layout of the BHEs in top view of the modelled office building including the position of the evacuated tube collectors installed on the building's roof for the four different preliminary set ups: 4, 7, 13 and 19 BHE's with the same total BHE length for the BTES.

Depending upon the depth of the proposed MD-BTES a vertical extent of the model is defined. The vertical extent is set such that the boundary parameters are kept considerably far from the MD-BTES. For a 1.0 km deep BHE a vertical model extent of 2.0 km has been set so that the 1st kind (temperature) boundary condition or other heat flux boundary conditions may not directly influence the BHEs. Boundary conditions have been set as shown in Figure 6. A subsurface temperature distribution with a geothermal gradient of 3 °C/km is set as initial condition. This model is now used incorporating 4th kind (BHE) boundary conditions at the BHE nodes with the BHE parameter setting and loading cycles for an operation period of 30 years.

5.2. Results

The simulation results (Figure 7) illustrate that the storage efficiency and the outlet temperature are higher if more BHEs can thermally interact with each other. Minimum outlet temperatures range from 40 °C to 60 °C after 30 years of operation. Thus, heat pumps are only needed during the coldest days of the heating period. Storage efficiencies are rather low, illustrating that either the heat demand of the building is too low for the chosen sizes of the different storage set ups and that more heat could be discharged from the storage in winter or that the heat input during summer was too high.
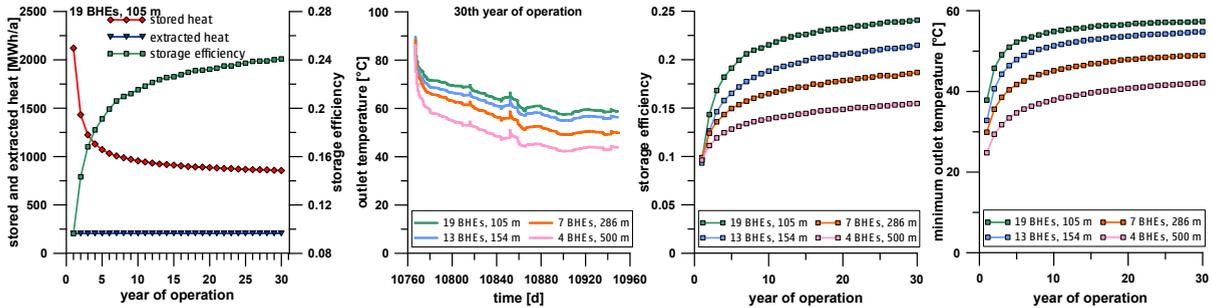
Fig. 6. (From left to right): Stored heat, extracted heat and storage efficiencies of the set up with 19 BHEs; comparison of the outlet temperatures in the 30th year of operation and of the storage efficiencies and minimum outlet temperatures (right) for the four different preliminary set ups.

To optimize the design and completion of the MD-BTES to maximize storage efficiency and to reach the desired temperature and power outputs as well as to evaluate the best economic scenario for such a coupled system two approaches are used in ongoing studies. The first approach [7] uses the software FEFLOW to model a variety of different geometrical scenarios as accurately as possible. For the second approach a MATLAB Toolbox [31] is designed to simulate a BHE heat storage system with similar numerical codes as used by FEFLOW but with other gridding and coupling algorithms, supposed to enable much shorter processing times. Furthermore, this toolbox incorporates mathematical optimization algorithms, which allow for an automatic optimization within predefined boundary conditions of each scenario. These parallel approaches are expected to define the best MD-BTES scenario for the project building.

6. Conclusions and Outlook

The largest energy consumer in industrial countries is building infrastructure with its heating and cooling demand. Innovative energy saving concepts in this field will have the biggest impact in terms of reducing CO_2 emissions. Especially the coupling of different renewable energy sources – solar thermal and geothermal – with already existing district heating systems – e.g. combined (biofuel-driven) heat and power stations (CHP) – as presented here, seems to be a very promising approach to cover the heating demand of renovated or old buildings at higher temperature levels with renewable energies. Since conventional heating systems are still installed in approximately more than 90 % of Germany's building stock, the presented concept is a viable option to reduce the heating energy demand and the related greenhouse gas emissions. Consequently, a high temperature storage and heating supply system without the application of a heat pump or specialized heat-pumps with increased coefficients of performance are needed. However, storage configurations like the MD-BTES systems can also be utilized for low temperature heating systems.

The design and completion of MD-BTES systems as described here are strongly depending on the knowledge about the subsurface and the energy flows between the heat source, the storage system and the building. The estimation of the BHE depth and completion design needs some iterative procedures. Coupled numerical-analytical modeling of the whole system combined with mathematical optimization algorithms will be used in future studies to estimate the optimal geometrical setup and depth of the MD-BTES.

Acknowledgements

References

[1] AGEB (ed). Anwendungsbilanzen für die Endenergiesektoren in Deutschland in 2011 und 2012 mit Zeitreihen von 2008 bis 2012. Berlin; 2013
[2] Hellstöm G. Ground Heat Storage, Thermal Analysis of duct Storage Systems. Department of Mathematical Physics, University of Lund; 1991.
[3] Bauer D, Marx R, Nußbicker-Lux J, Ochs F, Heidemann W, Müller-Steinhagen H. German central solar heating plants with seasonal heat storage. Solar Energy 2010:84(4):612-623.
[4] Homuth S, Bär K, Rühaak W, Sass I. Mitteltiefe kristalline Hochtemperaturspeicher – Dimensionierungsgrößen – Übertragbarkeit nördlichen Oberrheingraben (ORG). Proceedings Der Geothermiekongress 2012, Geothermische Vereinigung (GtV-BV e.V.), Essen; 2012.
[5] Homuth S, Rühaak W, Bär K, Sass I. Medium Deep High Temperature Heat Storage. Proceedings, European Geothermal Congress, Pisa, 2013.
[6] Kuntz D, Kübert M, Walker-Hertkorn S, Reisig O.A. Saisonale geothermische Wärmespeicher zur Direktheizung – ein Praxisbeispiel. Geothermische Energie 2013:76.
[7] Welsch B, Rühaak W, Schulte DO, Bär K, Homuth S, Sass I. A Comparative Study of Medium Deep Borehole Thermal Energy Storage Systems Using Numerical Modelling. Proceedings World Geothermal Congress 2015, Melbourne, Australia, 2015:7 p.
[8] Mielke P, Bauer D, Homuth S, Götz AE, Sass I. Thermal Effect of a Borehole Thermal Energy Store on the Subsurface. Geothermal Energy 2014:2,5. Springer, DOI 10.1186/s40517-014- 0005-1 .
[9] Fahlbusch K. Die geologischen Grundlagen der alten Wasserversorgung Darmstadts. Geol. Jb. Hessen 1980:108:223-240.
[10] Hoppe A, Lang S. The eastern master fault of the Upper Rhine Graben below the Science and Conference Centre in Darmstadt (Germany). Z. dt. Ges. Geowiss., 2007:158(1):113-117.
[11] Backhaus E. Die randliche „Rotliegend"-Fazies und die Paläogeographie des Zechsteins im Bereich des nördlichen Odenwaldes. Notizbl. Hess. L.-Amt Bodenforsch. 1965:93:112-140,
[12] Matthess G. Zur Vergrusung der magmatischen Tiefengesteine des Odenwaldes. Notizbl. Hess. L.-Amt Bodenforsch. 1964:92:160-178.
[13] Voges A, Toloczyki M, Trurnit P, Wittekindt H. Geologische Karte der Bundesrepublik Deutschland 1:1.000.000. BGR, Hannover; 1993.
[14] Bär,K. Untersuchung der tiefengeothermischen Potenziale von Hessen. PhD Thesis, TU Darmstadt, 2012:XXVI and 265 p.
[15] Stein E. The Geology of the Odenwald Crystalline Complex. Mineral. Petrol. 2001:72(1-3):7-28.
[16] Mezger JE, Felder M, Harms F-J. Crystalline rocks in the maar deposits of Messel: key to understand the geometries of the Messel Fault Zone and diatreme and the post-eruptional development of the basin fill. Z. dt. Ges. Geowiss. 2013:164(4):639-662.
[17] Beier M. Urbane Beeinflussung des Grundwassers: Stoffemissionen und-immissionen. PhD Thesis, TU Darmstadt; 2007.
[18] Greifenhagen G: Untersuchungen zur Hydrogeologie des Stadtgebietes Darmstadt mit Hilfe eines Grundwasserinformationssystems unter Verwendung von einer Datenbank, Datenmodellierung und ausgewählten statistischen Methoden. PhD Thesis, TU Darmstadt, (2000), 221 p.
[19] Bär K, Arndt D, Fritsche J-G, Götz A E, Kracht M, Hoppe A, Sass I. 3D-Modellierung der tiefengeothermischen Potenziale von Hessen – Eingangsdaten und Potenzialausweisung. Z. dt. Ges. Geowiss. 2011:162(4):371–388.
[20] Deutscher Wetterdienst (DWD), 2004: Testreferenzjahre von Deutschland, viewed 13th December 2010.
[21] Deutscher Wetterdienst (DWD), 2011: Climate data from selected German stations, viewed 13 December 2010.
[22] VDI-Gesellschaft Bauen und Gebäudetechnik, VDI-Fachbereich Facility-Management, VDI Richtlinie 2607 - Wirtschaftlichkeit gebäudetechnischer Anlagen - Blatt 11 - Rechenverfahren zum Energiebedarf beheizter und klimatisierter Gebäude; 2006.
[23] Deutsche Industrie Norm: Energy efficiency of buildings – Calculation of the net, final and primary energy demand for heating, cooling, ventilation, domestic hot water and lighting – Part 100 (18599-100), Deutsches Institut für Normung (DIN), Berlin; 2009.
[24] Honsberg C, Bowden S. Solar Radiation on a tilted Surface. http://pvcdrom.pveducation.org/SUNLIGHT/MODTILT.HTM; 2011.
[25] Deutsche Industrie Norm: Actions on structures - Part 4: Wind loads (1055-4:2005-03). Deutsches Institut für Normung (DIN), Berlin; 2005.
[26] Viessmann: VITOSOL technical guide, Author: Telford; 2006.
[27] Wittig V, Bracke R. Innovative Hydraulic DTH Drilling Technology based on Coiled Tubing for deep, hard rock Geothermal Drilling. Proceedings, European Geosciences Union (EGU) Kongress, Vienna / Wien; 2011.
[28] Riechers J. Wohin bohren wir? Masshaltigkeit konventioneller und innovativer hydraulischer GeoJEtting Bohrtechnik. unpublished BSc Thesis, Internationales Geothermiezentrum, Hochschule Bochum; 2011.
[29] Diersch H-JG, Bauer D, Heidemann W, Rühaak W, Schätzl P. Finite element modeling of borehole heat exchanger systems - Part 1: Fundamentals. Computers & Geosciences 2010a:37(8), DOI:10.1016/j.cageo.2010.08.003.
[30] Diersch H-JG, Bauer D, Heidemann W, Rühaak W, Schätzl P. Finite element modeling of borehole heat exchanger systems - Part 2. Numerical simulation. Computers & Geosciences 2010b:37(8):1136-1147.
[31] Schulte DO, Rühaak W, Chauhan S, Welsch B, Sass I. A MATLAB Toolbox for Optimization of Deep Borehole Heat Exchanger Storage Systems. Proceedings World Geothermal Congress 2015, Melbourne, Australia; 2015:5 p.

Appendix B – Characteristics of medium deep borehole thermal energy storage

Published as:

Characteristics of medium deep borehole thermal energy storage

Bastian Welsch[1,2,*,†], Wolfram Rühaak[1,2], Daniel O. Schulte[1,2], Kristian Bär[1] and Ingo Sass[1,2]

[1]Department of Geothermal Science and Technology, Technische Universität Darmstadt, Darmstadt, Germany
[2]Darmstadt Graduate School of Excellence Energy Science and Engineering, Darmstadt, Germany

SUMMARY

Seasonal energy storage is an important component to cope with the challenges resulting from fluctuating renewable energy sources and the corresponding mismatch of energy demand and supply. The storage of heat via medium deep borehole heat exchangers is a new approach in the field of Borehole Thermal Energy Storage. In contrast to conventional borehole storages, fewer, but deeper borehole heat exchangers tap into the subsurface, which serves as the storage medium. As a result, the thermal impact on shallow aquifers is strongly reduced mitigating negative effects on the drinking water quality. Furthermore, less surface area is required. However, there are no operational experiences, as the concept has not been put into practice so far. In this study, more than 250 different numerical storage models are compared. The influence of the characteristic design parameters on the storage system's behaviour and performance is analysed by variation of parameters like borefield layout, fluid inlet temperatures and properties of the reservoir rocks. The results indicate that especially larger systems have a high potential for efficient seasonal heat storage. Several GWh of thermal energy can be stored during summertime and extracted during the heating period with a high recovery rate of up to 83%. Medium deep borehole heat exchanger arrays are suitable thermal storages for fluctuating renewable energy sources and waste heat from industrial processes. Copyright © 2016 John Wiley & Sons, Ltd.

Correspondence

*Bastian Welsch, Darmstadt Graduate School of Excellence Energy Science and Engineering, Jovanka-Bontschits-Straße 2, 64287 Darmstadt, Germany.
†E-mail: welsch@geo.tu-darmstadt.de

1. INTRODUCTION

In 2011, about 25% of the global final energy consumption resulted from space heating and domestic hot water production [1]. Most of this heat is required in the winter season while there is a surplus of heat from various sources during summer. For example, solar thermal energy production is characterized by a high seasonality. Exploiting the full potential of solar thermal energy depends on economically competitive and reliable storage systems [2], which are able to bridge the seasonal offset between heat supply and heat demand. Thus, collector stagnation in summer is minimized and solar collector areas could be considerably reduced [3], especially in northern latitudes, where seasonal variations are high [4]. Furthermore, combined heat and power plants (CHP) often have to reduce their energy production because of the low heat demand in summer. Seasonal thermal storages can increase the operating time

and therefore the on-site heat and electricity production of CHPs. This leads to economic benefits and results in further savings of carbon dioxide emissions, compared with a CHP, which is operated without a seasonal storage [5–7]. Thermal energy storage systems can reduce energy costs and energy consumption, reduce equipment size, decrease the initial and maintenance costs and reduce pollutant emissions [8,9].

There are numerous methods for seasonal storage of thermal energy. Good overviews on the available technologies are given, for example, by Pinel *et al.* [2], Dincer and Rosen [8], Schmidt *et al.* [10], Xu *et al.* [11] and Hesaraki *et al.* [12]. Shallow borehole thermal energy storages (BTESs) are a promising technology and have been installed in several locations (e.g. [13–18]). They consist of several boreholes that are usually not deeper than 100 m. Some exceptions are known, for example, from Lund, Sweden [19] or Oshawa, Canada [20], where the

storage systems reach depths of 230 m and 200 m. The boreholes are equipped with borehole heat exchangers (BHEs). A BHE is a closed pipe system, which is embedded in a cement backfilling. A heat transfer fluid is circulated through the pipes. Heat is exchanged with the subsurface by conductive heat transport through the pipe wall and the backfill material. In this way, BTES can access a large storage volume at relatively low expenses [21]. A detailed technology description is given by Reuss [22].

The idea of using the ground as heat storage by shallow BHEs goes back to the 1970s/1980s [23–25]. In the 1980s and early 1990s, intensive research activities on shallow BTES were accomplished, particularly in Sweden and Finland: a first large-scale experimental and demonstration example was built in 1982/1983 at Luleå University of Technology, Sweden, consisting of 120 BHEs with a length of 65 m each [14,15]. Furthermore, the first numerical simulation models for BTES systems were developed (e.g. [26,27]). Lund and Östman [27] created a three-dimensional numerical model for BTES, which already accounted for convective heat flow in the storage region. They studied the behaviour of different BTES models in conjunction with variable dimensioning factors of a solar district heating system. Four different storage volumes were analysed, which all had a cubic geometry and a uniform BHE spacing. The deepest system they considered had a BHE length of 75 m. They also examined the influence of groundwater flow on the storage behaviour by simulating four different hydrogeological conditions. Nordell [28] developed a model for the design optimisation of shallow BTES, which also took account of economic aspects. He analysed sensitivities of different design and operational parameters as well as cost data on the optimum design of a storage system.

Although the viability of shallow BTES systems has been shown in several projects and simulation studies, there are some major difficulties linked to the concept. The major part of drinking water is produced from shallow aquifers. An increase of temperature can change the chemical (e.g. [29,30]) and biological (e.g. [31,32]) properties of the groundwater and thus have a negative impact on its quality [33–35]. Although most countries do not have any legal temperature limits for the heating and cooling of the groundwater [36,37], heat storage in the shallow subsurface is usually very restricted or not approved at all by the responsible water authorities. Furthermore, the return temperatures of shallow BTES are relatively low, and heat pumps are indispensable to provide the required supply temperatures for heating systems.

In contrast, storing heat at temperature levels of 90 °C or even more has a number of advantages compared with low temperature energy storage: higher loading temperatures in the summer season result in higher extraction temperatures during the heating period in winter. Consequently, the coefficient of performance of the heat pump increases, and a higher exergy efficiency of the heating system can be achieved [38]. Low temperature

heating systems, which are characterized by supply temperatures of 25 to 35 °C, could even be supplied directly without the use of a heat pump [39]. To mitigate the potentially hazardous impact on the shallow aquifers, the storage of high temperature heat in greater depths presents a viable alternative: fewer, but deeper BHEs with an insulation in the topmost section can protect the shallow aquifers and store the heat at depths up to several hundred metres [40]. As ground temperature increases with depth, a decreased lateral temperature gradient also reduces thermal losses. Additionally, these medium deep borehole thermal energy storages (MD-BTESs) require less space at the surface, which is especially advantageous in densely populated urban areas.

The dimensions of an MD-BTES differ significantly from those of a shallow BTES. Systems consisting of less than 50 BHEs and drilling depths of 100 m to 1000 m are taken into consideration. Compared with the relatively compact shape of shallow BTES, medium deep systems have an elongated geometry. Furthermore, medium deep systems can be operated at higher temperature levels, which in turn also leads to a different behaviour compared with shallow systems. Hence, the results of former studies are not generally transferable to MD-BTES. The concept has not been put into practice so far. There is no experience in operating an MD-BTES. As drilling costs increase with depth, the construction of an MD-BTES represents a large investment. Consequently, numerical simulations are necessary to predict the system performance and to estimate the influence of key parameters such as the dimension of the storage, the mode of operation and the underground properties.

This study presents comprehensive simulations of different MD-BTES configurations and examines the influence of the BHE length, the number of BHEs, the spacing between the boreholes, the fluid inlet temperatures and the rock properties on the system performance. The sensitivity of the parameters is assessed, and the setup of the simulation experiment is discussed. The study is part of a project, which assesses a potential MD-BTES system to be constructed at the Institute of Applied Geosciences, Technische Universität Darmstadt, Germany as described by Bär *et al.* [41].

2. METHODS

In order to quantify the influence of different design parameters on the performance of MD-BTES, numerical models of different storage setups were simulated, varying the parameters BHE length, number of BHEs and BHE spacing as listed in Table I(a). The simulation of all possible combinations of these parameter variations resulted in 200 different storage geometries. Figure 1 illustrates the five different BHE configurations resulting from the variation of the number of BHEs. In addition to the variation of the storage design, the influence of the heat transfer fluid temperature entering the storage system (inlet temperature)

Table I. Variation of influence parameters applied on the different storage models. Bold print denotes the base case design.

Variable	Value									
(a) Storage configuration										
BHE length [m]	100	200	300	400	500	600	700	800	900	1000
Number of BHEs[1]	7	13	19	28	37					
BHE spacing [m]	2.5	5	7.5	10						
(b) Fluid inlet temperatures										
During charging [°C]	70	80	**90**	100	110					
During discharging [°C]	10	20	**30**	40	50					
(c) Rock properties										
Thermal conductivity [$\mathrm{W\,m^{-1}\,K^{-1}}$]	1.4	2	**2.6**	3.2	3.8					
Volumetric heat capacity [$\mathrm{MJ\,m^{-3}\,K^{-1}}$]	2	2.15	**2.3**	2.45	2.6					
Hydraulic conductivity [$\mathrm{m\,s^{-1}}$]	$1\cdot10^{-9}$	$\mathbf{1\cdot10^{-8}}$	$1\cdot10^{-7}$	$5\cdot10^{-7}$	$1\cdot10^{-6}$	$5\cdot10^{-6}$	$1\cdot10^{-5}$	$1\cdot10^{-4}$		

[1]The number of borehole heat exchangers (BHEs) is the only non-continuous variable considered.
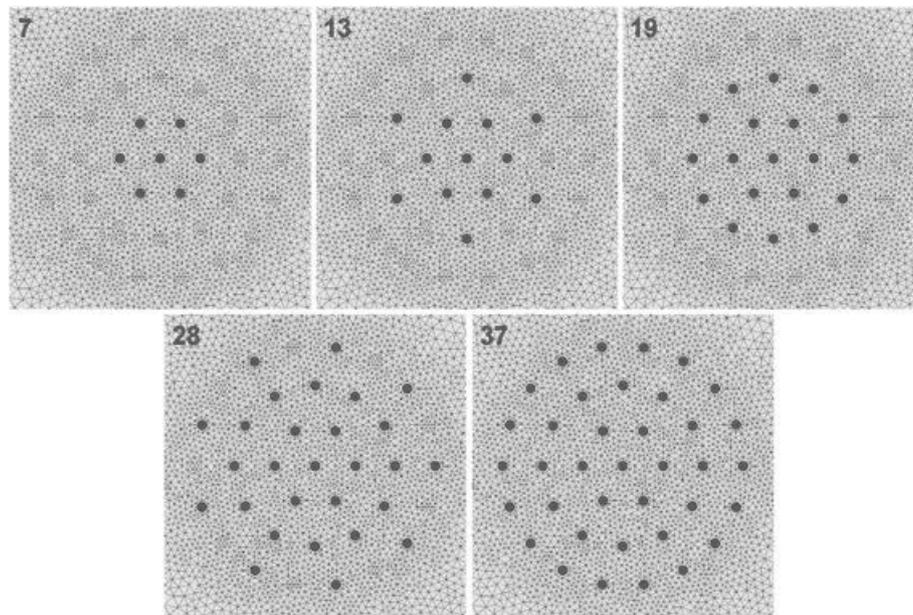
Figure 1. Different storage setups in top view with the corresponding number of borehole heat exchangers.

was studied in one characteristic storage setup by varying the inlet temperature values for the charging and discharging periods (Table I(b)). All possible temperature combinations were simulated. Furthermore, the effect of different geological and hydrogeological conditions was investigated by variation of the thermal conductivity, the volumetric heat capacity and the hydraulic conductivity of the entire model in one characteristic case (Table I(c)). In this partial study, only one parameter was varied, whereas the other parameters were kept at standard values.

In order to investigate the significance of heat losses at the surface and the effect of a hypothetical insulation, an additional set of storage models with an insulating top layer was simulated too.

The numerical simulations of the heat transport processes in the BHEs and in the subsurface were carried out using the finite element programme FEFLOW 6.2 [42,43]. The BHEs were modelled by 1D finite element representations as described by Diersch *et al.* [44]. The analytical BHE solution after Eskilson and Claesson [45] was

applied, as it has shown a high efficiency, robustness and a reasonable accuracy in long-term analyses [44,46]. In a previous study, FEFLOW simulations of the BTES in Crailsheim, Germany were in good agreement with measured data [47].

2.1. General model setup

In this study, all BHEs were implemented as coaxial pipes with annular inlet of the heat transfer fluid and centred outlet (CXA). The borehole diameter was set to 152 mm. For stability reasons, a steel pipe (carbon steel) was chosen as an outer casing with an outer diameter of 127 mm and a wall thickness of 5.6 mm. Furthermore, the relatively high thermal conductivity of the outer pipe ($54\,W\,m^{-1}\,K^{-1}$) is advantageous for the heat transfer rate between the fluid and the subsurface. Depending on the groundwater properties, low-grade carbon steel might be subject to corrosion. In such a case, more expensive stainless steel pipes should be preferred. Nakevska *et al.* [48] showed that it is advisable to use polyethylene (PE) pipes for the ascending portion of the loop (i.e. the inner pipe) because its relatively low thermal conductivity reduces the heat exchange between the up-streaming and down-streaming fluids. Therefore, the inner pipe was modelled as a PE-X pipe with an outer diameter of 75 mm, a wall thickness of 6.8 mm and a thermal conductivity of $0.4\,W\,m^{-1}\,K^{-1}$. The aforesaid BHE parameters were used in all considered storage models.

All simulations were run in a simple single-layered block-shaped underground model with the dimensions of $400\,m \times 400\,m \times 2000\,m$. According to Sanner [49], some low permeable sedimentary and crystalline rocks are suitable for the application of high temperature BTES. In this study, the subsurface was assumed to consist of a granodiorite with a thermal conductivity of $2.6\,W\,m^{-1}\,K^{-1}$, a volumetric heat capacity of $2.3\,MJ\,m^{-3}\,K^{-1}$ and a porosity of 1%. These are measured values, which were obtained from a field campaign at the proposed location for the study mentioned earlier [40].

In crystalline rock, groundwater flow is primarily restricted to interconnected fracture zones and fissures. MD-BTES tap into large rock volumes for which fracture heterogeneities are smoothed out as a result of spatial averaging. Thus, the subsurface can be treated in the models as a single continuum of porous material [43]. The estimated value for the hydraulic conductivity of the subsurface was $10^{-8}\,m\,s^{-1}$, which represents a reasonable value for the crystalline basement (cf. [50]). This barely allows for groundwater flow and makes conduction the dominant heat transport process. Hence, the groundwater flow was neglected and eliminated by setting the hydraulic gradient in the model to zero. A temperature boundary condition of $10\,°C$ was set on the uppermost slice as the mean annual surface temperature, whereas a temperature of $70\,°C$ was set on the lowest slice to factor in a geothermal gradient of $3\,K\,(100\,m)^{-1}$. Before running the actual storage simulations, a steady-state simulation of the underground model

was carried out to guarantee that the temperature boundary conditions are in equilibrium with the geothermal gradient. After the steady-state simulations, the temperature boundary conditions at the top of the model domain were deleted at the BHE positions and their neighbouring nodes to prevent a direct influence of the boundary condition on the BHE fluid temperatures. All parameters for the geological model and the BHEs are summarized in Table II.

To capture high temperature gradients between the BHEs and the surrounding rock during the simulation, the three-dimensional finite element mesh was locally refined: in the horizontal direction around the BHE nodes and in vertical direction close to the surface and close to the endpoints of the BHEs. An optimal mesh refinement around the BHE nodes was realized by using the approach of direct estimation of the nodal distances according to Diersch *et al.* [46]. The grids consist of triangular prisms, which are unstructured in horizontal direction and structured in vertical direction. The horizontal triangles were generated with the Triangle mesh generator [51], which is able to create high quality meshes that fulfil the Delauney criterion. This allows for a sound behaviour of the obtained solution (Galerkin method and upwinding method: shock capturing, iterative solver with a termination criterion of $1 \cdot 10^{-12}$, non-linear coupling with one iteration per time step and an allowed maximum L_∞ error of $1 \cdot 10^{-4}$): a fast convergence was achieved with negligible relative heat balance errors of less than $1 \cdot 10^{-8}$. For the majority of the models, the grid Peclet numbers (cf. [42]) were zero, as no convective heat transport was considered. The models for the groundwater flow variation study constitute an exception: maximum Peclet numbers were in the order of 2–3 for the three systems with the highest groundwater velocities. All remaining systems exhibited Peclet numbers well below 2. Such Peclet numbers are within an unproblematic range. An automatic time step control was applied, using the second-order Adams–Bashforth/trapezoid rule predictor-corrector method [43], which entails a fully implicit time integration scheme.

2.2. Borehole heat exchanger operation scenario

A very simplified loading and unloading scheme was applied in each simulation to simplify the comparison of the MD-BTES performance. Alternating operation between charging and discharging cycles was realized by a change of the inlet temperature every 6 months as shown in Figure 2a. During the charging periods, the inlet temperature was set to $90\,°C$, as this temperature can easily be supplied by solar thermal collectors but also describes the upper limit of the temperature resistance of the PE-X pipes. During heat extraction, the inlet temperature was set to $30\,°C$. This ensures that low temperature heating systems can be supplied without the use of a heat pump. The BHEs were connected

Table II. General model parameters for a base case design.

Underground parameters		Borehole heat exchanger parameters	
Parameter	Value	Parameter	Value
Thermal conductivity of solid	$2.6\,\mathrm{W\,m^{-1}\,K^{-1}}$	Borehole diameter	$0.1522\,\mathrm{m}$
Volumetric heat capacity of solid	$2.3\,\mathrm{MJ\,m^{-3}\,K^{-1}}$	Outer pipe diameter	$0.127\,\mathrm{m}$
Thermal conductivity of fluid	$0.65\,\mathrm{W\,m^{-1}\,K^{-1}}$	Outer pipe wall thickness	$0.0056\,\mathrm{m}$
Volumetric heat capacity of fluid	$4.2\,\mathrm{MJ\,m^{-3}\,K^{-1}}$	Inner pipe diameter	$0.075\,\mathrm{m}$
Porosity	0.01	Inner pipe wall thickness	$0.0068\,\mathrm{m}$
Surface temperature	$10\,^{\circ}\mathrm{C}$	Outer pipe thermal conductivity (steel)	$54\,\mathrm{W\,m^{-1}\,K^{-1}}$
Geothermal gradient	$0.03\,\mathrm{K\,m^{-1}}$	Inner pipe thermal conductivity (PE-X)	$0.4\,\mathrm{W\,m^{-1}\,K^{-1}}$
Hydraulic conductivity	$10^{-8}\,\mathrm{m\,s^{-1}}$	Grout thermal conductivity	$2\,\mathrm{W\,m^{-1}\,K^{-1}}$
Hydraulic gradient	0	Heat transfer fluid volumetric heat capacity (water)	$4.145\,\mathrm{MJ\,m^{-3}\,K^{-1}}$
Model length	$400\,\mathrm{m}$	Heat transfer fluid thermal conductivity (water)	$0.65\,\mathrm{W\,m^{-1}\,K^{-1}}$
Model width	$400\,\mathrm{m}$	Heat transfer fluid dynamic viscosity (water)	$504\cdot10^{-6}\,\mathrm{kg\,m^{-1}\,s^{-1}}$
Model depth	$2000\,\mathrm{m}$	Heat transfer fluid density (water)	$977\,\mathrm{kg\,m^{-3}}$
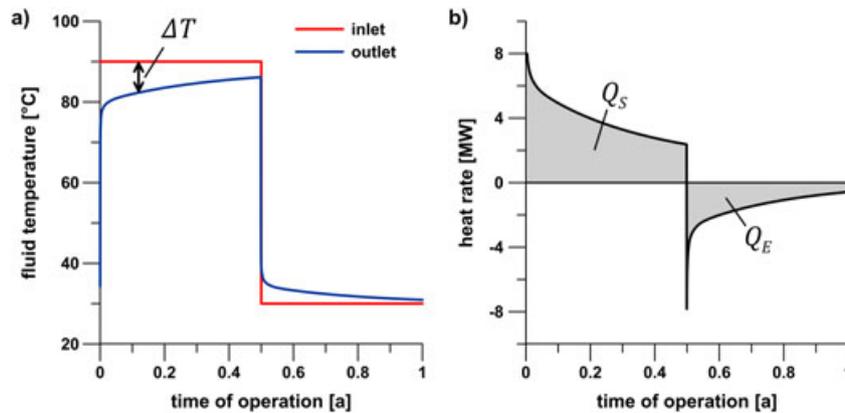
Figure 2. (a) Default inlet temperature and computed outlet temperature and (b) the corresponding calculated heat rate during the first year of operation of a characteristic medium deep borehole thermal energy storage (37 borehole heat exchangers with a length of 500 m and a spacing of 5 m). The hatched areas represent the total heat stored (Q_S) and the total heat extracted (Q_E) during the regarded time span.

to each other in a parallel arrangement, so that all BHEs were supplied with the same inlet temperature. Those temperatures were kept constant during the charging and discharging cycles, respectively. The flow rate for each BHE was set to $4\,\mathrm{l\,s^{-1}}$ for the whole simulation time. This value displays a reasonable compromise between a high heat exchange rate and a comparably low pressure drop in the BHEs. The latter depends on the fluid properties, which in turn depend on the fluid temperatures. For the considered inlet temperatures and the assumed pipe configuration, the calculated specific pressure loss (according to, e.g. Yamaguchi [52]) ranges from $295\,\mathrm{Pa\,m^{-1}}$ to $385\,\mathrm{Pa\,m^{-1}}$. The operation of the storage array is controlled by assigning a variable inlet temperature for a time span of 30 years with one exception: for the simulations of the variation of the underground properties, a time span of just 10 years was regarded.

2.3. Processing and analysis

In order to assess the different storage model setups, several key performance indicators are compared. First of all, the outlet temperatures of the single BHEs calculated during the numerical simulation were averaged to a mean storage outlet temperature. As an example, Figure 2a shows the mean outlet temperature of a high performance storage system. Because of the temperature difference between the heat transfer fluid in the BHEs and the surrounding rock, the subsurface is heated or cooled continuously. Consequently, this temperature difference decreases over time and reduces the BHE's heat transfer rate. The heat rate ΔQ, which is exchanged between the heat carrier fluid and the storage, is calculated as follows:

$$\Delta Q = \Delta T \cdot (\rho c)_f \cdot \dot{V} \tag{1}$$

Where ΔT is the temperature difference between the inlet and the outlet temperature of the fluid, $\dot{V}$ is the flow rate through the BHE array and $(\rho c)_f$ is the volumetric heat capacity of the fluid.

By integrating the heat rate over a charging or discharging cycle, the total heat stored or extracted during this period is calculated (Figure 2b). The ratio of the absolute values of extracted and stored heat, the storage efficiency η is defined by

$$\eta = \left| \frac{Q_E}{Q_S} \right| \tag{2}$$

Where Q_S is the stored heat and Q_E is the extracted heat during 1 year.

The total BHE length has to be taken into account to compare the total amount of extracted heat of the different systems. Thus, the specific heat extraction rate $\dot{q}$, which is the heat extraction rate referring to one extraction cycle normalized by the BHE length, is calculated as:

$$\dot{q} = Q_E \cdot \frac{1}{\Delta t \cdot L_{tot}} \tag{3}$$

Where Q_E is the heat extracted from the storage during the considered year, L_{tot} is the total BHE length of the considered storage system and Δt is the length of the heat extraction period.

3. RESULTS

In the simulations of the different storage model setups, the amount of stored heat ranges from about $420\,\mathrm{MWh\,a^{-1}}$ to more than $20\,\mathrm{GWh\,a^{-1}}$ in the 30th year of operation (Figure 3a). The corresponding amount of extracted heat lies between $150\,\mathrm{MWh\,a^{-1}}$ and $17\,\mathrm{GWh\,a^{-1}}$ (Figure 3b). Accordingly, the storage efficiency and the specific heat extraction rate range from 32% to almost 84% (Figure 3 c) and from $49\,\mathrm{W\,m^{-1}}$ to $113\,\mathrm{W\,m^{-1}}$, respectively (Figure 3d).

All simulations display typical BTES long-term behaviour: because of heat diffusion, not all of the stored heat can be recovered during the heat extraction period. A fraction of the stored thermal energy remains in the subsurface generating a heat plume and increasing the storage's average rock temperature. As a consequence, the elevated subsurface temperature leads to a decrease of heat storage and an increase of heat extraction (Figure 4). Thereby, the storage losses shrink and the storage efficiency η grows over time. This effect is especially strong during the first couple of charging and discharging cycles and diminishes later on, but still persists even after 30 years of operation (Figure 4). A complete list of all simulation results is included in the Supporting Information of this paper.

3.1. Influence of storage design

The storage size is determined by the number of BHEs and their length. Both variables correlate almost linearly with
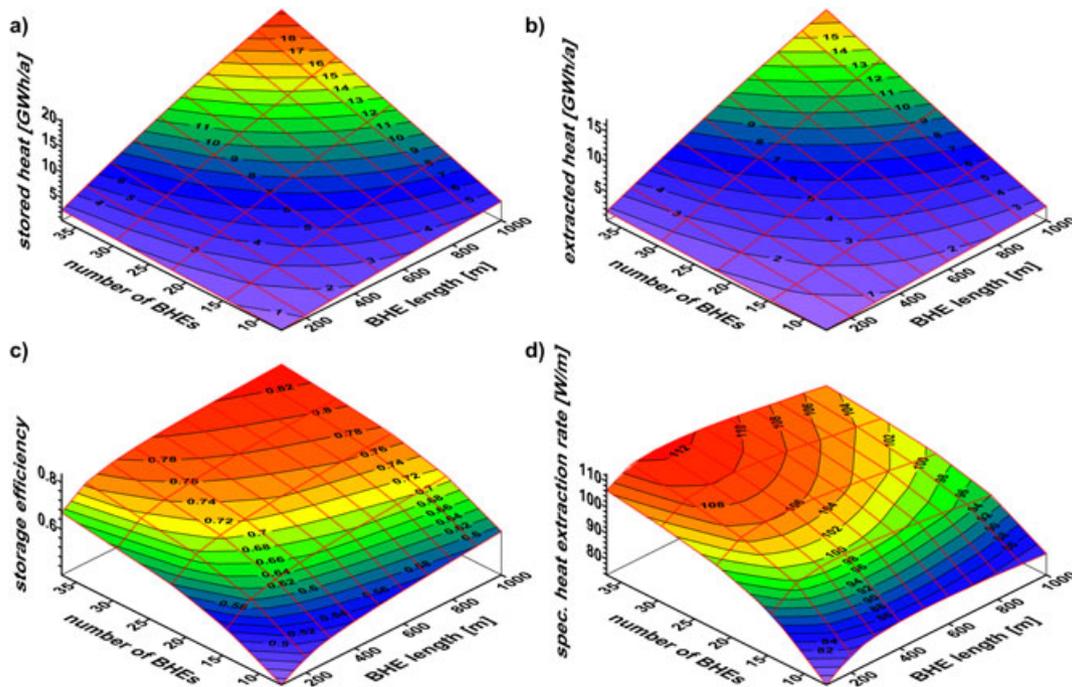
Figure 3. (a) Amount of stored heat, (b) amount of extracted heat, (c) storage efficiency and (d) specific heat extraction rate in the 30th year of operation depending on a change in the number of borehole heat exchangers (BHEs) and the BHE length for storage systems with a BHE spacing of 5 m. The results are illustrated as interpolated surfaces.
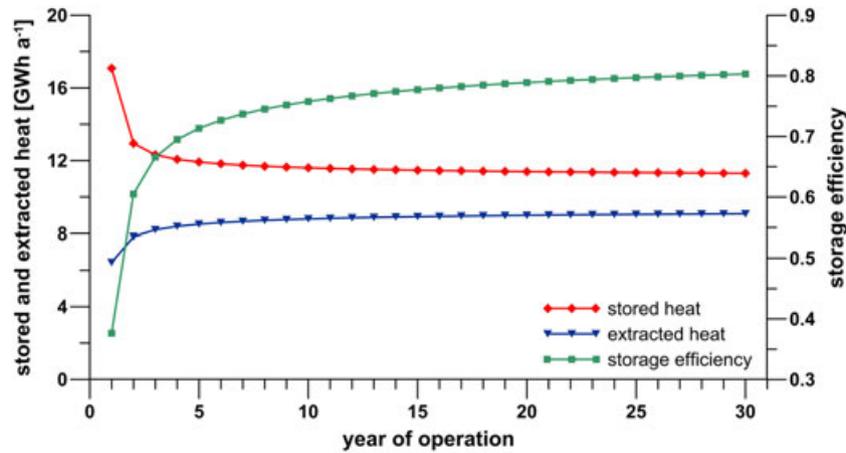
Figure 4. Temporal evolution of storage performance over 30 years of operation for a setup with 37 borehole heat exchangers with a length of 500 m and a spacing of 5 m.

the amounts of stored and extracted heat (cf. Figure 3a and b). Thus, larger storage systems have a higher capacity.

The storage efficiency rises continuously with the storage size, that is, the number of BHEs and their length (cf. Figures 3c, 5a and 6a): heat losses decrease with the increasing ratio of storage volume to storage surface. Furthermore, a higher number of BHEs in an MD-BTES means more thermal interaction between them: thermal energy that is lost due to heat diffusion can be recovered by neighbouring BHEs. Hence, heat losses concentrate on the storage fringe. For this reason, a lateral temperature gradient from the storage centre to the storage fringe develops with time, which leads to higher efficiencies of the inner BHEs compared with the peripheral ones. Moreover, the overall storage efficiency for the layouts of 13 and 28 BHEs is barely increased compared with the respectively next smaller system in the first year of operation (cf. kinks in Figure 5a). These are the borefield layouts, in which the outer BHE ring is occupied only on every second BHE position (Figure 1). As a result, the storage does not match the shape of an ideal circular cylinder, but has an overly

increased envelope area. Only after several years of operation this effect is compensated when a substantial heat plume has developed in the subsurface. This phenomenon has a short-term effect on the specific heat extraction rate as well (Figure 5b).

However, the variables' effect on the specific heat extraction rate and the storage efficiency is more complex. While the specific heat extraction rate generally grows with the number of BHEs, counter-intuitively, it reaches a maximum at a specific BHE length (cf. Figures 3d and 6b). The decrease in the specific heat extraction rate with larger depths can be explained by a prolonged dwell time of the fluid in the BHE pipes. As a result, heat losses increase in the upper parts of the borehole, where thermal energy is transferred back from the heated fluid to the colder subsurface. Beyond a specific depth, this effect outweighs the increased heat extraction in the bottom part of the BHE, which marks the BHE length for the maximum specific heat extraction rate.

Additionally, the non-linear decline in storage efficiency and specific heat extraction rate grows steeper with
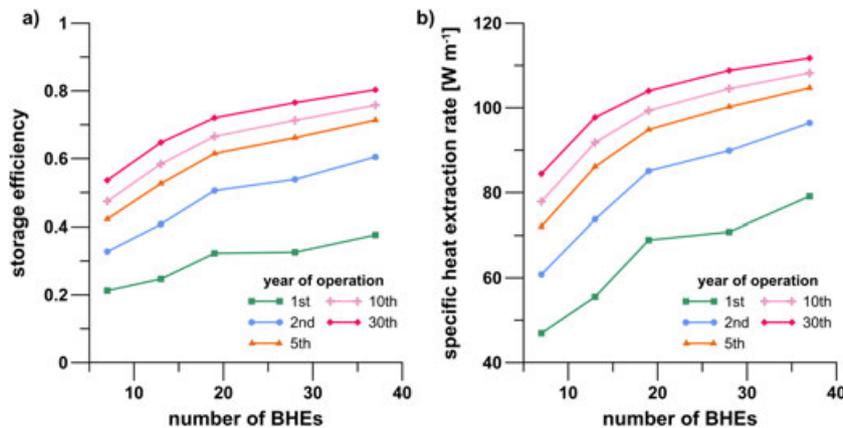
Figure 5. (a) Influence of the number of borehole heat exchangers (BHEs) on the storage efficiency and (b) the specific heat extraction rate in different years of operation, exemplarily illustrated for storage setups with a BHE length of 500 m and a spacing of 5 m.
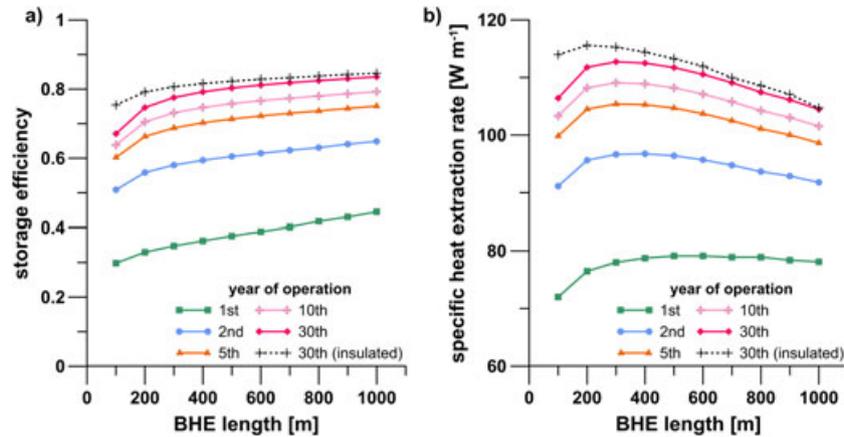
Figure 6. (a) Influence of the borehole heat exchanger (BHE) length on the storage efficiency and (b) specific heat extraction rate in different years of operation for storage setups with 37 BHEs and a spacing of 5 m; insulation layer thickness: 1 m; thermal conductivity of the insulation layer: $0.05\,\mathrm{W\,m^{-1}\,K^{-1}}$.

decreasing BHE length. The effect of heat losses at the top surface is more significant for shallow systems. Deeper BTES can compensate the heat losses by their higher capacity as the top surface does not increase with BHE length. Consequently, an insulating layer at the top of the storage is most effective for shallow BTES (Figure 6a and b). Furthermore, the specific lateral heat losses diminish with depth because of the geothermal gradient and the thereby reduced temperature difference between BHE fluid and surrounding rock. Insulating the upper portion of the BHEs by a low thermal conductivity grout would further reduce lateral heat losses [41,48]. However, multiple grout sections are not provided in FEFLOWs' analytical BHE solution.

Also, the BHE spacing has an effect on the storage performance. On the one hand, a narrow spacing results in a quick depletion of the storage reservoir during heat extraction. On the other hand, thermal interaction between BHEs is weak for a wide spacing, which equals to an inefficient heat recovery of the neighbouring BHEs. Consequently,

there must be an ideal radial distance between BHEs. The simulation results confirm this hypothesis and show peak specific heat extraction rates for a radial distance of 5 m (Figure 7b). The storage efficiency shows the same effect after a couple of years when the storage is charged and has developed a thermal plume (Figure 7a). A dependency of the optimal spacing on the BHE length cannot be observed.

3.2. Influence of the inlet temperature

The total amounts of stored and extracted heat are strongly dependent on and almost linearly correlated (Figure 8a) with the difference between the charging temperature (i.e. the inlet temperature during the heat storage period) and the discharging temperature (i.e. the inlet temperature during the heat extraction period). This implies that higher temperature differences result in higher specific heat extraction rates and higher storage capacities (Figure 8b). In general, the storage efficiency increases with higher
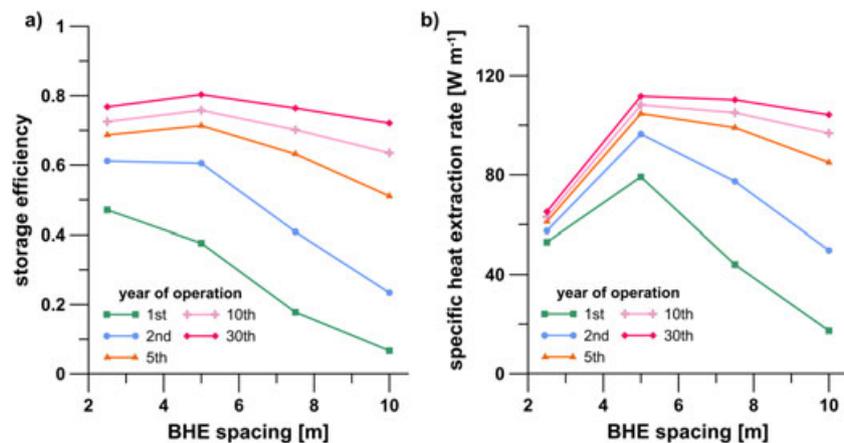
Figure 7. (a) Influence of the borehole heat exchanger (BHE) spacing on the storage efficiency and (b) the specific heat extraction rate in different years of operation, exemplarily illustrated for storage setups with 37 BHEs and a BHE length of 500 m.

charging temperatures and lower discharging temperatures. Yet, the variables' influence on the storage efficiency is interdependent (Figure 8c): While an increase of the charging temperature results in more stored heat, it also causes higher lateral heat losses. For high discharging temperatures and a consequently poor heat recovery, the increase of the charging temperature has a positive effect on the storage efficiency (Figure 8c, 50 °C discharging temperature line). However, if the discharging temperature is low, the positive effect is neutralized by effective heat recovery and the higher heat losses manifest in declining storage efficiencies (Figure 8c, 10 °C discharging temperature line).

3.3. Influence of general model variables

The heat transport processes in the subsurface are controlled by the thermo-physical and hydrogeological framework conditions. Figure 9 illustrates the influence of the variable rock properties on the storage performance in a characteristic storage setup. The thermal conductivity of the reservoir rock not only has a positive and nearly linear influence on the storage capacity but also enhances the lateral heat losses. Consequently, the rising storage capacity is accompanied by a slight decrease of storage efficiency (Figure 9a). In contrast to the thermal conductivity, an increase of the volumetric heat capacity has only a weak positive effect on the amounts of stored and extracted heat (Figure 9b). Thus, the influence of the volumetric heat capacity is considered to be negligible.

As advective dissipation of the stored heat by flowing groundwater has to be prevented, formations with a low hydraulic permeability are suitable reservoirs for BTES applications [48]. Parameter variations show that groundwater flow velocities larger than $2\,m\,a^{-1}$ lead to considerable advective losses of stored heat. This culminates in the worst case, where the subsurface temperature is set back to undisturbed conditions within the storage, whereas the entire plume of stored heat is displaced by

the groundwater flow. As a consequence, the discharge temperature is too high. Even in the winter period, heat is injected and not extracted resulting in a negative storage coefficient (Figure 9c).

These findings suggest that for locations, where groundwater flow is low, the thermal conductivity, and by extension, the thermal diffusivity of the reservoir rock determine the storage capacity of a given MD-BTES design. Where groundwater flow exceeds a certain level, it can have a strong negative influence on the storage capacity as well as on the storage efficiency.

4. DISCUSSION

Like any other model, the simulations cannot capture every physical detail and are affected by assumptive boundary conditions. Especially the homogeneous geological model and the operational scenario of 6 months of constant inlet temperatures and constant fluid flow rates represent oversimplifications, which certainly do not resemble realistic conditions. However, realistic values for these model parameters would add a lot of noise to the simulation results. Realistic stratigraphic models would have to consider geological uncertainty, while realistic charging and discharging temperature curves have a high temporal resolution and depend on simulation models or measured values, which are specific to a certain building. Consequently, the consideration of realistic values for these parameters would add a lot of complexity and detail to the model response and prevent a conclusive analysis of the other variables' effect. While simulations for the planning of a specific storage should factor in as much detail as possible, these model simplifications are necessary for our study to allow for the investigation of the parameters' sensitivity.

The simulations provide information on the characteristical MD-BTES system responses to the variation of a selection of geological, operational and design
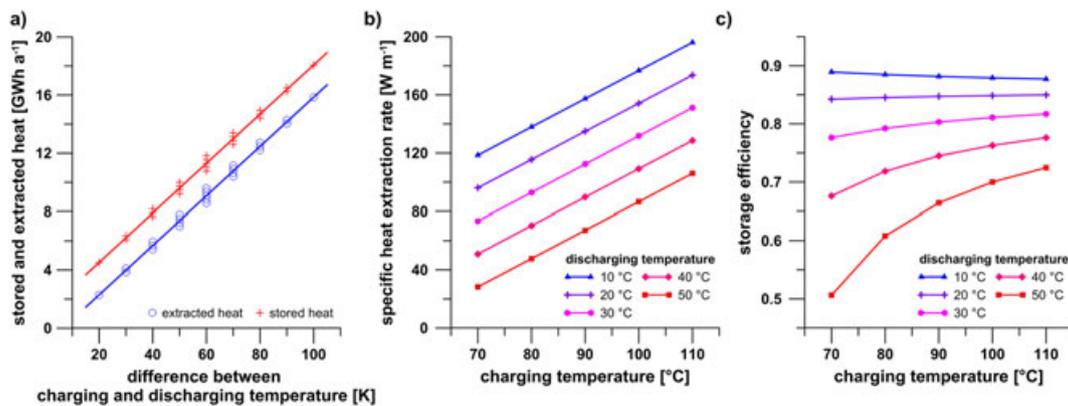
Figure 8. (a) Stored and extracted heat as a function of the difference between the charging temperature and the discharging temperature; correlation of the specific heat extraction rate (b) as well as the storage efficiency (c) and the charging temperature for different discharging temperatures. The results are shown for the storage system with 37 borehole heat exchangers (BHEs), a BHE length of 500 m and a spacing of 5 m in the 30th year of operation.
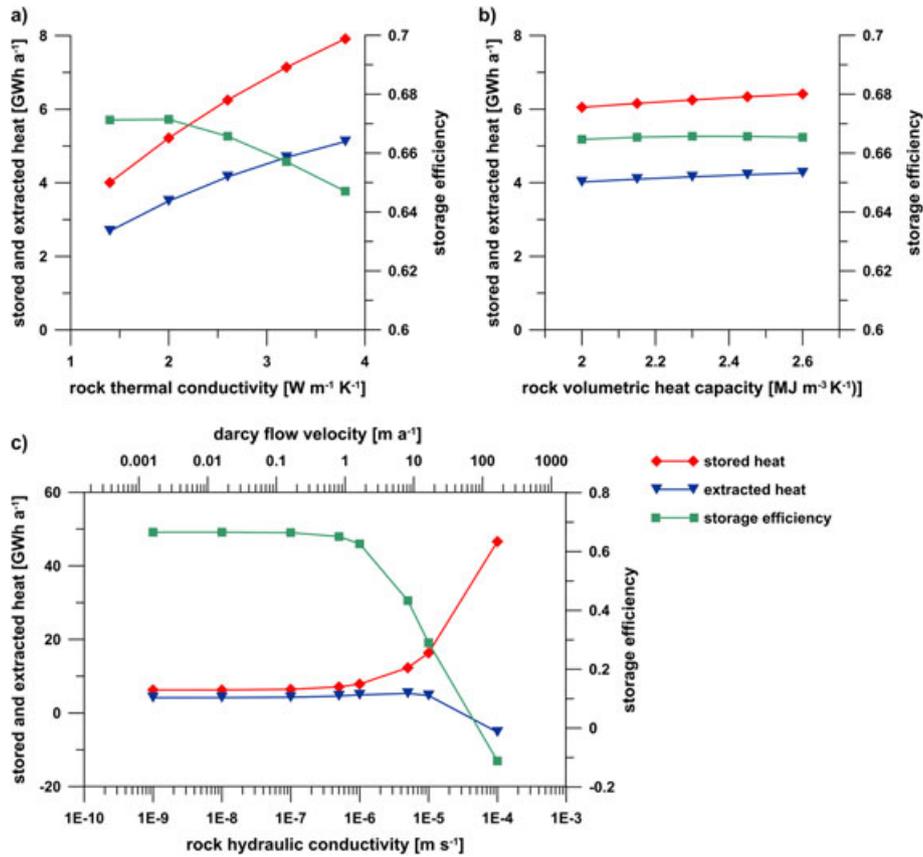
Figure 9. Storage performance in a characteristic storage setup (19 borehole heat exchangers, spacing 5 m and length 500 m) for the variations of (a) the thermal conductivity, (b) the volumetric heat capacity and (c) the hydraulic conductivity of the reservoir rocks. The results for the hydraulic conductivity variations are based on a hydraulic gradient of 5% in the underground model. The corresponding Darcy flow velocities are shown on the upper abscissa.

parameters and show that MD-BTES performance is sensitive to many of these variables. Evidently, many more parameters like thermo-physical properties of BHE materials and flow rates, for example, can have a significant influence. Yet, their number had to be restricted because of the design of the simulation experiments to limit the computational effort. Furthermore, the interdependent influence of variables has only been investigated for the borefield design (i.e. simultaneous change of the number of BHEs, their length and their spacing) and for the inlet temperatures during the charging and discharging cycles. However, the effect of changing charging and discharging temperatures indicates a correlation between several variables. Similarly, the value of the ideal BHE spacing depends on a balance between the thermal BHE interaction and the storage depletion, which is ultimately governed by the duration of the extraction and storage periods in correlation with the thermal diffusivity of the rock [22]. An interdependent effect of these variables on the system performance is obvious, but cannot be quantified because of the setup of variable variation across the simulation experiments. Therefore, future simulations may be based on experimental designs, which allow for the observation of such interdependency effects.

Our results confirm earlier findings (e.g. [10,17,18]) that BTES systems require several years of operation to reach a relatively balanced state. Although the system performance still rises even after 30 years of operation, the annual increase slows down significantly after the first couple of charging and discharging cycles. MD-BTES with a BHE spacing of 5 m achieve 80% of their final storage efficiency (i.e. storage efficiency in the 30th year) after 3–6 years (Figure 10). Furthermore, the strong dependency of the storage performance on its size indicates that under the considered scenario conditions, only large-scale applications are viable. With a heat demand of more than $6\,\mathrm{GWh\,a^{-1}}$, respective MD-BTES can exceed 70% storage efficiency, which is within the range of other underground thermal energy storages: Reuss *et al.* [39] carried out a numerical modelling study on a high temperature BTES, which resulted in a storage efficiency of 64% for the optimal storage design. Analyses of heat budget data of an Aquifer Thermal Energy Storage in Rostock and a BTES in Neckarsulm (both Germany) for the years 2008 to 2012 yielded an average storage efficiency of 69% and 79%, respectively [53]. Efficiencies of 46% are reported for the BTES in Anneberg, Sweden (quasi steady-state
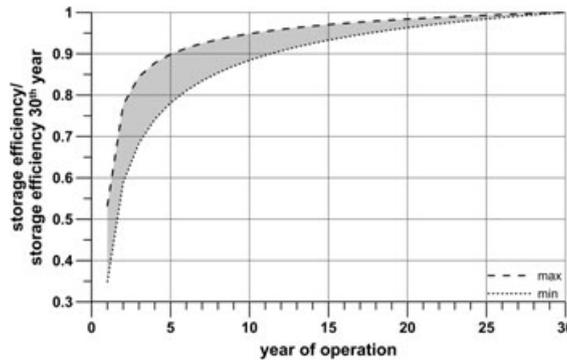
Figure 10. Range of the evolution of storage efficiency related to the storage efficiency in the 30th year of operation (systems with a borehole heat exchanger spacing of 5 m).

conditions, eighth year of operation) [54] and 54% for the BTES of the Drake Landing Solar Community, Okotoks, Canada (fourth year of operation) [17].

The present study emphasizes that higher discharging temperatures result in a significant decrease of the storage capacity and efficiency. Accordingly, the installation of a heat pump can be favourable for heating systems with high return temperatures of more than 50 °C (e.g. conventional radiators) as it reduces discharging temperatures. In contrast, panel heating systems like floor heating with low return temperatures (<30 °C) can reach high storage efficiencies without the utilization of a heat pump. Coupled simulations of all system components are necessary for an optimal fine-tuning of the heating and storage system and a potential heat pump.

5. CONCLUSIONS AND OUTLOOK

In the presented study, numerical simulations of various MD-BTES settings have been carried out. The effects of different storage configurations, fluid temperatures and subsurface properties were compared. The results reveal that with a proper dimensioning of the system and in convenient geological and hydrogeological framework conditions, MD-BTES are eminently suitable for seasonal heat storage. Furthermore, the collected data give reference points for an optimal design, favourable fluid temperatures to operate the storage and appropriate rock properties.

It is clarified that there is an optimal BHE spacing, where the highest storage efficiencies and the highest heat extraction rates are achieved. Increasing the number of BHEs or the BHE length enhances both the storage capacity as well as the storage efficiency. Under the very simplified operating procedure and subsurface conditions, storage efficiencies of up to 83% are reached. By adjusting supply temperatures for the heating system or increasing the loading temperature of the storage, the efficiencies can even be further improved. Groundwater flow has to be limited, as it can significantly affect the performance of MD-BTES by dissipating the stored heat out of the system.

Future work will focus on realistic charging and discharging scenarios to prove that MD-BTES will work not only under simplified assumptions but under realistic conditions as well. Therefore, coupled simulations of the storage system, the heat supply system and the heating system will be implemented. Further studies will be conducted to determine the actual impact on shallow groundwater aquifers to give evidence of the advantages of MD-BTES compared with shallow BTES systems. Moreover, the dependency of the storage performance on the BHE spacing puts high requirements on the verticality of the boreholes. Accordingly, suitable drilling technologies have to be identified and compared from a technical and economical perspective. In addition to that, a detailed economic analysis of the whole storage systems is planned to find an optimal system design from a financial point of view.

NOMENCLATURE

BTES	= borehole thermal energy storage
MD-BTES	= medium deep borehole thermal energy storage
BHE	= borehole heat exchanger
CHP	= combined heat and power plant

REFERENCES

1. IEA (International Energy Agency). Heating without global warming – market developments and policy considerations for renewable heat. OECD/IEA: Paris, 2014.

2. Pinel P, Cruickshank CA, Beausoleil-Morrison I, Wills A. A review of available methods for seasonal storage of solar thermal energy in residential applications. *Renewable and Sustainable Energy Reviews* 2011; **15** (7):3341–3359. doi:10.1016/j.rser.2011.04.013.

3. Dincer I, Dost S. A perspective on thermal energy storage systems for solar energy applications. *International Journal of Energy Research* 1996; **20**(6):547–557. doi:10.1002/(SICI)1099-114X(199606) 20:6<547::AID-ER173>3.0.CO;2-S.

4. Braun JE, Klein SA, Mitchell JW. Seasonal storage of energy in solar heating. *Solar Energy* 1981; **26** (5):403–411. doi:10.1016/0038-092X(81)90219-X.

5. Raine RD, Sharifi VN, Swithenbank J. Optimisation of combined heat and power production for buildings using heat storage. *Energy Conversion and Management* 2014; **87**:164–174. doi:10.1016/j. enconman.2014.07.022.

6. Mago PJ, Luck R. Evaluation of a base-loaded combined heating and power system with thermal storage for different small building applications. *International Journal of Energy Research* 2013; **37**(2):179–188. doi:10.1002/er.1892.

7. Mago PJ, Luck R, Knizley A. Combined heat and power systems with dual power generation units and thermal storage. *International Journal of Energy Research* 2014; **38**(7):896–907. doi:10.1002/er.3089.

8. Dincer I, Rosen MA. *Thermal Energy Storage: Systems and Applications* (2nd). Wiley: Hoboken, N.J., 2011.

9. Dincer I. Thermal energy storage systems as a key technology in energy conservation. *International Journal of Energy Research* 2002; **26**(7):567–588. doi:10.1002/er.805.

10. Schmidt T, Mangold D, Müller-Steinhagen H. Central solar heating plants with seasonal storage in Germany. *Solar Energy* 2004; **76**(1-3):165–174. doi:10.1016/j. solener.2003.07.025.

11. Xu J, Wang RZ, Li Y. A review of available technologies for seasonal thermal energy storage. *Solar Energy* 2014; **103**:610–638. doi:10.1016/j. solener.2013.06.006.

12. Hesaraki A, Holmberg S, Haghighat F. Seasonal thermal energy storage with heat pumps and low temperatures in building projects – a comparative review. *Renewable and Sustainable Energy Reviews* 2015; **43**:1199–1213. doi:10.1016/j.rser.2014.12.002.

13. Bauer D, Marx R, Nußbicker-Lux J, Ochs F, Heidemann W, Müller-Steinhagen H. German central solar heating plants with seasonal heat storage. *Solar Energy* 2010; **84**(4):612–623. doi:10.1016/j. solener.2009.05.013.

14. Nordell B. *A Borehole Heat Store in Rock at the University of Lulea, The Lulevarme Project 1982–1988*. Swedish Council for Building Research: Stockholm, Sweden, 1990.

15. Nordell B. *The Borehole Heat Store in Rock at the Lulea University of Technology, Constructional and Operational Experience, The Lulevarme Project 1982–1985*. Swedish Council for Building Research: Stockholm, Sweden, 1987.

16. Gao L, Zhao J, Tang Z. A review on borehole seasonal solar thermal energy storage. *Energy Procedia* 2015; **70**:209–218. doi:10.1016/j.egypro.2015.02.117.

17. Sibbitt B, Mcclenahan D, Djebbar R, Thornton J, Wong B, Carriere J, Kokko J. The performance of a high solar fraction seasonal storage district heating system – five years of operation. *Energy Procedia* 2012; **30**:856–865. doi:10.1016/j.egypro.2012.11.097.

18. Lundh M, Dalenbäck JO. Swedish solar heated residential area with seasonal storage in rock: initial evaluation. *Renewable Energy* 2008; **33**(4):703–711. doi:10.1016/j.renene.2007.03.024.

19. Andersson O, Ekkestubbe J, Ekdahl A. UTES (underground thermal energy storage) – applications and market development in Sweden. *Journal of Energy and Power Engineering* 2013; **7**(4):669–678.

20. Dincer I, Rosen MA. A unique borehole thermal storage system at University of Ontario Institute of Technology. In *Thermal Energy Storage for Sustainable Energy Consumption*, Paksoy H (ed.). Springer Netherlands: Dordrecht, 2007; 221–228.

21. Nordell B, Hellström G. High temperature solar heated seasonal storage system for low temperature heating of buildings. *Solar Energy* 2000; **69**(6):511–523. doi:10.1016/S0038-092X(00)00120-1.

22. Reuss M. 6 – the use of borehole thermal energy storage (BTES) systems. In: *Advances in Thermal Energy Storage Systems*, Cabeza LF (ed.), Woodhead Publishing, 2015, 117–147.

23. Andersson S, Eriksson A. Seasonal storage in hard rock – multiple well system. In *Thermal Storage of Solar Energy: Proceedings of an International TNO-*

Symposium Held in Amsterdam, The Netherlands, 5–6 November 1980, Ouden C (ed.). Springer Netherlands: Dordrecht, 1981; 249–258.

24. Beckmann G, Gilli PV. *Thermal Energy Storage: Basics-Design-Applications to Power Generation and Heat Supply*. Springer: Wien; New York, 1984.

25. Givoni B. Underground longterm storage of solar energy – an overview. *Solar Energy* 1977; **19**(6):617–623. doi:10.1016/0038-092X(77)90021-4.

26. Hellström G. *Duct Ground Heat Storage Model – Manual for Computer Code*. Department of Mathematical Physics, University of Lund: Lund, Sweden, 1989.

27. Lund PD, Östman MB. A numerical model for seasonal storage of solar heat in the ground by vertical pipes. *Solar Energy* 1985; **34**(4):351–366. doi:10.1016/0038-092X(85)90048-9.

28. Nordell B. Borehole heat store design optimization, Luleå University of Technology, Dissertation, 1994, 196.

29. Brons HJ, Griffioen J. Appelo CaJ, Zehnder AJB. (Bio)geochemical reactions in aquifer material from a thermal energy storage site. *Water Research* 1991; **25** (6):729–736. doi:10.1016/0043-1354(91)90048-U.

30. Griffioen J. Appelo CaJ. Nature and extent of carbonate precipitation during aquifer thermal energy storage. *Applied Geochemistry* 1993; **8**(2):161–176. doi:10.1016/0883-2927(93)90032-C.

31. Brielmann H, Griebler C, Schmidt SI, Michel R, Lueders T. Effects of thermal energy discharge on shallow groundwater ecosystems. *FEMS Microbiology Ecology* 2009; **68**(3):273–286.

32. Hall EK, Neuhauser C, Cotner JB. Toward a mechanistic understanding of how natural bacterial communities respond to changes in temperature in aquatic ecosystems. *The ISME Journal* 2008; **2**(5):471–481.

33. Hähnlein S, Bayer P, Ferguson G, Blum P. Sustainability and policy for the thermal use of shallow geothermal energy. *Energy Policy* 2013; **59**:914–925. doi:10.1016/j.enpol.2013.04.040.

34. Brielmann H, Lueders T, Schreglmann K, Ferraro F, Avramov M, Hammerl V, Blum P, Bayer P, Griebler C. Oberflächennahe Geothermie und ihre potenziellen Auswirkungen auf Grundwasserökosysteme. *Grundwasser* 2011; **16**(2):77–91. doi:10.1007/s00767-011-0166-9.

35. Bonte M, Stuyfzand PJ, Hulsmann A, Van Beelen P. Underground thermal energy storage: environmental risks and policy developments in the Netherlands and European Union. *Ecology and Society* 2011; **16**.

36. Hähnlein S, Bayer P, Blum P. International legal status of the use of shallow geothermal energy. *Renewable and Sustainable Energy Reviews* 2010; **14** (9):2611–2625. doi:10.1016/j.rser.2010.07.069.

37. Dehkordi SE, Schincariol RA. Guidelines and the design approach for vertical geothermal heat pump systems: current status and perspective. *Canadian Geotechnical Journal* 2014; **51**(6):647–662. doi:10.1139/cgj-2012-0205.

38. Kizilkan O, Dincer I. Borehole thermal energy storage system for heating applications: thermodynamic performance assessment. *Energy Conversion and Management* 2015; **90**:53–61. doi:10.1016/j.enconman.2014.10.043.

39. Reuss M, Beck M, Müller JP. Design of a seasonal thermal energy storage in the ground. *Solar Energy* 1997; **59**(4–6):247–257. doi:10.1016/S0038-092X (97)00011-X.

40. Schulte DO, Welsch B, Boockmeyer A, Rühaak W, Bär K, Bauer S, Sass I. Modeling insulated borehole heat exchangers. *Environmental Earth Sciences* 2016; **75**:1–12. doi:10.1007/s12665-016-5638-x.

41. Bär K, Rühaak W, Welsch B, Schulte D, Homuth S, Sass I. Seasonal high temperature heat storage with medium deep borehole heat exchangers. *Energy Procedia* 2015; **76**:351–360. doi:10.1016/j.egypro.2015.07.841.

42. FEFLOW finite element subsurface flow and transport simulation system – recent release 6.2 (DHI-WASY GmbH, Berlin, 2014).

43. Diersch H-JG. *Feflow – finite element modeling of flow, mass and heat transport in porous and fractured media*. Springer: Berlin; Heidelberg, 2014.

44. Diersch H-JG, Bauer D, Heidemann W, Rühaak W, Schätzl P. Finite element modeling of borehole heat exchanger systems: part 1. Fundamentals. *Computers & Geosciences* 2011; **37**(8):1122–1135. doi:10.1016/j.cageo.2010.08.003.

45. Eskilson P, Claesson J. Simulation model for thermally interacting heat extraction boreholes. *Numerical Heat Transfer* 1988; **13**(2):149–165. doi:10.1080/10407788808913609.

46. Diersch H-JG, Bauer D, Heidemann W, Rühaak W, Schätzl P. Finite element modeling of borehole heat exchanger systems: part 2. Numerical simulation. *Computers & Geosciences* 2011; **37**(8):1136–1147. doi:10.1016/j.cageo.2010.08.002.

47. Mielke P, Bauer D, Homuth S, Götz A, Sass I. Thermal effect of a borehole thermal energy store on the subsurface. *Geothermal Energy* 2014; **2**(1): 1–15, doi:10.1186/s40517-014-0005-1.

48. Nakevska N, Schincariol RA, Dehkordi SE, Cheadle BA. Geothermal waste heat utilization from in situ thermal bitumen recovery operations. *Groundwater* 2015; **53**(2): 251–260, doi:10.1111/gwat.12196.

49. Sanner B. High temperature underground thermal energy storage – state-of-the-art and prospects. In *Giessener geologische Schriften*, Vol. **67**. 1999; 82.

50. Stober I, Bucher K. Hydraulic properties of the crystal-line basement. *Hydrogeology Journal* 2007; **15** (2):213–224. doi:10.1007/s10040-006-0094-4.

51. Shewchuk JR. Triangle: engineering a 2D quality mesh generator and delaunay triangulator. In *Applied Computational Geometry Towards Geometric Engineering: FCRC'96 Workshop, WACG'96 Philadelphia, PA, May 27–28, 1996 Selected Papers*, Lin MC, Manocha D (eds.). Springer: Berlin; Heidelberg, 1996; 203–222.

52. Yamaguchi H. *Engineering Fluid Mechanics*. Springer: Dordrecht, 2008.

53. Bauer D, Drück H, Heidemann W, Marx R, Nußbicker-Lux J, Ochs F. *Solarthermie2000plus: Wissenschaftlich-technische Begleitung des Förderprogramms Solarthermie2000plus zu solar unterstützter Nahwärme und Langzeit-Wärmespeicherung*. Institute of Thermodynamics and Thermal Engineering (ITW): Stuttgart, Germany, 2013.

54. Heier J, Bales C, Sotnikov A, Ponomarova G. Evaluation of a high temperature solar thermal seasonal borehole storage. In: ISES Solar World Congress 2011.

SUPPORTING INFORMATION

Additional supporting information may be found in the online version of this article at the publisher's website:

Appendix C – Uncertainty in numerical models of borehole heat exchangers

Published as:

TECHNISCHE MITTEILUNG

CrossMark

Prognosefähigkeit numerischer Erdwärmesondenmodelle

Wolfram Rühaak · Sarah Steiner · Bastian Welsch · Ingo Sass

Zusammenfassung Für größere Erdwärmesondenanlagen werden standardmäßig numerische Berechnungen durchgeführt. Anlass sind neben der Dimensionierung (Bestimmung von Anzahl und Tiefe der benötigten Erdwärmesonden) vor allem genehmigungsrechtliche Fragestellungen, bei denen häufig eine möglichst realistische Modellierung gefordert wird.

Eine solche realistische Simulation ist technisch durchführbar, jedoch sehr aufwändig. Ein wichtiger Aspekt, der dabei in den Hintergrund gerät, ist die Quantifizierung der Parameterunsicherheiten aufgrund der natürlichen Heterogenität des geologischen Untergrundes.

Statt nur eine einzelne möglichst realistische Prognoseberechnung durchzuführen, kann die zusätzliche Berechnung von Ensemblemodellen, das heißt einer höheren Anzahl von sinnvoll vereinfachten Modellen, oftmals hilfreich sein. Durch Variation der Untergrundkennwerte im Bereich der vermuteten Unsicherheiten können Prognoseunsicherheiten bestimmt und dem Planer sowie dem Gutachter damit wichtige Zusatzinformationen zur Verfügung gestellt werden.

W. Rühaak (✉) · S. Steiner · B. Welsch · I. Sass
Darmstädter Exzellenz Graduiertenschule für
Energiewissenschaft und Energietechnik,
Jovanka-Bontschits-Straße 2,
64287 Darmstadt, Deutschland
E-Mail: ruehaak@geo.tu-darmstadt.de

I. Sass · B. Welsch · W. Rühaak
Institut für Angewandte Geowissenschaften, Fachgebiet
Angewandte Geothermie, Technische Universität Darmstadt,
Schnittspahnstraße 9,
64287 Darmstadt, Deutschland

S. Steiner
Institut für Massivbau, Technische Universität Darmstadt,
Franziska-Braun-Straße 3,
64287 Darmstadt, Deutschland

Uncertainty in numerical models of borehole heat exchangers

Abstract Large installations of borehole heat exchangers (BHEs) typically require numerical modeling. A reasonable system dimensioning (number and depth of BHEs) has to be found and regulatory requirements (minimizing environmental impact and avoiding competitive usage) have to be met. In the latter case, highly realistic models are typically demanded. Such realistic models are technically possible, but very laborious. One important issue, which is often neglected, is the quantification of parameter uncertainties due to heterogeneity of the geological subsurface.

Instead of a single forecast model, the additional computation of so-called ensemble models, i.e. a larger number of more simplified models, should be considered. By varying the relevant characteristics of the subsurface within the range of uncertainty, the quality of the forecast can be estimated, and the system designer can obtain valuable additional information.

Keywords Numerical modeling · Heat transport · Borehole heat exchanger · Uncertainty · Ensemble modeling

Einleitung

Mit einem Anteil von 57 % stellt der Bereich der Wärme- und Kälteversorgung den größten Teil des Energieverbrauchs in Deutschland dar (Stand 2012, AGEB 2013). Insbesondere hinsichtlich des Heizenergiebedarfs hat die Geothermie als regenerative und grundlastfähige Energiequelle Potenzial, langfristig fossile Energieträger wie Kohle, Erdöl und Erdgas abzulösen. Laut einer Prognose des Bundesverbands Erneuerbare Energie (BEE) wird

erwartet, dass im Jahr 2020 über 26.000 GWh Wärme durch geothermische Wärmepumpen und die direkte Nutzung tiefer Geothermie bereitgestellt werden (Hinrichs-Rahlwes & Pieprzyk 2009). Die Wärmebereitstellung in Deutschland mithilfe geothermischer Anlagen lag im Jahr 2013 bei ca. 9.500 GWh. Damit konnte ein Anteil von 0,64 % am gesamten Wärmebedarf in Deutschland durch Erdwärme gedeckt werden (BMWi 2014). Die Geothermie spielt demnach bei der Deckung des Heizenergiebedarfs eine noch eher untergeordnete Rolle. Als Gründe können hier zum einen die immer noch vergleichsweise hohen Investitionskosten gesehen werden, zum anderen können die noch bestehenden Unsicherheiten in der Dimensionierung und der Betriebserfahrung solcher Heizungsanlagen angeführt werden (Sass et al. 2014). Um die Geothermie als Energiequelle noch effizienter nutzen zu können sowie Unsicherheiten in der Planung und Auslegung zu minimieren, sind weitere Forschungsarbeiten notwendig.

Seit über 30 Jahren werden Erdwärmesonden in Kombination mit Wärmepumpen zum Heizen von Gebäuden eingesetzt (Hellström 1991, Banks 2008). Die Sonden sind dabei typischerweise zwischen 50 bis 100 m tief.

Immer häufiger kommen auch tiefe Erdwärmesonden zum Einsatz, wie beispielsweise in Weggis (Kohl et al. 2002), Heubach (Fritsche et al. 2012) und Aachen (Herzog 2006), die weit über 1000 m tief sein können.

Seit einigen Jahren werden vermehrt ganze Erdwärmesondenfelder angelegt und häufig auch zur saisonalen Wärmespeicherung genutzt. Ein bekanntes Beispiel ist der Erdsonden-Wärmespeicher in Crailsheim (z. B. Bauer et al. 2008). In selteneren Fällen werden Erdwärmesonden auch zur Kühlung von Gebäuden genutzt. Die genehmigungsrechtliche Situation für eine solche Kühlanwendung ist im Allgemeinen jedoch schwierig.

Erdwärmesonden können als technische Bauwerke verstanden werden, die in einen geologischen Untergrund eingebaut sind. Unsicherheiten hinsichtlich der konkreten technischen Eigenschaften einer Erdwärmesonde ergeben sich bereits aus dem Einbau der Sonde, da hierbei erhebliche Toleranzen auftreten können. Weitaus gravierender sind jedoch die Unsicherheiten hinsichtlich des Aufbaus und der Eigenschaften des Untergrundes.

Unter diesen Gesichtspunkten stellt sich gegebenenfalls die Frage, wie realitätsgetreu ein Modellierungsergebnis überhaupt sein kann.

Thermische Modellierung von Erdwärmesonden

Eine fachgerechte Auslegung von Erdwärmesonden ist eine wichtige Grundlage für eine nachhaltige Erdwärmenutzung. Eine korrekte Dimensionierung ist entscheidend für den technischen und wirtschaftlichen Erfolg der geother-

mischen Anlage. Für größere Anlagen (Heizlast >30 kW, Jahresbetriebsstunden >2.400 h, zusätzlich vorhandene Wärmequellen/-senken, wie zum Beispiel Kühlung) fordert die VDI (Richtlinie 4640, Blatt 2, 2001) daher eine auf den Einzelfall ausgerichtete Berechnung. Dabei sollen die Temperaturverläufe im Bereich der geothermischen Anlage, die sich aus dem Heizbedarf ergeben, über den vorgesehenen Betriebszeitraum ermittelt werden. Genehmigungsrechtlich müssen die Modelle außerdem sowohl die im Untergrund durch den Betrieb der Anlage maximal und minimal auftretenden Temperaturen als auch die laterale Ausbreitung der auftretenden Temperaturveränderungen quantifizieren. Je nach Anforderung und Komplexität des Untergrunds erfordert dies den Einsatz von auf analytischen oder numerischen Modellansätzen basierenden Simulationsprogrammen. Vorteile von analytischen Simulationsprogrammen, wie beispielsweise EED – Earth Energy Designer (Blomberg et al. 2008) oder dem Programm EWS (Huber 2011), sind deren kurze Rechenlaufzeiten sowie die Möglichkeit, Wärmepumpenkonfigurationen in die Berechnungen mit einzubeziehen. Die genannten Programme sind jedoch nicht in der Lage, variable Geometrien und vor allem den Einfluss einer Grundwasserströmung zu berücksichtigen. Hierzu ist die Kopplung der Erdwärmesondenberechnung mit einem numerischen Wärmetransportprogramm notwendig.

Mottaghy & Dijkshoorn (2012) haben 2006 die erste Implementierung einer Erdwärmesondenberechnung in dem numerischen Wärmetransport-Modellierungsprogramm SHEMAT vorgestellt. Diese Version wurde jedoch nicht für Anwender zur Verfügung gestellt. Ab 2009 wurde eine Implementierung der Berechnung von Erdwärmesonden alternativ nach Eskilson & Claesson (1988) oder Al-Khoury (Al-Khoury et al. 2005; Al-Khoury & Bonnier 2006) in dem verbreiteten Programm FEFLOW (Version 5.7) auf den Markt gebracht. Hiermit lag erstmals eine für Consulter einfach anwendbare Software für die Auslegungsberechnung sowie für Prognoseberechnungen (inklusive Ausbreitung von Temperaturfahnen und Einhaltung der gesetzlichen Auflagen hinsichtlich der im Untergrund auftretenden minimalen und maximalen Temperaturen) kommerziell frei verfügbar vor. Da FEFLOW bis heute das einzige öffentlich zugängliche Programm ist, welches diese Funktionalität bietet, beinhalten genehmigungsbehördliche Auflagen bei der Beantragung einer größeren Erdwärmesondenanlage oftmals die Forderung nach einer FEFLOW-Modellierung.

Steigt die zu erwartende negative Beeinflussung der Umwelt durch die Anlage (etwa durch Erwärmung des Untergrunds), steigen in der Regel auch die Erwartungen bezüglich der Realitätstreue der Modellierung. In manchen Fällen können eine Einbeziehung von Wetterdaten (zum Beispiel durch eine im Jahresgang variable Bodentemperatur) und eine Berücksichtigung des Einflusses von Gebäuden auf die Untergrundtemperatur sinnvoll sein. Auch

komplexe Betrachtungen der vorliegenden Grundwasserströmung in Hinblick auf den advektiven Wärmetransport können zu einer Verbesserung der Modellierungsergebnisse beitragen.

Wie jede numerische Modellierung ist auch die gekoppelte Simulation von Wärmetransport und Erdwärmesonden mit Unsicherheiten behaftet. Modelle zur Berechnung des gekoppelten advektiven und konduktiven Wärmetransports sind generell aufgrund der Nichtlinearität des zu berechnenden Gleichungssystems aufwendig (Rühaak et al. 2008, Diersch et al. 2011a 2011b, Diersch 2014). Die zusätzliche gekoppelte Berechnung von Erdwärmesonden kann dann zu Rechenzeiten in der Größenordnung von mehreren Tagen bis Wochen führen.

Unsicherheiten bei der Modellierung von Erdwärmesonden

Die Prognosen bei der thermischen Modellierung von Erdwärmesonden weisen typischerweise Unsicherheiten hinsichtlich aller geforderten Ergebnisse auf, das heißt hinsichtlich der Dimensionierung, der auftretenden minimalen/maximalen Temperaturen und auch der zeitlich-räumlichen Ausbreitung der durch den Betrieb hervorgerufenen Temperaturveränderung des Untergrundes.

Box & Draper (1987) schrieben: „*Remember that all models are wrong; the practical question is how wrong do they have to be to not be useful*". Numerische Modelle weisen per Definition Unsicherheiten auf. Modelle, die die Natur (Geologie, Wetter, etc.) widerspiegeln sollen, sind neben Unsicherheiten, die aus den mathematischen Verfahren selbst resultieren (Approximationsfehler), zudem mit großen Unsicherheiten hinsichtlich der angenommenen Parameter behaftet. Beispielsweise ist eine exakte Parametrisierung des geologischen Untergrundes bei dreidimensionalen Modellen prinzipiell nicht möglich. Die Frage ist also, welches Maß an Genauigkeit notwendig ist.

Besonders im geowissenschaftlichen Consulting wird häufig eine bestimmte Anpassungsgüte von zum Beispiel hydrogeologischen Modellen gefordert. Modelltechnisch wird diese Anpassung durch manuelle oder automatische (inverse) Kalibration erzielt. Eine bekannte Schattenseite dieser Kalibration ist, dass in vielen Fällen neu gewonnene Felddaten eine Rekalibrierung erfordern, da das Modell diese neuen Daten nicht korrekt vorhergesagt hat. Es ist also wenig robust und daher nur eingeschränkt prognosefähig.

Trotz dieser Unsicherheiten können Modelle wichtige Informationen liefern. Die Annahme einer Prognosefähigkeit innerhalb geringer Fehlertoleranzen (die häufig nur implizit benannt werden) ist jedoch in den meisten Fällen ein Missbrauch eines solchen Modells.

Die bei einer geothermischen Modellierung benötigten Parameter sind in Tabelle 1 zusammengefasst.

Die Unsicherheit der untergrundbezogenen Parameter (Wärmeleitfähigkeit, volumetrische Wärmekapazität und geothermischer Gradient) lässt sich durch einen *Thermal Response Test* (TRT) oder *Enhanced Thermal Response Test* (ETRT) einschränken. Beide können jedoch erst an einer bereits ausgebauten Bohrung durchgeführt werden. Vor allem zur Dimensionierung größerer Erdwärmeanlagen ist es empfehlenswert, das Verhalten der Erdwärmesonden unter angenommenen Randbedingungen bereits vor einem Abteufen der Bohrungen über einen entsprechenden Zeitraum zu simulieren.

Bei der aus einem TRT ermittelten Wärmeleitfähigkeit ist zu bedenken, dass es sich um einen aggregierten Wert handelt, was jedoch in vielen Fällen ausreichend ist. Der ETRT liefert demgegenüber tiefenaufgelöste Werte der Wärmeleitfähigkeit (Lehr & Sass 2014).

Die Wärmeleitfähigkeit in porösen Medien wird stark von der Wassersättigung bestimmt. Diese ist daher zumeist bedeutender als die Wärmeleitfähigkeit des Feststoffanteils im Untergrund. Zum Beispiel kann sich bei größeren jahreszeitlichen Schwankungen des Grundwasserspiegels die Entzugsleistung verändern. Strömendes Grundwasser führt durch den zusätzlichen konvektiven Wärmetransportanteil zu einer scheinbaren Erhöhung der Wärmeleitfähigkeit des Untergrundes. Bei TRT und ETRT wird eine effektive Wärmeleitfähigkeit ermittelt, die diesen Effekt widerspiegelt und deshalb für die Anlagenauslegung in einem rein konduktiven Wärmetransportmodell den korrekten Wert darstellt. Bei einem numerischen Wärmetransportmodell, welches die Grundwasserströmung selbst berücksichtigt, muss dieser Effekt jedoch aus den Daten herausgerechnet werden, da er sonst zweimal berücksichtigt würde. Mögliche Werte zur Korrektur können aus Huber (2013) abgeleitet werden.

Die wesentlich häufiger Verwendung findenden oberflächennahen Erdwärmesonden mit einer typischen Teufe zwischen 50 bis 150 m weisen andere Schwierigkeiten auf, als die deutlich seltener verbauten Erdwärmesonden mit Tiefen größer als 400 m. Im Hinblick auf die Unsicherheiten bei der Modellierung lassen beide Nutzungsarten viele Gemeinsamkeiten erkennen, jedoch auch einige wichtige Unterschiede. Beispielsweise ist der Aspekt der gegenseitigen Beeinflussung im Sondenfeld natürlich nicht von Relevanz bei einer Einzelsonde; weiterhin ist die geowissenschaftliche Untersuchung des Untergrundes bei tiefen Einzelsonden häufig aufwendiger als bei oberflächennahen Sonden. Aufgrund der Geologie Deutschlands werden oberflächennahe Erdwärmesonden häufig in quartären glazifluvialen Sedimenten abgeteuft, wohingegen tiefe Sonden in weiten Teilen im Festgestein abgeteuft werden. Dabei weisen die

Tab. 1 Unsicherheiten bei der Modellierung von Erdwärmesonden

	Parameter	Wie ermittelt	Unsicherheit
Untergrund	Wärmeleitfähigkeit	Bei kleinen Anlagen häufig aus Geographischen Informationssystemen (GIS) bzw. Web Map Service (WMS) und Literaturwerten (z. B. VDI 4640), bei größeren Anlagen aus Thermal Response Test (TRT) bzw. Enhanced TRT (ETRT)	Z. T. sehr hoch; TRT kann Unsicherheit verringern, ist aber teilweise ebenfalls mit größeren Unsicherheiten behaftet (bspw. Auswertungsfehler und durch Grundwasserströmung)
	Volumetrische Wärmekapazität	Bei kleinen Anlagen häufig aus GIS/WMS/Literaturwerten (z. B. VDI 4640), bei größeren Anlagen aus TRT bzw. ETRT	Z. T. sehr hoch; Einfluss nur relevant bei kurzzeitigen Lastwechseln; Ableitung aus TRT zumeist ungenau
	Oberflächentemperatur und Geothermischer Wärmefluss	GIS/WMS, Berechnung aus WLF und geothermischem Gradienten, letzterer durch Temperaturlog im Bohrloch	Hoch, jedoch ist die Schwankungsbreite relativ gering
	Grundwasserströmungsgeschwindigkeit und -richtung	Bei kleinen Anlagen häufig aus GIS/WMS, bei größeren Anlagen aus detailliertem Grundwasserströmungsmodell	Hohe Unsicherheit da Informationen über das Strömungsregime normalerweise nur großskalig vorliegen; Grundwasserströmung kann kleinräumige Variationen aufweisen (Tonlinsen etc.); hinsichtlich des Betriebs geht Grundwasserströmung in die (effektive) Wärmeleitfähigkeit ein
Erdwärmesonde	Wärmeleitfähigkeit des Hinterfüllmaterials	Datenblätter des Herstellers	Bei korrektem Einbau gering
	Volumetrische Wärmekapazität des Hinterfüllmaterials	Datenblätter des Herstellers	Bei korrektem Einbau gering; Einfluss nur relevant bei kurzzeitigen Lastwechseln
	Thermische Eigenschaften der Rohre	Datenbankwerte	Sehr gering
	Geometrie und Teufe der Bohrung und der eingebauten Rohre	–	Mittel bis groß; Anzahl der eingesetzten Abstandshalter bei U-Rohren ist wichtig; Abweichung der Bohrung vom Lot ist häufig unbekannt
Betrieb	Lastbetrieb	Technische Gebäudeplanung, Klimadaten	Hoch; variable Wetterbedingungen; über die Zeit veränderliches Nutzerverhalten

quartären Sedimente in den meisten Fällen eine höhere kleinräumige Variabilität auf als die Festgesteine.

Ein Modellbeispiel

Die Unsicherheitsbetrachtung soll Prognoseunsicherheiten bei der numerischen Modellierung aufgrund von abweichenden Untergrund- und Betriebsparametern quantifizieren. Als Fallbeispiel wurde hier die mitteltiefe Erdwärmesonde in Heubach herangezogen. Heubach liegt im nordöstlichen Bereich des kristallinen Odenwaldes, dem sogenannten Böllsteiner Odenwald. Die Bohrung für die 773 m tiefe Erdwärmesonde wurde dabei überwiegend in Gneisen mit veränderlichem Mineralgehalt abgeteuft (Fritsche et al. 2012). Für die thermische Modellierung der Untergrundverhältnisse wird ausschließlich von einem konduktiven Wärmetransport ausgegangen. Daraus ergibt sich der rein durch

Wärmeleitung bedingte zeitliche und räumliche Temperaturverlauf im homogen-isotropen Untergrund mit:

$$[1] \quad \rho c \frac{\partial T}{\partial t} = \lambda abla^2 T + H_{EWS}$$

H_{EWS} beschreibt eine externe Quelle/Senke. Durch ein Variieren des Lastgangs und somit auch des Wärmeeintrags im Untergrund wird dieser Term der Gleichung berücksichtigt. Zudem erfolgte die Untersuchung der Auswirkung einer Variation von Wärmeleitfähigkeit (λ), volumetrischer Wärmekapazität (ρc) und des geothermischen Gradienten ($ablaT$). Damit wurden alle direkten Einflussgrößen bei der Unsicherheitsbetrachtung berücksichtigt. Der Wertebereich der nachfolgend untersuchten Parameter ist weitgehend auf Grundlage von Literaturwerten festgelegt worden. Die Variation der Wärmeleitfähigkeit und der volumetrischen Wärmekapazität basiert auf im Labor gemessenen Kennwerten entsprechender Gesteine des Böll-

steiner Odenwaldes. Die bei der Tiefenbohrung in Heubach gewonnenen Gesteinsproben (Bohrkerne, Bohrklein) wurden ebenfalls untersucht. Die Kennwerte dieser Gesteine sind in die Bemessung des zu untersuchenden Wertebereichs nicht eingeflossen, da grundsätzlich von einem Wissensstand in der Planungsphase des Projekts ausgegangen wurde. In die Bestimmung der Wärmekapazität sind neben empirisch ermittelten Werten auch Kalorimetermessungen eingeflossen.

Die für die Unsicherheitsbetrachtung herangezogenen Kennwerte sollen möglichst einen breiten Wertebereich abdecken. Eine geeignete Methode, um dies zu erreichen, ist die Verwendung der Standardabweichung. Die Standardabweichung (σ) ist die Quadratwurzel der Varianz und damit ein Maß, um die Streuung von Messwerten um ihren Erwartungswert (μ) zu quantifizieren (Bättig 2015):

$$[2] \quad \sigma^2 = \left(x_1 - \mu\right)^2 \cdot \mathbb{P}\left(X = x_1\right) + \left(x_2 - \mu\right)^2 \cdot \mathbb{P}\left(X = x_2\right) + \ldots$$

Die Varianz stellt damit die zu erwartende quadratische Abweichung vom Mittelwert dar und kann für stete Wahrscheinlichkeitsmodelle beschrieben werden durch (Bättig 2015):

$$[3] \quad \sigma^2 = \int_{-\infty}^{\infty} \left(x - \mu\right)^2 \cdot f\left(x\right) dx$$

Dabei ist μ der Mittelwert (Erwartungswert) der Messwerte (hier Wärmeleitfähigkeiten bzw. volumetrische Wärmekapazitäten) und $f(x)$ die Dichtefunktion. Ein stetes Wahrscheinlichkeitsmodell, anhand dessen die Streuung der Werte veranschaulicht werden kann, ist die Normalverteilung (*Gauß-Verteilung*) mit der Dichtefunktion:

$$[4] \quad f_{Gauss}\left(x | \overline{x}, \sigma\right) = \frac{1}{\sqrt{2\pi\sigma^2}} \cdot exp\left\{-0,5 \cdot \left(\frac{x - \overline{x}}{\sigma}\right)^2\right\}$$

Der Parameter $\overline{x}$ stellt dabei den Modus dar. Es ist der Median und auch der Mittelwert (Erwartungswert) der Normalverteilung (Bättig 2015). Die Häufigkeitsverteilung sowie der Graph der Gauß-Verteilung der Wärmeleitfähigkeit und der volumetrischen Wärmekapazität sind in Abbildung 1 dargestellt.

Für beide Datensätze konnte eine Normalverteilung anhand verschiedener Methoden nachgewiesen werden.

Für einen Messwert x in einem normalverteilten Wertebereich gilt dabei:

$$[5] \quad \mathbb{P}\left(\mu - \sigma < x \leq \mu + \sigma\right) = 0,6828$$

$$[6] \quad \mathbb{P}\left(\mu - 2\sigma < x \leq \mu + 2\sigma\right) = 0,955$$

$$[7] \quad \mathbb{P}\left(\mu - 3\sigma < x \leq \mu + 3\sigma\right) = 0,997$$

Demnach liegen in einem normalverteilten Modell die Werte mit einer Wahrscheinlichkeit von etwa 68,3 % zwischen $\left(\mu - \sigma\right)$ und $\left(\mu + \sigma\right)$ und mit etwa 95,5 % Wahrscheinlichkeit zwischen $\left(\mu - 2\sigma\right)$ und $\left(\mu + 2\sigma\right)$ (Bättig 2015).

Ausgehend vom Mittelwert wurden nun die Werte für $\left(\mu - \sigma\right)$ $\left(\mu + \sigma\right)$ $\left(\mu - 2\sigma\right)$ und $\left(\mu + 2\sigma\right)$ der Wärmeleitfähigkeit und der volumetrischen Wärmekapazität als Parameter für die Unsicherheitsbetrachtung festgelegt (Tab. 2).

Die Variation des geothermischen Gradienten soll die üblichen Werte für Gebiete in Hessen, die außerhalb des Oberrheingrabens gelegen sind, umfassen. Der Oberrheingraben bildet eine sogenannte Wärmeanomalie. Der Aufstieg heißer Tiefenwässer im Grabensystem führt lokal zu Temperaturgradienten von bis zu 10 K (100 m)$^{-1}$ (Pribnow & Schellschmidt 2000). In der Bemessung der Parameter für die Sensibilitätsbetrachtung des geothermischen Gradienten sollen diese Gradienten daher nicht beachtet werden. In Arndt et al. (2011) werden auf Grundlage von Temperaturdaten für die Bereiche Hessens außerhalb des Oberrheingrabens empirisch ermittelte Temperaturgradienten von 2,4 K (100 m)$^{-1}$ bis 4,0 K (100 m)$^{-1}$ veranschlagt. Im Mittel nimmt in Mitteleuropa die Temperatur um etwa 3,0 K (100 m)$^{-1}$ mit der Tiefe zu. Darauf aufbauend wurden für die Unsicherheitsbetrachtung geothermische Gradienten von 2,5 K (100 m)$^{-1}$ bis 3,5 K (100 m)$^{-1}$ in Intervallen von 0,25 K (100 m)$^{-1}$ untersucht.

Neben den Untergrund- und Gesteinskennwerten ist der Heizenergiebedarf eine wichtige Größe bei der Dimensionierung von geothermischen Anlagen. Die Bemessung der mitteltiefen Erdwärmesonde in Heubach basiert auf einem Lastgang, der in einem kalten Jahr den Entzugsbedarf decken soll. Dabei soll eine jährliche Wärmemenge von etwa 120 MWh a^{-1} entzogen werden. Bemessen wurde dieses Lastprofil an den klimatischen Daten von 2010.

Alle Modelle wurden über eine Laufzeit von vier Jahren simuliert. Mit dem Ziel, vier vollständige Heizperioden abzubilden, wurde der Startpunkt der Simulationen auf den ersten Oktober des Ausgangsjahres gesetzt.

Einschränkungen singulärer Prognosemodelle

Die Güte und Zuverlässigkeit einer einzelnen Prognosemodellierung ist abhängig vom Grad der Kenntnis des geologischen Untergrunds und seiner Eigenschaften. Sofern die genauen Untergrundverhältnisse nicht durch eine Bohrung erschlossen wurden, basiert die Prognosemodellierung auf Annahmen der Gesteinskennwerte und der Temperaturver-

Abb. 1 a Häufigkeitsverteilung der gemessenen Wärmeleitfähigkeiten der Gesteine des Böllsteiner Odenwaldes sowie der dazugehörige Graph der Normalverteilung. Im Bereich μ−σ bis μ+σ (*dunkelgrau*) befinden sich 68,28% und im Bereich μ−2σ bis μ+2σ (*hellgrau*) 95,5% aller Messwerte. Dabei sind μ der Mittelwert und σ die Standardabweichung. **b** Häufigkeitsverteilung der aus den Ergebnissen der Kalorimetermessungen berechneten volumetrischen Wärmekapazitäten der Gesteinsproben
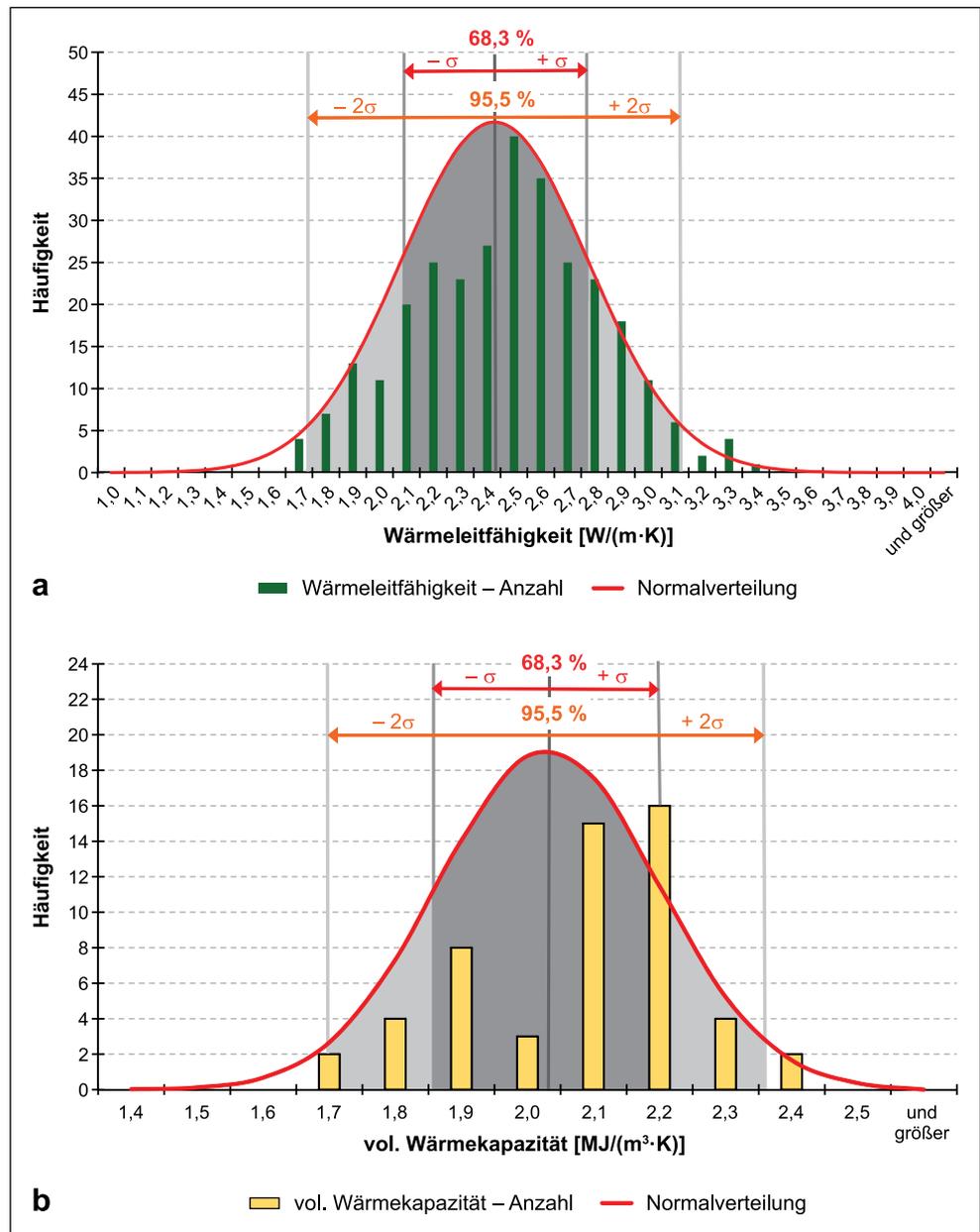
Tab. 2 Übersicht der gewählten Parameter der Wärmeleitfähigkeit und der volumetrischen Wärmekapazität für die Unsicherheitsbetrachtung

	μ−2σ	μ−σ	M	μ+σ	μ+2σ
Wärmeleitfähigkeit [W/(m·K)]	1,73	2,08	2,43	2,77	3,12
Vol. Wärmekapazität [MJ/(m³·K)]	1,7	1,86	2,03	2,2	2,36

teilung. Eine einzelne Prognosemodellierung spiegelt dabei nur einen für die angenommenen Verhältnisse gültigen Fall wieder. Wie stark diese Prognose mit einer Unsicherheit behaftet ist, kann daraus nicht abgeleitet werden. Je nach Art und Anforderung der geplanten Geothermieanlage variiert auch die Bedeutung der geothermischen, hydrogeo-

logischen und reservoirgeologischen Eigenschaften. Die entsprechenden Modelle müssen daher unterschiedliche Detailgrade aufweisen.

Insbesondere bei großen und kostenintensiven geothermischen Nutzungssystemen kann es sinnvoll sein, begleitend zu einem Prognosemodell, dem die am ehesten zu vermutenden Parameter zugrunde liegen, ein Ensemble an Prognosesimulationen mit variierenden Ausgangsbedingungen zu erstellen. Hierdurch kann ein Bereich definiert werden, in dem die aus der Anlage gewonnenen Fluidtemperaturen mit einer gewissen Wahrscheinlichkeit liegen sollten. Außerdem kann dadurch der für das spezifische Projekt geltende Einfluss der verschiedenen Parameter in einer vergleichsweise frühen Planungsphase abgeschätzt

werden. Um den rechnerischen Aufwand solcher Ensemblemodelle in einem vertretbaren Rahmen zu halten, bietet es sich an, zum Beispiel für die Parametrisierung des Untergrundes von homogenen Bedingungen auszugehen. Für die Erdwärmesonde in Heubach wurde neben dem Einfluss der einzelnen Parameter auf die Modellierungsergebnisse auch der gekoppelte Einfluss von Wärmeleitfähigkeit und volumetrischer Wärmekapazität untersucht. Um eine mögliche Überlagerung der Einflüsse beider Parameter zu erfassen, wurden Modelle erstellt, in denen beide Parameter gemeinsam variiert wurden.

Abbildung 2 zeigt die Simulationsergebnisse der ersten Heizperiode. Dargestellt sind die Abweichungen der mittleren täglichen Fluidtemperaturen der verschiedenen Modelle relativ zum Mittelwert-Modell. Die Nulllinie steht demnach für das Mittelwert-Modell, dem eine Wärmeleitfähigkeit des Untergrundes von 2,43 W m^{-1} K^{-1} und eine volumetrische Wärmekapazität von 2,03 MJ m^{-3} K^{-1} zugrunde liegen. Das Modell mit den um zwei Standardabweichungen verringerten Wärmeleitfähigkeiten (1,73 W m^{-1} K^{-1}) und volumetrischen Wärmekapazitäten (1,70 MJ m^{-3} K^{-1}) zeigte in den Monaten mit verstärktem Wärmeentzug (Dezember bis Februar) bereits im ersten Betriebsjahr Abweichungen in den mittleren täglichen Fluidtemperaturen von bis zu −5,3 K.

Bei der getrennten Betrachtung beider Parameter konnte die Wärmeleitfähigkeit des Untergrundes als maßgebliche Größe für diese Temperaturunterschiede ausgemacht werden. Die Untersuchungen zur Prognoseunsicherheit der volumetrischen Wärmekapazität ergaben für die jährliche mittlere Fluidtemperatur maximale Abweichungen von weniger als 0,5 K zwischen dem Modell mit 1,70 MJ m^{-3}

K^{-1} und dem Modell mit 2,36 MJ m^{-3} K^{-1}. Der hier gezeigte geringe Einfluss der volumetrischen Wärmekapazität sollte allerdings nicht verallgemeinert werden. Unter veränderten Betriebsbedingungen, wie zum Beispiel unter Einbeziehung einer saisonalen Speicherung von Wärme, könnte der Einfluss größer werden.

Durch eine Prognosemodellierung anhand mehrerer Szenarien werden die Unsicherheiten bei gegebenem Wissensstand in Form der Spannweite der Modellergebnisse widergegeben. Durch zusätzliche Vorerkundungsmaßnahmen können solche Unsicherheiten eingegrenzt werden. Eine Prognose auf Basis eines Ensembles an Simulationen kann bei der Projektentwicklung also als Entscheidungshilfe für zusätzliche Vorerkundung dienen. Parameter, die bei der Ensemblemodellierung einen geringen Einfluss zeigen, könnten von Vorerkundungsmaßnahmen ausgeschlossen werden, um dadurch Kosten zu sparen.

Fazit

Numerische Modelle sind ein hilfreiches Werkzeug, um vor Bau einer Erdwärmesondenanlage eine Auslegung zu konzipieren. Aufgrund der großen Anzahl von zum Teil erheblichen Unsicherheiten bei den Eingangsparametern ist die Berechnung eines einzigen Prognosemodells kritisch zu hinterfragen.

Die Autoren halten die zusätzliche Berechnung sogenannter Ensemblemodelle, wie sie schon lange in der Meteorologie üblich ist (z. B. Krahe et al. 2009), für einen möglichen Ansatz. Der Auftraggeber erhält nun nicht mehr ein einziges Ergebnis, sondern ergänzend eine statistisch sinnvoll quantifizierte Spanne von möglichen Ergebnissen

Abb. 2 Differenz der mittleren Fluidtemperaturen der Variationsmodelle relativ zum Mittelwert-Modell
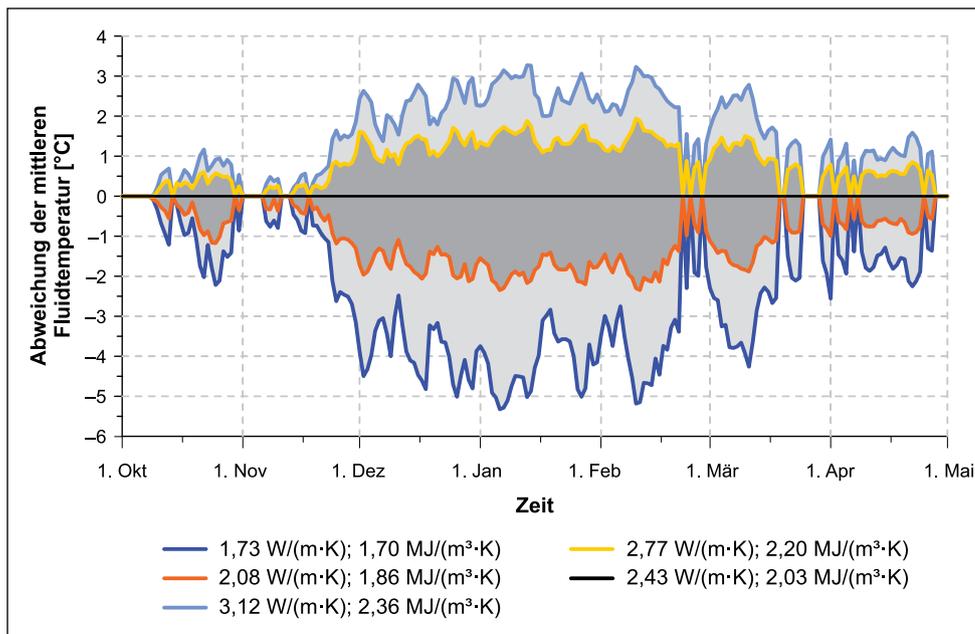
mit einem Hinweis auf den Variationsbereich mit der höchsten Wahrscheinlichkeit.

Aus dem Consulting ist bekannt, dass immer wieder relativ allgemeine Sensitivitätsbetrachtungen gefordert werden. Die hier vorgestellte Vorgehensweise ist nicht als eine solche Sensitivitätsbetrachtung zu verstehen. Die Gleichung 1 ist wohlbekannt, die Sensitivitäten der Parameter folgen den physikalischen Gesetzmäßigkeiten. Die unbekannte Parametersensitivität ergibt sich aus einer zeitlichen Variabilität: Je schneller thermische Lasten wechseln, desto relevanter ist die volumetrische Wärmekapazität, je stationärer das Problem wird, desto relevanter wird die Wärmeleitfähigkeit. Für eine sinnvolle Sensitivitätsbetrachtung wären also vielfache Modellvariationen bei verschiedener zeitlicher Variabilität erforderlich. Tatsächlich sind die Unsicherheiten hinsichtlich der zeitlichen Variabilität häufig größer als bei den hier vorgestellten Parameter-Unsicherheitsbetrachtungen. Letztlich können Ensemblemodelle also die Frage der Sensitivität durchaus mitbeantworten, sie sind jedoch nicht hierauf beschränkt.

Literatur

AGEB – Arbeitsgemeinschaft Energiebilanzen e. V. (Hrsg.): Anwendungsbilanzen für die Endenergiesektoren in Deutschland in den Jahren 2011 und 2012 mit Zeitreihen von 2008 bis 2012. Berlin (2013)

Al-Khoury, R., Bonnier, P.G.: Efficient finite element formulation for geothermal heating systems, part II: transient. Int. J. Numer. Meth. Engng. **67**,725–745 (2006)

Al-Khoury, R., Bonnier, P.G., Brinkgreve, R.B.J.: Efficient finite element formulation for geothermal heating systems, part I: steady state. Int. J. Numer. Meth. Engng. **63**, 988–1013 (2005)

Arndt, D., Bär, K., Fritsche, J.G., Kracht, M., Sass, I., Hoppe, A.: 3D structural model of the Federal State of Hesse (Germany) for geopotential evaluation. Z. Dtsch. Ges. Geowiss. **162**(4), 353–369 (2011)

Banks, D.: An introduction to thermogeology: ground source heating and cooling. S. 352. Blackwell Publishing, Oxford, UK (2008)

Bättig, D.: Angewandte Datenanalyse; Der Bayes'sche Weg – Statistik und ihre Anwendungen. S. 366. Springer, Berlin (2015)

Bauer, D., Heidemann, W., Marx, R., Nußbicker-Lux, J., Ochs, F., Panthalookaran, V., Raab, S.: Solar unterstützte Nahwärme und Langzeit-Wärmespeicher (Juni 2005 bis Juli 2008). Forschungsbericht zum BMU-Vorhaben 0329607J. Stuttgart (2008)

Blomberg, T., Claesson, J., Eskilson, P., Hellstrom, G., Sanner, B.: EED-Earth energy designer 3.16. BLOCON SWEDEN. www.blocon.se (2008)

BMWi – Bundesministerium für Wirtschaft und Technologie (Hrsg.): Erneuerbare Energien im Jahr 2013 – Erste vorläufige Daten zur Entwicklung der erneuerbaren Energien in Deutschland auf der Grundlage der Angaben der Arbeitsgruppe Erneuerbare Energien-Statistik (AGEE-Stat). Stand 28. Februar 2014 (2014)

Box, G.E.P., Draper, N.R.: Empirical model building and response surfaces. S. 688. John Wiley & Sons, New York (1987)

Diersch, H.-J.G.: Finite element modeling of flow, mass and heat transport in porous and fractured media, Bd. XXXV, S. 996. Springer, Berlin (2014)

Diersch, H.-J.G., Bauer, D., Heidemann, W., Rühaak, W., Schätzl, P.: Finite element modeling of borehole heat exchanger systems – part 1. Fundamentals. Comput. Geosci. **37**(8), 1122–1135 (2011a)

Diersch, H.-J.G., Bauer, D., Heidemann, W., Rühaak, W., Schätzl, P.: Finite element modeling of borehole heat exchanger systems – part 2. Numerical simulation. Comput. Geosci. **37**(8), 1136–1147 (2011b)

Eskilson, P., Claesson, J.: Simulation Model for thermally interacting heat extraction boreholes. Numer. Heat Tranf. **13**(2), 149–165 (1988)

Fritsche, J.G., Kött, A., Kracht, M., Nesbor, H.-D., Reischmann, T.: Geologische und geothermische Ergebnisse aus dem Projekt: Mitteltiefe Erdwärmesonde Heubach. Hessisches Landesamt für Umwelt und Geologie, 7. Tiefengeothermie-Forum Hessen. Darmstadt, 8. Oktober 2012 (2012)

Hellström, G.: Ground heat storage, thermal analyses of Duct Storage Systems. Department of Mathematical Physics, University of Lund, Sweden (1991)

Herzog, C.: Die Geothermiebohrung „RWTH-1" – Technische, geologische und bergrechtliche Aspekte eines Geothermieprojektes in öffentlicher Trägerschaft. Dissertation. Preuße, A. (Hrsg.): Schriftenreihe Institut für Markscheidewesen, Bergschadenkunde und Geophysik im Bergbau an der Rheinisch-Westfälischen Technischen Hochschule Aachen **1–2005** (2006)

Hinrichs-Rahlwes, R., Pieprzyk, B.: Ausbauprognose der Erneuerbare-Energien-Branche für Deutschland. http://www.bee-ev.de/_downloads/publikationen/studien/2010/100125_BEE-Roadmap_AusbauEE_2020.pdf. Zugegriffen: Oktober 2014 (2009)

Huber, A.: Benutzerhandbuch zum Programm EWS, Version 4.7 – Berechnung von Erdwärmesonden. http://www.hetag.ch/download/Bed_EWS47.pdf. Zugegriffen: Oktober 2014 (2011)

Huber, H.: Experimentelle und numerische Untersuchungen zum Wärmetransportverhalten oberflächennaher, durchströmter Böden. Mitteilungen des Instituts für Werkstoffe und Mechanik im Bauwesen der Technischen Universität Darmstadt **40** (2013)

Kohl, T., Brenni, R., Eugster, W.: System performance of a deep borehole heat exchanger. Geothermics. **31**(6), 687–708 (2002)

Krahe, P., Nilson, E., Carambia, M., Maurer, T., Tomassini, L., Bülow, K., Jacob, D., Moser, H.: Wirkungsabschätzung von Unsicherheiten der Klimamodellierung in Abflussprojektionen – Auswertung eines Multimodell-Ensembles im Rheingebiet. Hydrol. Wasserbewirtsch. **5**, 316–331 (2009)

Lehr, C., Sass, I.: Thermo-optical parameter acquisition and characterisation of geologic properties – A 400 meter deep BHE in a karstic alpine marble aquifer. Environ. Earth Sci. **72**(5), 1403–1419 (2014)

Mottaghy, D., Dijkshoorn, L.: Implementing an effective finite difference formulation for borehole heat exchangers into a heat transport code. Renew. Energy. **45**, 59–71 (2012)

Pribnow, D., Schellschmidt, R.: Thermal tracking of upper crustal fluid flow in the Rhine Graben. Geophys. Res. Lett. **27**(13), 1957–1960 (2000)

Rühaak, W., Rath, V., Wolf, A., Clauser, C.: 3D finite volume groundwater and heat transport modeling with non-orthogonal grids using a coordinate transformation method. Adv. Water Resour. **31**(3), 513–524 (2008)

Sass, I., Brehm, D., Coldewey, W.G., Dietrich, J., Klein, R., Kellner, T., Kirschbaum, B., Lehr, C., Marek, A., Mielke, P., Müller, L., Panteleit, B., Pohl, S., Porada, J., Schiessl, S., Wedewardt, M., Wesche, D.: Empfehlung Oberflächennahe Geothermie – Planung, Bau, Betrieb und Überwachung – EA Geothermie. S. 300. Ernst & Sohn, Berlin (2014)

VDI: Richtlinie 4640, Blatt 2: Thermische Nutzung des Untergrunds – Erdgekoppelte Wärmepumpenanlagen. Düsseldorf (2001)

Appendix D – BASIMO – borehole heat exchanger array simulation and optimization tool

Published as:

Schulte DO, Rühaak W, **Welsch B** and Sass I (2016): BASIMO – borehole heat exchanger array simulation and optimization tool, *Energy Procedia*, v. 97, p. 210-217, doi:/10.1016/j.egypro.2016.10.057.

European Geosciences Union General Assembly 2016, EGU
Division Energy, Resources & Environment, ERE

BASIMO – borehole heat exchanger array simulation and optimization tool

Daniel Otto Schulte[a,b,*], Wolfram Rühaak[a,b], Bastian Welsch[a,b], Ingo Sass[a,b]

[a]*Technische Universität Darmstadt, Institute of Applied Geosciences, Department of Geothermal Science and Technology, Schnittspahnstrasse 9, 64287 Darmstadt, Germany*
[b]*Darmstadt Graduate School of Excellence Energy Science and Engineering, Technische Universität Darmstadt, Jovanka-Bontschits-Straße 2, 64287 Darmstadt, Germany*

Abstract

Innovative applications and novel modifications of borehole heat exchangers (BHE) require new simulation tools. Currently, features like inclined or partly insulated boreholes necessitate fully discretized models. However, those models come at high computational cost. We present a tool, which uses an analytical solution for the BHE coupled with a numerical solution for the subsurface heat transport. A tetrahedron mesh bypasses the limitations of structured grids for borehole path geometries, while BHE properties changing with depth are considered. The tool benefits from the fast analytical solution of the BHEs while still allowing for a detailed consideration of the BHE properties.

Keywords: borehole heat exchangers; numerical modelling; mathematical optimization; borehole thermal energy storage

1. Introduction

Globally, space heating and domestic hot water production constitute about a quarter of the final energy consumption [1]. In countries, which are affected by winter seasons, this fraction can be substantially higher (cf. [2]). Renewable energy sources like solar collectors are increasingly used to cover the heat demand [3, 4]. They have the

---

* Corresponding author. Tel.: +49-6151-16-25675; fax: +49-6151-16-23601.
  E-mail address: schulte@geo.tu-darmstadt.de

potential to reduce the consumption of fossil fuels and to mitigate the CO_2 emissions. However, like the demand, the renewable heat supply is subject to seasonality in higher latitudes. Excess heat is available in summer, while the heat demand is highest in winter. Consequently, renewable heat sources rely on seasonal storage systems [3-8]. Shallow arrays of borehole heat exchangers are already in use for seasonal heat storage at comparably low temperature levels [9-12]. In many countries legal regulations restrict alterations of the groundwater that may have a negative impact on the drinking water quality [13]. Excessive heating of the shallow subsurface can induce microbial growth and, therefore, has to be prevented in these aquifers [14].

Instead, medium deep borehole thermal energy storage systems (BTES) can store the heat in greater depth at high temperature levels evading the topmost aquifers. For that purpose, medium deep BTES have to be fitted with an insulation in the upper section of the borehole. This can be achieved by larger borehole diameters and the use of insulating grouting material in the regarding borehole section. [15-17]

Compared to shallow installations, drilling is an even more critical cost factor for the construction of a medium deep BTES. Thus, simulations of the storage operation are imperative prior to the investment. Furthermore, the design of the BHE array has to be optimized to avoid badly sized systems. Consequently, a simulator for the BHE array should allow for mathematical optimization [17]. Also, a partly insulated borehole corresponds to depth-dependent BHE properties and implies additional special requirements to numerical models. These requirements rule out most of the available simulation tools like EED [18], FEFLOW [19] or line source-based approaches (e.g. [20, 21]). Up to now, only fully discretized models could fulfill these requirements. However, fully discretized models come at high computational cost and are not a viable option for the simulation of entire arrays of BHEs.

In this paper, we present BASIMO: a **B**orehole heat exchanger **A**rray **SIM**ulation and **O**ptimization tool. It comprises a simulator that employs the finite element method (FEM) to calculate the transient conductive heat transport in the subsurface. The thermal response of the BHEs is calculated using an adapted analytical solution based on thermal resistance and capacity models (TRCM), which allows for the consideration of partly insulated boreholes, but still grants fast computation compared to fully discretized models [22]. As the simulator is MATLAB-based, it can be readily used with the MATLAB Global Optimization Toolbox [23] for the mathematical optimization of the storage performance with respect to variable system parameters. For elaborate optimization problems, the computational time can be reduced using a previously trained proxy model [17]. Furthermore, it is possible to link BASIMO to building models for coupled BTES-building simulations.

2. BASIMO

BASIMO was initially developed for the design optimization of BTES [17]. On the one hand, this determines the required features for the simulator, namely the consideration of borehole insulation and the possibility to couple the simulator to mathematical optimization algorithms. On the other hand, it allows for certain simplifications: BTES systems typically target low permeable rocks for heat storage, as groundwater flow decreases the storage efficiency [15]. Therefore, BASIMO neglects the convective heat transport in the subsurface, which decreases the computational cost significantly. Nevertheless, BASIMO can also be used for the simulation of regular BHE arrays in mere heat extraction scenarios as long as groundwater flow is non-existent. BASIMO applies a dual continuum approach where the numerical calculation of the subsurface heat transport is separated from the simulation of the thermal interactions within the BHEs. The latter can be solved analytically, which significantly saves computation time otherwise required for the full discretization of the borehole. The program structure of the simulator is illustrated in Fig. 1.

Input   **Processing**   **Output**
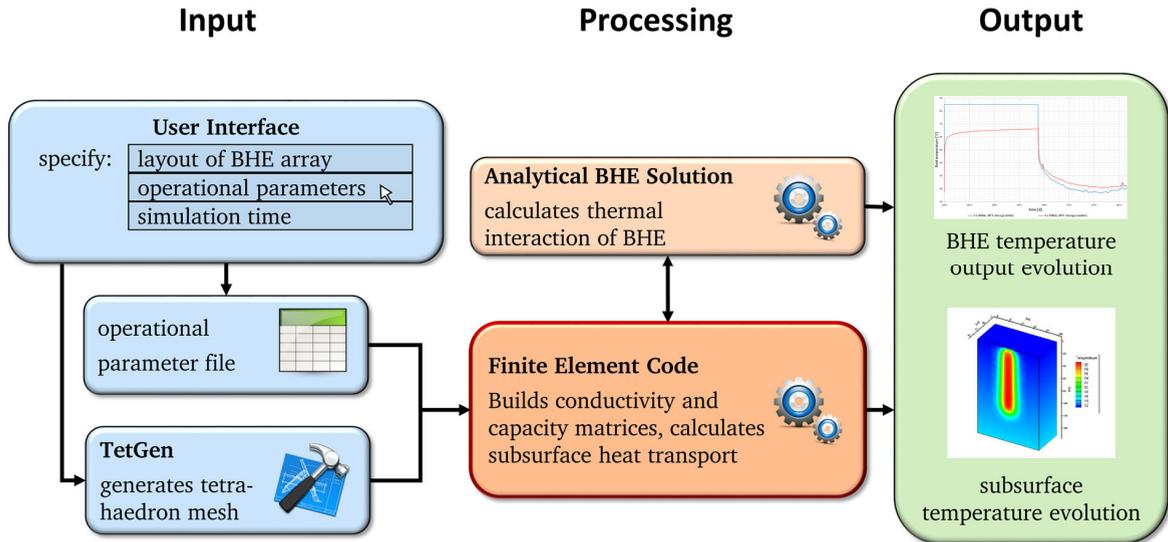
Fig. 1. Schematic of the program structure of the BASIMO simulator, arrows indicate the interaction of the program components.

2.1. Finite Element Method and Tetrahedron Mesh

The core of BASIMO is an improved MATLAB FEM implementation (Galerkin method of weighted residuals [24]) originally developed by Alberty et al. [25]. It calculates the transient heat diffusion in the subsurface by numerically solving Fourier's Law of heat conduction for the model domain, which is discretized as a tetrahedron mesh generated with TetGen [26]:

$$\rho_s c_s \frac{\partial T}{\partial t} = \nabla \cdot (\lambda_s \nabla T) + q_Q \tag{1}$$

With ρ_s: soil density, c_s: volumetric heat capacity of the soil, T: Temperature, t: time, λ_s: thermal conductivity of the soil and q_Q: heat sources and sinks as internal heat generation per unit volume. The tetrahedron mesh is unstructured and eliminates any restrictions for the bore path geometry. Consequently, inclined BHEs can be modeled in BASIMO (Fig. 2a), whereas semi-structured triangular meshes or fully structured rectangular meshes, typical for most available simulators, only allow for the consideration of vertical boreholes.

The principles of the FEM in heat transfer problems have been described for instance by Reddy and Gartling [27]. Ultimately, the weak formulation of the partial differential equation (1) summarized over the entire model domain can be expressed in a short matrix notation:

$$\mathbf{M\dot{T}} + \mathbf{KT} = \mathbf{F(T)} \tag{2}$$

Where $\mathbf{M}$ represents the heat capacity matrix, $\mathbf{K}$ is the thermal conductivity matrix and $\mathbf{F}$ is the right-hand side vector including source terms, whereas $\mathbf{T}$ is the solution vector, i.e. the subsurface temperature. The BHEs act as heat sources or sinks in the FEM mesh and contribute to the right-hand side $\mathbf{F}$. As the heat transfer from and to the BHEs depends on the temperature of the surrounding reservoir rock, their contribution to the source terms in $\mathbf{F}$ depends on the solution vector $\mathbf{T}$. Consequently, the system of equations (2) is non-linear. A predictor-corrector method is used with a second order Adams-Bashforth predictor and a Crank-Nicolson corrector to solve the system of equations. It

allows for automated time stepping after a few initial time steps provide the acceleration vectors of **T** required for the predictor. A Picard iteration scheme is applied on the corrector to consider the non-linearity. [27]

As MATLAB is an interpreted programming language, the program's execution can have significant performance drawbacks compared to compiled code. Especially the assembly of the conductivity and capacity matrices **M** and **K** becomes very slow for large models. This problem is bypassed using C/C++ code [28], which assembles the matrices outside of MATLAB and speeds up the computation by several orders of magnitude. In the same way, other libraries can be integrated, for example, to replace MATLAB's solver by GPU based routines.

2.2. Analytical Solution for Borehole Heat Exchangers

The thermal interaction of the BHEs is calculated by a one-dimensional analytical thermal resistance and capacity model [29-31]. Fed with inlet temperature and flow rate data, it provides the temperature distribution in the inlet and outlet pipes in predefined depth levels. The solution takes into account all thermal and hydraulic parameters of the BHE materials and the borehole wall temperature. In the finite element mesh, the BHEs are discretized as vertical or inclined (Fig. 2a) lines of mesh nodes. The temperature at these nodes defines the borehole wall temperature and is passed to the analytical solution. In return, the analytical solution sets heat sources based on the thermal resistances within the BHEs and the difference between the borehole wall temperature and the calculated BHE fluid temperature at the corresponding nodes (see above). The same solution is used in the commercial software FEFLOW [19], but has been improved for BASIMO to take into account BHE properties changing with depth [22]. This allows for the consideration of insulation within sections of the borehole (Fig. 2b).
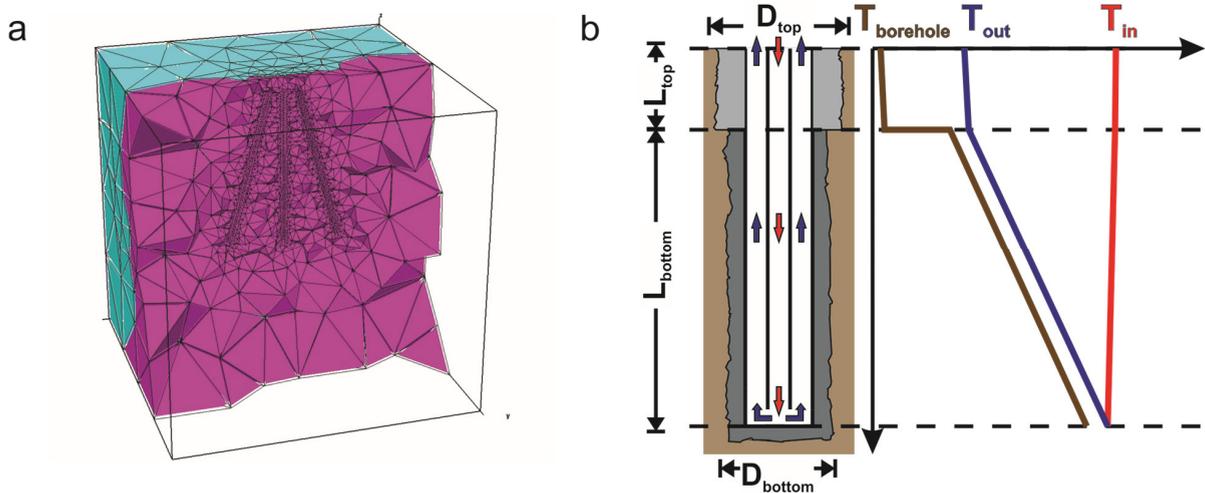
Fig. 2. (a) Cross section of a tetrahedron mesh of a reservoir with inclined BHEs; (b) schematic of an insulated coaxial BHE with centered inlet (not to scale) and the corresponding temperature profiles of the borehole wall and of the fluid in the inlet and the outlet pipe , D: borehole section diameter, L: borehole section length (simplified after [22]).

2.3. User Input and Model Output

BASIMO allows for a detailed model description by the user. Except for the geometry of the BHE array, the model is parametrized by self-explanatory Excel sheets. The user can change the model settings by editing these files without having to tamper with the code. This way, the model can be generated with a simple stratigraphy of the subsurface, where each layer is defined by its bottom depth and can be assigned a different bulk thermal conductivity, density and specific heat capacity.

In a similar manner, the operation of the BHEs is set up by user-defined time steps, for which the BHEs can be assigned a mass flow rate and a corresponding inlet temperature or heat extraction rate. As the analytical solution for the BHEs cannot handle heat extraction rates by itself, an additional Picard iteration loop in BASIMO determines the corresponding inlet temperature. Furthermore, BASIMO allows the user to choose between U-pipe, double U-pipe and coaxial BHEs in the operation setup, which includes the choice between central or annular inlet for coaxial BHEs. These settings apply for all BHEs in the array alike.

The BHEs, on the other hand, are each dealt with independently in a separate file. A detailed configuration allows for the consideration of the following parameters:

- Borehole diameters (two independent sections for possible insulation)
- Pipe diameters
- Pipe wall thicknesses
- Shank space (U-pipe and double U-pipe only)
- Pipe thermal conductivities
- Fluid specific heat capacity
- Fluid thermal conductivity
- Fluid dynamic viscosity
- Fluid density
- Grout thermal conductivities (two independent sections for possible insulation)
- Length of insulation

The temperature dependency of the thermo-physical parameters is not taken into account. The borehole insulation can be disregarded by keeping the borehole diameters and the grout thermal conductivities the same.

Lastly, it is possible, to change a few settings, which concern the numerical calculation and the program output of BASIMO. Depending on the model size and the scheduled operation time, these settings can greatly influence the stability, the accuracy and the simulation time:

- Time integration weighting coefficient of the corrector to change from Crank-Nicolson to fully implicit
- Time stepping control tolerance error
- Picard iteration tolerance error
- Maximum number of Picard iterations
- Initial time step size
- Maximum time step acceleration factor
- Maximum time step size
- Switch for graphical output during the simulation
- Switch for detailed data output for post-processing

BASIMO provides a subroutine for generating the finite element mesh. It first spatially delimits the model domain and then defines the bore paths of the BHEs as lines of nodes in a Cartesian coordinate system before calling TetGen [26] to generate the tetrahedral mesh of finite elements. While the geometrical arrangement of the BHEs is predefined by templates depending on the number of BHEs (Fig. 3), the user can chose their number, their length and their respective distance towards each other. Also, the inclination angle can be defined. In that case, all BHEs radially dip away from the center. If there is a central BHE in the particular arrangement, it remains vertical. The templates try to place the BHEs in a compact arrangement, as a low enveloping surface to storage volume ratio is important for BTES systems. However, BASIMO will also accept user-defined meshes as long as they come with separate files that specify the coordinates of the mesh nodes for each BHE.
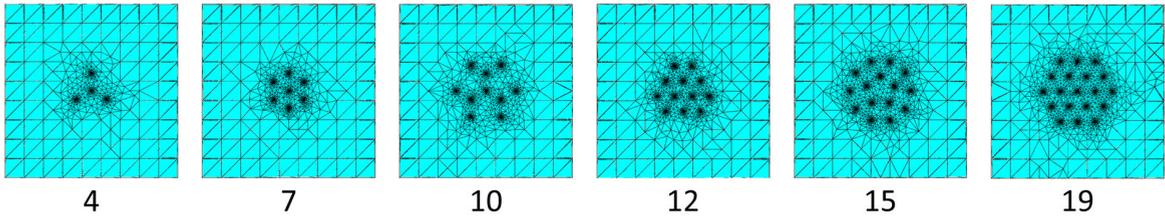
Fig. 3. Exemplary templates for the arrangements of BHEs in the discretized tetrahedron mesh (overhead perspective) and the corresponding number of boreholes, model edge length: 100 m.
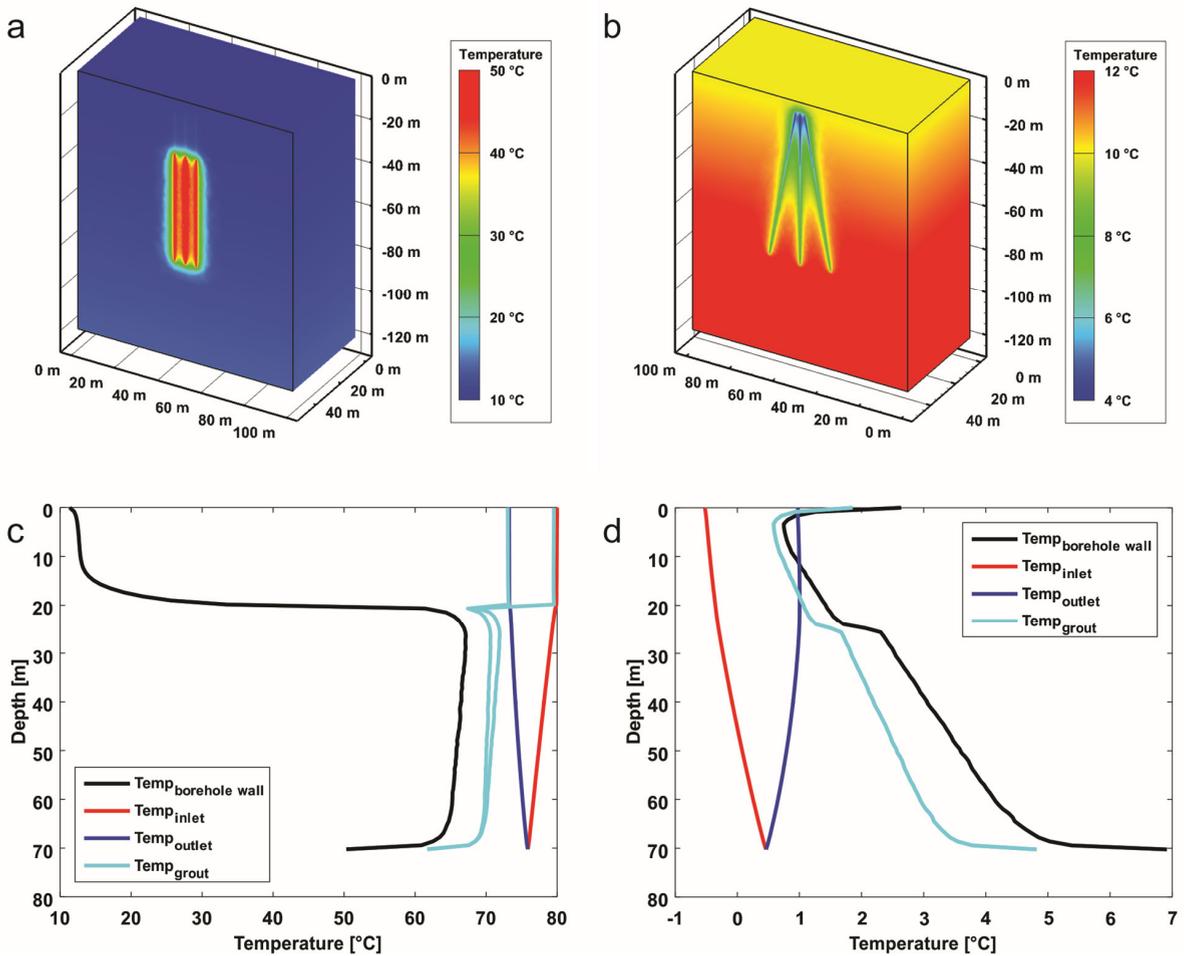
Fig. 4. BASIMO outputs: model cross sections (post-processed) showing the subsurface temperature distribution in a 7 BHE x 70 m array(cf. Fig 3) after 90 days of (a) heat storage in a homogeneous reservoir (granite) with borehole insulation and (b) heat extraction from a stratified reservoir with inclined boreholes (10°); corresponding BHE temperature profiles after 90 days of (c) heat storage in a homogeneous reservoir with borehole insulation and (d) heat extraction from a stratified reservoir with inclined boreholes (10°); stratification: 0-20 m: sandstone, 20-120 m: quartzite.

As mentioned above, BASIMO can return various simulation outputs. Every simulation provides time series of the BHE return temperatures and the final temperature distribution of the subsurface (Fig. 4a & Fig 4b). The latter can also be saved as a time series of distinct time steps for post-processing purposes. Furthermore, it is possible to activate a graphical output during the simulation, which plots the time step size and the inlet and outlet temperature during the simulation, as well as the current temperature profile of the BHE (i.e. borehole wall, downstream pipe and upstream pipe temperature, Fig. 4c & Fig 4d).

2.4. Optimization

Since the code of BASIMO is written in MATLAB, it can be easily embedded in a subroutine called as an objective function or as a nonlinear constraint function in the MATLAB Global Optimization Toolbox [23]. This way, various design or operational parameters can be optimized with regard to characteristic performance indicators. For example, BASIMO can minimize the size of a BHE array for heat storage (i.e. number and length of BHEs), which corresponds to the investment costs, for a specified amount of heat to be provided by the BTES [17]: BASIMO is called as constraint function to ensure sufficient heat provision by the considered array designs. Similarly, the outlet temperature of a single BHE can be optimized by finding the ideal length of borehole insulation [22]. In this case, BASIMO is the objective function called by the optimization algorithm.

Despite the advantages of BASIMO over other programs, simulations of large systems can still be lengthy. This can pose an impasse for some optimization problems that require a large number of function calls to converge on a solution. The problem can be overcome by generating a proxy model from considerably fewer training simulations by arbitrary polynomial chaos expansion [17, 32]. Whereas the computational effort for large models is still high, they only have to be computed once. The resulting proxy model can be evaluated by the optimization algorithm in a matter of seconds, as it consists only of a polynomial instead of a numerical model.

The adaptability of the MATLAB code not only enables its use in optimization algorithms. With only a few simple changes to the code it is possible to couple BASIMO with building models, which consider the heating infrastructure like heat pumps and buffer storages on the surface. Heat demand profiles with a high temporal resolution can be taken into account. This way, the dynamic interplay of the involved system components can be simulated with unprecedented and realistic detail. [33]

3. Outlook

BASIMO is a versatile tool specifically tailored for the simulation and the optimization of BTES systems. It closes capability gaps of currently available simulators like the consideration of borehole insulation and unrestricted bore path geometries, while still maintaining reasonable computational performance. In benchmarks simulations, BASIMO showed good agreement with other simulators [17, 22]. The code is still under development. Future work will focus on the implementation of the transient convective heat transport calculation in the subsurface and on further performance improvements.

Acknowledgements

References

[1] IEA (International Energy Agency). *Heating Without Global Warming – Market Developments and Policy Considerations for Renewable Heat*. Paris: OECD/IAE; 2014.
[2] AGEB (Arbeitsgemeinschaft Energiebilanzen). *Anwendungsbilanzen für die Endenergiesektoren in Deutschland in 2011 und 2012 mit Zeitreihen von 2008 bis 2012*. Berlin: AGEB; 2013.
[3] Schmidt T, Mangold D, Müller-Steinhagen H. Central solar heating plants with seasonal storage in Germany. *Sol Energy* 2004;76:165-174.
[4] Bauer D, Marx R, Nußbicker-Lux J, Ochs F, Heidemann W, Müller-Steinhagen H. German central solar heating plants with seasonal heat storage. *Sol Energy* 2010;84:312-320.

[5] Dinçer İ, Rosen MA. *Thermal Energy Storage*. Hoboken: John Wiley & Sons, Ltd; 2011.

[6] Pine. P, Cruickshank CA, Beausoleil-Morrison I, Wills A. A review of available methods for seasonal storage of solar thermal energy in residential applications. *Renewable and Sustainable Energy Reviews* 2011;15:3341-3359.

[7] Xu J, Wang R, Li Y. A review of available technologies for seasonal thermal energy storage. *Solar Energy* 2014;103:610-638.

[8] Hesaraki A, Holmberg S, Haghighat F. Seasonal thermal energy storage with heat pumps and low temperatures in building projects – A comparative review. *Renew Sust Energ Rev* 2015;43:1199-1213.

[9] Lundh M, Dalenbäck JO. Swedish solar heated residential area with seasonal storage in rock: Initial evaluation. *Renewable Energy* 2008;33:703-711.

[10] Sibbitt B, McClenahan D, Djebbar R, Thornton J, Wong B, Carriere J, Kokko J. The Performance of a High Solar Fraction Seasonal Storage District Heating System – Five Years of Operation. *Energy Procedia* 2012;30:856-865.

[11] Mielke P, Bauer D, Homuth S, Götz A, Sass I. Thermal effect of a borehole thermal energy store on the subsurface. *Geothermal Energy* 2014;2:1-15.

[12] Reuß M. The use of borehole thermal energy storage (BTES) systems. In: *Advances in Thermal Energy Storage Systems*, Cabeza LF editor. Cambridge: Woodhead Publishing; 2015. p. 117-147.

[13] Haehnlein S, Bayer P, Blum P. International legal status of the use of shallow geothermal energy. *Renewable and Sustainable Energy Reviews* 2010;14:2611-2625.

[14] Griebler C, Kellermann C, Stumpp C, Hegler F, Kuntz D Walker-Hertkorn S. *Auswirkungen thermischer Veränderungen infolge der Nutzung oberflächennaher Geothermie auf die Beschaffenheit des Grundwassers und seiner Lebensgemeinschaften – Empfehlungen für eine umweltverträgliche Nutzung, Texte 54/2015*. Dessau-Roßlau: Umweltbundesamt; 2015.

[15] Bär K, Rühaak W, Welsch B, Schulte D, Homuth S, Sass I. Seasonal High Temperature Heat Storage with Medium Deep Borehole Heat Exchangers. *Energy Procedia* 2015;76:351-360.

[16] Sass I, Welsch B, Schulte D. *Mitteltiefe Erdwärmesondenspeicher – Lösungen für den Nutzungskonflikt Grundwasserschutz versus Geothermienutzung?* At: 7. Bochumer Grundwassertag, Bochum, Germany; 17.03.2016.

[17] Schulte DO, Rühaak W, Oladyshin S, Welsch B, Sass I. Optimization of Medium-Deep Borehole Thermal Energy Storage Systems. *Energy Technology* 2016;4:104-113.

[18] Hellström G, Sanner B. *Software for dimensioning of deep boreholes for heat extraction*. In: Proceedings of the Calorstock'94, Espoo, Finland; 1994.194-200.

[19] Diersch HJG. *FEFLOW Finite Element Modeling of Flow, Mass and Heat Transport on Porous Media*. Berlin, Heidelberg: Springer-Verlag; 2014.

[20] de Paly M, Hecht-Méndez J, Beck M, Blum P, Zell A, Bayer P. Optimization of energy extraction for closed shallow geothermal systems using linear programming. *Geothermics* 2012;43:57-65.

[21] Bayer P, de Paly M, Beck M. Strategic optimization of borehole heat exchanger fields for seasonal geothermal heating and cooling. *Applied Energy* 2014;136:445-453.

[22] Schulte DO, Welsch B, Boockmeyer A, Rühaak W, Bär K, Bauer S, Sass I. Modeling Insulated Borehole Heat Exchangers. *Environmental Earth Sciences* 2016, in press.

[23] The MathWorks. MATLAB 2015b Global Optimization Toolbox. Natick, Massachusetts: The Mathworks, Inc; 2015.

[24] Zienkiewics OC, Taylor RL, Thu JZ. *The Finite Element Method: Its Basis and Fundamentals*. 6th ed. Oxford: Butterworth-Heinemann; 2005.

[25] Alberty J, Carstensen C, Funken SA. Remarks around 50 lines of Matlab: short finite element implementation. *Numerical Algorithms* 1999;20:117-137.

[26] Si H. Constrained Delaunay tetrahedral mesh generation and refinement. *Finite elements in Analysis and Design* 2010;46:33-46.

[27] Reddy JN, Gartling DK. *The Finite Element Method in Heat Transfer and Fluid Dynamics*. 3rd ed. Boca Raton: CDC Press; 2010.

[28] Rühaak W, Bense VF, Sass I. 3D hydro-mechanically coupled groundwater flow modelling of Pleistocene glaciation effects. *Computers & Geosciences* 2014;37:88-99.

[29] Bauer D, Müller-Steinhagen H, Diersch HJG. Thermal resistance and capacity models for borehole heat exchangers. *International Journal of Energy Research* 2011;35:312-320.

[30] Diersch HJG, Bauer D, Heidemann W, Rühaak W, Schätzl P. Finite element modeling of borehole heat exchanger systems: part 1. Fundamentals. *Computers & Geosciences* 2011;37:1122-1135.

[31] Eskilson P, Claesson J. Simulation model for thermally interacting heat extraction boreholes. *Numerical Heat Transfer* 1988;v13:149-165.

[32] Oladyshin S, Nowak W. Polynomial Response Surfaces for Probabilistic Risk Assessment and Risk Control via Robust Design. In: *Novel Approaches and Their Applications in Risk Assessment*, Luo Y editor. Rijeka: InTech; 2012. p. 317-344.

[33] Welsch B, Rühaak W, Schulte DO, Bär K, Sass I. Advanced Coupled Simulation of Borehole Thermal Energy Storage Systems and Above Ground Installations. At: European Geoscience Union General Assembly 2016, Vienna, Austria; 17.-22.04.2016.

Appendix E – Optimization of Medium-Deep Borehole Thermal Energy Storage Systems

Published as:

     FULL PAPER

Optimization of Medium-Deep Borehole Thermal Energy Storage Systems

Daniel Otto Schulte,*[a, b] Wolfram Rühaak,[a, b] Sergey Oladyshkin,[c] Bastian Welsch,[a, b] and Ingo Sass[a, b]

Arrays of medium-deep borehole heat exchangers are characterized by their slow thermal response and large storage capacity. They represent suitable thermal energy storage systems for seasonally fluctuating heat sources such as solar energy or district heating grids. However, the economic feasibility of these systems is compromised by high investment costs, especially by the expensive drilling of the boreholes. This study presents an approach for the simulation and optimization of borehole thermal energy storage systems. To exemplify the concept, a software tool is used to optimize the number and length of borehole heat exchangers with regard to a specific annual heat demand. The tool successfully determines the ideal size of the thermal energy storage. Furthermore, the prediction of the system's performance also indicates that borehole thermal energy storage systems only operate efficiently in large-scale applications. With the presented tool, many aspects of borehole thermal energy storage systems can be simulated and optimized.

Introduction

Approximately 65% of the total end energy consumption in private households accounts for heating in Germany.[1] Consequently, there is a high potential for energy conservation in this sector. Renewable energy sources such as solar collectors are increasingly used to cover this heat demand, to reduce the consumption of fossil fuels, and to mitigate CO_2 emissions. In summer, solar thermal collector panels provide excess heat when the heating demand is low. Yet, during the winter time, a secondary system has to provide the heat, as the situation is reversed. Likewise, the increased use of district heating grids is supposed to play an important role in the future of renewable energies.[2,3] They are often powered by combined heat and power plants (CHPs). Whereas electricity is needed throughout the year, the seasonality of the heat demand renders CHPs inefficient during summer when the heat demand is low. Thus, seasonal storage can enhance the efficiency of CHPs in district heating grids and solar collector systems by shifting excess heat to the winter time.

Early considerations for solar thermal energy systems envisaged water tanks for seasonal heat storage. As the water tank is the most expensive component in the system, it is imperative to exploit the decreasing price per storage volume with increasing size.[4] Whereas such water tanks require considerable space on the surface, borehole thermal energy storage (BTES) systems need only a small amount of space to tap into a large volume of subsurface rock, which can serve as the heat storage. Additionally, geothermal heat feeds such a system. This combination of solar heat usage, seasonal storage, and geothermal heat has already been demonstrated in practice to be highly efficient with shallow BTES systems.[5–8] Furthermore, because of this combination, a secondary heating system to back up the solar collectors is rendered dispensable.

However, shallow aquifers are often used for the extraction of drinking water. In Germany and many other countries, legal regulations often restrict alterations of groundwater that may have a negative impact on drinking water quality.[9] Thus, excessive heating, which can induce microbial growth, has to be prevented in these aquifers.[10,11] Given that solar collectors can provide a temperature output of 100 °C and above[12] and that district heating grids operate at supply temperatures of approximately $\geq 80\,°C$,[13] storage of the excess amount of heat in greater depth is favorable. Ideally, a medium-deep borehole thermal energy storage (MD-BTES) system should reach a couple of hundred meters deep and should be thermally insulated at the topmost part. Shallow borehole heat exchangers (BHEs) are often polymer U pipes or double U pipes, whereas deeper BHEs are usually coaxial pipe systems with a high thermal conductivity outer

[a] D. O. Schulte, Dr. W. Rühaak, B. Welsch, Prof. Dr. I. Sass
Graduate School of Excellence Energy Science and Engineering
Technische Universität Darmstadt
Jovanka-Bontschits-Strasse 2, 64287 Darmstadt (Germany)
E-mail: schulte@geo.tu-darmstadt.de

[b] D. O. Schulte, Dr. W. Rühaak, B. Welsch, Prof. Dr. I. Sass
Geothermal Science and Technology
Technische Universität Darmstadt
Schnittspahnstrasse 9, 64287 Darmstadt (Germany)

[c] Dr. S. Oladyshkin
Institute for Modelling Hydraulic and Environmental Systems (LS3)
University of Stuttgart
Pfaffenwaldring 5A, 70569 Stuttgart (Germany)

steel pipe. The inner pipe is insulated to reduce the thermal interaction between the up- and down-streaming fluids. In summer, the warm fluid is injected into the inner pipe for heat storage, whereas in winter the cold fluid is injected into the annular gap for heat extraction.[14]

Typically, permeability decreases with depth, which prevents removal of heat from the storage by ground water flow. Furthermore, the stored heat will not dissipate as fast as in shallow storage systems owing to a reduced lateral temperature gradient. Consequently, the extraction temperatures will be higher than those for shallow BTES systems, which only permit moderate injection temperatures. This increases the performance of the heat pump and possibly allows for use with conventional radiator heating systems, which require a higher supply temperature.[14]

MD-BTES systems are operated in seasonal charging and discharging cycles. Excess thermal energy is stored in summer. During winter, it is extracted again for heating purposes. The performance is quantified by the heat, which is stored and extracted during each cycle [Eq. (1)] (Figure 1).
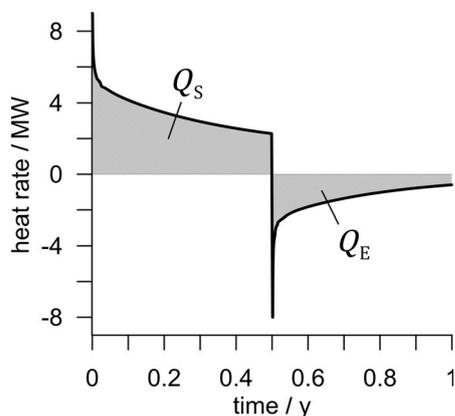
Figure 1. Evolution of heat storage and extraction; Q_S: stored heat, Q_E: extracted heat.

$$Q_{S/E} = \int_t \Delta T \cdot \rho_f \cdot c_f \cdot \dot{V} \, dt \qquad (1)$$

in which $Q_{S/E}$ is the stored/extracted heat, ΔT is the temperature difference between the inlet and outlet, ρ_f is the working fluid density, c_f is the specific heat capacity of the working fluid, $\dot{V}$ is the working fluid flow rate, and t is the time of operation.

The ratio of extracted heat to stored heat defines the storage coefficient S [Eq. (2)], whereas the specific heat extraction rate Q_{spec} describes the system's efficiency of heat exchange between BHEs and the subsurface [Eq. (3)]:

$$S = \left| \frac{Q_E}{Q_S} \right| \qquad (2)$$

$$Q_{spec} = \frac{Q_E}{l_{tot} \cdot t_E} \qquad (3)$$

in which Q_{spec} is the specific heat extraction rate, l_{tot} is the total drilled length, and t_E is the time of operation in the heat extraction mode.

In general, the difference between the inlet and outlet temperatures of the working fluid in the BHEs decreases over the charging or discharging cycle because of continuous heat exchange with the reservoir (Figure 2). Owing to diffu-
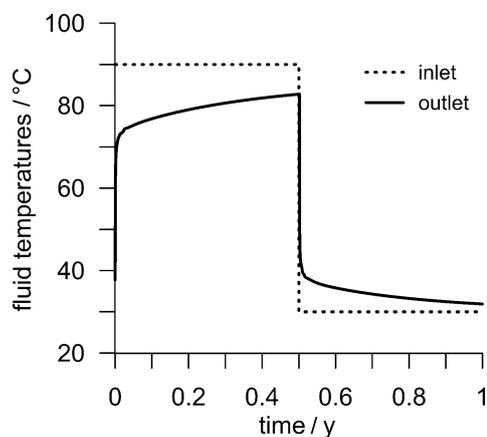
Figure 2. Evolution of the BHE inlet and outlet temperatures.

sion processes, not all of the stored heat can be recovered. Some of the thermal energy remains in the reservoir and begins to create a thermal plume in the subsurface. This thermal plume decreases the lateral temperature gradient between the BHEs and the surrounding rock, which results in declining heat storage over summer, but enhanced heat extraction in winter and increased storage efficiency (Figure 3).

Drilling is the critical cost factor in the development of a geothermal reservoir. Deeper boreholes significantly raise the costs for a high-temperature underground storage system. It is necessary to simulate the performance of a planned system prior to the investment of building a storage platform. The design of the borehole heat exchanger array has
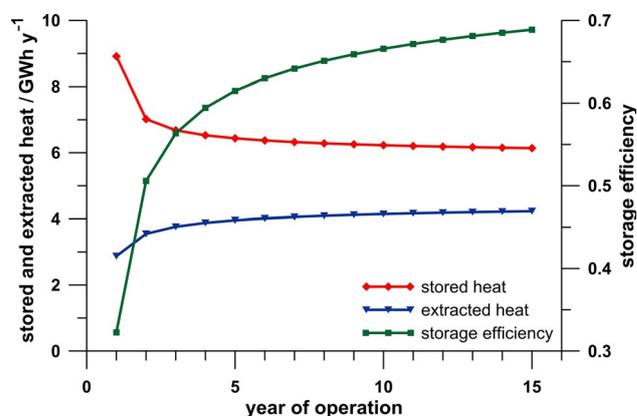
Figure 3. Evolution of storage performance; model: 19 BHEs, BHE length: 500 m, BHE spacing: 5 m, flow rate: 4 L s⁻¹, inlet temperature during storage: 90 °C, inlet temperature during extraction: 30 °C.

to be optimized for the heating purpose to avoid an over-sized and, therefore, overpriced system. Earlier optimization approaches used analytical 2D finite line source models.[15,16] We present a MATLAB-based toolbox, which can numerically simulate and optimize the 3D design of an MD-BTES system. Instead of using finite line source models, the thermal interactions of the BHEs are considered by a more detailed solution.

In the proxy model-based optimization section, the basic methods that are used in the optimization process are explained. Afterwards, the optimization of the performance of the MD-BTES system is demonstrated by an arbitrary example. Finally, we discuss the results with respect to real-case applications.

Proxy Model Based Optimization

To optimize the design of an MD-BTES system, many configurations representative for the range of variability of the design parameters have to be evaluated. The seasonal operation is numerically simulated for each configuration to predict the thermal behavior of the MD-BTES system. Given that the performance of an MD-BTES system changes significantly over the first couple of cycles, several years of operation have to be simulated. As a result, the computational time for a simulation is too long to allow the direct use of the numerical model in an optimization algorithm. To bypass this problem, a surrogate proxy model is trained by numerical simulations. The proxy model can be evaluated in a matter of seconds by the optimization algorithm. However, as the proxy model is not exact, the following iterative procedure is performed to assure robustness of the optimization: The best solution for the proxy model is verified by an additional numerical simulation with the parameters found by the optimization algorithm. In case the verification differs too much from the proxy model prediction, the numerical simulation can serve as an additional training simulation to refine the proxy model for a new optimization. This process is repeated until the mismatch of the optimal solution between proxy model and numerical model is sufficiently small (Scheme 1).

Physical model formulation

Simulation of the operation of an MD-BTES system comprises simulation of subsurface heat transport and thermal interaction of the BHEs with the surrounding rock. The transient subsurface heat diffusion is calculated by solving Fourier's law of heat conduction for the model domain [Eq. (4)]:

$$\rho_s c_s \frac{\partial T}{\partial t} = \nabla \cdot \lambda \nabla T + q \tag{4}$$

in which ρ_s is the soil density, c_s is the volumetric heat capacity of soil, T is the temperature, t is the time, λ is the thermal conductivity, and q is the heat sources and sinks. Given that low-permeable rock bodies with negligible ground water
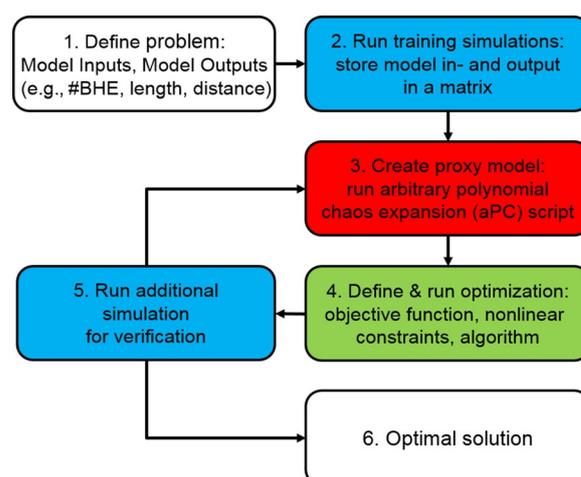
Scheme 1. General process of optimizing the design of an MD-BTES system.

flow are targeted for MD-BTES systems, convective heat transfer is disregarded. Also, temperature dependency of the material parameters is not taken into account. The standard Galerkin method[17] is applied in an adapted MATLAB[18] implementation for finite elements[19] on an unstructured tetrahedron mesh.[20] A predictor–corrector method is used with a second-order Adams–Bashforth predictor and a Crank–Nicolson corrector for automated time stepping.[21]

The thermal interaction of the BHEs is calculated by a 1D analytical thermal-resistance and capacity model.[22–24] Fed with inlet temperature and flow rate data, it provides the temperature distribution in the inlet and outlet pipes in predefined depth levels. The solution takes into account all thermal and hydraulic parameters of the BHE materials and the borehole wall temperature. In the finite element mesh, the BHEs are discretized as vertical lines of mesh nodes. The temperature at these nodes defines the borehole wall temperature and is passed to the analytical solution. In return, the analytical solution sets heat sources on the basis of the thermal resistances within the BHEs and the difference between the borehole wall temperature and the calculated BHE fluid temperature at the corresponding nodes. This results in a contribution to the right-hand side term of the respective equations.[25] As the heat source terms depend on the temperature, which is the solution vector, the system of equations is nonlinear [Eq. (5)]:

$$M\dot{T} + KT = F(T) \tag{5}$$

in which M is the heat capacity matrix, K is the thermal conductivity matrix, F is the right-hand side vector including source terms, and T is the solution vector for temperature. A Picard iteration scheme is applied on the corrector to solve the system of nonlinear equations, whereas the predictor provides a tentative solution to start the iteration loop.[26]

Prior to the study, the code was tested and showed good agreement with FEFLOW[25] in a benchmark simulation. For the benchmark, the BHE outlet temperatures in the
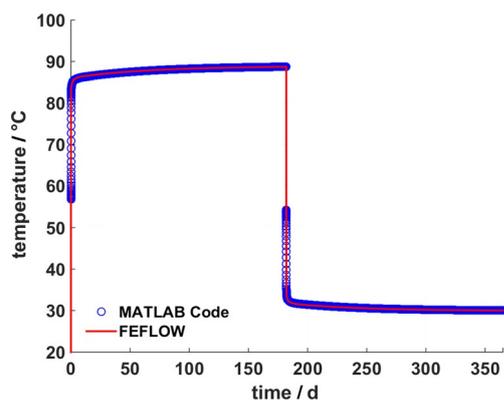
Figure 4. Comparison of BHE outlet temperatures of the central pipe of a BHE array in the MATLAB implementation and in FEFLOW; model: 7 BHEs of 100 length, 182 days of heat storage (90 °C inlet temperature) and 183 days of heat extraction (30 °C inlet temperature) at 2.5 L s^{-1} injection rate.

MATLAB implementation and in FEFLOW were compared against each other (Figure 4).

Proxy model by arbitrary polynomial chaos expansion

The physical model described in the previous section is used to construct a proxy model on the basis of the theory of polynomial chaos expansion (PCE). The basic idea of PCE was introduced by Wiener[27] and consists in the construction of the proxy model (response surface) of the original model with the help of an orthonormal polynomial basis in the parameter space. Simply, the dependency of the model output on all relevant input parameters is approximated by projection onto a high-dimensional polynomial. The key attractive features of all PCE techniques are the high-order approximation of the model combined with its computational speed.

Formally, we will consider the vector of N input parameters $\omega = \{\omega_1, \ldots, \omega_N\}$ for the physical model that is simply denoted as $\Omega = f(\omega)$. Our goal is to capture the influence of all parameters ω on the model output Ω. According to PCE theory, the model output Ω can be approximated by polynomials $\Psi_i(\omega)$ [Eq. (6)]:

$$\Omega(\omega) \approx \sum_{i=1}^{M} c_i(\omega) \Psi_i(\omega) \qquad (6)$$

The number M of polynomials $\Psi_i(\omega)$ and the corresponding coefficients c_i depend on the total number of analyzed input parameters N and on the order d of the polynomial representation [Eq. (7)]:

$$M = \frac{(N+d)!}{(N! \cdot d!)} - 1 \qquad (7)$$

The coefficients $c_i(\omega)$ quantify the dependency of the model output Ω on the input parameters ω for each desired point in the parameter space, which results in a surrogate for model Ω.

In the current paper, we will apply a recent generalization of the PCE technique known as the arbitrary polynomial chaos (aPC).[28] In aPC, the multidimensional orthonormal polynomial basis can be constructed for arbitrary probability distribution shapes of input parameters and, in addition, can even work with unknown distribution shapes if only a few statistical moments can be inferred from limited data or from expert elicitation. To project the MD-BTES model response onto an orthogonal polynomial basis, a uniform distribution is assumed for the modeling variables, which is simply dictated by equal interest to all possible outcomes of the physical model. The orthogonal polynomial basis of order d can be constructed according to Equation (4) in Oladyshkin and Nowak.[28]

To determine the unknown coefficients $c_i(\omega)$ of the proxy model, the original model is run at least once, but preferably more often, for every input parameter by using so-called training simulations with various sets of the input parameters (see details in the next section). Such training simulations are used to create an initial prediction for the following optimization procedure. However, to assure robustness of the overall modeling procedure, the quality of the proxy model is iteratively improved by incorporating additional simulations indicated by the optimization algorithm: specifically, the performance of the ideal design found by the optimization algorithm is validated by an additional numerical simulation. The approximation error of the proxy model must not be bigger than 1%. If the verification simulation results in a violation of this criterion, it is used as an additional training simulation for refinement of the proxy model. Thus, a new projection of the model onto the orthonormal basis is performed by using all cumulatively available training simulation within the least-squares collocation method.[29,30] The optimization is then repeated by using the refined proxy model for the constraint function. From a practical point of view, the computational costs of our framework are dominated by the model calls required for constructing the surrogate model.

Mathematical optimization

Drilling is the cost-critical factor and needs to be optimized. Thus, the fitness function y for this study is the total drilled borehole length, which is simply the product of the number of BHEs and their length [Eq. (8)]. Additionally, the borehole length is penalized against the number of BHEs, because drilling costs rise exponentially with depth:[31]

$$y = x_1 \cdot x_2 \cdot e^{(a \cdot x_2)} \qquad (8)$$

in which x_1 is the number of BHEs, x_2 is the BHE length, and a is a scaling factor. The optimization algorithm tries to minimize the value for y by altering the number of BHEs and their length. Each parameter combination represents a certain design for an MD-BTES system, the performance of which has to meet a specific requirement. In the presented

study, it has to cover a building's heat demand after a certain amount of operation time. This represents a constraint to the optimization algorithm: the MD-BTES system cannot be indefinitely small, as this would lead to a vanishingly low performance.

The design parameters for MD-BTES systems can include discrete variables such as the number of BHEs or industrial standard sizes for pipes. Consequently, the optimization algorithm has to be able to handle discrete features. Genetic algorithms[32] can solve mixed integer optimization problems, that is, the variable parameters are real or integer values. Hence, the optimal design for an MD-BTES system is determined with a genetic algorithm, which is included in the MATLAB Global Optimization Toolbox.[33] The integer variables can relate to discrete ordinate values or even categories. Each combination of variables constitutes an individual, whereas a set of individuals represents a population. For every iteration, called generation in genetic algorithm terminology, the individuals of a population are tested by their fitness function score. The algorithm tries to minimize the score partly by combining variable values of individuals with a low score and partly by choosing random values for the individuals of the next population, which are tested in the following generation. A defined number of best individuals, called elite, make it to the next generation unaltered, regardless of the algorithm's choices.

As mentioned before, predicting the performance of an MD-BTES system requires a numerical simulation. The genetic algorithm has to evaluate hundreds of parameter combinations to converge on an optimal solution. It only stops if the best individual's score cannot be improved more than a predefined fitness function tolerance after a predefined number of so-called stall iterations. Given that the performance of each tested configuration has to be checked against the constraint, this results in an enormous computational effort: depending on the model size a single numerical simulation can take a few days up to several weeks. To overcome this problem, we use a proxy model generated from significantly fewer numerical training simulations by arbitrary polynomial chaos expansion,[34] as mentioned in the previous section. Whereas the computational effort for larger models is still high, they have to be rendered only once. The resulting proxy model calculates the performance of the MD-BTES system in a matter of seconds, as only a polynomial function has to be evaluated instead of a numerical model.

Specifically tailored optimization of the simulation model can converge on an optimal solution with less model evaluations without the help of a proxy model. However, the performance of an MD-BTES system depends on many more parameters than the number of BHEs and their length (e.g., thermal properties of rock and BHE materials, radial distance of BHEs, operational parameters such as flow rate, etc.). A pre-existing proxy model can be easily expanded by additional training simulations to incorporate more model parameters. Furthermore, it is possible to formulate more than one optimization objective on the basis of the additional variable parameters. In general, this can be included in the fitness function as well as in the constraints to add to the detail of the model. The genetic algorithm in MATLAB's Global Optimization Toolbox is capable of multiobjective optimization. Whereas renewed optimization under altered considerations requires laborious changes to a specifically tailored solution and profound mathematical knowledge, the rather generic approach of using a genetic algorithm on a proxy model is a ready-to-use tool that allows quick re-evaluations of the optimization problem. Therein lies the main potential of this approach.

Training Model Setup

For the proxy training simulations, the varying MD-BTES configurations are applied to a standard model, which includes constant parameters for the subsurface (Table 1) as well as for the BHE materials (Table 2).

The finite element mesh is 100 m by 100 m wide with the BHE array in its center, whereas the depth of the model is variable and always 50 m more than the BHE length for the considered scenario. An initial temperature field is set, which corresponds to a geothermal gradient of 3 K per 100 m. Dirichlet boundary conditions are defined accordingly: 10 °C as an average annual near-surface temperature at the top,

Table 1. Geological model parameters.

Parameter	Value
thermal conductivity	2.6 W m^{-1} K^{-1}
density	2600 kg m^{-3}
specific heat capacity	800 J kg^{-1} K^{-1}
surface temperature boundary condition	10 °C
geothermal gradient	0.03 K m^{-1}

Table 2. BHE material and operational parameters.

Parameter	Value
radial distance between BHE	5 m
borehole diameter	0.1522 m
outer pipe, outer diameter	0.127 m
outer pipe, wall thickness	0.0056 m
outer pipe, thermal conductivity (steel)	54 W m^{-1} K^{-1}
inner pipe, outer diameter	0.075 m
inner pipe, wall thickness	0.0068 m
inner pipe, thermal conductivity (PE)	0.4 W m^{-1} K^{-1}
grout, thermal conductivity	2 W m^{-1} K^{-1}
working fluid dynamic viscosity (water)	0.000504 kg m^{-1} s^{-1}
working fluid density (water)	977 kg m^{-3}
working fluid specific heat capacity (water)	4145 J kg^{-1} K^{-1}
working fluid thermal conductivity (water)	0.65 W m^{-1} K^{-1}
flow rate	2.5 L s^{-1}
heat storage period	182 days
injection temperature during heat storage	90 °C
heat extraction period	183 days
injection temperature during heat extraction	30 °C
simulated time of operation	7 years

whereas the boundary condition at the bottom depends on the depth of the model for each respective scenario.

Predefined geometric relations determine the layout of the MD-BTES system for the different number of BHEs (Figure 5). The axial reference distance between the BHEs is set to 5 m. Preliminary simulations have shown that the ideal axial distance depends on the thermal properties of the subsurface and the BHE materials rather than the number or length of BHEs.
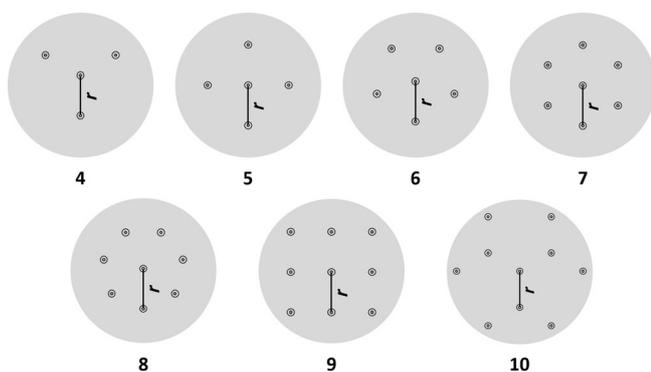
Figure 5. Templates for BHE array layouts, r: axial reference distance.

As a result, only the number and length of the BHEs are variable, and the performance of the MD-BTES system is evaluated on the basis of their variation. For each configuration, the same basic operational scenario is simulated. The MD-BTES system is charged and discharged at constant inlet temperatures and at a constant flow rate (Table 2), whereas the change of flow direction in the coaxial pipe for winter and summer time is accounted for.

To minimize the time for which a redundant heating system is required, an MD-BTES system has to meet the heat demand soon after its construction, which is typically long before the break-even point is reached. Whereas longer simulations would be beneficial for the economical assessment of the long-term operation, they are not necessary for finding the ideal design of an MD-BTES system, which can cover a specified heat demand after a few years. Hence, the basic operational scenario is only simulated for seven years to reduce the computational effort. The long-term operation can be simulated once the ideal design has been determined.

For the numerical simulation of the subsurface heat transport, the initial time step size is set to 1 s and is limited to a maximum of 4 h. It cannot grow by more than 20% per time step. The error tolerances for the time step control and Picard iterations are set to 0.001 and 0.005, respectively. If the Picard scheme fails to converge below the tolerance level within five iterations, the time step size is reduced by 20% and the time step is repeated.

The parameter space is sampled by a full factorial design[35] of experiments with nine levels for the BHE length and seven levels for the number of BHEs (Table 3). The resulting 63 numerical simulations each provide values for stored and extracted heat, storage coefficient, and specific

Table 3. Sampled parameter variations for proxy training.

BHE length [m]	100	133	166	200	233	300	366	433	500
Number of BHEs	4		5	6	7		8	9	10

heat extraction rate for all 7 heat charging/discharging cycles. Including the years of operation as an additional variable parameter, a total of 441 sample points serve as input to the aPC. The polynomial order for the proxy model is chosen in such a way that it is in good agreement with the training data without overfitting them (see the results).

The resulting aPC proxy model is a function of the number of BHEs, their length, and the year of operation and is used to constrain the fitness function as previously mentioned. It returns the value for extracted heat in MWh in the specified extraction cycle. Individuals must yield an aPC function value that satisfies a predefined constraint function to qualify as a possible solution. For the optimization, only the performance after the seventh year of operation is considered. Thus, the operational time is kept constant in the optimization and is only used afterwards with the proxy model to display the temporal evolution of the optimal performance of the MD-BTES system.

Comparably to Tester et al.,[31] the BHE length is penalized in the fitness function exponentially with a scaling factor $a = 7.51 \times 10^{-4}$. In a real case, the scaling factor should be deducted empirically from typical drilling cost data for the local geology.

For this study, two optimization scenarios are considered. In both cases, the constraint for the fitness function is set to 500 MWh minimum heat extraction. This resembles roughly the annual heat demand of a midsized energetically modernized office building. The second scenario includes, in addition, a constraint of 200 m on the minimum BHE depth to take into account a legal requirement (in this case fictional). In both cases, the objective of the genetic algorithm is to determine the smallest possible MD-BTES system that still provides enough heat to cover the annual demand. Preliminary simulations have shown that the increase in the system efficiency slows down after a few years (see Figure 3) Therefore, the requirement has to be met only after seven years of operation to rule out systems that turn out to be oversized later on. All settings for the genetic algorithm are summarized in Table 4.

Optimization of the Performance of the MD-BTES System

All 63 training simulations reflect the typical behavior of BTES systems: the storage efficiency increases over time (Figure 6) and bigger storage systems perform better than smaller ones. After seven years of operation, the storage coefficient ranges from approximately 22 to 50% (Figure 7), and the recovered heat during extraction ranges from approximately 90 to 1800 MWh depending on the storage size

Table 4. Settings for the genetic algorithm.

Parameter	Value
number of independent variables	3
integer variables	1, 3
lower bound, number of BHEs	4
upper bound, number of BHEs	10
lower bound, BHE length	100 m
upper bound, BHE length	500 m
lower bound, operational time	7 years
upper bound, operational time	7 years
fitness function	$y = x_1 \cdot x_2 \cdot e^{(a \cdot x_2)}$
scaling factor a	7.51×10^{-4}
population size	200
generations	500
number of elite individuals	3
stall generation limit	20
fitness function tolerance	1×10^{-6}
constraint C_1	500 MWh
constraint C_2	200 m
constraint function for scenario 1 and 2	$0 \geq -aPC\mathrm{proxy}(x_1, x_2)^{[a]} + C_1$
constraint function for scenario 2 only	$0 \geq -x_2 + C_2$
error tolerance (numerical to proxy model)	1%
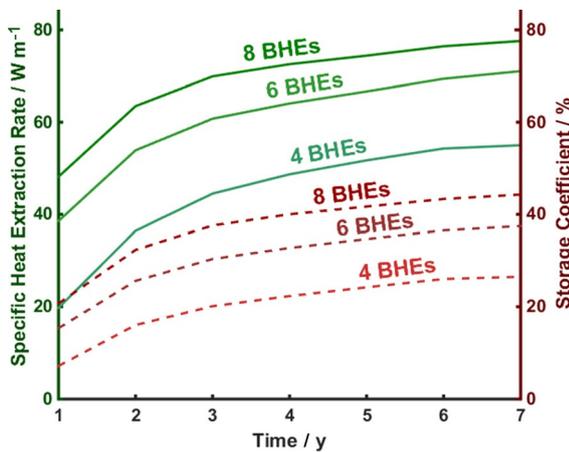
Figure 6. Temporal evolution of the performance of a 250 m deep MD-BTES system with 4, 6, and 8 BHEs.

(Figure 8). The specific heat extraction rate reaches values of up to 86 W m^{-1} (Figure 9).

Whereas the MATLAB implementation does not allow for parallel processing, several simulations can be run simultaneously in multiple MATLAB instances depending on the available CPU nodes. The computation time for each simulation ranges from 50 h (smallest model, 4 BHEs of 100 m length) to 95.3 days (biggest model, 10 BHEs of 500 m length), which corresponds to 0.17 and 7.89 % of the total computation time of 1208.5 days, respectively. A complete list of all simulation results and the computational time is included in the Supporting Information.

The proxy model allows for fast evaluation in between the sampled training simulations. The quality of the proxy model is quantified by a mean relative approximation error (MRAE), which is the sum of relative approximation errors normalized by the sample size for each model output at the training sample points [Eq. (9)]:

Figure 7. Response surface of the storage coefficient after seven years of operation as a function of the number of BHEs and BHE length.
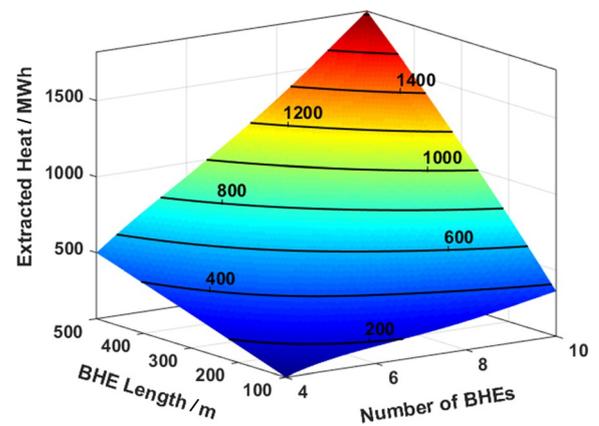
Figure 8. Response surface of extracted heat in the seventh year of operation as a function of the number of BHEs and BHE length.
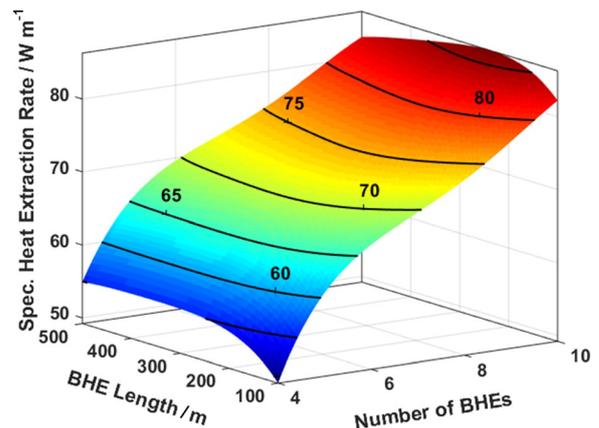
Figure 9. Response surface of specific heat extraction rate after seven years of operation as a function of the number of BHEs and BHE length.

$$\mathrm{MRAE}_i = \left| \frac{\sum_{j=1}^{n} {}^{y_{i,j,\mathrm{numerical}} - y_{i,j,\mathrm{proxy}}} / {y_{i,j,\mathrm{numerical}}}}{n} \right| \qquad (9)$$

in which y_i is the model output, j is the training simulation index, and n is the number of training simulations. By simple testing the polynomial degree can be set as high as fourth order. All MRAE values are summarized in Table 5. A

Table 5. Approximation errors of the fourth polynomial order proxy model.

Model output	MRAE [%]
specific heat extraction rate	0.0028
storage coefficient	0.0132
stored heat per cycle	0.0279
extracted heat per cycle	0.0868

higher polynomial degree could achieve better MRAE values but would also lead to overfitting owing to the well-known polynomial properties. However, a moderate order of the proxy model such as four is sufficient to capture the model's nonlinearity and also to assure acceptable accuracy with MRAEs below 0.1 %.

In the first optimization scenario, the genetic algorithm fails to improve the solution any further without violating the constraint function after 55 generations and 11 000 evaluations of the fitness function. The second scenario converges on an optimum after 46 generations and 9200 function evaluations. These are approximate numbers as the irreproducible selection of individuals for a new generation involves random processes. Finding the ideal solution, however, is reproducible. For an annual heat demand of 500 MWh extracted in the described operation, the ideal BHE arrays have to have 10 BHEs of 134 m length (total drilled length: 1340 m) for scenario one and 7 BHEs of 220 m length (total drilled length: 1540 m) for scenario two. The MD-BTES system would operate at 43.6 and 40.7 % storage efficiency with a specific heat extraction rate of 84.4 and 74.2 W m^{-1}, respectively, in the seventh year of operation. Any configuration with fewer, but deeper, BHEs also located on the intersection of the model response surface of extracted heat and the 500 MWh plane would provide the required heat as well (Figure 10). However, those solutions have been ruled out by the genetic algorithm, as the increased length is exponentially penalized relative to the number of BHEs in the fitness function.

The ideal MD-BTES designs found by the genetic algorithm are each verified by an additional numerical simulation and are compared against the proxy model prediction with respect to the relative approximation error (RAE) (Table 6). In the second scenario, the RAE does not violate the previously defined tolerance criterion of 1 %. Hence, no further iteration is required and an MD-BTES system with 7 BHEs of 220 m length can be regarded as the solution to the optimization problem of scenario two. However, the verification of the first scenario fails: the numerical simulation of an MD-BTES system with 10 BHEs of 134 m length returns 494 MWh extracted heat in the last cycle, which results in a RAE of 1.2 % and a violation of the 1 % criterion. Consequently, the proxy model is refined with the numerical verifi-
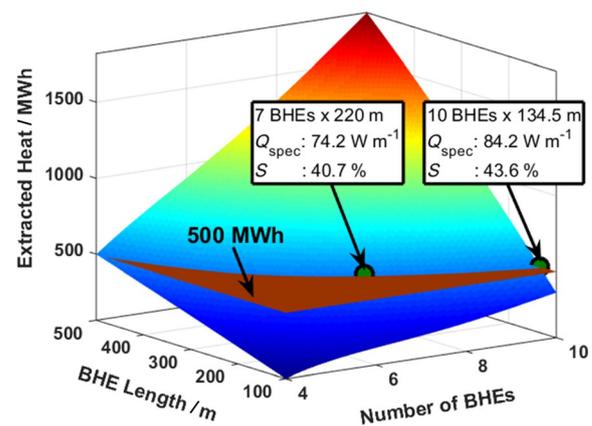
Figure 10. Response surface of extracted heat in the seventh cycle showing the two optimal solutions found by the genetic algorithm.

Table 6. Verification of the optimal solutions on the unrefined proxy model.

Model output	Specific heat extraction rate [W m^{-1}]	Storage coefficient [%]	Heat per cycle [MWh] stored	extracted
Scenario 1				
numerical	83.9	43.5	1136.8	494
proxy	84.3	43.5	1129.9	500
RAE	<1%	<1%	<1%	>1%
Scenario 2				
numerical	74.5	40.7	1238.1	503
proxy	74.2	40.7	1229.6	500
RAE	<1%	<1%	<1%	<1%

cation simulation. Renewed optimization of scenario one with the refined proxy model yields an optimal MD-BTES design of 10 BHEs with 134.5 m. An additional numerical verification shows that the RAE criterion is now satisfied (Table 7).

Discussion

Optimization using a proxy model

The low MRAE values indicate good quality of the proxy model's predictions of the storage performance for low computational costs. This is especially true for the center region of the parameter space. However, as a result of the lack of training points beyond the parameter space boundaries, the proxy model predictions become less accurate at the edges of the response surfaces and even more so in the corners. A corner is a point in multidimensional parameter space at which every variable has its lower or upper boundary value. Therefore, it is important to choose the parameter space for the training simulations in such a way that the optimal solution can be expected to be nowhere close to a corner.

In the first scenario, the optimal solution converges inevitably on the proxy model boundary of two variables. On the one hand, the performance of the MD-BTES system is evalu-

Table 7. Verification of the optimal solutions on the refined proxy model.

Model Output	Specific heat extraction rate [W m^{-1}]	Storage coefficient [%]	Heat per cycle [MWh] stored	extracted
numerical	84.3	43.5	1143.6	498
proxy	84.2	43.6	1134.4	500
RAE	<1%	<1%	<1%	<1%

ated for the seventh year of operation, which is the upper boundary for the simulation time. On the other hand, because it is unconstrained, it converges at the top boundary for the number of BHEs owing to the fitness penalty on the BHE length. Still, the MRAE compared to verification simulation barely violates the 1% tolerance criterion by 0.2 percentage points and only one refinement iteration of the proxy model is required. However, if more variables are considered, it is advisable to use a more sophisticated experimental design to handle the exponential increase in training simulations. Typically, experimental designs such as the Latin hypercube[35] or Box–Behnken[36] design sample the parameter space much more efficiently but provide proxy models that are less accurate at their boundaries. Therefore, for more complex cases we recommend using wider boundaries for the training simulations than required for the optimization. In this way, the algorithm can converge on an optimization variable's boundary without reaching the edge of the proxy model parameter space.

Implications of the optimal solution for the design of MD-BTES systems

The solutions for both scenarios indicate that storage efficiency increases more quickly with the number of BHEs than with their depth: The proxy model returns a heat supply of nearly 300 MWh for a hypothetical MD-BTES system with 7 BHEs and 134.5 m length. To raise this value to the required 500 MWh, the total drilled borehole length has to be increased by approximately 600 m for the 7 BHEs of 220 m array (i.e., deeper boreholes), but only by approximately 400 m for the 10 BHEs of 134.5 m array (i.e., additional boreholes). However, with only 134.5 m depth the solution of scenario one barely qualifies as a medium-deep BTES system. As a consequence, a possibly decreased efficiency of the MD-BTES system with fewer, but deeper, BHEs has to be accepted to meet legal requirements of minimum depth.

Furthermore, both scenarios are characterized by over 50% storage losses. Although the storage performance would further increase over time, this improvement already slows down significantly after a few years of operation (see Figures 3 and 6). A larger MD-BTES system would operate at higher efficiencies but would also store and extract more heat in each cycle. Hence, a heat demand of 500 MWh can be considered too low for the proposed operational scenario. MD-BTES systems are rather suited for large-scale applications with a heat demand of several GWh. On the basis of

previous estimates,[37] MD-BTES systems are then expected to achieve over 80% storage efficiency.

Extension of the optimal MD-BTES system design to real field

Whereas the genetic algorithm easily determines the ideal design of an MD-BTES system, the actual solution to the optimization problem depends on several assumptive boundary conditions and simplifications. In particular, the operational scenario of continuous storage charging and discharging cycles is unrealistic. In a real case, it should be based on annual heat demand and supply curves with high temporal resolution. Such curves can be provided by comprehensive building model simulations that take into account the interaction of infrastructural installations and weather conditions. This would greatly influence the long-term behavior of MD-BTES systems and possibly lead to a different result even if the total annual heat demand is the same. However, every application requires its own building model, and building models are not the scope of this study. For the sake of simplicity, the presented operational scenario is sufficiently suitable to demonstrate the concept of MD-BTES design optimization.

Another crucial factor is the choice of the parameter space. Many parameters that influence the performance of an MD-BTES system, including thermal conductivities and heat capacities of the BHE materials and the reservoir rock, are kept constant and are not considered as variables. In a real case study, some of the modeling parameters such as subsurface thermal conductivity could also be subject to uncertainty. The aPC method is specially designed to account for uncertain parameters.[34] Hence, the presented procedure could be extended to optimization under geological uncertainty.

Conclusions

We showed in an arbitrary example that the presented software tool can predict the performance of a medium-deep borehole thermal energy storage system and optimize its design efficiently. Careful definition of the problem and selection of the variable parameters and their boundaries is imperative to obtain significant results. The application of a proxy model generated by arbitrary polynomial chaos expansion greatly accelerates the optimization algorithm. The possibility to rerun optimizations considering different boundary conditions with little additional computational cost gives this approach an advantage over simulation codes tailored for a specific optimization problem. Our generic and modular approach allows for easy adaptation to other optimization problems with different objectives.

Acknowledgements

[1] Bundesministerium für Wirtschaft und Energie (Arbeitsgemeinschaft Energiebilanzen e.V.), *Anwendungsbilanzen für die Endenergiesektoren in Deutschland in den Jahren 2011 und 2012 mit Zeitreihen von 2008 bis 2012*, http://www.ag-energiebilanzen.de/, Berlin, **2013**.

[2] H. Lund, B. Möller, B. V. Mathiesen, A. Dyrelund, *Energy* **2010**, *35*, 1381–1390.

[3] I. Sass, R. Bracke, W. Rühaak, *Proceedings World Geothermal Congress*, **2015**, 35014.

[4] D. Lindenberger, T. Bruckner, H. M. Groscurth, R. Kümmel, *Energy* **2000**, *25*, 591–608.

[5] D. Bauer, W. Heidemann, R. Marx, J. Nußbicker-Lux, F. Ochs, V. Panthalookaran, S. Raab, *Forschungsbericht zum BMU-Vorhaben 0329607J (Juni 2005 bis Juli 2008)*, http://www.itw.uni-stuttgart.de/dokumente/Publikationen/publikationen_09-01.pdf, University of Stuttgart, Stuttgart, **2008**.

[6] D. Bauer, R. Marx, J. Nußbicker-Lux, F. Ochs, W. Heidemann, H. Müller-Steinhagen, *Solar Energy* **2010**, *84*, 612–623.

[7] P. Mielke, D. Bauer, S. Homuth, A. Götz, I. Sass, *Geotherm. Energy* **2014**, *2*, 1–15.

[8] B. Sibbitt, D. McClenahan, R. Djebbar, J. Thornton, B. Wong, J. Carriere, J. Kokko, *Energy Procedia* **2012**, *30*, 856–865.

[9] S. Haehnlein, P. Bayer, P. Blum, *Renewable Sustainable Energy Rev.* **2010**, *14*, 2611–2625.

[10] C. Griebler, C. Kellermann, C. Stumpp, F. Hegler, D. Kuntz, S. Walker-Hertkorn, in *54/2015* (Ed.: Umweltbundesamt), http://www.umweltbundesamt.de/sites/default/files/medien/378/publikationen/texte_54_2015_auswirkungen_thermischer_veraenderungen_infolge_der_nutzung_obenflaechennaher_geothermie_0.pdf, **2015**, p. 159.

[11] Guideline 4640/2 of the Society of German Engineers (VDI), https://www.vdi.de/richtlinie/vdi_4640_blatt_2-thermische_nutzung_des_untergrundes_erdgekoppelte_waermepumpenanlagen/, **2001**.

[12] S. A. Kalogirou, *Prog. Energy Combust. Sci.* **2004**, *30*, 231–295.

[13] H. Gadd, S. Werner, *Appl. Energy* **2014**, *136*, 59–67.

[14] K. Bär, W. Rühaak, B. Welsch, D. Schulte, S. Homuth, I. Sass, *Energy Procedia* **2015**, *76*, 351–360.

[15] P. Bayer, M. de Paly, M. Beck, *Appl. Energy* **2014**, *136*, 445–453.

[16] M. de Paly, J. Hecht-Méndez, M. Beck, P. Blum, A. Zell, P. Bayer, *Geothermics* **2012**, *43*, 57–65.

[17] O. C. Zienkiewicz, R. L. Taylor, J. Z. Zhu, *The Finite Element Method: Its Basis and Fundamentals*, 7th ed., Butterworth-Heinemann, Oxford, **2013**.

[18] MATLAB 2014b, The MathWorks, Inc., Natick, MA, **2014**.

[19] J. Alberty, C. Carstensen, S. Funken, *Numer. Algorithms* **1999**, *20*, 117–137.

[20] H. Si, *Finite Elem. Anal. Design* **2010**, *46*, 33–46.

[21] P. M. Gresho, D. F. Griffiths, D. J. Silvester, *SIAM J. Sci. Comput.* **2008**, *30*, 2018–2054.

[22] D. Bauer, W. Heidemann, H. Müller-Steinhagen, H. J. G. Diersch, *Int. J. Energy Res.* **2011**, *35*, 312–320.

[23] H. J. G. Diersch, D. Bauer, W. Heidemann, W. Rühaak, P. Schätzl, *Comput. Geosci.* **2011**, *37*, 1122–1135.

[24] P. Eskilson, J. Claesson, *Numer. Heat Trans.* **1988**, *13*, 149–165.

[25] H. J. G. Diersch, *FEFLOW: Finite Element Modeling of Flow, Mass and Heat Transport on Porous and Fractured Media*, Springer, Berlin, **2014**.

[26] J. N. Reddy, D. K. Gartling, *The Finite Element Method in Heat Transfer and Fluid Dynamics*, 3rd ed., CRC Press, Boca Raton, FL, **2010**.

[27] N. Wiener, *Am. J. Math.* **1938**, *60*, 897–936.

[28] S. Oladyshkin, W. Nowak, *Reliab. Eng. Sys. Saf.* **2012**, *106*, 179–190.

[29] J.-S. Chen, L. Wang, H.-Y. Hu, S.-W. Chi, *Int. J. Numer. Methods Eng.* **2009**, *80*, 163–190.

[30] H. Moritz, *Rev. Geophysics* **1978**, *16*, 421–430.

[31] J. W. Tester, E. M. Drake, M. J. Driscoll, M. W. Golay, W. A. Peters, *Sustainable Energy: Choosing Among Options*, MIT Press, Cambridge, MA, **2005**.

[32] D. E. Goldberg, *Genetic Algorithms in Search, Optimization, and Machine Learning*, Addison-Wesley, Reading, MA, **1989**.

[33] MATLAB 2014b and Global Optimization Toolbox, The MathWorks, Inc., Natick, Ma, **2014**.

[34] S. Oladyshkin, W. Nowak in *Novel Approaches and Their Application in Risk Assessment* (Ed.: Y. Luo), InTech, Rijeka, **2012**.

[35] K. Siebertz, D. van Bebber, T. Hochkirchen, *Statistische Versuchsplanung—Design of Experiments (DoE)*, Springer, Berlin, **2010**.

[36] G. E. P. Box, D. W. Behnken, *Technometrics* **1960**, *2*, 455–475.

[37] B. Welsch, W. Rühaal, D. O. Schulte, K. Bär, S. Homuth, I. Sass, *Proceedings World Geothermal Congress* **2015**, 38006.

Appendix F – Modeling insulated borehole heat exchangers

Published as:

CrossMark

Modeling insulated borehole heat exchangers

Daniel Otto Schulte[1,2] · Bastian Welsch[1,2] · Anke Boockmeyer[3] · Wolfram Rühaak[1,2] ·
Kristian Bär[2] · Sebastian Bauer[3] · Ingo Sass[1,2]

Abstract In the heating sector, borehole heat exchangers have become popular for supplying renewable energy. They tap into the subsurface to extract geothermal energy for heating purposes. For advanced applications, borehole heat exchangers require insulation in the upper part of the borehole either to meet legal requirements or to improve their performance. A priori numerical heat transport models of the subsurface are imperative for the systems' planning and design. Only fully discretized models can account for depth-dependent borehole properties like insulated sections, but the model setup is cumbersome and the simulations come at high computational cost. Hence, these models are often not suitable for the simulation of larger installations. This study presents an analytical solution for the simulation of the thermal interactions of partly insulated borehole heat exchangers. A benchmark with a fully discretized OpenGeoSys model confirms sufficient accuracy of the analytical solution. In an application example, the functionality of the tool is demonstrated by finding the ideal length of a borehole insulation using mathematical optimization and by quantifying the effect of the insulation on the borehole heat exchanger performance. The presented method allows for accommodation of future advancements in borehole heat exchangers in numerical simulations at comparatively low computational cost.

This article is part of a Topical Collection in Environmental Earth Sciences on "Subsurface Energy Storage", guest edited by Sebastian Bauer, Andreas Dahmke, and Olaf Kolditz.

✉ Daniel Otto Schulte
schulte@geo.tu-darmstadt.de

1   Graduate School of Excellence Energy Science and Engineering, Technische Universität Darmstadt, Jovanka-Bontschits-Straße 2, 64287 Darmstadt, Germany

2   Geothermal Science and Technology, Technische Universität Darmstadt, Schnittspahnstraße 9, 64287 Darmstadt, Germany

3   Geohydromodelling, Christian-Albrechts-Universität zu Kiel, Ludewig-Meyn-Straße 10, 24118 Kiel, Germany

Introduction

Public awareness on renewable energies focuses mostly on the electricity supply. Yet, countries in high latitudes spend vast amounts of energy on heating. For example, in Germany, heating purposes alone account for more than half of the total end energy consumption (Ageb 2013). The use of borehole heat exchangers (BHEs) is an increasingly popular way to supply renewable heat all over the world (Angelino et al. 2014; Lund and Freeston 2005). BHEs are typically installed in vertical boreholes; a heat carrier fluid is circulated in closed-loop pipes. A cement grout used as backfill material ensures a good thermal connection to the borehole wall and protects the groundwater from possible contamination by antifreeze contained in the pipes. Heat is extracted from the subsurface rock by thermal conduction in the grout and by convection in the pipes (Sass et al. 2016a). Typically, at the surface a heat pump raises the temperature to the required level for the specific heating purpose. Its efficiency depends on the outlet temperature of the BHE and on the required temperature level for heating. Higher outlet temperatures reduce the required temperature lift and consequently the heat pump's energy consumption.

As the subsurface temperature increases with depth due to the geothermal gradient, deeper BHEs can provide higher outlet temperatures. However, heat losses in the shallow

subsurface can eliminate the temperature gains originating from the deeper section of the boreholes (Nakevska et al. 2015) and render the increased investment costs for deeper BHEs worthless. Thus, a thermal insulation in the upper section of a borehole is favorable for deeper BHEs. Furthermore, legal regulations in some countries may restrict the temperature increase of the uppermost aquifer to a certain maximum to protect drinking water from negative biological or chemical alterations (Haehnlein et al. 2010). Hence, a thermal insulation has been proposed for the upper part of medium deep borehole thermal energy storages (BTES) as well (Bär et al. 2015). On the one hand, a backfill material with reduced thermal conductivity and an increased borehole diameter are supposed to reduce the heat losses and the consequent warming of the shallow subsurface due to an increased thermal resistance between the pipes and the borehole wall. On the other hand, a backfill material with a high thermal conductivity can enhance the heat exchange at elevated ambient temperatures in the bottom part of the BHE (Sass et al. 2016a).

In the past, BHEs rarely exceeded 100 m depth. Therefore, no partial thermal insulation was necessary. On the contrary, due to the small temperature differences between the heat carrier fluid and the borehole wall, a high thermal conductivity of a single grout was favorable along the entire borehole. Consequently, simulation models did not need to account for grout thermal conductivities or borehole diameters changing with depth. Based on Eskilson and Claessons's solution (1988), Bauer et al. (2011) and Diersch et al. (2011a) developed a thermal resistance and capacity model (TRCM) which reduces a BHE to a one-dimensional discretization of nodes in a finite element mesh. This model accounts for a detailed description of the geometry of different BHE types and their material parameters. While it is more accurate than many line source models as it calculates depth-dependent grout and fluid temperatures within the BHE, it cannot accommodate changing borehole diameters or backfill material properties along the borehole length. Thus, up to now only fully discretized 3D numerical models have been able to simulate BHEs with vertically varying thermal conductivities. However, these models are laborious to set up, require expensive computations and lack the efficiency of fast analytical solutions, especially for larger models with multiple BHEs as needed for borehole thermal energy storages.

In this paper, Eskilson and Claessons's solution is improved to a model, which considers boreholes with an upper and a bottom section, with both different borehole diameters and different thermal conductivities of the backfill material represented in a TRCM. Our approach is independent from the specific BHE type and can handle coaxial, U-pipe and double U-pipe BHEs. The novel solution is linked to a numerical subsurface heat transport model and tested against a fully discretized numerical

benchmark model for a coaxial BHE. Finally, in an application example the model is combined with a mathematical optimization algorithm to determine the ideal length of the insulated section for a double U-pipe BHE.

An extended analytical solution

Eskilson and Claesson's analytical BHE solution (Eskilson and Claesson 1988) describes the fluid temperature in the downstream and upstream pipes T_{in} and T_{out} in °C as two codependent functions of depth z (in the range of $\zeta = 0$ to the total borehole length L) and the current borehole wall temperature T_b at time t.

$$T_{in}(z, t) = T_{in}(0, t)f_1(z) + T_{out}(0, t)f_2(z)$$
$$+ \int_0^z T_b(\zeta, t)f_4(z - \zeta)\, d\zeta \tag{1}$$

$$T_{out}(z, t) = -T_{in}(0, t)f_2(z) + T_{out}(0, t)f_3(z)$$
$$- \int_0^z T_b(\zeta, t)f_5(z - \zeta)\, d\zeta \tag{2}$$

The functions f_1, f_2, f_3, f_4 and f_5 are given by the following expressions:

$$
\begin{aligned}
f_1(z) &= e^{\beta z}[\cosh(\gamma z) - \delta \sinh(\gamma z)] \\
f_2(z) &= e^{\beta z} \frac{\beta_{12}}{\gamma} \sinh(\gamma z) \\
f_3(z) &= e^{\beta z}[\cosh(\gamma z) + \delta \sinh(\gamma z)] \\
f_4(z) &= e^{\beta z}\left[\beta_1 \cosh(\gamma z) - \left(\delta\beta_1 + \frac{\beta_2 \beta_{12}}{\gamma}\right)\sinh(\gamma z)\right] \\
f_5(z) &= e^{\beta z}\left[\beta_2 \cosh(\gamma z) + \left(\delta\beta_2 + \frac{\beta_1 \beta_{12}}{\gamma}\right)\sinh(\gamma z)\right]
\end{aligned}
\tag{3}
$$

The functions' auxiliary variables α, β, β_1, β_2, β_{12}, γ and δ, which are based on the TRCMs of the involved BHE components, are calculated according to the BHE type after Bauer et al. (2011), whereas the derivation of the functions f_1–f_5 can be found in Eskilson and Claesson (1988). Since the solution describes only local steady-state conditions, time t is omitted from the following equations for better readability. The analytical solution has to be linked to a numerical subsurface model by deriving a heat source term from the difference between the borehole wall temperature and the fluid temperature (Diersch et al. 2011a) to account for transient heat transport in the subsurface. Then, the numerical model calls the analytical solution every time step, providing the time-dependent borehole wall temperature.

As the upstream and downstream pipes form a closed loop, the fluid temperature must be the same at the bottom. Hence, Eqs. (1) and (2) can be equalized at $z = L$ and
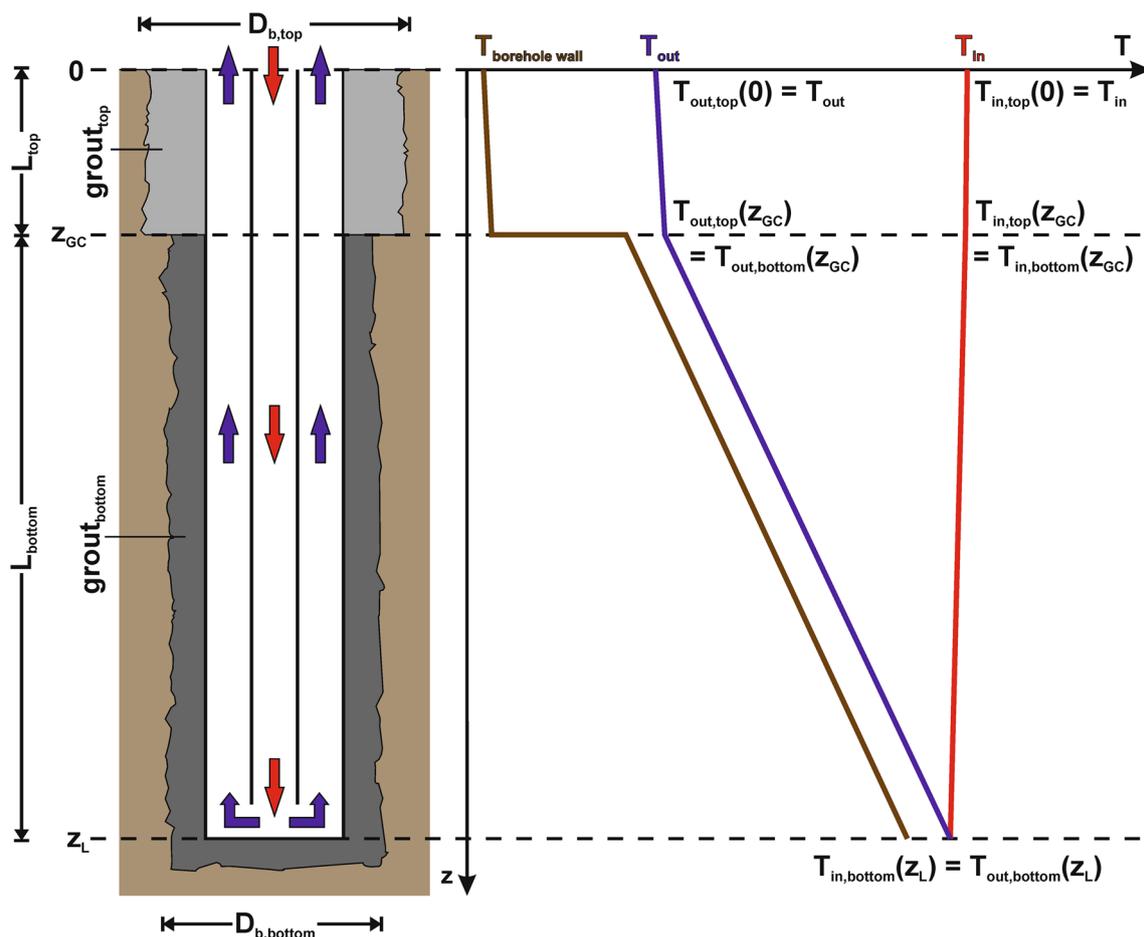
Fig. 1 Sketch of a coaxial BHE (*centered inlet*) with the insulated uppermost borehole section and the initial corresponding temperature profile for heat storage operation. The step-like offset of the borehole wall temperature at z_{gc} is smoothed out after prolonged operation due to vertical heat transport in the subsurface

resolved for $T_{out} = T_{out}(z = 0)$ for a given inlet temperature of the BHE $T_{in} = T_{in}(z = 0)$:

$$T_{out} = T_{in} \frac{f_1(L) + f_2(L)}{f_3(L) - f_2(L)} + \int_0^L \frac{T_s(\zeta) f_4(L - \zeta) + f_5(L - \zeta)}{f_3(L) - f_2(L)} d\zeta \tag{4}$$

Determining the outlet temperature T_{out} is the imperative first step, as Eqs. (1) and (2) require both the inlet and the outlet temperature of the BHE to calculate the depth-dependent temperature profile in the downstream and upstream pipes. However, Eq. (4) shows that the solution for the outlet temperature integrates functions f_4 and f_5 over the entire borehole length L. Likewise, functions f_1, f_2 and f_3 depend on the total borehole length L as well. Hence, borehole properties changing with depth cannot be accounted for in this equation, as they are constants in the auxiliary variables of the functions f_1–f_5. Instead, a BHE with a borehole insulation in the upper part requires a split calculation.

As the design splits the BHE into two sections with different grout properties and drilling diameters (Fig. 1), Eqs. (1) and (2) apply for the upper and lower section separately. This allows for an independent consideration of different TRCMs with different auxiliary variable values for the functions f_1–f_5 in each section. The downstream and upstream pipes are connected in the bottom section. Therefore, Eqs. (1) and (2) cannot be equalized for the bottom of the upper part at the interface between the two different grout types at depth z_{gc} to derive Eq. (4). However, at the interface the fluid temperatures $T_{in, top}(z_{gc})$ and $T_{out, top}(z_{gc})$ of the upper section of the wellbore are equal to the inlet and outlet temperatures $T_{in, bottom}$ and $T_{out, bottom}$ of the bottom section.

$$\begin{aligned} T_{in, bottom} &= T_{in, top}(z_{GC}) \\ T_{out, bottom} &= T_{out, top}(z_{GC}) \end{aligned} \tag{5}$$

Equation (4) is still valid for the bottom section, but the inlet and outlet temperatures are unknown. Thus, substitution according to (5) gives

$$T_{\text{out, bottom}} = T_{\text{in, bottom}} \frac{f_{1,\text{bottom}}(L_{\text{bottom}}) + f_{2,\text{bottom}}(L_{\text{bottom}})}{f_{3,\text{bottom}}(L_{\text{bottom}}) - f_{2,\text{bottom}}(L_{\text{bottom}})}$$

$$+ \int_{z_{\text{GC}}}^{z_L} \frac{T_s(\zeta) f_{4,\text{bottom}}(L_{\text{bottom}} - \zeta) + f_{5,\text{bottom}}(L_{\text{bottom}} - \zeta)}{f_{3,\text{bottom}}(L_{\text{bottom}}) - f_{2,\text{bottom}}(L_{\text{bottom}})} d\zeta \equiv$$

$$T_{\text{out, top}}(z_{\text{GC}}) = T_{\text{in, top}}(z_{\text{GC}}) \frac{f_{1,\text{bottom}}(L_{\text{bottom}}) + f_{2,\text{bottom}}(L_{\text{bottom}})}{f_{3,\text{bottom}}(L_{\text{bottom}}) - f_{2,\text{bottom}}(L_{\text{bottom}})} \cdot$$

$$+ \int_{z_{\text{GC}}}^{z_L} \frac{T_s(\zeta) f_{4,\text{bottom}}(L_{\text{bottom}} - \zeta) + f_{5,\text{bottom}}(L_{\text{bottom}} - \zeta)}{f_{3,\text{bottom}}(L_{\text{bottom}}) - f_{2,\text{bottom}}(L_{\text{bottom}})} d\zeta$$

$$\text{(6)}$$

Inserting (1) and (2) for $T_{\text{in, top}}(z_{\text{GC}})$ and $T_{\text{out, top}}(z_{\text{GC}})$, the resulting equation can be solved for $T_{\text{out, top}}$:

$$T_{\text{out, top}} = T_{\text{in, top}}$$

$$\times \frac{\kappa + v \int_0^{z_{\text{GC}}} T_b(\zeta) f_{4,\text{top}}(L_{\text{top}}) d\zeta + \int_0^{z_{\text{GC}}} T_b(\zeta) f_{5,\text{top}}(L_{\text{top}}) d\zeta + \mu}{\lambda}$$

$$\text{(7)}$$

with

$$\kappa = v f_{1,\text{top}}(L_{\text{top}}) + f_{2,\text{top}}(L_{\text{top}})$$

$$\lambda = f_{3,\text{top}}(L_{\text{top}}) - v f_{2,\text{top}}(L_{\text{top}})$$

$$\mu = \int_{z_{\text{GC}}}^{z_L} \frac{T_b(\zeta) \left(f_{4,\text{bottom}}(L_{\text{bottom}}) + f_{5,\text{bottom}}(L_{\text{bottom}}) \right)}{f_{3,\text{bottom}}(L_{\text{bottom}}) - f_{2,\text{bottom}}(L_{\text{bottom}})} d\zeta$$

$$v = \frac{f_{1,\text{bottom}}(L_{\text{bottom}}) + f_{2,\text{bottom}}(L_{\text{bottom}})}{f_{3,\text{bottom}}(L_{\text{bottom}}) - f_{2,\text{bottom}}(L_{\text{bottom}})}$$

$$\text{(8)}$$

Subsequently, the depth-dependent temperature profiles in the downstream and upstream pipes can be calculated with (1) and (2) using $T_{\text{in, top}}$ and $T_{\text{out, top}}$ for the upper insulated section of the wellbore and $T_{\text{in, bottom}} = T_{\text{in, top}}(z_{\text{GC}})$ and $T_{\text{out, bottom}} = T_{\text{out, top}}(z_{\text{GC}})$ for the lower section. The new solution now takes into account borehole properties changing with depth and can be coupled to a numerical subsurface model as described in Diersch et al. (2011a).

Benchmarking

The enhanced analytical solution is integrated in a MATLAB (The MathWorks 2015a) finite element method (FEM)-based simulator called BASIMO (borehole heat exchanger array simulation and optimization tool, Schulte et al. 2016). In a benchmark problem, it is compared against a benchmark simulation of a fully discretized detailed numerical 3D model using OpenGeoSys (OGS; Kolditz et al. 2012). OGS is a process and object-oriented simulator (Kolditz and Bauer 2004) that uses a FEM to solve the arising thermal and hydraulic processes. The OGS model is based on the same principle as introduced in

Boockmeyer and Bauer (2014) and was successfully verified against detailed experimental data for a BHE (Boockmeyer and Bauer 2014). The OGS model can account for spatially varying and temperature–dependent material parameters and is applied for the simulation of heat storage in the subsurface (Bauer et al. 2013, 2015).

A simple heat storage and extraction operation scenario is set up for the benchmark: A partly insulated 100-m coaxial BHE is located in the center of the model domain, which is 100 m by 100 m wide and 150 m deep. The initial temperature distribution corresponds to a geothermal gradient of 0.03 K/m. Dirichlet boundary conditions are set accordingly: 10 °C at the top and 14.5 °C at the bottom. An enlarged drilling diameter and a reduced thermal conductivity of the grout provide a borehole insulation from the surface to 30 m depth (Fig. 2).

Heat is stored for 182 days with an inlet temperature of 90 °C and a flow rate of 2.5 l/s. Subsequently, the heat extraction period lasts 183 days with the same flow rate and an inlet temperature of 5 °C. The change of the flow direction from the centered inlet for heat storage to the inlet through the annular gap for heat extraction is considered. Table 1 summarizes the material properties, the BHE geometry and the according abbreviations used in Fig. 2.

Both simulators are set up with the model described above. In the benchmark, the temporal evolution of the outlet temperatures is compared against each other. As the simulators use independent time-stepping schemes, results are saved after 1 day and after 10 days of storage and extraction operation, respectively, to ensure at least two comparison points per period. The results show that the improved analytical solution lacks in accuracy to match the fully discretized model for the early time steps during transient input situations (Fig. 3a, c), but achieves a very good fit after a few hours of simulation time (Fig. 3b, d). After 10 days of operation, the temperature difference is less than 0.14 °C. At the end of the storage and extraction periods, the BHE outlet temperature differs less than 0.02 °C between the BASIMO and the OGS model.

It is not possible to quantify the difference in the outlet temperature for the entire time domain without interpolation of the results due to the different time-stepping schemes. Instead, the heat balance Q, which represents the heat exchanged with the subsurface and requires the integration for the storage and the extraction period, is considered:

$$Q = \int (T_{\text{in}} - T_{\text{out}}) f \, \rho_f \, c_f \, t \, dt \tag{9}$$

with T_{in}: inlet temperature, T_{out}: outlet temperature, f: flow rate of the heat carrier fluid, ρ_f: density of the heat carrier fluid, c_f: specific heat capacity of the carrier fluid and t: time. The results of the benchmark and the relative

Fig. 2 Schematic of the coaxial BHE used in the benchmark (not to scale)
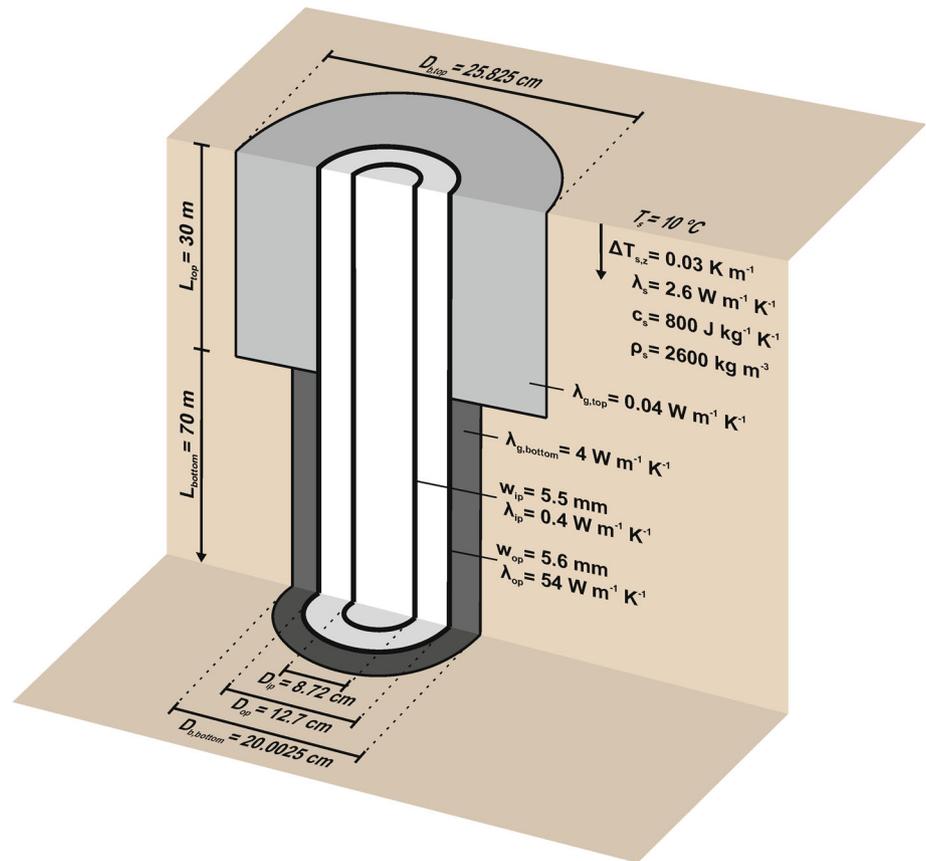
Table 1 Model parameters and BHE properties for benchmark simulation

Parameter	Value	Unit	Abbreviation
Rock thermal conductivity	2.6	$W \cdot m^{-1} \cdot K^{-1}$	λ_s
Rock density	2600	$kg \cdot m^{-3}$	ρ_s
Rock specific heat capacity	800	$J \cdot kg^{-1} \cdot K^{-1}$	c_s
Rock volumetric heat capacity	2.08	$MJ \cdot m^{-3} \cdot K^{-1}$	ρc_s
Upper section borehole diameter	0.25825	m	$D_{b, top}$
Upper section grout thermal conductivity	0.04	$W \cdot m^{-1} \cdot K^{-1}$	$\lambda_{g, top}$
Upper section length	30	m	L_{top}
Lower section borehole diameter	0.200025	m	$D_{b, bottom}$
Lower section grout thermal conductivity	4	$W \cdot m^{-1} \cdot K^{-1}$	$\lambda_{g, bottom}$
Lower section length	70	m	L_{bottom}
Outer pipe outer diameter	0.127	m	D_{op}
Outer pipe wall thickness	0.0056	m	w_{op}
Outer pipe thermal conductivity (steel)	54	$W \cdot m^{-1} \cdot K^{-1}$	λ_{op}
Inner pipe outer diameter	0.0872	m	D_{ip}
Inner pipe wall thickness	0.0055	m	w_{ip}
Inner pipe thermal conductivity (polyethylene)	0.4	$W \cdot m^{-1} \cdot K^{-1}$	λ_{ip}
Heat carrier fluid dynamic viscosity (water)	0.000504	$kg \cdot m^{-1} \cdot s^{-1}$	μ
Heat carrier fluid density (water)	977	$kg \cdot m^{-3}$	ρ_f
Heat carrier fluid specific heat capacity (water)	4145	$J \cdot kg^{-1} \cdot K^{-1}$	c_f
Heat carrier fluid thermal conductivity (water)	0.65	$W \cdot m^{-1} \cdot K^{-1}$	λ_f
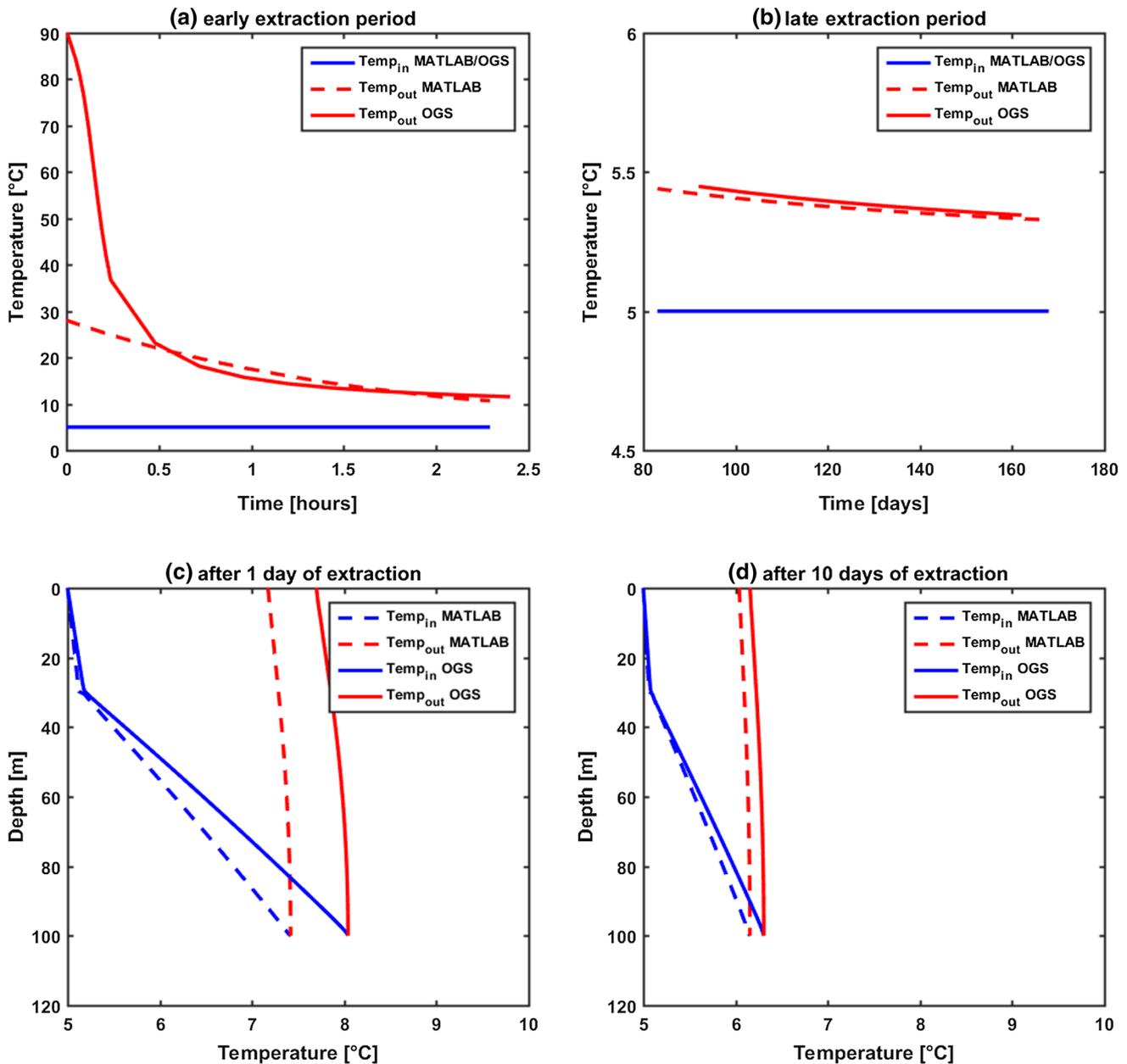
Fig. 3 Comparison of the coaxial BHE model responses. *Top*: **a** short-term and **b** long-term evolution of the BHE outlet temperature. *Bottom*: BHE temperature profiles after **c** 1 day and after **d** 10 days of extraction

difference of the models are summarized in Table 2. The amount of transferred heat differs by 1.6 and 5 % during storage and extraction, respectively. Considering only the first 10 days of the storage and extraction periods, increased errors of 6.8 and 13.54 % indicate the strong influence of the analytical solution's inaccuracy during the first time steps, whereas the remaining storage and extraction periods yield smaller errors (Table 2). The accuracy of the analytical solution and sources for the remaining error are addressed in the "Discussion" section below.

Application example

In most applications, double U-pipe BHEs are coupled with heat pumps (Sass et al. 2016a). Deeper boreholes are often fitted with coaxial BHEs instead (Bär et al. 2015; Schulte et al. 2016; Welsch et al. 2015). They benefit from the fact that the inner pipe is not in contact with the grout and can be designed to have a low thermal conductivity, which can reduce heat losses of the upstream fluid within. For double U-pipe BHEs, the full length of the downstream and upstream pipes acts as a heat exchange surface with the

Table 2 Benchmark results

Period	Q_{MATLAB} (MWh)	Q_{OGS} (MWh)	Error: $(Q_{OGS}-Q_{MATLAB})/Q_{OGS}$ (%)
Storage$_{total}$	106.57	108.29	1.6
Storage$_{0-10\ days}$	8.34	8.95	6.8
Storage$_{10-182\ days}$	98.24	99.34	1.1
Extraction$_{total}$	−23.55	−24.77	5.0
Extraction$_{0-10\ days}$	−3.84	−4.45	13.54
Extraction$_{192-365\ days}$	−19.70	−20.33	3.1

Table 3 Model parameters and BHE properties for application example

Parameter	Value	Unit	Variable
Rock thermal conductivity	2.6	$W \cdot m^{-1} \cdot K^{-1}$	λ_s
Rock density	2600	$kg \cdot m^{-3}$	ρ_s
Rock specific heat capacity	800	$J \cdot kg^{-1} \cdot K^{-1}$	c_s
Rock volumetric heat capacity	2.08	$MJ \cdot m^{-3} \cdot K^{-1}$	ρc_s
Upper section borehole diameter	0.25825	m	$D_{b,\ top}$
Upper section grout thermal conductivity	0.04	$W \cdot m^{-1} \cdot K^{-1}$	$\lambda_{g,\ top}$
Lower section borehole diameter	0.13	m	$D_{b,\ bottom}$
Lower section grout thermal conductivity	4	$W \cdot m^{-1} \cdot K^{-1}$	$\lambda_{g,\ bottom}$
Depth of diameter and grout change	variable	m	z_{gc}
Pipe outer diameter	0.032	m	D_p
Pipe wall thickness	0.0029	m	w_p
Diagonal shank space	0.06	m	s_p
Pipe thermal conductivity (polyethylene)	0.38	$W \cdot m^{-1} \cdot K^{-1}$	λ_p
Heat carrier fluid dynamic viscosity (water)	0.000504	$kg \cdot m^{-1} \cdot s^{-1}$	μ
Heat carrier fluid density (water)	977	$kg \cdot m^{-3}$	ρ_f
Heat carrier fluid specific heat capacity (water)	4145	$J \cdot kg^{-1} \cdot K^{-1}$	c_f
Heat carrier fluid thermal conductivity (water)	0.65	$W \cdot m^{-1} \cdot K^{-1}$	λ_f

surrounding rock and the grout material. Thus, double U-pipe BHEs suffer growing heat losses in the upstream pipes with increasing borehole length: the heat extracted at the bottom of the BHE is lost to the shallow subsurface and the cooler downstream pipes (so-called thermal short-circuiting) before it reaches the surface. Consequently, only lower inlet temperatures can compensate the heat losses and maintain the required difference between inlet and outlet temperature for the desired heat extraction rate. This, however, directly translates to an increased power consumption of the heat pump and an efficiency loss. Assuming an ideal Carnot process, the efficiency of a heat pump can be calculated by determining the theoretical maximum coefficient of performance (COP):

$$COP_{theor,\ max} = \frac{T_{hot}}{T_{hot} - T_{cold}} \quad (10)$$

where T_{hot} represents the required temperature level for the specific heating purpose and T_{cold} the outlet temperature of the BHE (all temperatures in Kelvin). Although being a simplification, which neglects internal losses, the theoretical maximum COP reflects the influence of the outlet temperature and can give an estimate on the change of the system performance.

In a synthetic simulation example, a 400-m double U-pipe BHE is to be fitted with a borehole insulation in the upper section. Again, BASIMO (Schulte et al. 2016) is used to simulate the BHE's operation. The vertical BHE is located in the center of the model with a horizontal extension of 100 m by 100 m. The model domain is 450 m deep. Dirichlet boundary conditions and initial conditions concur with a geothermal gradient of 0.03 K/m and a surface temperature of 10 °C. Table 3 and Fig. 4 plot the considered material properties and the BHE specifications. A simple scenario to simulate the BHE operation applies: Heat is extracted at a constant rate of 20 kW for 30 days at a flow rate of 0.5 l/s. For the given fluid heat capacity and density, this equates to a required difference of about 9.88 °C between inlet and outlet temperature. Strong coupling by a Picard iteration loop (Reddy and Gartling 2010) enforces this requirement by altering the inlet temperature for every time step accordingly. The beneficial effect of the insulation is quantified by comparing the outlet temperature against the results of a BHE without insulation, which serves as the base case.

Fig. 4 Schematic of the double
U-pipe BHE used in the
application example (not to
scale)
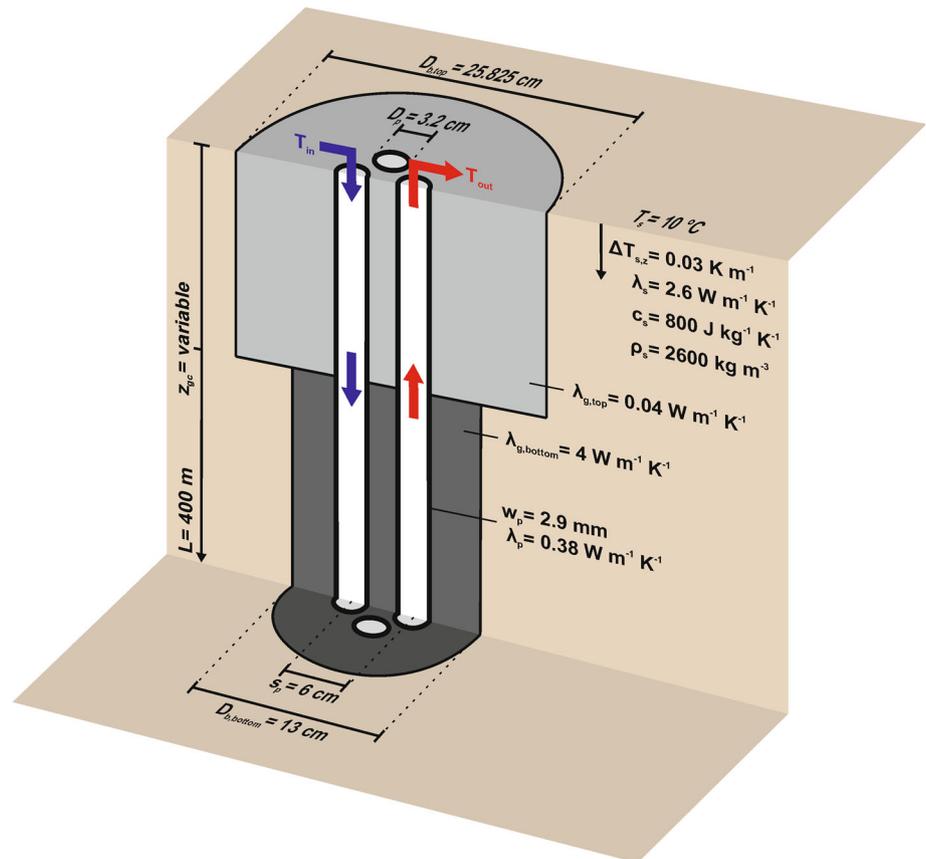
An entirely insulated borehole will perform worse than a
BHE without any insulation. Hence, an ideal length of
borehole insulation must exist. A basic optimization algo-
rithm contained in the MATLAB Optimization Toolbox
(Brent 1973; The MathWorks 2015b) for finding the min-
imum of a single-variable function on a fixed interval is
used to determine the ideal length. The optimization
algorithm calls the simulator repeatedly, varying the length
of the borehole insulation (i.e., the depth of borehole
diameter and grout change) within preset boundaries until
it fails to improve the outlet temperature of the BHE with
respect to a tolerance criterion for the variable (i.e., length
of insulation) or the function value (i.e., the outlet tem-
perature, Table 4).

After 15 iterations, the optimization algorithm con-
verges on an optimal solution of approximately 142 m
(Fig. 5a) for the insulation length. At the end of the 30-day
period, the outlet temperature of the insulated double
U-pipe BHE is 2.36 °C. Compared to the outlet tempera-
ture of the same BHE without insulation, this represents an
increase of approximately 1.7 °C (Fig. 5b). The effect of
the insulation becomes apparent by comparing the tem-
perature profiles of both BHEs after 30 days of operation
(Fig. 6a, b). The insulation reduces the heat extraction in
the upper section of the downstream pipe. As a result, the

Table 4 Optimization algorithm settings

Parameter	Value	Unit
Lower variable boundary	10	m
Upper variable boundary	390	m
Maximum number of iterations	20	[–]
Variable tolerance	0.1	m
Function tolerance	0.001	°C

heat carrier fluid cannot reach temperatures as high as at
the bottom of the uninsulated borehole. However, the
insulation also mitigates the heat loss in the upstream pipe,
ultimately providing a higher outlet temperature at the top
of the insulated borehole.

Assuming an ideal Carnot heat pump, which raises the
temperature to a target level of 35 °C (i.e., T_{hot}), the the-
oretical maximum COP for the insulated BHE is 9.44,
whereas the BHE without an insulated borehole only
achieves a theoretical COP of 8.97. This equates to a
performance increase of about 5 %. Table 5 gives a
selection of the optimization iterations' results. The first
iteration with an insulation length of 244.85 m shows how
an insulation that is too long negatively affects the BHE
performance.
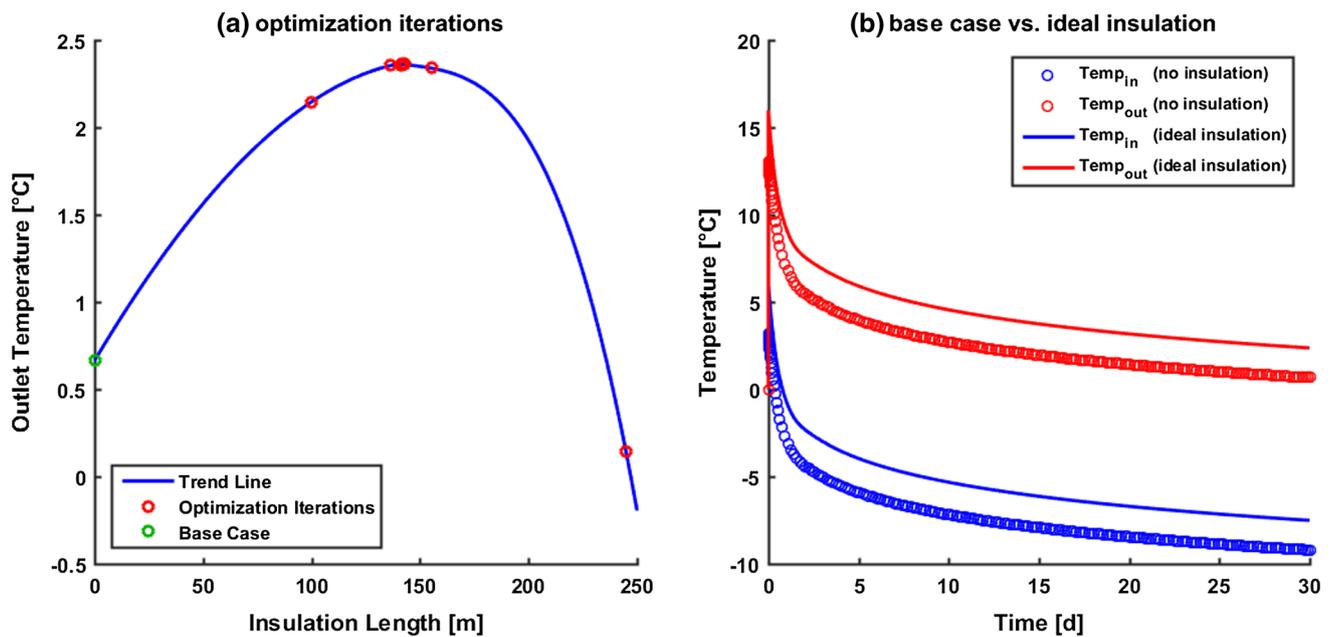
Fig. 5 Optimization results: **a** Temp$_{out}$ after 30 days of operation for each iteration, **b** Temp$_{in}$ and Temp$_{out}$ evolution of the base case and the ideally insulated BHE

Discussion

Although the presented solution only accounts for two borehole sections with different borehole diameters and backfill materials, the method is expandable to any number of segments by further substitution in Eq. (7). Additional segmentation results in nested functions, but is only limited by the increment size of the one-dimensional discretization of the borehole. However, for better readability the calculation rule for two sections sufficiently describes the concept.

In general, any other parameter included in the TRCM (e.g., pipe properties) can be altered as well. Yet, for the purpose of modeling a borehole insulation, the scope in this study is restricted to the borehole diameter and the thermal conductivity of the backfill material. As the solution for modeling insulated BHEs represents an improvement solely on Eskilson and Claesson's work (Eskilson and Claesson 1988), the TRCM providing the parameters for functions (3) is not affected. Consequently, our novel solution can handle improved TRCMs as long as they provide the required parameters for the auxiliary functions (3). For example, future TRCMs can be expanded to include additional standpipes in the thermal resistance network.

Despite the adequate benchmark results, the two simulations still show an observable mismatch. The conceptual differences between the fully discretized OGS model and the FEM-coupled analytical solution can contribute to this error in various ways. Most importantly, the OGS model is transient, whereas the analytical model is a local steady-state solution coupled to a transient FEM algorithm. Consequently, the FEM-coupled analytical model struggles to match the numerical model in transient input situations on short timescales. Diersch et al. (2011b) have shown that the analytical solution overestimates the outlet temperature during the first time steps of storage operation. However, the errors vanish with increasing time step size until further inlet temperature changes occur. The same is true for the presented analytical solution for insulated BHEs: The outlet temperature difference between the BASIMO and the OGS model decreases to less than 0.02 °C in the long-term prediction. After changing from storage to extraction operation, the difference in outlet temperature soars up before the error diminishes again.

Another source of error in the FEM-coupled analytical model is the grid spacing around the BHE nodes. The nodes representing the BHEs are dimensionless singularities in the finite element mesh, whereas the actual BHE cross section has an extent. Thus, the heat exchange with the FEM model does not occur exactly where the borehole wall would be. In a semi-structured triangular prism mesh, numerical accuracy can be attained by choosing a specific, optimal distance of the horizontally neighboring nodes depending on the borehole diameter (Diersch et al. 2011b). However, the simulator for borehole thermal energy storage (Schulte et al. 2016) uses a tetrahedral finite element mesh. This inhibits the possibility of placing all neighboring nodes at an equal distance. The nodes sharing a tetrahedron element with a BHE node inherently have

Fig. 6 Temperature profiles of **a** the double U-pipe BHE without insulation and **b** the ideally insulated double U-pipe BHE after 30 days of operation
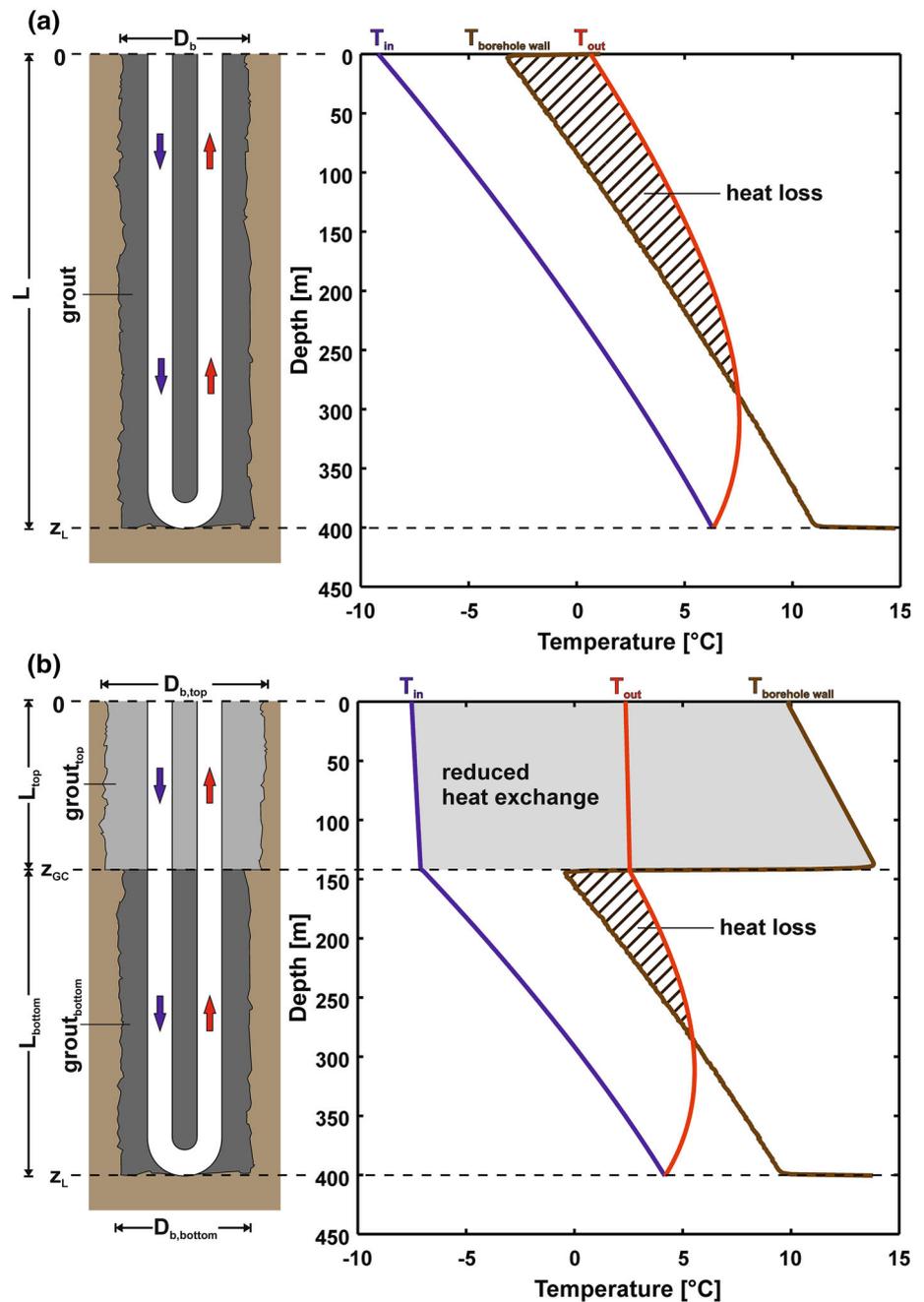
different distances from one another. Consequently, this problem cannot be overcome by optimal conditions of mesh spacing as suggested by Diersch et al. (2011b). Solving this problem to achieve better accuracy is, however, subject of further research. Altogether, the FEM-coupled analytical solution still achieves an acceptable accuracy compared to the fully discretized OGS model. The greater portion of the error can be attributed to the shortcomings in transient situations on short timescales, but since typical simulations of BHE arrays usually span

several years of operation, this deficit is negligible for most applications.

In the past, considerations of insulation focused on the pipes used in BHEs (Acuña et al. 2011; Acuña and Palm 2013) to mitigate thermal short-circuiting. However, the application example shows that an insulation of the borehole can have significant impact on the output temperature of a BHE. Despite its beneficial effect on deep BHEs and although it has been proposed for BTES systems for environmental reasons (Bär et al. 2015), to our knowledge

Table 5 Selection of optimization iteration results (after 30 days of operation)

Iteration	Insulation length (m)	Inlet and Outlet temperature (°C)	Target temperature (°C)	COP$_{theor, max}$	Relative change of COP$_{theor, max}$ compared to base case
0 (base case)	0	−9.21/0.66	35	8.97	not applicable
1	244.85	−9.73/0.15	35	8.84	−1.46 %
2	99.71	−7.73/2.14	35	9.38	+4.50 %
3	155.15	−7.54/2.34	35	9.43	+5.14 %
15 (optimal)	142.15	−7.52/2.36	35	9.44	+5.21 %

thermal borehole insulation has not been put into practice so far. Consequently, the development of grouts for BHEs has focused on enhancing the thermal conductivity (Lee et al. 2010) rather than reducing it. Thus, the thermal conductivity of the insulating grout in the application example does not refer to any available BHE grout, but to polyurethane. Polyurethane may very well be a potential candidate for a BHE insulating grout as it is watertight, has a very low thermal conductivity and is already in use for sealing wellbores in other applications (Mansure 2002; Zawislanski and Faybishenko 1999). Thus, a thermal conductivity as low as $0.04 \text{ W m}^{-1} \text{ K}^{-1}$ is a reasonable assumption.

It is necessary to evaluate the effect of the borehole insulation on the system performance for each scenario specifically. Heat pump specifications, heat losses and the load profile for the heat demand have to be taken into account. As building specifications are beyond the scope of this paper, the performance increase of the synthetic application scenario can only consider the improvement of the theoretical maximum COP neglecting all losses an actual heat pump would have. However, the results still provide a good estimate on the magnitude of a possible performance gain by an insulated borehole.

A gain of 5 % in heat pump performance may appear miniscule considering the increased costs for drilling with a larger borehole diameter and fitting the BHE with the insulation. Simply extending the BHE or adding a second BHE instead of using insulation could achieve the same efficiency gain. At least for U-pipe and double U-pipe BHEs extending the borehole length is not a viable option due to the increased thermal short-circuiting mentioned above. A comparative simulation shows that an uninsulated BHE with the same specifications, but twice the length (i.e., 800 m) provides an outlet temperature of 1.95 °C after 30 days in the described operational scenario. This corresponds to a theoretical maximum COP of 9.32 and a relative COP increase of 3.9 %. Extending the BHE proves to be effective, but even so the borehole insulation provides better results. Furthermore, doubling the borehole length represents a considerable rise in investment costs and does

not even factor in the increased power consumption for the circulation pump, which is about twice as high.

On the other hand, using two BHEs without insulation instead of an ideally insulated one can be a cost-saving alternative. Applying the mathematical optimization algorithm on a system of two identical BHEs without insulation, which are 5 m apart and have the load of 20 kW split equally among them, yields a required length of 162.60 m each to match the outlet temperature of the ideally insulated BHE. While the setup with two shorter BHEs results in saving about 19 % of total borehole length as well as pumping power (considering the described scenario with 0.5 l/s per BHE) compared to the single insulated 400 m BHE, the two BHEs without insulation also require more space at the surface. With only 5 m distance in between, the BHEs will eventually influence each other, which will result in decreasing outlet temperatures. If the reservoir is not replenished by heat storage cycles or prolonged recovery phases, the distance between the BHEs has to be increased even further. For arrays of BHEs this can raise the required surface area significantly. As mentioned before, recharging the reservoir by heat storage cycles can have a negative impact on the drinking water quality in the topmost aquifer and can therefore be legally restricted. BHEs as short as ∼160 m are likely to affect this aquifer along a large part of their length, which limits the possibilities of replenishment by heat storage. Therefore, a borehole insulation is a favorable option to increase BHE efficiency where deeper boreholes are required due to limited space in urban areas (Gehlin et al. 2016) or even a necessity, when legal regulations require a reduction of the thermal impact on the topmost aquifer (Bär et al. 2015; Sass et al. 2016b).

Summary and conclusion

Particular advanced applications for borehole heat exchangers require some of the borehole properties to change with depth. This study presents an efficient analytical solution for modeling such depth-dependent

properties. The solution can accommodate future developments on thermal resistance and capacity networks for borehole heat exchangers. If coupled to a transient model for the subsurface heat transport, it is sufficiently accurate to save expensive and cumbersome simulations of fully discretized borehole heat exchangers. This method allows for the implementation of properties like increased borehole diameters and thermal resistances, which can act as borehole insulation, even for simulations of larger arrays of borehole heat exchangers.

References

Acuña J, Palm B (2013) Distributed thermal response tests on pipe-in-pipe borehole heat exchangers. Appl Energy 109:312–320. doi:10.1016/j.apenergy.2013.01.024

Acuña J, Mogensen P, Palm B (2011) Distributed thermal response tests on a multi-pipe coaxial borehole heat exchanger. HVAC&R Res 17:1012–1029. doi:10.1080/10789669.2011.625304

Ageb AE (2013) Anwendungsbilanzen für die Endenergiesektoren in Deutschland in den Jahren 2011 und 2012 mit Zeitreihen von 2008 bis 2012. Bundesministerium für Wirtschaft und Technologie, Berlin

Angelino L, Dumas P, Latham A (2014) EGEC Market Report 2013/2014 Update, 4 edn. European Geothermal Energy Council—EGEC

Bär K, Rühaak W, Welsch B, Schulte D, Homuth S, Sass I (2015) Seasonal high temperature heat storage with medium deep borehole heat exchangers. Energy Procedia 76:351–360. doi:10.1016/j.egypro.2015.07.841

Bauer D, Heidemann W, Müller-Steinhagen H, Diersch HJG (2011) Thermal resistance and capacity models for borehole heat exchangers. Int J Energy Res 35:312–320. doi:10.1002/er.1689

Bauer S, Beyer C, Dethlefsen F, Dietrich P, Duttmann R, Ebert M, Feeser V, Görke U, Köber R, Kolditz O, Rabbel W, Schanz T, Schäfer D, Würdemann H, Dahmke A (2013) Impacts of the use of the geological subsurface for energy storage: an investigation concept. Environ Earth Sci 70:3935–3943. doi:10.1007/s12665-013-2883-0

Bauer S, Pfeiffer T, Boockmeyer A, Dahmke A, Beyer C (2015) Quantifying induced effects of subsurface renewable energy storage. Energy Procedia 76:633–641. doi:10.1016/j.egypro.2015.07.885

Boockmeyer A, Bauer S (2014) High-temperature heat storage in geological media: high-resolution simulation of near-borehole processes. Géotechnique Lett 4:151–156. doi:10.1680/geolett.13.00060

Brent RP (1973) Algorithms for minimization without derivatives. Dover, Mineola

Diersch HJG, Bauer D, Heidemann W, Rühaak W, Schätzl P (2011a) Finite element modeling of borehole heat exchanger systems: part 1. Fundam Comp Geosci 37:1122–1135. doi:10.1016/j.cageo.2010.08.003

Diersch HJG, Bauer D, Heidemann W, Rühaak W, Schätzl P (2011b) Finite element modeling of borehole heat exchanger systems:

part 2. Numer Simul Comp Geosci 37:1136–1147. doi:10.1016/j.cageo.2010.08.002

Eskilson P, Claesson J (1988) Simulation model for thermally interacting heat extraction boreholes. Numer Heat Transf 13:149–165

Gehlin SEA, Spitler JD, Hellström G (2016) Deep boreholes for ground source heat pump systems—scandinavian experience and future prospects. Paper presented at the ASHRAE Winter Meeting, Orlando, Florida, 23–27 Jan 2016

Haehnlein S, Bayer P, Blum P (2010) International legal status of the use of shallow geothermal energy. Renew Sustain Energy Rev 14:2611–2625. doi:10.1016/j.rser.2010.07.069

Kolditz O, Bauer S (2004) A process-oriented approach to computing multi-field problems in porous media. J Hydroinformatics 6:225–244

Kolditz O, Bauer S, Bilke L, Böttcher N, Delfs JO, Fischer T, Görke UJ, Kalbacher T, Kosakowski G, McDermott CI, Park CH, Radu F, Rink K, Shao H, Shao HB, Sun F, Sun YY, Singh AK, Taron J, Walther M, Wang W, Watanabe N, Wu Y, Xie M, Xu W, Zehner B (2012) OpenGeoSys: an open-source initiative for numerical simulation of thermo-hydro-mechanical/chemical (THM/C) processes in porous media. Environ Earth Sci 67:589–599. doi:10.1007/s12665-012-1546-x

Lee C, Lee K, Choi H, Choi H-P (2010) Characteristics of thermally-enhanced bentonite grouts for geothermal heat exchanger in South Korea. Sci China Ser E-Technol Sci 53:123–128. doi:10.1007/s11431-009-0413-9

Lund JW, Freeston DH, Boyd TL (2005) Direct application of geothermal energy: 2005 Worldwide review. Geothermics 34:691–727. doi:10.1016/j.geothermics.2005.09.003

Mansure AJ (2002) Polyurethane grouting geothermal lost circulation zones. Paper presented at the IADC/SPE Drilling Conference, Dallas, Texas, 26–28 Feb 2002

Nakevska N, Schincariol RA, Dehkordi SE, Cheadle BA (2015) Geothermal waste heat utilization from in situ thermal bitumen recovery operations. Groundwater 53:251–260. doi:10.1111/gwat.12196

Reddy JN, Gartling DK (2010) The finite element method in heat transfer and fluid dynamics, 3rd edn. CRC Press, Boca Raton

Sass I, Brehm D, Coldewey WG, Dietrich J, Klein R, Kellner T, Kirschbaum B, Lehr C, Marek A, Mielke P, Müller L, Panteleit B, Pohl S, Porada J, Schiessl S, Wedewardt M, Wesche D (2016a) Shallow geothermal systems—recommendations on design, construction, operation and monitoring. Ernst & Sohn, Berlin

Sass I, Welsch B, Schulte DO (2016b) Mitteltiefe Erdwärmesondenspeicher—Lösung für den Nutzungskonflikt Grundwasserschutz versus Geothermienutzung? Paper presented at the 7. Bochumer Grundwassertag, Bochum, 17 Mar 2016

Schulte DO, Rühaak W, Oladyshkin S, Welsch B, Sass I (2016) Optimization of medium-deep borehole thermal energy storage systems. Energy Technol 4:104–113. doi:10.1002/ente.201500254

The MathWorks (2015a) MATLAB 2015b. The MathWorks Inc, Natick

The MathWorks (2015b) MATLAB 2015b Global Optimization Toolbox. The MathWorks Inc, Natick

Welsch B, Rühaak W, Schulte DO, Bär K, Homuth S, Sass I (2015) A comparative study of medium deep borehole thermal energy storage systems using numerical modeling. In: Proceedings World Geothermal Congress, Melbourne, 19–24 Apr 2015

Zawislanski PT, Faybishenko B (1999) New casing and backfill design for neutron logging access boreholes. Ground Water 37:33–37. doi:10.1111/j.1745-6584.1999.tb00955.x

Appendix G – Environmental and Economic Assessment of Borehole Thermal Energy Storage in District Heating Systems

Published as:
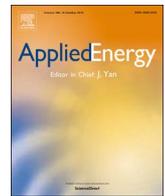
Environmental and economic assessment of borehole thermal energy storage in district heating systems

Bastian Welsch[a,c,*], Laura Göllner-Völker[b,c], Daniel O. Schulte[a,c], Kristian Bär[a], Ingo Sass[a,c], Liselotte Schebek[b,c]

[a] Technische Universität Darmstadt, Geothermal Science and Technology, Schnittspahnstraße 9, 64287 Darmstadt, Germany
[b] Technische Universität Darmstadt, Material Flow Management and Resource Economy, Franziska-Braun-Straße 7, 64287 Darmstadt, Germany
[c] Darmstadt Graduate School of Excellence Energy Science and Engineering, Otto-Berndt-Straße 3, 64287 Darmstadt, Germany

HIGHLIGHTS

- Economic and environmental LCA of medium deep BTES in DH generation is carried out.
- Various system compositions and changing boundary conditions are investigated.
- Pareto fronts illustrate optimal system designs with and without BTES.
- Economic and environmental assumptions affect optimal system designs considerably.
- Combinations of BTES, solar heat & a small CHP are competitive with CHP-based systems.

GRAPHICAL ABSTRACT
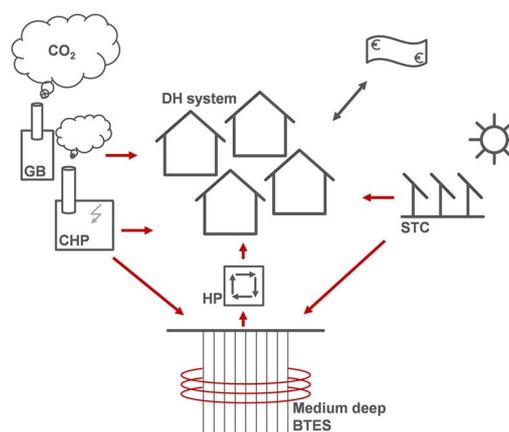
ARTICLE INFO

ABSTRACT

District heating will play an important role for heat provision in temperate and cold climate zones in the future. However, in the context of decarbonizing the heating sector, conventional heat sources have to be replaced by renewable energies. This replacement correlates to the necessity to integrate the fluctuating energy source of solar radiation and thus requires seasonal thermal energy storage. More recently, borehole thermal energy storage systems have been integrated into such district heating concepts. Yet, the potential greenhouse gas emission reduction and the financial benefits of these innovative district heating concepts have not been assessed with respect to the environmental burden and the associated investment cost of the modernization. This study presents a comprehensive environmental and economic life cycle assessment of a fictional district heating system with varying shares of shallow to medium deep borehole thermal energy storage and alternative heat sources replacing conventional capacity. In an exemplary district heating system covering 25 GW h of annual heat demand, borehole thermal energy storage can decrease the greenhouse gas emissions of combined heat and power plants and solar thermal collectors by over 40%. Boundary conditions assumed for the development of the energy market and the existence of subsidies have a significant impact on the emission savings and the levelized cost of heat. Considering a probable increase of energy costs and a growing share of renewables in the electricity mix, a combination of solar thermal collectors and borehole thermal energy storage with a small heat and power plant is the best solution, which is economical even without subsidies. The results of the study promote the construction of medium deep borehole thermal energy storage systems that can help to increase the share of renewable energy in the heating sector at reasonable cost.

Nomenclature

Abbreviations

BAU	business as usual scenario
BAU SUB	business as usual scenario including subsidies
BHE	borehole heat exchanger
BTES	borehole thermal energy storage
CHP	combined heat and power
DH	district heating
ECO	economic/environmental scenarios
EUA	European Union Emission Allowance
EU ETS	European Union Emissions Trading System
EVO	evolution scenario
EVO SUB	evolution scenario including subsidies
GB	gas boiler
GHG	greenhouse gas
HP	heat pump
LCA	life cycle assessment
P1 – P4	selection of Pareto efficient system designs
SI	supplementary information
STC	solar thermal collector
TES	thermal energy storage

Symbols

A_{STC}	solar collector area, [m^2]
CED	cumulative energy demand, [TJ]
L_{BHE}	length of borehole heat exchangers, [m]
N_{BHE}	number of borehole heat exchangers, [–]
α_{CHP}	coefficient of share of cogeneration in the peak load demand, [–]
EF	emission factor, [kg CO_2eq/kW h]
F	operation costs, [€]
GWP	global warming potential, [t CO_2eq]
I	investment costs, [€]
$LCOH$	levelized cost of heat, [€ct/kW h]
M	maintenance costs, [€]
P	thermal power demand/supply, [kW]
Q	thermal energy demand/supply, [kW h]
R	revenue, [€]
a	year of operation, [–]
r	interest rate, [–]

1. Introduction

By 2050, more than 80% of European residents are expected to live in urban areas [1]. Such populous areas are usually characterized by a high heat density and are therefore particularly suitable for the implementation of district heating (DH) grids. DH is considered an essential component in successfully transitioning to a sustainable and decarbonized heating sector (e.g. [2–6]). For this purpose, a large amount of fluctuating renewable energy sources must be integrated in future DH grids in order to replace conventional heat sources, while simultaneously guaranteeing the security of supply.

The concept of fourth generation district heating (4GDH, [7]) comprises a significant reduction of grid supply temperatures down to 55 °C [8]. Grid losses are thereby lowered and the energy and exergy efficiency is improved [8,9]. Moreover, low-carbon heat sources like geothermal energy or industrial waste heat, which are characterized by low-temperatures, can be integrated more efficiently (e.g. [10,11]).

Another auspicious technology for substituting fossil heat sources in DH grids is large solar thermal collector (STC) fields [12–14]. However, especially in the temperate and cold climate zones, there is a seasonal mismatch between solar supply and heat demand [15]. Seasonal thermal energy storage (TES) systems are able to offset this mismatch, thus increasing the performance of solar thermal heating systems [16] and reducing the required STC size [17].

There are several seasonal TES technologies available (for an overview see [18,19]). However, their requirements are diametrically opposed: high storage capacities are desired, but the costs and the space required need to be minimized [20]. With respect to heat storage on a district level, chemical and latent heat storage solutions are not competitive yet [19]. Only a couple of sensible heat storage technologies meet the requirements for large-scale TES. These can be differentiated into large above-ground water tanks and underground thermal energy storage (UTES) like water or gravel-water pit storage [21,22], cavern storage or aquifer storage [23,24]. Another promising type of UTES are borehole thermal energy storage (BTES) systems [25–27]. BTES utilizes the subsurface as a heat storage medium via a borehole heat exchanger (BHE) array. Even though initial costs are very high for BTES systems, specific costs in relation to the storage capacity are relatively low compared to other storage technologies [13,28]. The functionality of BTES has already been demonstrated in several projects (e.g. [12,29–34]). A basic overview of installed systems and their technology

is given by Gehlin [26]. Recent studies propose the novel concept of medium deep BTES [35–40]. They can reach storage efficiencies of more than 80% [35]. Compared to shallow systems (usually < 100 m in depth), medium deep BTES consist of fewer but deeper BHEs (up to 1000 m). They require less floor area than shallow systems with a similar storage capacity and can significantly inhibit the thermal impairment of sensitive aquifers in the shallow subsurface [41]. Therefore, the utilization of medium deep BTES is more independent of the geological conditions and could lead to a more widespread application of seasonal heat storage. Nevertheless, deeper wellbores require more sophisticated and therefore more expensive drilling methods and the environmental impact of such systems has not been investigated yet. Consequently, uncertain financial implications and vague environmental benefits inhibit their market introduction.

Several studies deal with the optimization or the assessment of DH systems in terms of profitability and/or environmental impact. Most of these studies concentrate on specific technologies like heat pumps (HP) [42–44], combined heat and power (CHP) [5,45,46], the integration of industrial excess heat [47] or energy conservation measures [48–51]. Truong & Gustavsson [52] compare different DH production technologies under changing economic or environmental boundary conditions but do not include any TES in their considerations. Certainly, some valuable publications already address the integration of solar thermal technology into DH systems in combination with heat storage (e.g. [16,53–59]). But they either concentrate on specific case studies, look at economic or environmental impacts only or disregard potential changes in the economic or environmental boundary conditions. With a few exceptions (e.g. [60]), most studies assessing the environmental impacts of DH heat production only take into account the use phase. Tulus et al. [61] is the only study that combines an economic and environmental life cycle assessment (LCA) to optimize central solar heating plants including a seasonal TES. Their results show that optimally sized solar thermal storage systems can significantly reduce both costs and environmental impact, compared to a gas-fired boiler (GB). However, their case study did not consider the effects of changing economic and environmental boundary conditions. It lacks a combination of BTES with CHP as well as a comparison to CHP technology, which has a much higher relevance in future DH grids than GB. Furthermore, they only take into account water tank storages, which differ significantly in their behavior and economics from BTES systems.

Accordingly, a comprehensive study, comprising an economic and an environmental LCA of different heating concepts for DH systems under different economic and environmental boundary conditions, is missing. Moreover, the financial and environmental effects associated with the integration of BTES into district heating concepts have not been jointly addressed so far. Thus, we present a dedicated economic and environmental life cycle analysis of district heating concepts integrating shallow to medium deep BTES. Several BTES-assisted heat generation plant options for DH systems, including GB, CHP and STC, are assessed with respect to their levelized cost of heat (*LCOH*) and their global warming potential (*GWP*), and are compared against reference heat generation scenarios without seasonal TES. In addition to solar thermal energy, surplus heat from a CHP, which is usually driven in heat-match mode, is considered for BTES charging as well.

2. Methods

The economic and environmental impacts connected to district heating concepts that include medium deep BTES were evaluated for a synthetically generated district heating load profile with an annual heat demand of 25 GW h by conducting the following steps:

1. Definition of boundary conditions: Seven system combinations of the considered heat generation technologies were assembled for comparison of options (Fig. 1), including four combinations without any seasonal TES and three including a BTES system. To compare these seven technical combinations, four environmental and economic scenarios (ECO scenarios, Table 1) were developed.
2. Model implementation: based on the selected heat generation options, an integrated energy balance and economic/environmental assessment model was developed, which considers the various economic and environmental boundary conditions. The environmental burdens were ascertained in terms of an LCA.
3. Parameter study: the system components CHP, STC and BTES were varied in size and the economic and environmental effects of the generated variants for the four ECO scenarios were calculated. The analysis of the acquired data was performed in two consecutive steps: Firstly, an **identification of Pareto efficient system**

combinations and designs was conducted. Secondly, a **case analysis** was carried out, in which a selection of four of the previously identified Pareto efficient system designs were compared in detail to demonstrate economic and environmental effects of seasonal TES against reference scenarios. They serve as a measure for the performance of the respective BTES-assisted heat generation plant design.

4. Sensitivity analysis: at the end, a comprehensive sensitivity study was carried out on the four selected heat generation systems in order to determine the influence of different variables on the *LCOH* of the four selected Pareto efficient system designs.

As the following subchapters can only give a summary of these steps, much of the detailed information has been omitted. However, more on the methodology is given in the attached supplementary information (SI) file (Appendix A).

Table 1
Economic and environmental scenarios.

Scenario	Gas price [ct/kW h]	Electricity price for CHP feed-in [ct/kW h]	Electricity price for industry [ct/kW h]	Emission factor grid electricity [g/kW h]	Subsidies included
BAU	3.08[a]	3.66[b]	13.08[c]	532[d]	
BAU SUB	3.08[a]	3.66[b]	13.08[c]	532[d]	✓
EVO	Projected[e] (4.59)	Projected[e] (6.59)	Projected[e] (14.34)	Projected[f] (322)	
EVO SUB	Projected[e] (4.59)	Projected[e] (6.59)	Projected[e] (14.34)	Projected[f] (322)	✓

[a] Average gas price for industry in Germany 2015 [64].
[b] 3.16 ct/kW h average price for baseload power at the European Power Exchange EPEX spot 2015 [65] plus 0.5 ct//kW h for avoided grid charges.
[c] Average value for 2015 [64].
[d] Current German electricity mix [62].
[e] 30 year time series starting at BAU value and ending at the given value in brackets, based on [63], (see SI 2).
[f] 30 year time series starting at BAU value and ending at the given value in brackets, determined according to [62], (see SI 2).

Fig. 1. Technical reference and storage scenarios.

2.1. Boundary conditions

2.1.1. System components and combinations

As a basic assumption, a DH system with a GB was considered. The DH grid was not specified in detail. It was only represented by a synthetically generated hourly heat load demand curve with an annual heat demand of 25 GW h (see also Section 2.2.1) and a constant supply temperature of 55 °C. Seven different combinations (Fig. 1) consider the partial replacement of the GB's heat supply capacity with the following three components and their combinations: a CHP, an STC field and a medium deep BTES, which is assisted by a heat pump (HP). In the first three system combinations, the heat demand was satisfied without any seasonal TES. These combinations represent the heat generation in conventional district heating systems, whereas the latter three combine the respective conventional heat generation options with a HP-assisted BTES. The size of the individual components CHP, STC and BTES in the respective combinations may vary in size, influencing the outputs significantly. However, all system combinations still comprise a GB, which is dimensioned to cover the residual load and providing back-up capacity. The HP, which is connected to the BTES system, was sized according to the capacity of the storage. It is needed to yield the required grid supply temperature from the BTES.

2.1.2. Environmental and economic scenarios (ECO scenarios)

To fulfill the life cycle approach, the environmental burdens and costs of the production (for more details see Sections 2.2.2 and 2.2.3) and use phase of the identified components were evaluated. During the use phase, several assumptions regarding prices and the electricity mix influence the results. Therefore, two of the four ECO scenarios investigated the effects of steady prices and emission factors (business as usual, BAU scenarios) in comparison to a hypothetical price development and the projected reduction of the grid electricity emission factor due to an expected increasing share of renewables in the grid mix (evolution, EVO scenarios).

Since circumstances vary from country to country, it was not possible to define boundary conditions, which are universally valid. Due to the good data availability, the ECO scenarios in this study are based on the German energy environment.

2.1.2.1. BAU scenario.
In the BAU scenario (see also Table 1) a constant gas price of 3.08 ct/kW h was assumed, whereas the CHP-produced electricity can be sold to the grid for 3.66 ct/kW h. If the system combination lacks a CHP, external electricity has to be purchased, which is charged with an electricity tariff for industry of 13.08 ct/kW h. As the CHP replaces existing electricity production, the CO_2 emissions of the cogenerated electricity were derived from the *Gemis 4.93* database [62] considering the current German electricity mix.

2.1.2.2. EVO scenario.
Based on the predictions by Schlesinger et al. [63], the EVO scenario anticipates a development of the prices and the German electricity mix. The respective CO_2 emission factors were determined according to *Gemis 4.93* [62]. A figure showing the assumed time series of the annual energy prices and the emission factor of the electricity mix is provided in the supplementary (see SI 2).

2.1.2.3. BAU SUB & EVO SUB scenarios.
Germany offers several state subsidies for the deployment of CHPs, renewable energies and TES that can be exploited. Therefore, these subsidies were taken into account in two sub-scenarios (BAU SUB & EVO SUB) complementary to the other ones (Table 2).

Costs for European greenhouse gas (GHG) emission allowances (EUA) were not factored in, since the *European Union Emissions Trading System* (EU ETS) only applies to combustion plants exceeding a rated thermal input of 20 MW, which is clearly beyond the regarded system size.

Table 2
Subsidies considered in scenarios BAU SUB and EVO SUB.

System	Public funding line	Amount
CHP	German Act on Combined Heat and Power (KWKG 2016) [66]	Continued support of 30,000 full load hours: 3.1 Cent per kW h of electricity sold to the grid
BTES	German Act on Combined Heat and Power (KWKG 2016) [66]	30% of investment cost
STC	KfW (German Promotional bank) program: "Renewables Energy Premium" (KfW 2016) [67]	Investment support: 40% of investment cost

2.2. System modelling

The heating system analysis required a model (Fig. 2) that calculates the system response based on the size of the different components (system design). For each system design, the system response was evaluated in terms of costs and environmental effects according to the underlying ECO scenario. Since the DH grid itself is assumed to be identical for all system designs, it was excluded from the assessment. In the following, the three steps of the assessment are explained in detail.

2.2.1. Heating system model

The DH system was modeled on the basis of an energy balance calculation, which was implemented in MATLAB 2016 [68]. It considers an urban quarter with 40% single family homes, 40% multi-family homes and 20% commercial buildings. Ambient temperature data from a test reference year dataset of Germany (BBR [69], medium weather conditions, region 12) were used to generate an hourly heat load curve with a total annual heat demand Q_{DH} of 25 GW h for a 30 year valuation period (see supplementary information SI 1).

The design of the heat generation system is defined by three input variables:

- Size of the CHP, characterized by the coefficient of share of cogeneration α_{CHP}
- Size of the STC field, characterized by the collector area A_{STC}
- Size of the BTES, characterized by the length L_{BHE} of the BHEs, while the number N_{BHE} of BHEs is kept constant at 37[1].

Based on these parameters, the required sizes of the GB and the HP were determined automatically, always guaranteeing to supply the 25 GW h of heat.

For every hour of the simulation period the heat balance was calculated according to the supply and demand curves. The balance equations (see SI 3) define, whether a component of the system is producing heat or not and whether the seasonal storage system is charged or discharged. An explicit order of priority for the feed-in of different heat sources into the DH grid was predefined: if available, solar thermal energy has priority over cogenerated heat. This ensures that the most environmentally friendly heat is utilized first. Then cogenerated heat, which has a higher exergy, is favored over the low exergy heat from the storage system. Ultimately, excess production of cogenerated heat and heat from the GB has to be avoided. Consequently, these systems may have to operate in partial load.

The hourly values of the thermal power P of each technology are determined in the energy balance model and are used to determine the hourly natural gas consumption of these technologies as well as the electrical power output of the CHP. Furthermore, the auxiliary electricity (for example, for the operation of circulation pumps and the heat pump) is determined according to either the components' size or the

---

[1] The number of 37 BHEs originates from a circular alignment of the BHEs (cf. Welsch et al. [12]).
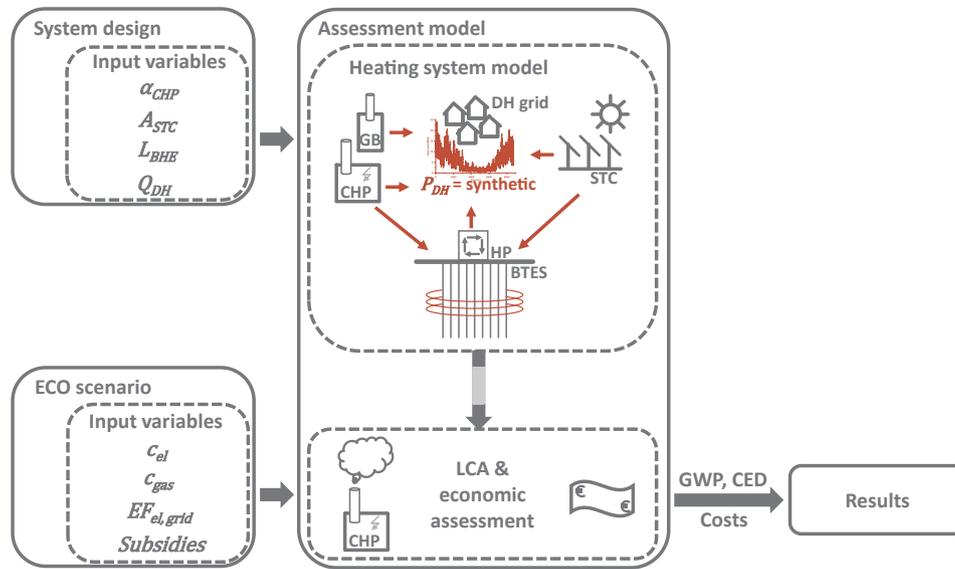
Fig. 2. Schematic illustration of the assessment model.

power values. Detailed information about the modelling of the system components, the calculation of the energy consumption and supply of each technology is given in SI 3. Additional references and datasets that are used in the heating system model are listed in Table 3.

The cost analysis and the LCA were based on annual energy amounts. For this purpose, the sum of the respective hourly power values for each system component or energy source P provides the annual energy amounts Q_a:

$$Q_a = \int P dt \tag{1}$$

2.2.2. Economic assessment

The economic output of the system configurations was compared using the approach of *LCOH* (cf. [70,71]). The *LCOH* represents the financial mathematic average for the specific cost of heat in euro cent per Kilowatt-hour over the assumed valuation period a_{end}. It was calculated from the net present value, which consists of the investment costs I, maintenance costs M, operation costs F (i.e. fuel/electricity costs), the revenue R of the system and the assumed interest rate r, and is divided by the system's discounted thermal energy output Q:

$$LCOH = \frac{\sum_{a=0}^{a_{end}} (I_a + M_a + F_a - R_a) \cdot (1 + r)^{-a}}{\sum_{a=0}^{a_{end}} Q_a \cdot (1 + r)^{-a}} \cdot 100 \tag{2}$$

Investment costs only arise at the beginning $a = 0$. If the valuation period a_{end} exceeds a component's lifetime, the respective investment cost can occur more than once. In return, a residual value was deducted at the end, if the period under consideration is exceeded by a component's lifetime. Detailed information about the cost elements of the various system components and their calculations can be found in SI 4. Further references and datasets that are used in the economic analysis are listed in Table 3.

2.2.3. Life cycle assessment

The environmental impact of DH systems is composed of GHG emissions during the operation, and also related environmental effects during the production and the implementation of system components as well as their disposal. LCA, as specified in the standards ISO 14040/44 [72,73], is a method for weighting the environmental effects of product systems. In this study, the OpenLCA software [74] was employed to compile the environmental effects resulting from the production

process of the regarded system components. For this purpose, the following databases were incorporated: *ecoinvent 3.1 cutoff* [75], *GaBi 5* [76] and *Gemis 4.93* [62].

2.2.3.1. Goal and scope definition. The LCA conducted within this study allowed for a comparison of environmental burdens of different district heating concepts. In this context, the functional unit was defined as 25 GW h heat annually delivered to the DH grid for 30 years. It was assumed that the DH system is located in Germany. Transportation of goods was only considered in terms of raw material transport, which has already been taken into account in the applied datasets. Transportation from the production site to the buildings was not included as it is expected to have only a minor effect on the overall results. Aside from that, the disposal phase (end-of-life) of the components was disregarded as well. This is a common practice in many LCA: firstly, it is assumed that the impact of the disposal phase is negligible compared to the production and use phase, and secondly, recycling processes may advance and are therefore difficult to predict. Another argument for this approach is that subsurface installations of BTES systems have a much longer life than 30 years, and reliable data about the dismantling of BTES is not available yet.

2.2.3.2. Life cycle inventory (LCI) and impact assessment (LCIA). Initially, several datasets were compiled, which describe the environmental impacts connected to the production phases of the respective system components. Subsequently, the applicability of this

Table 3
Further datasets and references applied in the three submodels of the assessment tool sorted by the respective system component.

	Heating model	Economic model	LCA	
			Production	Use Phase
STC	[68,69,78]	[79]	[75,79]	[62]
CHP	[80–82]	[80]	[75]	[62]
BTES	[35]	[83]	[75,83]	[62]
HP	[84]	[85]	[75,86]	[62]
GB		[87]	[75]	[62]

data was evaluated. Finally, suitable datasets were adapted for our approach. They were normalized to either the nominal power (CHP, GB, HP) or the size (STC, medium deep BTES) of the respective component in order to facilitate the inclusion of the LCA data into the assessment tool. The environmental impact during the use phase essentially results from natural gas combustion and electricity consumption. Therefore, these burdens are assessed on the basis of the gas and electricity consumption of the respective system component.

The midpoint impact category of global warming potential (*GWP*) according to CML 2001 [77] was chosen to evaluate the environmental burdens. In addition, the cumulative energy demand (*CED*) was appraised. However, the focus was set to the *GWP*, as the differences between *GWP* and *CED* are only marginal in the systems assessment. Additionally, the emission factor (*EF*) $\left[\frac{kgCO_2eq}{kWh}\right]$ was evaluated to allow for comparison with differently sized systems. The *EF* is defined as the ratio of summarized *GWP* values for production and operation of each component and the overall heat production of the according system:

$$EF = \frac{GWP}{Q_{th,tot}} = \frac{1}{Q_{th,tot}} \cdot \sum_{i=1}^{n} \left(GWP_{prod,i} + \sum_{a=1}^{a_{life}} GWP_{a,op,i} \right) \tag{3}$$

Detailed information about data sources and handling as well as the calculation of the environmental impact of the different system components is given in SI 5. References and datasets used in the LCA are listed in Table 3.

2.3. Parameter study

The three technical components CHP, STC and BTES were varied in size and combined to a full factorial experimental design, as illustrated in Table 4, resulting in 9241 different system designs. For each of these system designs the *LCOH* and the *GWP* were calculated (Fig. 4).

The analysis of the results is divided into two steps (see also Fig. 3):

- Identification of Pareto efficient system designs
- Case analysis

In the first step, the best of the sampled system designs were determined for each configuration and ECO scenario. Subsequently, selected optimal designs were compared across different ECO scenarios in order to illustrate advantages and disadvantages of the integration of medium deep BTES into DH concepts under various boundary conditions.

2.3.1. Identification of Pareto efficient system combinations & designs

The search for an optimal system design represents a multi-objective optimization problem, composed of two generally independent

objective functions. More specifically, the most economic heating supply system is usually not the system with the lowest global warming potential. Instead, several Pareto efficient solutions exist. Each of them represents a system design, for which neither the *GWP* nor the *LCOH* can be improved without impairing the other. Thus, the first step deals with the identification of Pareto efficient system designs for all scenarios and combinations under consideration.

28 different sets of Pareto efficient system designs can be identified for the relevant combinations of the seven technical configurations and the four ECO scenarios. Three characteristic Pareto efficient system designs were identified for each of the sets where possible (for some, optimization resulted in a single optimal solution). These subsets consist of the system designs with the minimum *LCOH*, the minimum *GWP* and a compromise solution.

The former two represent the Pareto efficient solutions to the multi-objective optimization problem:

$$\min_{L_{BHE}, A_{STC}, \alpha_{CHP} \in R} LCOH(L_{BHE}, A_{STC}, \alpha_{CHP})$$
$$\min_{L_{BHE}, A_{STC}, \alpha_{CHP} \in R} GWP(L_{BHE}, A_{STC}, \alpha_{CHP})$$
subject to
$$0 \leqslant L_{BHE} \leqslant 1000$$
$$0 \leqslant A_{STC} \leqslant 100,000$$
$$0 \leqslant \alpha_{CHP} \leqslant 1 \tag{4}$$

The compromise solution is defined as the point, where the reduction of *GWP* equals the increase of the *LCOH*. It represents a system design, which achieves a relatively large reduction in the *GWP* associated with only a moderate increase in the *LCOH*.

2.3.2. Case analysis

A selection of compromise solutions for four specific system combinations labeled P1–P4 was chosen for a detailed analysis and comparison of the environmental and economic effects induced by BTES systems (Table 5). The Pareto efficient system identification (see Section 3.1.1) revealed that BTES systems are most favorable when assuming progression scenarios (EVO & EVO SUB). However, subsidies are a regional regulatory procedure that manipulates the results to some extent. For this reason, the four cases, P1 to P4, were selected from the compromise solutions of EVO (see Table 6). The case analysis comprises a comparison of all ECO scenarios on the example of these four system designs. It should be noted that they are not necessarily Pareto optimal designs in a scenario other than EVO.

P1 consists of a CHP ($\alpha_{CHP} = 35\%$) and a GB representing a conventional DH system. P2 illustrates the effects of adding an STC field with an area of 20,000 m² to P1. P3 and P4 both consider a medium deep BTES system for seasonal storage of STC heat. P3 additionally includes a small CHP with $\alpha_{CHP} = 5\%$ for self-supply of electricity.

Table 4
Variation of the technical input parameters.

	α_{CHP} [%]			A_{STC} [m²]			L_{BHE} [m]			n
	Range		Interval	Range		Interval	Range		Interval	
	Min	Max		Min	Max		Min	Max		
GB-only	0	0	–	0	0	–	0	0	–	1
CHP	5	100	5	0	0	–	0	0	–	20
STC	0	0	–	5000	100,000	5000	0	0	–	20
CHP + STC	5	100	5	5000	100,000	5000	0	0	–	400
CHP + BTES	5	100	5	0	0		0	1000	50	400
STC + BTES	0	0	–	5000	100,000	5000	0	1000	50	400
CHP + STC + BTES	5	100	5	5000	100,000	5000	0	1000	50	8000
									Sum	9241[a]

[a] The 20 system designs consisting of a GB and a BTES were removed, as the combination of a GB and a BTES system is illogical from an energetic, environmental and economic point of view.
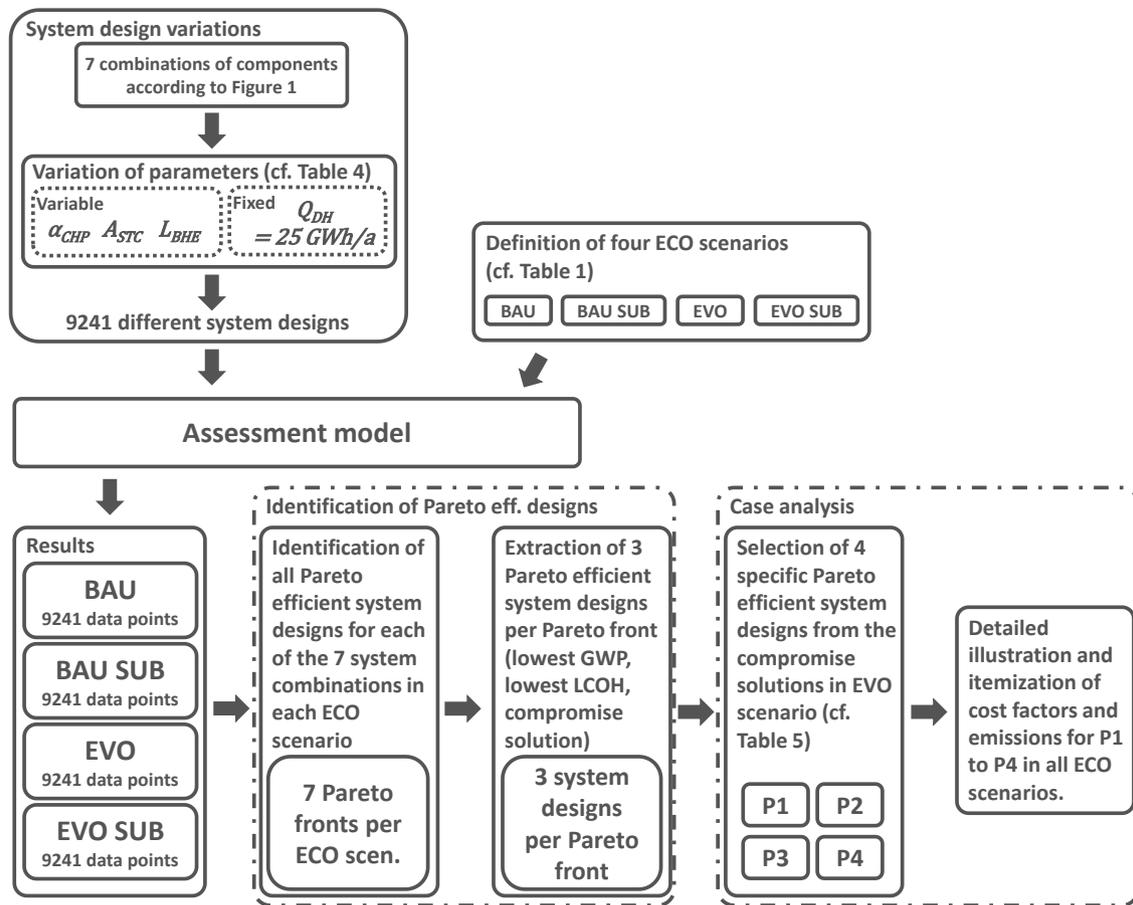
Fig. 3. Schematic illustration of different steps of the parameter study.

2.4. Sensitivity analysis

Finally, the influence of the most important cost factors on the *LCOH* was assessed in a sensitivity analysis to give an estimate of the uncertainty of the results. It was carried out as an OAT (one-at-a-time) analysis in which one single parameter was varied after another with reference to a base case. It assessed the influence of the investment costs, the energy costs and the interest rate on the *LCOH*. The BAU scenario was taken as a basis and the sensitivity was evaluated for the selected compromise solutions of the system configurations determined before (P1–P4).

3. Results

3.1. Parameter study

In the different technical combinations[2] and ECO scenarios under consideration, the *LCOH* ranged from approximately 3.6 ct/kW h (assuming BAU SUB) to almost 10.43 ct/kW h (expecting EVO) (Fig. 4). The total *GWP* for the production phase and 30 years of operation varied between 67,000 t CO_2eq and 215,000 t CO_2eq, mostly depending on the technical scenario and the size of the subsystems (Fig. 4). This corresponds to an average emission factor *EF* of 90 g CO_2eq/kW h to 290 g CO_2eq/kW h. These variations in heat price and GHG emissions illustrate that the economic and environmental evaluation of district heating concepts is highly sensitive to the system design as well as the economic-environmental assumptions made.

---

[2] All system combinations comprise a GB, which covers a certain share of the heat load. Therefore, the GB is not further mentioned when referring to system combinations.

3.1.1. Identification of Pareto efficient system combinations

Fig. 5 displays the Pareto fronts of the six different system combinations and the base case, which are presented for the four ECO scenarios. Table 6 summarizes the respective compromise solutions of the system combinations. The system designs identified as lowest *LCOH* and lowest *GWP* systems are summarized in SI 6.

3.1.1.1. GB-only.
The GB-only base case was invariant and therefore does not constitute a Pareto front. It always obtained the highest *GWP*. As investment costs are relatively low for the GB, the *LCOH* depend mainly on the gas price. As a result, the GB achieved the lowest *LCOH* in BAU. Without any energy price development, other technologies only become competitive if subsidies are introduced (BAU SUB). In EVO and EVO SUB the *LCOH* for the GB rose with the predicted increase of energy costs.

3.1.1.2. CHP.
Replacing GB capacity with a CHP led to a significant reduction of the GHG emissions of up to 54%. These relatively large emission savings are attributed to the high CO_2-credits for replacing electricity in the grid by cogenerated electricity. In BAU the compromise solution with $\alpha_{CHP} = 50\%$ can reduce the *GWP* by almost 53% compared to the base case. However, the reduction of the *GWP* was also associated with rising *LCOH*. With an increasing share of renewables, emission factors of the grid electricity were expected to fall resulting in an impairment of the CO_2-credits associated with the replacement of grid electricity in EVO/EVO SUB. Additionally, an expected increase of the gas price also effected the *LCOH*. Subsidies reduced the *LCOH* below the base case and collapsed the Pareto fronts to a single optimum solution with $\alpha_{CHP} = 55\%$ (BAU SUB and EVO SUB).
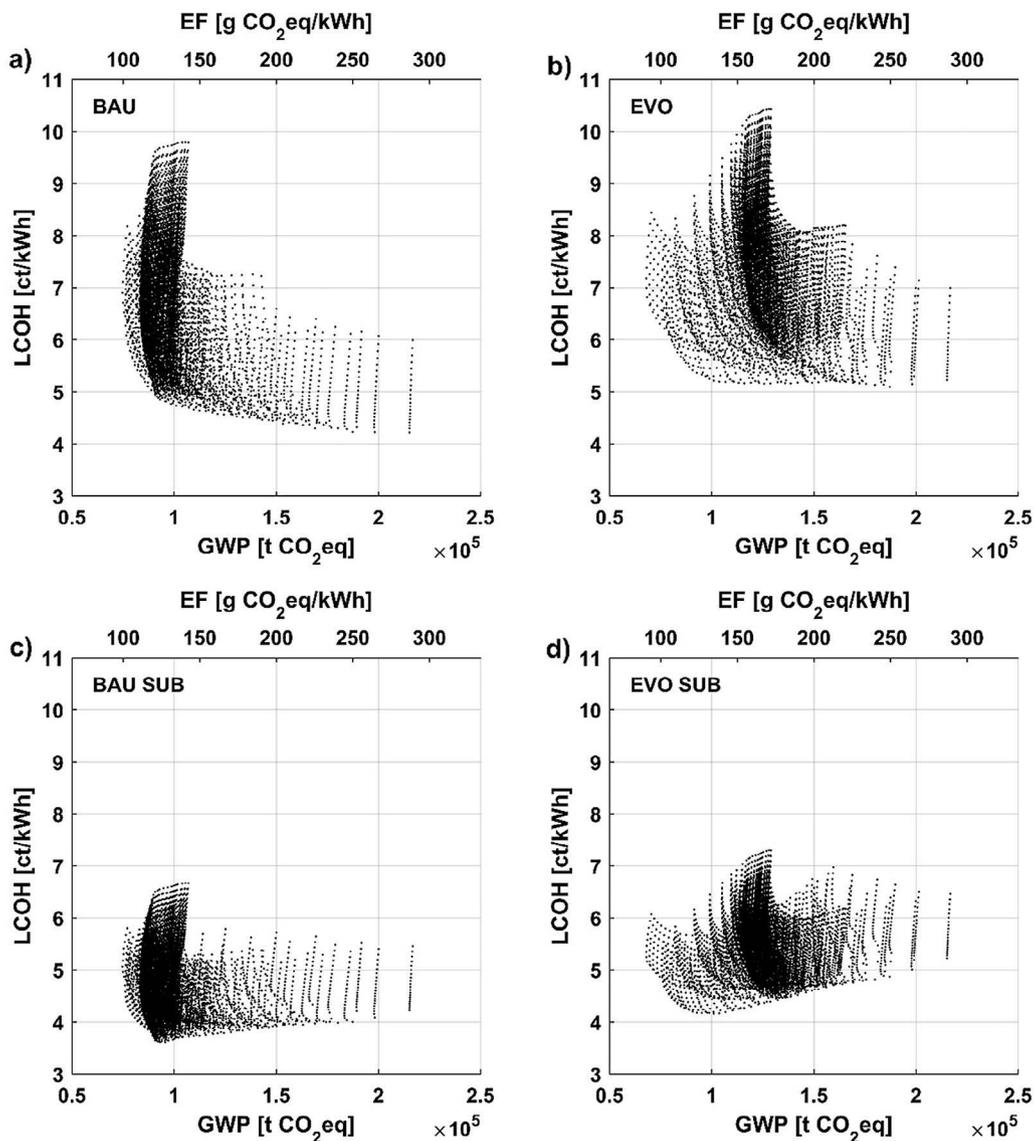
Fig. 4. Total range of *LCOH* and *GWP* for the four ECO scenarios.

Table 5
System combinations chosen for the detailed case analysis.

No	Combination	Share of cogeneration [–]	STC area [m²]	BHE length [m]
P1	CHP (+GB)	0.35	0	0
P2	CHP + STC (+GB)	0.35	20,000	0
P3	CHP + STC + BTES (+GB)	0.05	45,000	650
P4	STC + BTES (+GB)	0	55,000	750

3.1.1.3. STC. Replacing GB capacity with STC can also reduce the *GWP* markedly. Emissions from STC originated from the electricity required for operation, but also to a great extent from the production. Considering an increasing share of renewables in the grid electricity mix, the reduction potential can even exceed CHP systems, if the STC field is large enough (EVO and EVO SUB). However, STC entail high specific investment costs and the heat production of large STC systems exceeds the heat demand during the summer months. Thus, the *LCOH*

increased over-proportionately compared to the achieved reductions in the *GWP*. Subsidies can attenuate the effect (BAU SUB and EVO SUB), but even so, large STC become the most expensive solution. Nevertheless, small STC fields can provide economical *GWP* reductions even without subsidies (BAU and EVO).

3.1.1.4. CHP + STC. In all ECO scenarios, the combination of STC and CHP amplified the reduction of the *GWP* and the *LCOH* with regard to a separate replacement of GB capacity. Due to the aforementioned exponential increase of *LCOH* with STC share, the Pareto optimal systems consist of moderately sized CHP and small-sized STC. An increasing share of renewables in the grid electricity mix and the associated impairment of the CO_2-credits for CHP (EVO and EVO SUB) allowed for slightly larger STC fields (Table 6). Where subsidies were considered (BAU SUB & EVO SUB), the *LCOH* for almost all Pareto optimal CHP + STC systems were competitive compared to the base case: in BAU SUB, the CHP + STC system with $\alpha_{CHP} = 45\%$ and $A_{STC} = 10,000\,\mathrm{m}^2$ even yields the overall lowest *LCOH* of 3.6 ct/kW h with a *GWP* reduction of 56%.

Table 6

Heating system compositions with the compromise solution between lowest *LCOH* and lowest *GWP* for different technical and economical/environmental scenarios.

		GB-only	CHP	STC	CHP + STC	CHP + BTES	STC + BTES	CHP + STC + BTES
BAU	α_{CHP} [–]	0.00	0.50	0.00	0.45	0.50	0.00	**0.05**
	A_{STC} [m^2]	0	0	10,000	10,000	0	50,000	**40,000**
	L_{BHE} [m]	0	0	0	0	50	650	**550**
	$LCOH$ [ct/kW h]	4.22	4.86	4.23	4.81	5.00	5.50	**4.77**
	GWP [t CO$_2$eq]	215,246	101,352	187,423	95,685	100,518	94,852	**98,362**
BAU SUB	α_{CHP} [–]	0.00	0.55	0.00	**0.55**	0.55	0.00	0.50
	A_{STC} [m^2]	0	0	25,000	**10,000**	0	55,000	10,000
	L_{BHE} [m]	0	0	0	**0**	50	700	50
	$LCOH$ [ct/kW h]	4.22	3.68	4.03	**3.62**	3.75	4.37	3.69
	GWP [t CO$_2$eq]	215,246	100,086	169,451	**92,153**	99,424	87,919	92,305
EVO	α_{CHP} [–]	0.00	*0.35*	0.00	*0.35*	0.40	*0.00*	***0.05***
	A_{STC} [m^2]	0	*0*	15,000	*20,000*	0	*55,000*	***45,000***
	L_{BHE} [m]	0	*0*	0	*0*	50	*750*	***650***
	$LCOH$ [ct/kW h]	5.23	*5.75*	5.13	*5.69*	5.95	*6.13*	***5.37***
	GWP [t CO$_2$eq]	215,246	*157,422*	179,943	*133,759*	154,300	*79,204*	***92,767***
EVO SUB	α_{CHP} [–]	0.00	0.55	0.00	0.50	0.55	0.00	**0.05**
	A_{STC} [m^2]	0	0	35,000	25,000	0	55,000	**50,000**
	L_{BHE} [m]	0	0	0	0	50	800	**750**
	$LCOH$ [ct/kW h]	5.23	4.68	4.84	4.51	4.76	4.81	**4.27**
	GWP [t CO$_2$eq]	215,246	151,473	160,671	126,703	151,447	76,845	**86,660**

Bold print highlights the technical system composition with the optimal solution for the respective ECO scenario. Italics denote the Pareto efficient combinations P1–P4 selected for the case analysis (see Table 5).
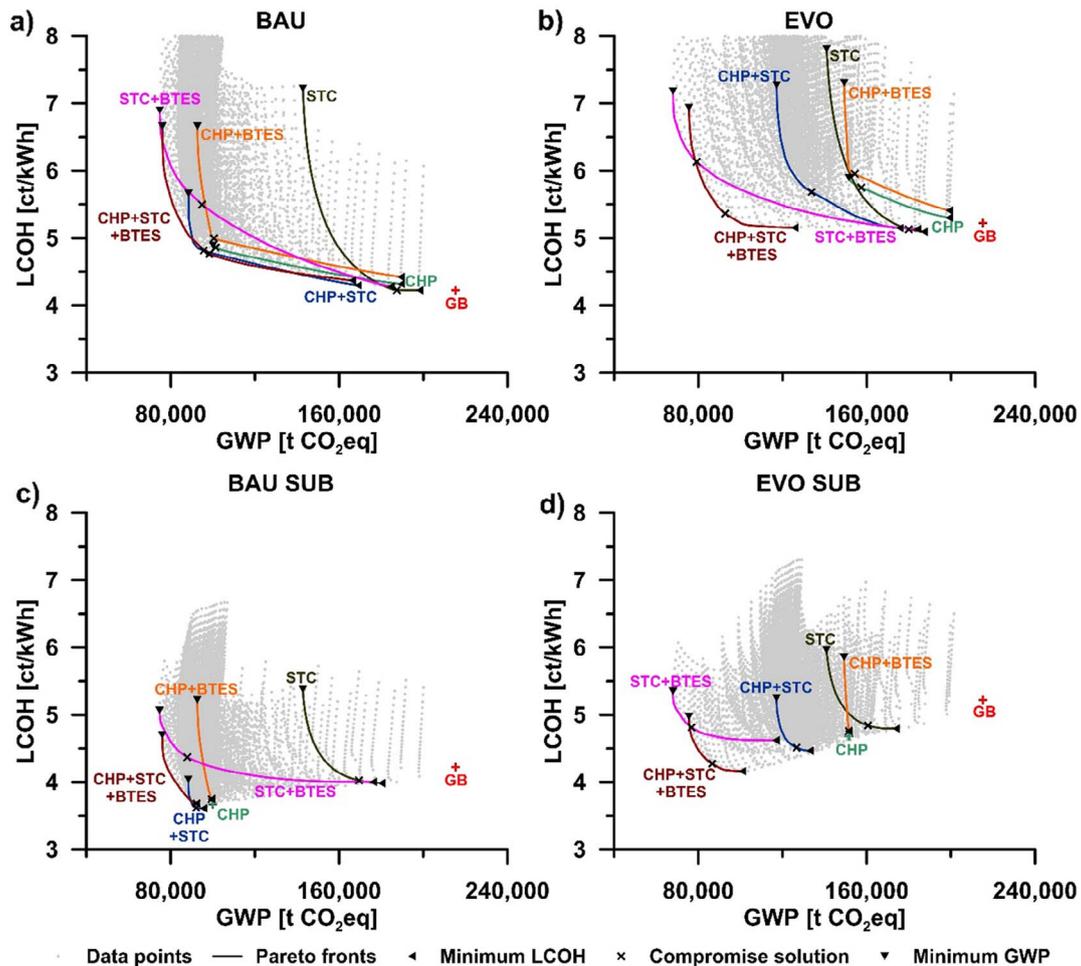
Fig. 5. Comparison of Pareto fronts for the different system compositions for (a) scenario BAU, (b) scenario EVO, (c) scenario BAU SUB and (d) scenario EVO SUB.

3.1.1.5. CHP + BTES. Adding a BTES to the CHP yielded almost no benefits regardless of the considered ECO scenario. Acting as a heat sink, the storage prolonged the running time of the CHP during the summer season, while it provided heat during winter time replacing GB capacity. However, the functional interaction of a heat-matching CHP and a BTES is complex (see Fig. 6a and b): a CHP that is too small does not provide enough thermal energy in summer to charge the storage appropriately, whereas a larger CHP shortens the discharge period and thus restrains the heat provision of the storage. Both cases resulted in inefficient storage operation. Subsequently, the earnings by an increased electricity production were too low to compensate for the high investment costs of the BTES, even when subsidies were taken into account. Hence, any CHP + BTES design was more expensive than the Pareto optimal CHP-only systems and *GWP* reductions attributed to the BTES were characterized by a steep increase in *LCOH* (see Fig. 5a and b). Furthermore, storage losses canceled out the CO_2-credits for replacing grid electricity rendering the reduction of GHG emissions almost insignificant.

3.1.1.6. STC + BTES. In contrast to the fossil fuel burning CHP, STC operation is almost emission-free (see above). Instead of adding a medium deep BTES to CHP, the combination with an STC field therefore entails a strong *GWP* reduction in both BAU and both EVO scenarios. An STC area of $A_{STC} = 70{,}000 \, m^2$ and a BTES with a depth of $L_{BHE} = 1000 \, m$ was the environmentally best system design across all ECO scenarios with the lowest *GWP* of 74,000 t CO_2eq and 68,000 t CO_2eq for BAU/BAU SUB and EVO/EVO SUB, respectively. This corresponds to a reduction of approximately 65% and 68% compared to the base case. The remaining GHG emissions can be attributed to the production and the electricity required for operation, and the GB, which covers the peak load.

Fig. 6c and d illustrate the synergies of STC and BTES systems. Due to the residual heat demand in summer, collector fields that were too small could not generate surplus heat to charge a BTES system. Thus, the integration of storage was only reasonable for solar thermal systems exceeding a critical size (approximately 15,000 m² in this particular case). Then, the integration of a medium deep BTES reduced costs and GHG emissions. Therefore, the capacity of both components had to be
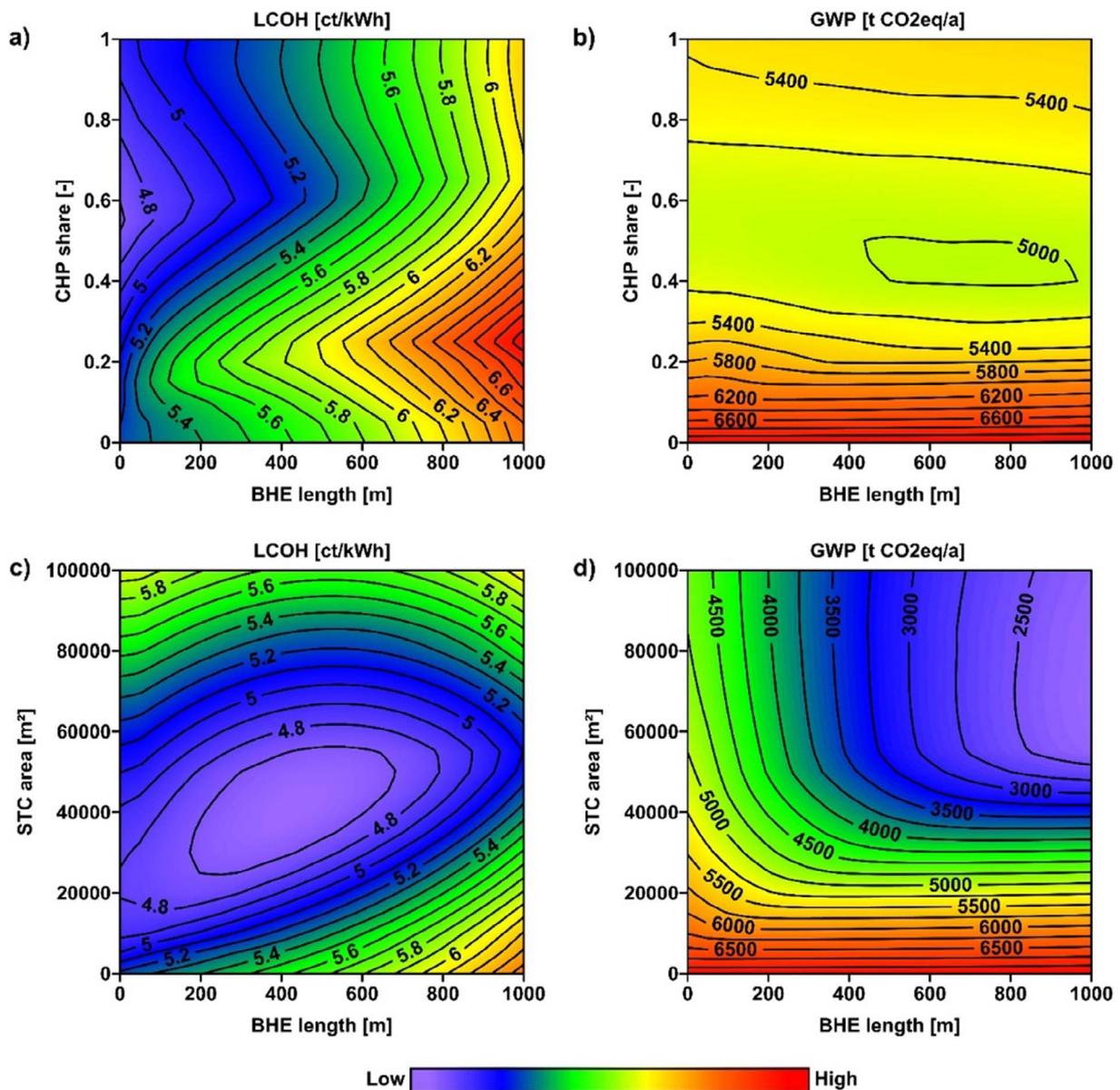
Fig. 6. Influence of the CHP share and the BHE length on the (a) *LCOH* and (b) *GWP*, influence of the STC area and BHE length on the (c) *LCOH* and (d) *GWP*, exemplary for the EVO scenario.

carefully balanced in order to maximize synergies. An oversizing of the STC or the medium deep BTES led to an increase of costs. Consequently, there is a global minimum in *LCOH* for a specific system combination (Fig. 6c) and only a simultaneous increase of the components' size allowed for an additional reduction of the *GWP* (Fig. 6d).

3.1.1.7. CHP + STC + BTES. STC + BTES systems still require a power supply for operation. Adding a small CHP to the STC + BTES combination allowed for the use of self-supplied electricity, which lowered the *LCOH* significantly in all ECO scenarios without straining the *GWP* too much (Fig. 5a–d). Accordingly, Pareto optimal designs typically had a CHP share just sufficient to cover the electricity demand for BTES and STC operation. Only in BAU SUB, subsidies for CHPs had a sufficient effect to allow for a share of $\alpha_{CHP} = 50\%$. Diminishing CO_2-credits for replacing grid electricity in the EVO scenario prohibited large CHP shares, even with subsidies (EVO SUB).

Compared to Pareto optimal CHP + STC designs, the CHP + STC + BTES systems exhibited a comparable *GWP* and *LCOH* in BAU and BAU SUB. In BAU, they even constituted the compromise solution with a slight advance. As high shares of CHP became less attractive with increasing energy costs and decreasing CO_2-credits, the replacement of CHP capacity by STC and BTES with a residual CHP share for self-supplied electricity became more favorable. Thus, CHP + STC + BTES systems represent the best solution in the EVO and EVO SUB scenarios (Table 6).

3.1.2. Case analysis

As subsidies take no effect on the environmental impact, the environmental assessment only considered BAU and EVO. For the economical assessment, the selected cases were analyzed under consideration of all ECO scenarios. This means they are not necessarily Pareto optimal designs in a scenario other than EVO.

The fractions of thermal energy supplied to the DH grid by the different system components for the four cases are displayed in Fig. 7 (averaged over 30 years of production). Although the CHP in case P1 has a share in the peak load demand of $\alpha_{CHP} = 35\%$, it contributes almost 83% of the total heat production. In case P2, the solar thermal energy covers approximately 22% of the annual heat demand. It mainly replaces cogenerated heat, while the share of the GB is only reduced by approximately 2.5 percentage points. In P3, 72% of the annual heat demand can be covered by the BTES-assisted STC field. Approximately 9 percentage points account for the auxiliary power for the HP, resulting in a solar fraction of approximately 63%. The CHP contributes 10% of the annual heat production leaving 18% to be covered by the GB. Sparing self-supplied electricity in case P4 allowed for a larger STC field and a larger BTES to substitute the heat production of the CHP, which increased the combined STC + BTES + HP share to 82% and the solar fraction to 76%.

3.1.2.1. Environmental effects. Generally, the share of solar thermal energy increased from P1 through P4. In BAU, this resulted in a perceptible decrease of the total *GWP* (Fig. 8a): while the integration of an STC field in P2 led to a reduction from approximately 113,000 t CO_2eq to 101,000 t CO_2eq by approximately 11%, adding a BTES in P3 reduced the *GWP* by another 9% to approximately 91,000 t CO_2eq. *GWP* savings of a markedly reduced CHP capacity were mostly equalized by the increase of emitted CO_2-equivalents of the auxiliary systems (GB, HP & circulation pumps for STC and BTES). Sparing the CHP altogether did not require additional GB capacity, but could be replaced by a larger STC field and a larger BTES. Thus, P4 allowed for an additional decrease of the *GWP* of 6% down to 85,500 t CO_2eq compared to P3. In total, the *GWP* declined by 24% from P1 through P4.

In EVO, the decreasing CO_2-credits for cogenerated electricity scaled up the *GWP* of CHP-provisioned heat. This amplified savings resulting from the replacement of CHP capacity (Fig. 8d): thereby, the STC decreased the *GWP* from almost 157,500 t CO_2eq to approximately 134,000 t CO_2eq by 15% in P2. Adding a BTES in P3 reduced the CHP share in the total heat production to only 10% and improved the *GWP* by 31% to approximately 93,000 t CO_2eq. Excluding the CHP altogether in P4 reduced the *GWP* by another 15% to approximately 79.000 t CO_2eq, which equals a reduction in the *GWP* of almost 50% compared to case P1.

By comparison, the *CED* behaves similarly to the *GWP* (Fig. 8b & e): with regard to P3 and P4, the CHP-dominated cases performed relatively better in BAU and worse in EVO. As a result, the reduction in the *CED* from P1 to P4 in EVO equates to approximately 53%, but only 21% in BAU.

The positive impact of enlarging the solar capacity and the storage capacity was slightly compromised by the relatively high *GWP*, which is associated with the production of the collectors and the BTES system (see Fig. 9). In combination with the generally decreasing total *GWP* from P1 through P4, this led to a notable increase in the significance of the production process in the total *GWP*, which is depicted in Fig. 8c & f.

3.1.2.2. Economic effects. In general, investment costs increased from P1 through P4 (Figs. 10a & 11), whereas operating costs and electricity sales decreased (Figs. 10b–d & 11). A comparison of the cases across all ECO scenarios illustrated the effects of the different boundary conditions (Fig. 11). Firstly, the increasing energy prices in EVO and EVO SUB raised the *LCOH* of all systems. Despite the growth in electricity sales (Fig. 10c and d), the fossil fuel-dominated cases P1 and P2 were affected most with an increase of 1.00 ct/kW h and 0.80 ct/kW h, respectively (Figs. 10d, 11). P3 and P4, on the other hand, were affected significantly less with a rise of 0.40 ct/kW h and 0.35 ct/kW h, respectively. Secondly, subsidies decreased the *LCOH*. They affected the sale of cogenerated electricity, as well as the investment costs for STC and BTES. Therefore, the resulting reduction depended on the capacities of the different system components (see Fig. 7 versus Fig. 11). However, despite the almost equal share of subsidizable heat production in all four cases, the *LCOH* reduction increased from approximately 0.82 ct/kW h in P1 to over 1.36 ct/kW h in P4, which implies that subsidies for STC and BTES investment outweighed subsidies for CHP electricity sales. P2 and P3 showed almost equal *LCOH* reductions of around 1.18 ct/kW h. In P3, most of the cogenerated electricity was used for self-supply. Accordingly, it was not subsidized.
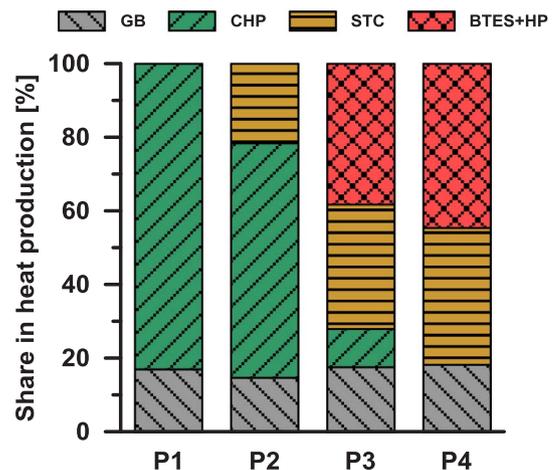
Fig. 7. Share in average annual heat production of the different system components.
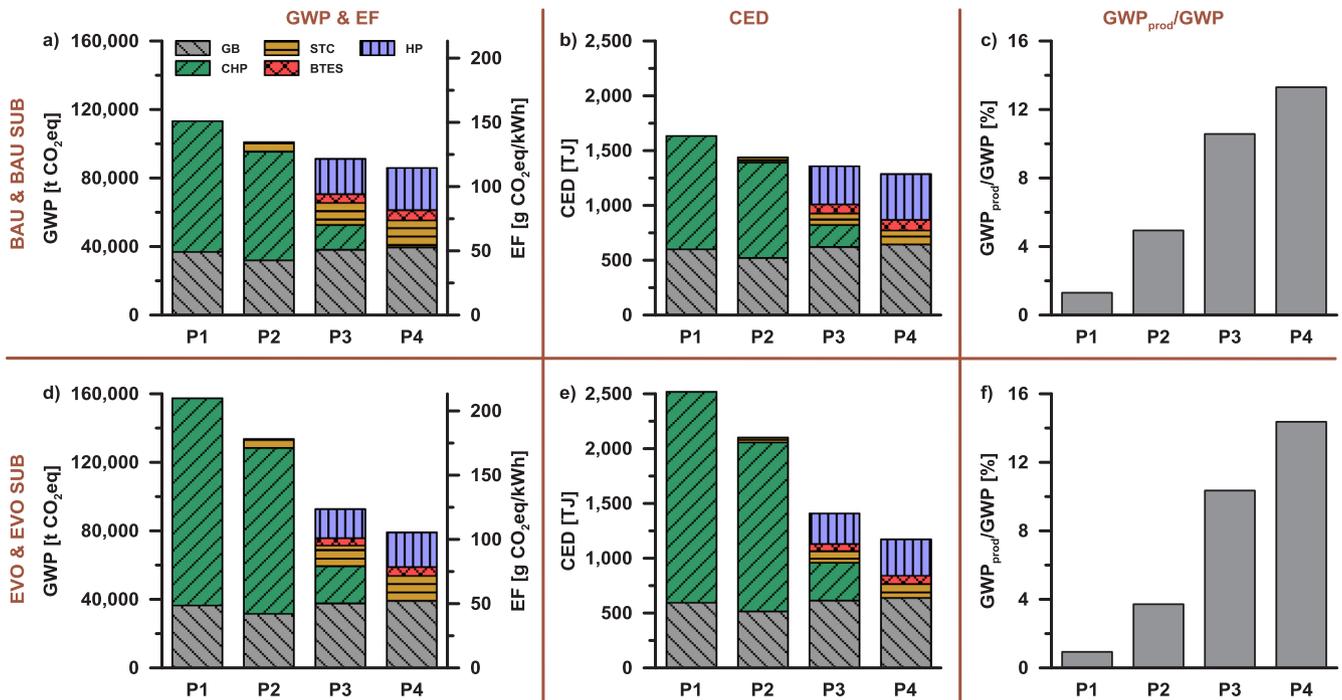
Fig. 8. Comparison of *GWP* (a + d), *CED* (b + e) and share of *GWP* associated with the production process in the overall *GWP* (c + f) for the four selected system designs and BAU and EVO, respectively.
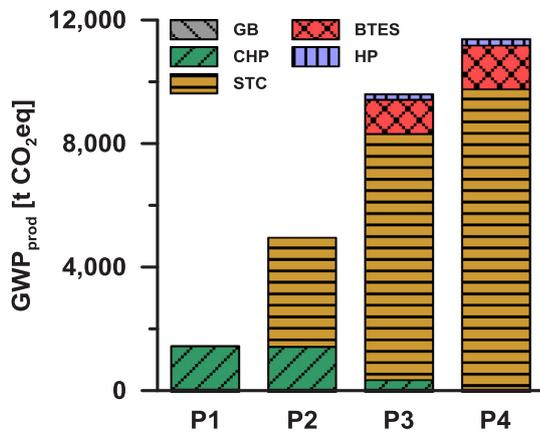
Fig. 9. *GWP* accounted to the production phase of each system component for the four scenarios under consideration.

3.2. Sensitivity analysis

For a sensitivity analysis of the *LCOH* in BAU, investment and energy costs were varied by up to 20% (Fig. 12). Differences between the four cases P1 to P4 indicate the sensitivity's dependency on the system composition. The results agree with the general correlation between the sensitivity and the operation-to-investment-cost ratio: the production of systems with a large STC and BTES share in the total heat supply was more expensive than CHP and GB-dominated systems. Thus, the *LCOH* can change by 0.92 ct/kW h and 1.08 ct/kW h in P3 and P4, respectively, if the investment costs vary by 20%. On the contrary, in P1 and P2 the *LCOH* only changed by 0.09 ct/kW h and 0.36 ct/kW h, respectively.

Inversely, a large share of operation costs in the *LCOH* resulted in a strong dependency on the energy prices. Despite the positive effect of electricity sales, the *LCOH* of CHP and GB-dominated systems was more sensitive to variations in energy costs. Assuming a coupled variation of the electricity price and the gas price by 20%, the *LCOH* can change by 0.73 ct/kW h and 0.59 ct/kW h, in P1 and P2 respectively, whereas P3

and P4 were only affected by changes of 0.29 ct/kW h and 0.36 ct/kW h, respectively.

4. Discussion

4.1. Limitations

The model-based study of complex systems, such as DH grids, requires many simplifications and assumptions, not only because of computational limitations, but mainly because too much detail in the model results in too much noise, which can obscure meaningful results. In order to investigate the impact of some of the adjusting parameters, other potentially influential variables have to be disregarded to suppress the effects of interdependencies.

Firstly, most simplifications result from a lack of adequate cost and LCA data for some of the system components. Particularly the LCA databases used for the environmental burdens were not designated for the dimensions of some of the system components. Thus, the study relies on values extrapolated from smaller units. For STC fields and HP, these extrapolations are linear and positive scaling effects were not taken into account. Moreover, there is no real field data available for BTES at all. They had to be compiled from data of the employed materials and estimates for fuel consumption. Despite these shortcomings, this is a conservative approach that does not overestimate the environmental benefits of the respective renewable technologies.

Secondly, the modelling of the DH system based on an energy balance is sensitive to errors. As a major simplification, the approach assumes that the thermal energy can always be transferred completely, not considering the fluid temperatures of the respective heat source and the grid. This means that the transfer of thermal energy is always in agreement with the first law of thermodynamics, but the model does not check for consistency with the second law. However, in this context the approach is expected to be viable: grid temperatures are relatively low as well as the return temperatures of the BTES. Consequently, the GB, the CHP and the STC are expected to generate fluid temperatures that are always high enough to ensure the feed-into the grid or the BTES. As the HP energy consumption is particularly sensitive to the
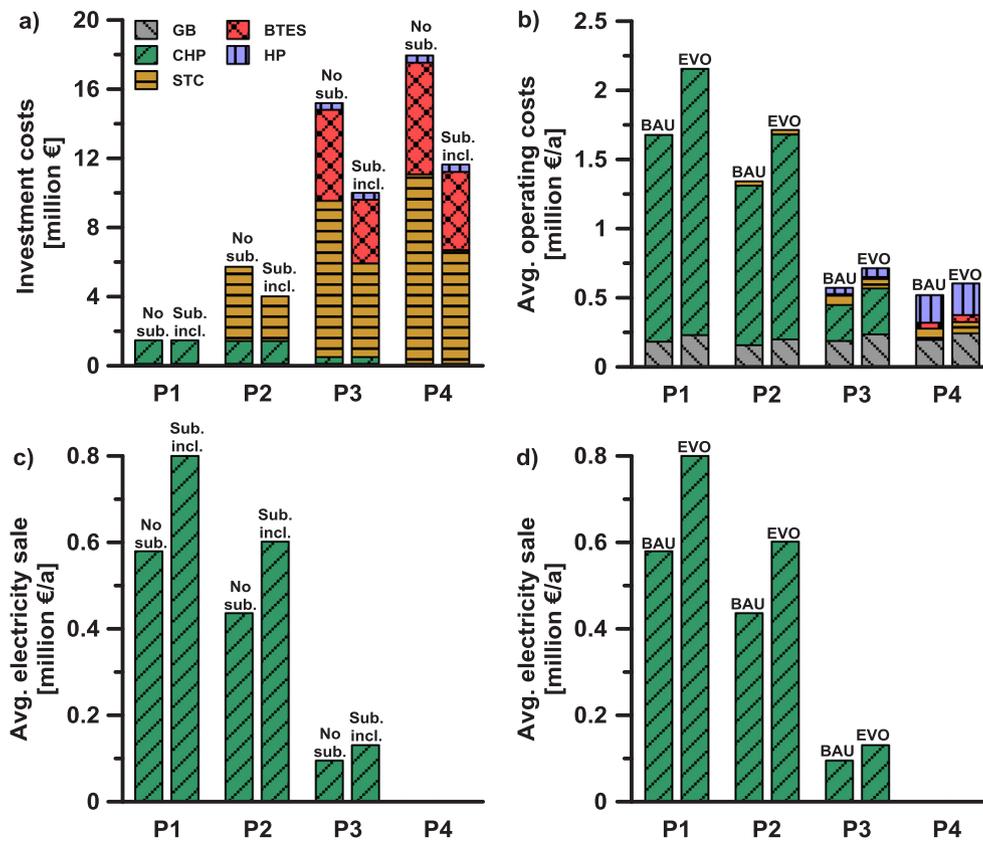
Fig. 10. Comparison of (a) investment costs, (b) average operating costs and (c + d) average electricity sale for the four selected system designs and different ECO scenarios.

BTES outlet, temperature cannot be disregarded for this particular subsystem. Realistic values for the BTES outlet temperature were determined by simulations to calculate a temperature-dependent coefficient of performance (see SI 3).

Lastly, the model disregards the distribution network of the DH grid. The production and operation of the grid itself can have a significant impact on the *LCOH* and the *GWP*. Nonetheless, as the heat demand remains unchanged, the impact is assumed to be the same for all systems and scenarios. A comprehensive model would have to consider the variabilities and possible saving potentials in the distribution network and in the heat demand at the end-consumer's level. However, this study focuses on the environmental and economic assessment of the heat-generating system components, especially of medium deep BTES. Disregarding the details of the DH grid and the end-consumers admittedly represents a simplification, but it eliminates noise irrelevant to the study from the results.

Aside from these simplifications, many assumptions are required to obtain meaningful results. Most assumptions are reflected in the different ECO scenarios. This includes subsidies, energy prices and the future energy mix in the electricity grid. Evidently, these assumptions are subject to uncertainty, which is not considered in this study. Therefore, the ECO scenarios are to be understood as the boundary points of a range of possible developments in the energy market. However, the development of the heat demand is not taken into account, but considered to remain constant at 25 GW h/a. As regulations in Germany require building reconstructions to include energy-saving measures [88], the energy demand per household has decreased over the past few decades. This trend will presumably continue, but has been identified as problematic for the efficiency and economic viability of existing DH grids [7,89]. Thus, more households will have to be connected to DH grids, if this technology is to play a role in the future. Therefore, the total heat demand will probably not decrease, and its development does not have to be considered in a study that focuses on

the environmental and economic assessment of the heat-generating system components.

Another disputable assumption is the proposed CO_2-credit for co-generated electricity according to the emission factor of the grid mix. Replacement of grid electricity depends on regulations and the merit order, which means that, technically, the CO_2-credit cannot be attributed to power sources' emission factor with regard to their share in the grid mix. However, the replacement does not always comply with regulations, as a local overcapacity has to be balanced locally as well [90,91]. This makes predictions of the replaced electricity source and the associated CO_2-credit very difficult. For this reason, the CO_2-credit for replacing grid mix electricity is assumed as an average value, as it is usually handled in most other LCA studies too, and complies with the requirements for co-products set by DIN EN ISO 14040/44.

The EVO scenarios consider a development in the energy market, while possible regulatory changes are disregarded. A regulatory tool often criticized for not being effective is the EUA. In this study, the EUA was not considered, as it only applies to larger combustion plants and, were it applied, it would not have a large effect on the *LCOH* (Fig. 13). However, it is possible that the EU ETS will be extended to smaller plants and that the EUA price will be increased in the future in an attempt to meet the stipulations of the Paris Agreement [92]. Fig. 13 illustrates the effect on the *LCOH* of such an extension as the EU ETS and an increase of the EUA price. The differences between the BAU and EVO scenarios also show the interdependency of developments on the energy market: with a progressing grid electricity mix, renewable sources (STC and BTES) are less affected by the allowance price. As a consequence, both regulatory and market development aspects will need to be taken into account in future studies, if regulatory changes become more likely.
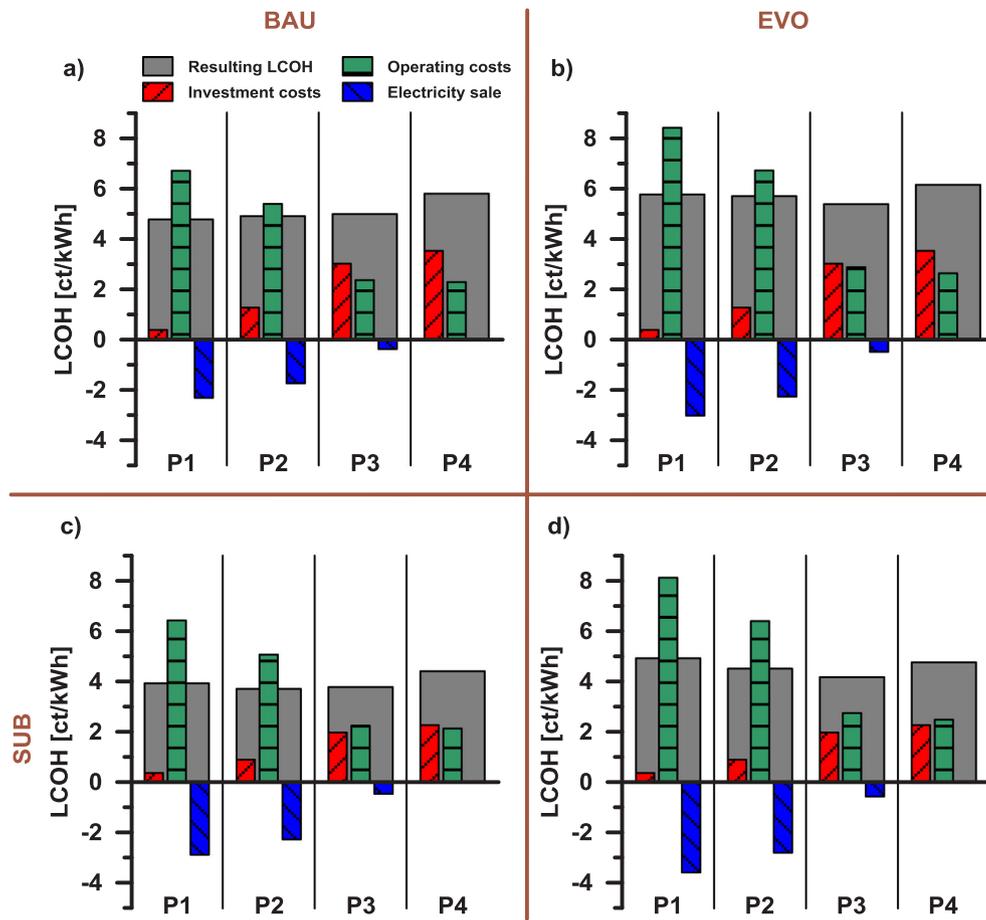
Fig. 11. Comparison of *LCOH* for the four selected layouts and the four ECO scenarios.

4.2. Discussion of results

The results provide different Pareto optimal system designs for the ECO scenarios under consideration with relatively similar *GWP* reductions. Only the subsidies cause an offset in the *LCOH* of the different Pareto optimal systems. Therefore, the optimal solutions appear equally good. However, the probabilities of the different assumptions about the existence of subsidies and the development of the energy market, which are pictured in the four ECO scenarios, are not equal. The development rate of renewable energies has not been steady in the past, and future trends are hard to predict. Yet, it is very likely that the share of renewable energy in the grid electricity mix will increase, and the emission factor of grid electricity can be expected to decrease. If the Pareto optimal solutions are weighted by the probability of the respective scenario, the STC + BTES solution with a small CHP unit for self-supplied electricity becomes the most favorable.

The combination of CHP + BTES is not favorable in any ECO scenario. CHP operation is considered to follow the heat load. Therefore, CHPs are dimensioned according to the base load of heat to avoid overcapacities. Thus, electricity sales are limited as they correspond to the heat provision. BTES allows for CHP operation to be decoupled from the heat demand as thermal energy can be stored for later use, even if the heat demand is low. As a result, CHP operation can follow the electricity demand instead and thereby realize higher prices for electricity sales. Then, the increased revenue could compensate the high investment costs for BTES and decrease the *LCOH*. The CHP operation following the electricity demand could not be investigated in this study, as it would require the consideration of a fluctuating electricity market but it can potentially make a CHP + BTES system as competitive as a CHP + STC + BTES system.

4.3. Comparison with other seasonal TES technologies

Storage capacities of efficient medium deep BTES designs for the assumed DH system lay in the range of 10 GW h/a. This corresponds to an equivalent water volume of approximately 140,000 m^3 (assuming a ΔT of 60 °C). Specific investment costs for such a BTES were approximately 38 €/(m^3 water eq.). Compared to this, specific investment costs for water storage tanks are rather high [21] (> 100 €/(m^3 water eq.), cf. [13,93]). Water pit storage systems are an affordable alternative (< 30 €/(m^3 water eq.), cf. [93]). However, such systems consist of a large excavation with an elevated rampart around it. The ground has to be stable enough to transfer the additional load from the water volume. Furthermore, pit systems constitute a significant interference in the landscape, which might cause discrepancies in the population. Gravel-water pits have a much lower landscape impact but require up to double the storage volume [21]. ATES systems can exploit sufficient storage volumes for reasonable prices and have a low landscape impact, but they rely on very specific hydrogeological site conditions. Firstly, hydraulic conductivities need to be high enough while groundwater flow has to be low and secondly, the mineral content of the utilized groundwater has to be limited. Although, BTES systems are restricted to geological formations, where groundwater flow is limited as well, the general geological requirements are much lower than that of ATES systems. Moreover, BTES systems are almost invisible and entail therefore almost no landscape impact. A further advantage of BTES systems is its very simple expandability by additional BHEs. Advantages of medium deep BTES systems over shallow ones are already elaborated in the introduction.
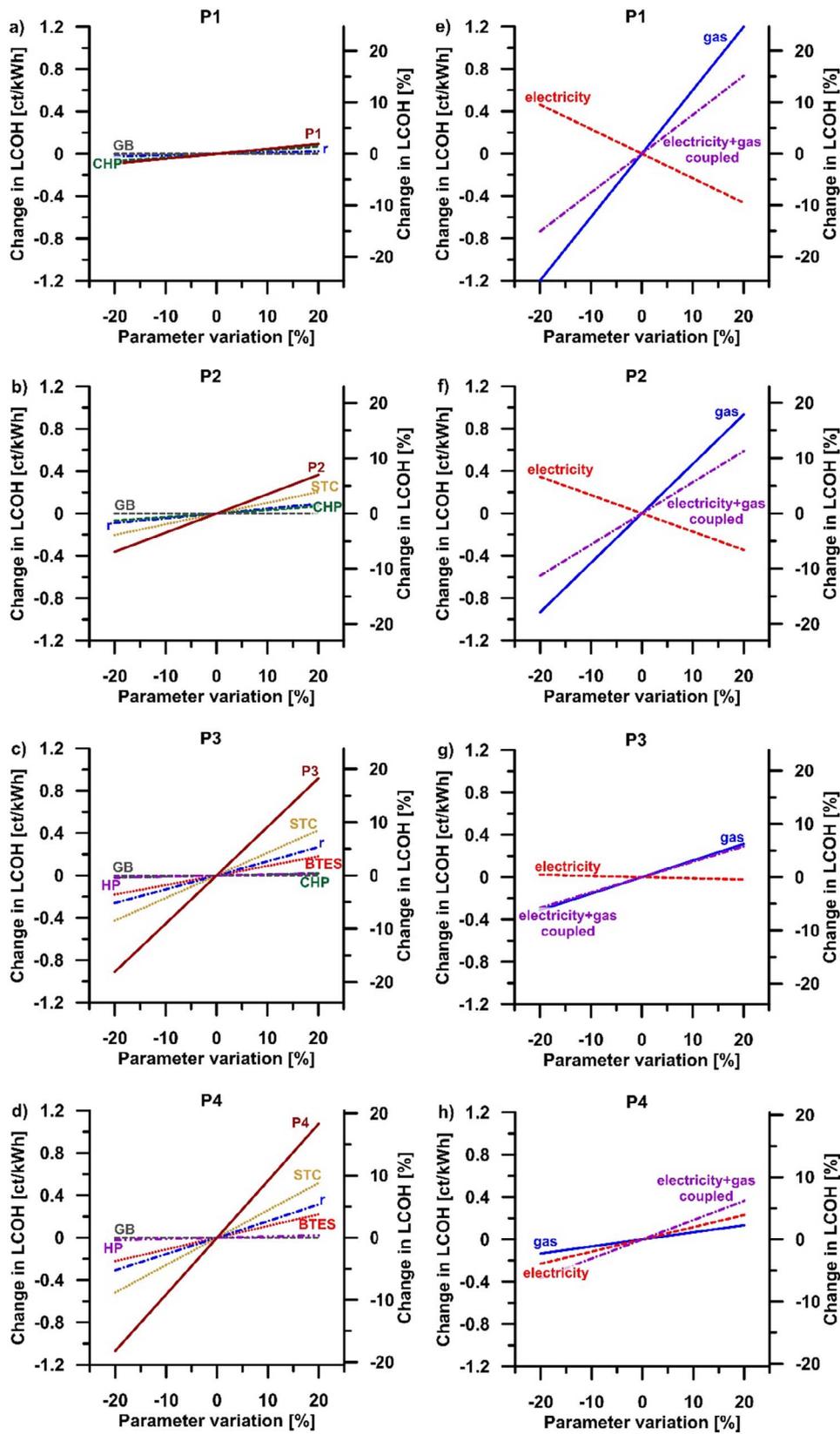
Fig. 12. Influence of investment costs (a–d) and the energy costs (e–h) on the *LCOH* for the four cases P1 to P4, considering the BAU scenario.
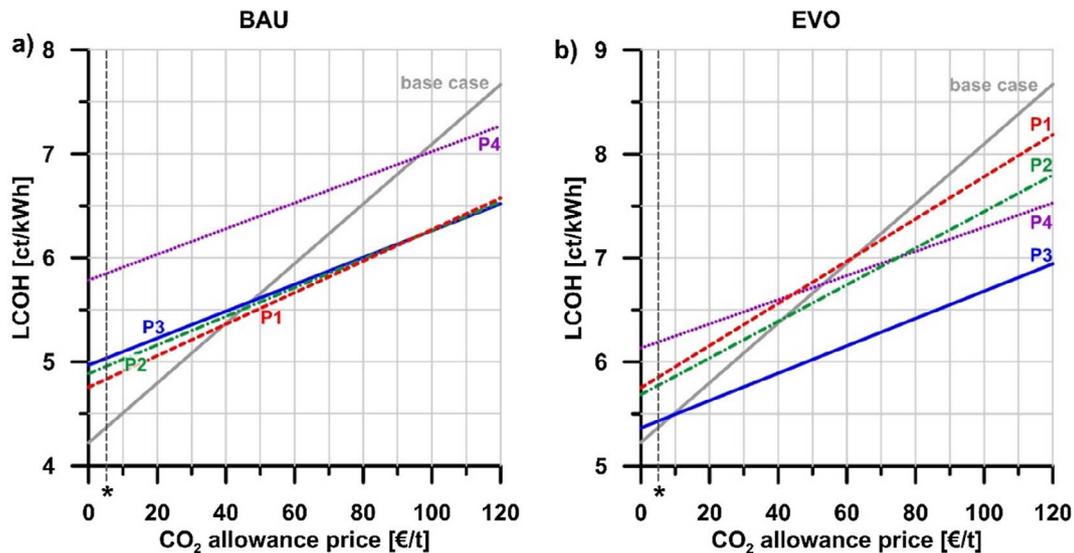
Fig. 13. Effect of implementing a CO_2 emissions allowance costs on *LCOH* for different scenarios. The dashed vertical lines (*) mark the current price level of EUAs at approximately 5 €/t.

5. Conclusions

Medium deep BTES is an advancement of conventional BTES technology, which is more independent from geological site conditions and has a much lower impact on landscape than competing technologies for large-scale seasonal heat storage. Consequently, its market introduction could result in a wider applicability of seasonal storage in DH systems but is opposed by high investment costs and uncertain environmental benefits.

Based on a life cycle approach, this study analyzes the economic and environmental effects of integrating medium deep BTES systems into a hypothetical low temperature DH grid under varying shares of STC-, CHP- and GB-capacity and under different ECO scenarios. Even though the ECO scenarios under consideration are based on German boundary conditions, the general conclusions concerning favorable conditions for BTES integration are transferable to other countries as well. The results are depicted as Pareto fronts, which illustrate the trade-off between cost efficiency and the reduction of *GWP*. Our approach allows for the identification of specific system designs that combine a large reduction in the *GWP* with reasonable *LCOH*. The basic results concerning the integration of medium deep BTES in district heating systems can be concluded as follows:

- The results are very sensitive to changes in the economic and environmental boundary conditions.
- The most promising system designs combine a large STC field and a large medium deep BTES system with a small CHP, which supplies the HP and circulating pumps with cogenerated electricity.
- Under the current market conditions, disregarding existing subsidies (BAU), this CHP + STC + BTES combination can significantly reduce the *GWP* by 54%, while increasing the *LCOH* by 13%, compared to the most economic system (i.e. GB-only). Nevertheless, it has to compete with highly efficient CHP-based technology combinations, which can achieve similar results.
- Assuming a very likely future rise in energy prices and a decrease in the electricity mix emission factor (EVO), CHP-based combinations are less attractive. The most favorable compromise solution without seasonal storage can achieve a *GWP* reduction of 29% by an increase in *LCOH* of 12%, compared to the most economic combination (i.e. GB + small STC). In contrast, the CHP + STC + BTES combination reduces the *GWP* by 33% or 50%, when accepting a rise in the *LCOH* by only 1.2% or 5.5%, respectively.
- Including German state subsidies in EVO SUB, CHP + STC + BTES depicts the most economic system combination. However, in the

current market situation (BAU SUB) the subsidies offer an advantage to CHP-based systems. This leads to a crowding out of storage capacities.
- Less than 15% of the *GWP* of the CHP + STC + BTES combination can be attributed to the production phase. However, investment costs for STC, BTES and HP make up approximately 45% to 60% of the *LCOH*, constituting a major potential for savings.

All in all, our study highlights that medium deep BTES systems in combination with a large STC field and a small CHP can be a cost-effective alternative to large CHPs for mitigating GHG emissions in district heating systems. Our assessment tool can easily be adapted to other economic/environmental scenarios as well as to specific DH systems. Furthermore, the tool could be expanded by further heating or storage technologies. Thus, we provide an instrument, which could be used by system engineers or policy makers to assess the economic and environmental effects of different system designs or regulatory measures. Furthermore, the tool could be applied by DH operators to plan the integration of a BTES into an existing system, to gauge the current performance of their heating system, or assess the consequences of, for example, changes in energy prices or the electricity mix.

The construction of a pilot storage system should be the next step to assess the general practicability of the concept of medium deep BTES. Moreover, it could gather more precise data about the economics and environmental burden of the drilling process. Finally, a pilot storage system would serve as the first operational experience of such a system.

Acknowledgement

Appendix A. Supplementary material

Supplementary data associated with this article can be found, in the online version, at http://dx.doi.org/10.1016/j.apenergy.2018.02.011.

References

[1] United Nations, Department of Economic and Social Affairs, Population Division. World Urbanization Prospects: The 2014 Revision, (ST/ESA/SER.A/366); 2015.
[2] Sass I, Bracke R, Rühaak W. Urban heating. In: Proceedings of the World Geothermal Congress; 19-25 April 2015; Melbourne, Australia; 2015.
[3] Connolly D, Lund H, Mathiesen BV, Werner S, Möller B, Persson U, et al. Heat

roadmap Europe: combining district heating with heat savings to decarbonise the EU energy system. Energy Policy 2014;65:475–89. http://dx.doi.org/10.1016/j.enpol.2013.10.035.

[4] Lund H, Möller B, Mathiesen BV, Dyrelund A. The role of district heating in future renewable energy systems. Energy 2010;35:1381–90. http://dx.doi.org/10.1016/j.energy.2009.11.023.

[5] Björnebo L, Spatari S, Gurian PL. A greenhouse gas abatement framework for investment in district heating. Appl Energy 2018;211:1095–105. http://dx.doi.org/10.1016/j.apenergy.2017.12.003.

[6] Rezaie B, Rosen MA. District heating and cooling: review of technology and potential enhancements. Appl Energy 2012;93:2–10. http://dx.doi.org/10.1016/j.apenergy.2011.04.020.

[7] Lund H, Werner S, Wiltshire R, Svendsen S, Thorsen JE, Hvelplund F, et al. 4th Generation district heating (4GDH): integrating smart thermal grids into future sustainable energy systems. Energy 2014;68:1–11. http://dx.doi.org/10.1016/j.energy.2014.02.089.

[8] Li H, Svendsen S. Energy and exergy analysis of low temperature district heating network. Energy 2012;45:237–46. http://dx.doi.org/10.1016/j.energy.2012.03.056.

[9] Kauko H, Kvalsvik KH, Rohde D, Hafner A, Nord N. Dynamic modelling of local low-temperature heating grids: a case study for Norway. Energy 2017. http://dx.doi.org/10.1016/j.energy.2017.07.086.

[10] Gadd H, Werner S. Achieving low return temperatures from district heating substations. Appl Energy 2014;136:59–67. http://dx.doi.org/10.1016/j.apenergy.2014.09.022.

[11] Schmidt D, Kallert A, Blesl M, Svendsen S, Li H, Nord N, et al. Low temperature district heating for future energy systems. Energy Proc 2017;116:26–38. http://dx.doi.org/10.1016/j.egypro.2017.05.052.

[12] Bauer D, Marx R, Nußbicker-Lux J, Ochs F, Heidemann W, Müller-Steinhagen H. German central solar heating plants with seasonal heat storage. Solar Energy 2010;84:612–23. http://dx.doi.org/10.1016/j.solener.2009.05.013.

[13] Schmidt T, Mangold D, Müller-Steinhagen H. Central solar heating plants with seasonal storage in Germany. Solar Energy 2004;76:165–74. http://dx.doi.org/10.1016/j.solener.2003.07.025.

[14] Fisch MN, Guigas M, Dalenbäck JO. A review of large-scale solar heating systems in Europe. Solar Energy 1998;63:355–66. http://dx.doi.org/10.1016/S0038-092X(98)00103-0.

[15] Dincer I, Rosen MA. Thermal energy storage: systems and applications. 2nd ed. Hoboken, N.J.: Wiley; 2011.

[16] Sillman S. Performance and economics of annual storage solar heating systems. Solar Energy 1981;27:513–28. http://dx.doi.org/10.1016/0038-092X(81)90046-3.

[17] Braun JE, Klein SA, Mitchell JW. Seasonal storage of energy in solar heating. Solar Energy 1981;26:403–11. http://dx.doi.org/10.1016/0038-092X(81)90219-X.

[18] Xu J, Wang RZ, Li Y. A review of available technologies for seasonal thermal energy storage. Solar Energy 2014;103:610–38. http://dx.doi.org/10.1016/j.solener.2013.06.006.

[19] Pinel P, Cruickshank CA, Beausoleil-Morrison I, Wills A. A review of available methods for seasonal storage of solar thermal energy in residential applications. Renew Sustain Energy Rev 2011;15:3341–59. http://dx.doi.org/10.1016/j.rser.2011.04.013.

[20] Tian Y, Zhao CY. A review of solar collectors and thermal energy storage in solar thermal applications. Appl Energy 2013;104:538–53. http://dx.doi.org/10.1016/j.apenergy.2012.11.051.

[21] Novo AV, Bayon JR, Castro-Fresno D, Rodriguez-Hernandez J. Review of seasonal heat storage in large basins: water tanks and gravel–water pits. Appl Energy 2010;87:390–7. http://dx.doi.org/10.1016/j.apenergy.2009.06.033.

[22] Kübler R, Fisch N, Hahne E. High temperature water pit storage projects for the seasonal storage of solar energy. Solar Energy 1997;61:97–105. http://dx.doi.org/10.1016/S0038-092X(97)00040-6.

[23] Lizana J, Chacartegui R, Barrios-Padura A, Valverde JM. Advances in thermal energy storage materials and their applications towards zero energy buildings: a critical review. Appl Energy 2017;203:219–39. http://dx.doi.org/10.1016/j.apenergy.2017.06.008.

[24] Thomsen PD, Overbye PM. Energy storage for district energy systems. In: Wiltshire R, editor. Advanced district heating and cooling (DHC) Systems Oxford: Woodhead Publishing; 2016. p. 145–66. http://dx.doi.org/10.1016/B978-1-78242-374-4.00007-0.

[25] Lizana J, Chacartegui R, Barrios-Padura A, Ortiz C. Advanced low-carbon energy measures based on thermal energy storage in buildings: a review. Renew Sustain Energy Rev 2018;82:3705–49. http://dx.doi.org/10.1016/j.rser.2017.10.093.

[26] Gehlin S. Borehole thermal energy storage. In: Rees SJ, editor. Advances in ground-source heat pump systems Woodhead Publishing; 2016. p. 295–327. http://dx.doi.org/10.1016/B978-0-08-100311-4.00011-X.

[27] Reuss M. 6 – The use of borehole thermal energy storage (BTES) systems. In: Cabeza LF, editor. Advances in thermal energy storage systems Woodhead Publishing; 2015. p. 117–47. http://dx.doi.org/10.1533/9781782420965.1.117.

[28] Tveit T-M, Savola T, Gebremedhin A, Fogelholm C-J. Multi-period MINLP model for optimising operation and structural changes to CHP plants in district heating networks with long-term thermal storage. Energy Convers Manage 2009;50:639–47. http://dx.doi.org/10.1016/j.enconman.2008.10.010.

[29] Nordell B. A borehole heat store in rock at the University of Lulea, The Lulevarme Project 1982–1988. Stockholm, Sweden: Swedish Council for Building Research; 1990.

[30] Lundh M, Dalenbäck JO. Swedish solar heated residential area with seasonal storage in rock: initial evaluation. Renew Energy 2008;33:703–11. http://dx.doi.org/10.1016/j.renene.2007.03.024.

[31] Sibbitt B, McClenahan D, Djebbar R, Thornton J, Wong B, Carriere J, et al. The performance of a high solar fraction seasonal storage district heating system – five years of operation. Energy Proc 2012;30:856–65. http://dx.doi.org/10.1016/j.egypro.2012.11.097.

[32] Nordell B, Scorpo AL, Andersson O, Rydell L. The HT BTES plant in Emmaboda: report from the first three years of operation 2010-2013. Luleå tekniska universitet; 2014.

[33] Rapantova N, Pospisil P, Koziorek J, Vojcinak P, Grycz D, Rozehnal Z. Optimisation of experimental operation of borehole thermal energy storage. Appl Energy 2016;181:464–76. http://dx.doi.org/10.1016/j.apenergy.2016.08.091.

[34] Nordell B. LARGE-SCALE SEASONAL HEAT STORAGE IN ROCK – Construction and operation experiences. Proceedings of the International Symposium on Engineering in Complex Rock Formations: Pergamon; 1988. p. 351–6. doi: 10.1016/B978-0-08-035894-9.50050-0.

[35] Welsch B, Rühaak W, Schulte DO, Bär K, Sass I. Characteristics of medium deep borehole thermal energy storage. Int J Energy Res 2016;40:1855–68. http://dx.doi.org/10.1002/er.3570.

[36] Schulte DO, Rühaak W, Oladyshkin S, Welsch B, Sass I. Optimization of medium-deep borehole thermal energy storage systems. Energy Technol 2016;4:104–13. http://dx.doi.org/10.1002/ente.201500254.

[37] Bär K, Rühaak W, Welsch B, Schulte D, Homuth S, Sass I. Seasonal high temperature heat storage with medium deep borehole heat exchangers. Energy Proc 2015;76:351–60. http://dx.doi.org/10.1016/j.egypro.2015.07.841.

[38] Welsch B, Rühaak W, Schulte DO, Bär K, Homuth S, Sass I. A comparative study of medium deep borehole thermal energy storage systems using numerical modelling. In: Proceedings of the world geothermal congress; 19–25 April 2015; Melbourne, Australia; 2015.

[39] Schulte DO, Rühaak W, Welsch B, Sass I. BASIMO – borehole heat exchanger array simulation and optimization tool. Energy Proc 2016;97:210–7. http://dx.doi.org/10.1016/j.egypro.2016.10.057.

[40] Bär K, Rühaak W, Welsch B, Schulte D, Homuth S, Sass I. Seasonal high temperature heat storage with medium deep borehole heat exchangers – a conceptual case study. In: Proceedings of the European Geothermal Congress; 19–24 Sept 2016; Strasbourg, France; 2016.

[41] Schulte DO, Welsch B, Boockmeyer A, Rühaak W, Bär K, Bauer S, et al. Modeling insulated borehole heat exchangers. Environ Earth Sci 2016;75:1–12. http://dx.doi.org/10.1007/s12665-016-5638-x.

[42] Molyneaux A, Leyland G, Favrat D. Environomic multi-objective optimisation of a district heating network considering centralized and decentralized heat pumps. Energy 2010;35:751–8. http://dx.doi.org/10.1016/j.energy.2009.09.028.

[43] Østergaard PA, Andersen AN. Booster heat pumps and central heat pumps in district heating. Appl Energy 2016;184:1374–88. http://dx.doi.org/10.1016/j.apenergy.2016.02.144.

[44] Genchi Y, Kikegawa Y, Inaba A. CO_2 payback–time assessment of a regional-scale heating and cooling system using a ground source heat–pump in a high energy–consumption area in Tokyo. Appl Energy 2002;71:147–60. http://dx.doi.org/10.1016/S0306-2619(02)00010-7.

[45] Khoshgoftar Manesh MH, Navid P, Amidpour M, Hamedi MH. New procedure for optimal design of cogeneration system with considering environmental impacts and total cost. Clean Technol Environ Policy 2013;15:893–919. http://dx.doi.org/10.1007/s10098-012-0576-0.

[46] Torchio MF. Comparison of district heating CHP and distributed generation CHP with energy, environmental and economic criteria for Northern Italy. Energy Convers Manage 2015;92:114–28. http://dx.doi.org/10.1016/j.enconman.2014.12.052.

[47] Weinberger G, Amiri S, Moshfegh B. On the benefit of integration of a district heating system with industrial excess heat: an economic and environmental analysis. Appl Energy 2017;191:454–68. http://dx.doi.org/10.1016/j.apenergy.2017.01.093.

[48] Lidberg T, Gustafsson M, Myhren JA, Olofsson T, Ödlund L. Environmental impact of energy refurbishment of buildings within different district heating systems. Appl Energy 2017. http://dx.doi.org/10.1016/j.apenergy.2017.07.022.

[49] Lundström L, Wallin F. Heat demand profiles of energy conservation measures in buildings and their impact on a district heating system. Appl Energy 2016;161:290–9. http://dx.doi.org/10.1016/j.apenergy.2015.10.024.

[50] Truong NL, Dodoo A, Gustavsson L. Effects of heat and electricity saving measures in district-heated multistory residential buildings. Appl Energy 2014;118:57–67. http://dx.doi.org/10.1016/j.apenergy.2013.12.009.

[51] Gustafsson M, Gustafsson MS, Myhren JA, Bales C, Holmberg S. Techno-economic analysis of energy renovation measures for a district heated multi-family house. Appl Energy 2016;177:108–16. http://dx.doi.org/10.1016/j.apenergy.2016.05.104.

[52] Truong NL, Gustavsson L. Cost and primary energy efficiency of small-scale district heating systems. Appl Energy 2014;130:419–27. http://dx.doi.org/10.1016/j.apenergy.2014.05.031.

[53] Buoro D, Pinamonti P, Reini M. Optimization of a distributed cogeneration system with solar district heating. Appl Energy 2014;124:298–308. http://dx.doi.org/10.1016/j.apenergy.2014.02.062.

[54] Lindenberger D, Bruckner T, Groscurth HM, Kümmel R. Optimization of solar district heating systems: seasonal storage, heat pumps, and cogeneration. Energy 2000;25:591–608. http://dx.doi.org/10.1016/S0360-5442(99)00082-1.

[55] Ucar A, Inalli M. Thermal and economical analysis of a central solar heating system with underground seasonal storage in Turkey. Renew Energy 2005;30:1005–19. http://dx.doi.org/10.1016/j.renene.2004.09.015.

[56] Ucar A, Inalli M. A thermo-economical optimization of a domestic solar heating plant with seasonal storage. Appl Therm Eng 2007;27:450–6. http://dx.doi.org/10.

1016/j.applthermaleng.2006.06.010.

[57] Paiho S, Hoang H, Hukkalainen M. Energy and emission analyses of solar assisted local energy solutions with seasonal heat storage in a Finnish case district. Renew Energy 2017;107:147–55. http://dx.doi.org/10.1016/j.renene.2017.02.003.

[58] Raluy RG, Serra LM, Guadalfajara M, Lozano MA. Life cycle assessment of central solar heating plants with seasonal storage. Energy Proc 2014;48:966–76. http://dx.doi.org/10.1016/j.egypro.2014.02.110.

[59] Wang H, Yin W, Abdollahi E, Lahdelma R, Jiao W. Modelling and optimization of CHP based district heating system with renewable energy production and energy storage. Appl Energy 2015;159:401–21. http://dx.doi.org/10.1016/j.apenergy.2015.09.020.

[60] Ghafghazi S, Sowlati T, Sokhansanj S, Bi X, Melin S. Life cycle assessment of base–load heat sources for district heating system options. Int J Life Cycle Assess. 2011;16:212–23. http://dx.doi.org/10.1007/s11367-011-0259-9.

[61] Tulus V, Boer D, Cabeza LF, Jiménez L, Guillén-Gosálbez G. Enhanced thermal energy supply via central solar heating plants with seasonal storage: a multi-objective optimization approach. Appl Energy 2016;181:549–61. http://dx.doi.org/10.1016/j.apenergy.2016.08.037.

[62] IINAS – International Institute for Sustainability Analysis and Strategy. GEMIS model and database, version 4.93, < http://iinas.org/gemis.html > ; 2016.

[63] Schlesinger M, Hofer P, Kemmler A, Kirchner A, Koziel S, Ley A, et al. Entwicklung der Energiemärkte – Energiereferenzprognose. Studie im Auftrag des Bundesministeriums für Wirtschaft und Technologie, < http://www.bmwi.de/Redaktion/DE/Publikationen/Studien/entwicklung-der-energiemaerkte-energiereferenzprognose-endbericht.html > ; 2014. [accessed 07.06.2017].

[64] German Federal Statistical Office (Statistisches Bundesamt). Daten zur Energiepreisentwicklung: Lange Reihen von Januar 2000 bis Dezember 2016. Wiesbaden; 2017. p. 54.

[65] European Energy Exchange AG. Quarterly Prices According to CHP Law, < www.eex.com/en/market-data/power/spot-market/kwk-index > ; 2017.

[66] German Act on Combined Heat and Power Generation of 2016 – Gesetz für die Erhaltung, die Modernisierung und den Ausbau der Kraft-Wärme-Kopplung (Kraft-Wärme-Kopplungsgesetz – KWKG). (December 21, 2015).

[67] KfW Bankengruppe. KfW-Programm Erneuerbare Energien "Premium"; 2016.

[68] The MathWorks Inc. MATLAB 2016a. Natick, MA; 2016.

[69] BBR. Updated and enhanced test reference years (TRY) of Germany for medium and extreme weather conditions; 2011.

[70] Short W, Packey DJ, Holt T. A manual for the economic evaluation of energy efficiency and renewable energy technologies. National Renewable Energy Laboratory; 1995.

[71] Moomaw W, Burgherr P, Heath G, Lenzen M, Nyboer J, Verbruggen A. Annex II: methodology. In: Edenhofer O, Pichs-Madruga R, Sokona Y, Seyboth K, Matschoss P, Kadner S, editors. IPCC special report on renewable energy sources and climate change mitigation. Cambridge, United Kingdom and New York, NY, USA: Cambridge University Press; 2011.

[72] DIN EN ISO 14040:2009-11. Environmental management – life cycle assessment – principles and framework (ISO 14040:2006); German and English version EN ISO 14040:2006; 2009; 2006.

[73] DIN EN ISO 14044:2006-10. Environmental management – Life cycle assessment – Requirements and guidelines (ISO 14044:2006); German and English version EN ISO 14044:2006; 2006.

[74] GreenDelta GmbH. openLCA – the Life Cycle and Sustainability Modeling Suite. 1.5.

[75] Wernet G, Bauer C, Steubing B, Reinhard J, Moreno-Ruiz E, Weidema B. The ecoinvent database version 3 (part I): overview and methodology. Int J Life Cycle Assess 2016;21:1218–30. http://dx.doi.org/10.1007/s11367-016-1087-8.

[76] Thinkstep AG. GaBi: Software and database contents for Life Cycle Engineering. 5 ed; 2011.

[77] Guinée JB, editor. Handbook on life cycle assessment: operational guide to the ISO standards XI. Dordrecht: Kluwer Academic Publishers; 2002. p. 692. http://dx.doi.org/10.1007/0-306-48055-7.

[78] Solar-Institute Jülich. CARNOT 6.0 for MATLAB 2013b; 2016.

[79] Mauthner F, Herkel S. Classification and benchmarking of solar thermal systems in urban environments. In: International Energy Agency – Solar Heating and Cooling Programme – Task 52: Solar Heat and Energy Economics in Urban Environments, editor. Technology and Demonstrators: Technical Report Subtask C – Part C1; 2016.

[80] ASUE. BHKW-Kenndaten 2011 – Module, Anbieter, Kosten. In: Arbeitsgemeinschaft für sparsamen und umweltfreundlichen Energieverbrauch e.V., editor. 2011.

[81] EPA. Catalog of CHP Technologies. In: U.S. Environmental Protection Agency Combined Heat and Power Partnership, editor 2015.

[82] Schaumann G, Schmitz KW, editors. Kraft-Wärme-Kopplung. 4th ed.XIII. Berlin: Springer; 2010. p. 455.

[83] Homuth S, Hornich W, Krenn H, Sass I, Spahn T. Down-the-hole water-powered hammer drilling method for medium-deep geothermal energy drilling. Oil Gas European Mag 2016;132:39–41.

[84] Fischer D, Madani H. On heat pumps in smart grids: a review. Renew Sustain Energy Rev 2017;70:342–57. http://dx.doi.org/10.1016/j.rser.2016.11.182.

[85] Croteau R, Gosselin L. Correlations for cost of ground-source heat pumps and for the effect of temperature on their performance. Int J Energy Res 2015;39:433–8. http://dx.doi.org/10.1002/er.3243.

[86] Greening B, Azapagic A. Domestic heat pumps: life cycle environmental impacts and potential implications for the UK. Energy 2012;39:205–17. http://dx.doi.org/10.1016/j.energy.2012.01.028.

[87] Gebhardt M, Kohl H, Steinrötter T. Preisatlas – Ableitung von Kostenfunktionen für Komponenten der rationellen Energienutzung. Duisburg-Rheinhausen: Institut für Energie und Umwelttechnik e.V. (IUTA); 2002. p. 356.

[88] EnEV. Energieeinsparverordnung 2014 – Nichtamtliche (konsolidierte) Lesefassung. EnEV 2014, < http://www.enev-online.com/enev_2014_volltext/ > ; 2013. p. 3951–89. [accessed 17.09.2017].

[89] Persson U, Werner S. Heat distribution and the future competitiveness of district heating. Appl Energy 2011;88:568–76. http://dx.doi.org/10.1016/j.apenergy.2010.09.020.

[90] Stoll P, Brandt N, Nordström L. Including dynamic CO_2 intensity with demand response. Energy Policy 2014;65:490–500. http://dx.doi.org/10.1016/j.enpol.2013.10.044.

[91] Seier M, Schebek L. Model-based investigation of residual load smoothing through dynamic electricity purchase: the case of wastewater treatment plants in Germany. Appl Energy 2017;205:210–24. http://dx.doi.org/10.1016/j.apenergy.2017.07.116.

[92] United Nations/Framework Convention on Climate Change. Adoption of the Paris Agreement. Paris: United Nations; 2015.

[93] Schmidt T, Mangold D, Sørensen PA, From N. Large-scale heat storage. In: Proceedings of the IRES 2011 6th International Renewable Energy Storage Conference, Eurosolar; Berlin, Germany; 2011.

0 ed, < http://www.openlca.org/ > ; 2017.

Appendix H – Co-Simulation of Geothermal Applications and Heating, Ventilation and Air Conditioning Systems

Published as:

European Geosciences Union General Assembly 2017, EGU
Division Energy, Resources & Environment, ERE

Co-Simulation of Geothermal Applications and HVAC Systems

Bastian Welsch[a,b,]*, Wolfram Rühaak[c], Daniel O. Schulte[a,b], Julian Formhals[a,b],
Kristian Bär[a], Ingo Sass[a,b]

[a]*Technische Universität Darmstadt, Department of Geothermal Science and Technology, Schnittspahnstraße 9, 64287 Darmstadt, Germany*
[b]*Darmstadt Graduate School of Excellence Energy Science and Engineering, Jovanka-Bontschits-Straße 2, 64287 Darmstadt, Germany*
[c]*Federal Institute for Geosciences and Natural Resources, Stilleweg 2, 30655 Hannover, Germany*

Abstract

An interface is developed to couple the finite element program FEFLOW with the MATLAB-SIMULINK software. The TCP/IP based data exchange routine allows for a co-simulation of borehole heat exchangers and of HVAC components, so that each subsystem can be modeled in its specialized simulation environment. Hereby, the interaction of the subsystems is taken into account, which leads to a more precise representation of the systems' dynamic behavior. Furthermore, the concept supports the application of mathematical optimization algorithms that can be utilized to automatically determine several design parameters for an overall improved system performance.

© 2017 The Authors. Published by Elsevier Ltd.
Peer-review under responsibility of the scientific committee of the European Geosciences Union (EGU) General Assembly 2017 – Division Energy, Resources and the Environment (ERE).

Keywords: Coupling; co-simulation; optimization; geothermal; HVAC; borehole heat exchanger; FEFLOW; MATLAB

1. Introduction

Large scale geothermal applications are eminently suitable for the substitution of fossil based energy sources, particularly in the district heating sector in combination with low supply temperatures. Furthermore, shallow and medium deep borehole thermal energy storage (BTES) systems are very promising technologies with regard to the seasonal storage of solar thermal energy [1-4]. However, these systems are most efficient if they are large enough, i.e. when the storage capacities lie in the range of several GWh of heat per year. Such a heat demand is only present

---

* Corresponding author. Tel.: +49-6151-16-22096; fax: +49-6151-16-23601.
  E-mail address: welsch@geo.tu-darmstadt.de

in large district heating grids, which usually consist of several subsystems like heat sources (e.g. solarthermics or a combined heat and power plant), geothermal applications (e.g. a borehole thermal energy storage system), heat consumers (e.g. space heating systems), diurnal storages (i.e. water tanks), additional heat sources for peak load coverage (e.g. a heat pump or a gas boiler) and the distribution network. For the design and the optimization of an integrated system, numerical simulations of all subsystems are imperative. Borehole thermal energy storage systems are usually simulated with finite element programs under consideration of groundwater flow and heat transport in the subsurface. In contrast, the heating, ventilation and air conditioning (HVAC) installations are often analyzed with modular transient simulation software packages for modeling physical systems. The separate simulation of the borehole energy storage and HVAC installations is well-established, but represents a simplification. In reality, the subsystems interact dynamically with each other. The fluid temperatures of the heat generation system, the heating system and the underground storage are interdependent IFM and affect the performance of each subsystem. Coupled simulation models, which co-simulate the subsystems are required, to take these interdependencies into account.

There are different program codes for the simulation of the interaction of borehole heat exchangers (BHEs) with the subsurface (e.g. BASIMO [5]). Here, the program FEFLOW [6, 7] is used to compute the subsurface heat transport including a one-dimensional solution for the BHEs [8, 9]. The Carnot Blockset [10] for MATLAB-SIMULINK [11] is deployed for the simulation of the HVAC components. This allows for a readily combination with the MATLAB optimization toolbox, which provides various powerful mathematical optimization algorithms.

2. Implementation

Simulation software packages from different developers usually do not contain pre-defined coupling interfaces and in addition to that, might be based on different program languages. Hence, a major challenge is to develop a robust and versatile communication architecture between them. We decided to use a client-server network connection based on the Transmission Control Protocol/Internet Protocol (TCP/IP). The TCP/IP protocol suite specifies how data has to be packetized, addressed, transmitted, routed and received at the destination. It assures that data loss is identified and corrected and it allows for a bidirectional communication. Furthermore, it offers the possibility to run the different simulation packages on separate computers (Fig. 1).
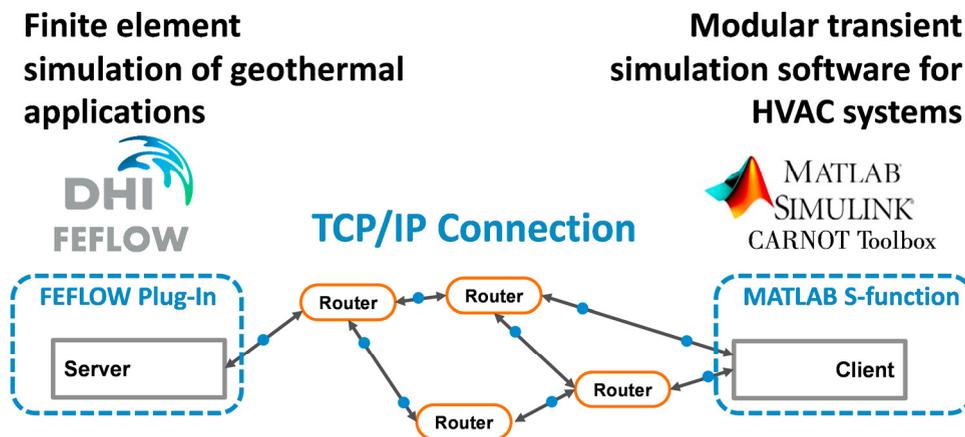

Fig. 1. Principle of the socket-client connection between FEFLOW and SIMULINK.

To establish such a connection, it is necessary that both software packages allow for the execution of proprietary source code. FEFLOW has a programming interface (IFM), which provides the possibility to read or change several model parameters during a simulation and also to execute C++ code. In SIMULINK, so called S-function blocks are available that can be integrated into the model and contain own MATLAB code or C++ code, as well.

The following routine is executed to establish the connection, send data via the interfaces and close the connection (cf. Fig. 2): FEFLOW operates as the server, which passively waits for a connection. Therefore, a TCP

socket is established and a port number is assigned to the socket. A socket is the endpoint of a network-based connection. The socket address is composed of the IP address of the host and the port number. SIMULINK is instructed to serve as the client. It also creates a socket, which then calls the address of the server socket. After the server has accepted the connection, data can be sent and received. Finally, after the connection is no longer needed, the sockets are closed to release the ports.
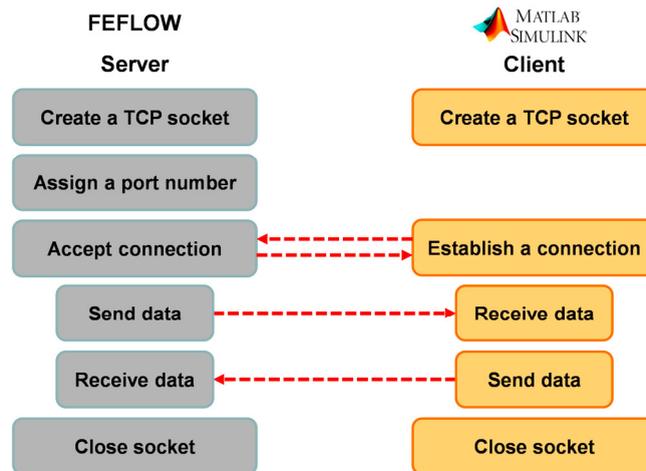

Fig. 2. Implementation scheme of the socket-client connection between FEFLOW and SIMULINK.

The connection is established shortly before the simulations are started. Subsequently, the transfer parameters are exchanged at distinct communication times. The communication time step size is constant and has to be defined in advance. Both programs generally maintain their own simulation time step control. However, it has to be ensured, that the simulation time steps coincide at the communication time steps.

3. Application example: optimal buffer storage size

3.1. System and model description

The following simplified BTES system is used to demonstrate the capability of the approach (cf. Fig. 3): A borehole storage of a specific size (37 BHE, 100 m each) is considered to be charged by a solar thermal collector system with a given collector area (15.000 m², corresponds to approx. 6 GWh of heat gain per year). A water tank between the collectors and the seasonal storage serves as a buffer storage, which cushions the daily peak loads that occur during the solar heat generation. Thus, the capacity of the buffer storage is expected to have a strong influence on the heat amount that can be transferred from the collectors into the BTES. Consequently, identifying the optimal volume of the water tank V_{buf} will maximize the heat $Q_{BTES,stor}$ that can be stored in the BTES. As this scenario only focuses on the charging process of the BTES, the representation of the heating system is not necessary.

Since there are two separated closed fluid circuits, both have to be actuated by circulation pumps. The operation of these pumps is temperature-controlled. As soon as a trigger temperature in the collectors of 60 °C is exceeded, the collector circuit is started. Accordingly, the circulation is stopped when the collectors' return temperature falls below a certain trigger temperature of 30 °C. A second operational constraint of the solar circulation pump is implemented: the collector outlet temperature has to be at least two degree centigrade above the collector inlet temperature. This shall prevent the occurrence of negative collector outputs. Likewise, the operation of the BTES fluid circuit is controlled in a similar manner: it starts operating as soon as the temperature at a sensor close to the top of the buffer storage tank exceeds a threshold of 70 °C and it stops when the sensor temperature drops beneath 42 °C. Furthermore, the pump is switched of, when the supply temperature of the BTES undercuts the return temperature. Thereby, the BTES operation is restricted to charging conditions only.
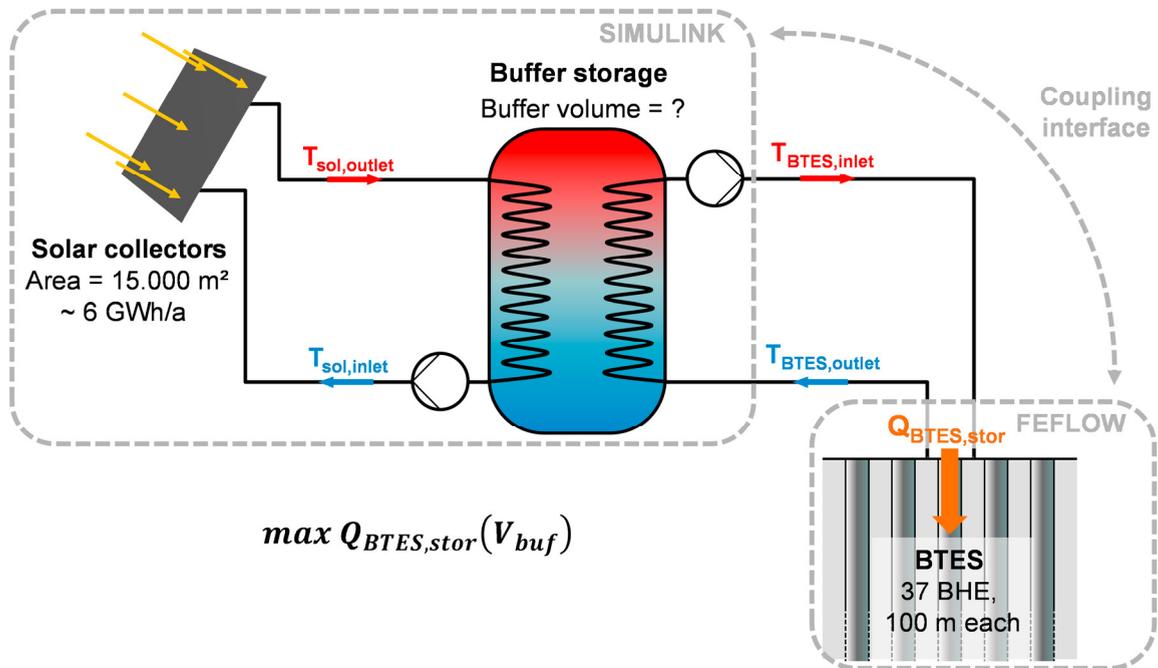
Fig. 3. Schematic of the application example setup.

While the HVAC-system components such as the solar collectors, the buffer storage tank, the circulation pumps and the control system are modeled in MATLAB-SIMULINK with the Carnot Blockset [10], the BTES is represented in a FEFLOW 3D finite element model. Both models are connected through TCP/IP and co-simulated using the approach presented herein. Therefore, the BTES supply temperature, as well as the volume flow rate in the BTES circuit are transferred from the HVAC model to the BTES model. Whereas, the BTES model only sends back the BTES return temperature. The values are exchanged at predefined communication intervals of five minutes of simulated time. Hourly solar radiation data and ambient temperature data from a test reference year dataset of Germany [12] (medium weather conditions, region 12) serve as input parameters for the solar collectors and the buffer storage tank.

3.2. Simulation results

Fig. 4 illustrates the simulation results for the first day of operation. In the morning hours, the sun raises and the solar insulation starts to increase. At about 9:50 the trigger temperature for the solar circulation pump is reached and the charging of the buffer storage starts. About one hour later, the trigger temperature of the BTES circuit is also exceeded. From that point on, heat is also transferred from the buffer storage to the BTES. In the afternoon, the solar yield decreases. Consequently, the temperature of the buffer storage decreases as well. At about 17:15 the solar yields are too low and the solar circuit pump is switched off. Since the buffer storage still contains enough heat, the charging of the BTES continues until the switch-off criterion for the BTES circulation pump is reached as well at about 2:15 in the night.

In summary, it can be stated that the simulation results are realistic and have a high level of detail. The co-simulation of the components allows for a very close inspection of the interaction processes of the components.
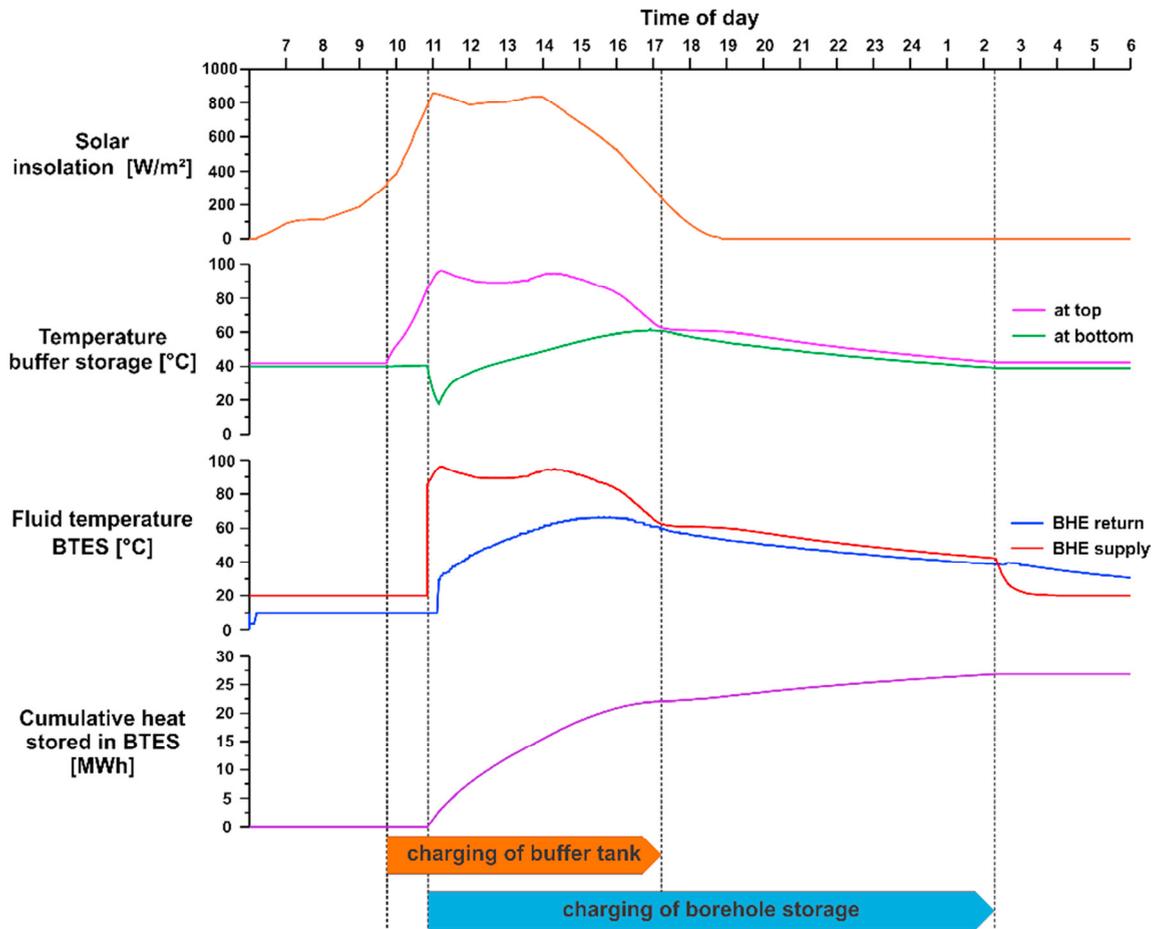
Fig. 4. Course of different system parameters during the first day of simulation.

3.3. Optimization procedure

Only with this very detailed inspection of the system's behavior resulting from the coupled simulation, it is possible to improve the system's performance by enhancing single or multiple components. In the presented scenario, an optimized buffer storage capacity can maximize the amount of solar heat that is stored in the BTES. This can be realized by applying a mathematical optimization algorithm, which automatically iterates the buffer storage volume until the optimum is found within a confidence interval.

In this example, the MATLAB function called *fminbnd* is deployed, which is part of the MATLAB Optimization Toolbox. It is based on Brent's algorithm as described in [13] and combines a golden-section search and a parabolic interpolation for finding a minimum on a fixed interval. Therefore, the objective function, which is the amount of stored heat at the optimal buffer storage capacity, has to be formulated as follows:

$$max(Q_{BTES,stor}(V_{buf})) = -min(-Q_{BTES,stor}(V_{buf})) \tag{1}$$

The principle of the optimization procedure is shown in Fig. 5. In every optimization iteration, the function *fminbnd* systematically chooses a buffer storage tank volume, which lies inside a predefined parameter range and passes this value to a MATLAB function called *StartSim*. This function in turn starts both, the FEFLOW model as well as the SIMULINK model and sets the buffer storage tank volume in the SIMULINK model to the chosen value. Subsequently, both models connect to each other via their TCP/IP interfaces and start to co-simulate.
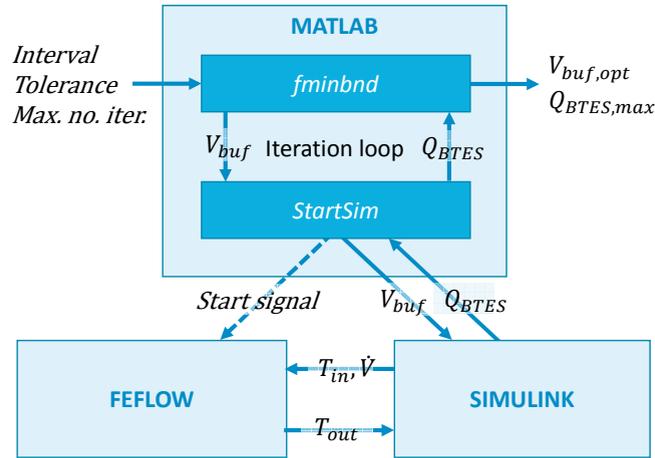
Fig. 5. Flowchart of the optimization process.

Due to the relatively small communication step size of 5 minutes, the simulation of one day takes up to one hour. For this reason, the simulation of three consecutive days is deemed to be sufficient. After this final simulation time is reached, the amount of heat that has been stored into the BTES is returned from the model to the *StartSim* function and from there to the optimization algorithm. The iteration procedure is repeated until a maximum is found for the amount of stored heat within a pre-set termination tolerance.
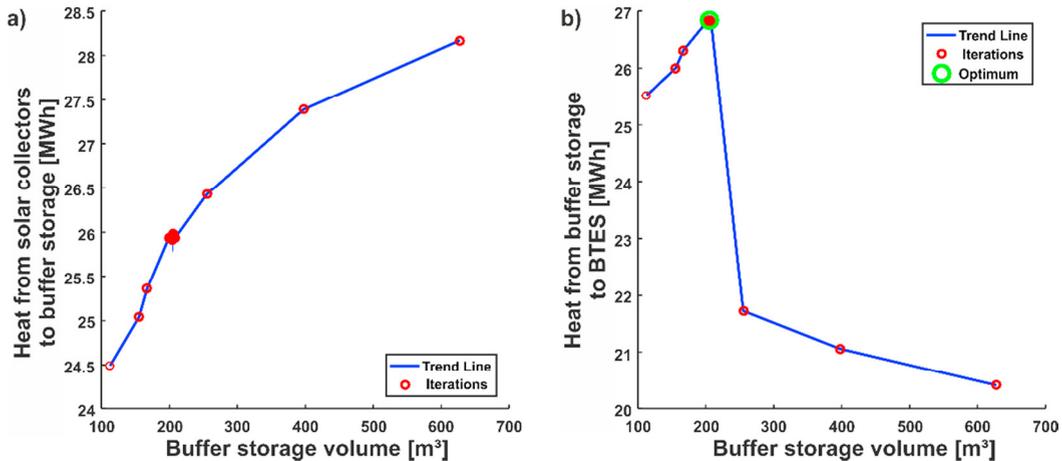

Fig. 6. Heat amount that is transferred (a) from the solar collectors to the buffer storage and (b) from the buffer storage to the BTES for the respective iteration of the buffer volume.

The optimization algorithm finds the optimum after 21 optimization iterations at a water tank volume of about 205 m³ and an error < 0.015%. It is obvious that from the seventh iteration on, the algorithm is already very close to the optimum value (error < 3.5%). Therefore, choosing a larger termination tolerance could decrease the iteration number significantly.

Fig. 6a illustrates the heat amount that is transferred from the solar thermal collectors to the buffer storage depending on the water tank size. Increasing the water tank volume leads to an increase in the buffer storage capacity. As a result, the efficiency of the collectors increases with the heat amount that is transferred from the collectors to the buffer storage.

The heat amount that is subsequently stored from the buffer storage to the BTES (Fig. 6b) increases with the water tank size as well, until a maximum is reached. Beyond this point, a significant decrease in the BTES load can

be observed. With increasing water tank size, the buffer storage temperature generally decreases. This leads to a shortened time span in which the trigger criterion for the pump operation in the BTES circuit is satisfied. As a consequence, the duration of the charging cycle decreases and the amount of stored heat diminishes. The water tank size resulting in a maximum BTES load can be considered ideal for the specific system setup and control strategy.

4. Transmission error

The applied coupling approach has to be regarded as a loose coupling, since no iteration process between the two simulation environments is implemented in the procedure. The values received from the respectively other model at a distinct communication step are kept constant until the subsequent communication step is reached. Accordingly, the accuracy of the co-simulation is very sensitive to the communication step size.

Therefore, a simple variation study is conducted, in which a 24 h synthetic thermal load profile is created through a constant flow of heat carried fluid with varying temperatures in MATLAB-SIMULINK. The synthetic load profile consists of several constant load steps with different magnitudes. Fluid flow rate and temperature are passed to a BHE model in FEFLOW via the coupling interface. Simultaneously, the thermal load that is applied by the analytical BHE solution to the FEFLOW finite element mesh is gathered and summed up to a total heat amount at the end of the simulation. Afterwards, the recorded heat amount in FEFLOW is compared to the heat amount that theoretically results from the synthetic load profile and a relative transmission error is calculated. Furthermore, the computation time for one load cycle is captured.

The co-simulation is repeated several times, varying the communication step size as well as the load profiles itself (profiles of two different days) and the duration of the particular load steps (1h, 2h, 4h). The transmission error generally depends on the ratio of the communication step size to the load step size. Therefore, a relative communication step size is defined as the communication step size normalized by the duration of the particular load steps. For instance, the relative step size is 1, when the communication step has the same length as the load steps and it is 0.1 when 10 communication steps are performed during one load step. Additionally, the computation speed-up related to the slowest model for each communication step size variation series is calculated.
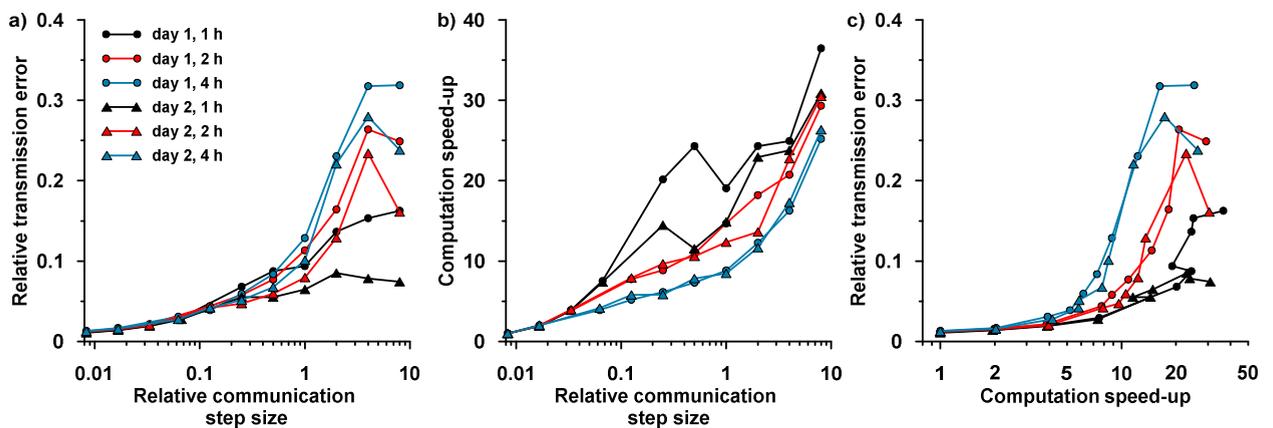

Fig. 7. a) Relative transmission error and b) computation speed-up against the relative communication step size, c) comparison of transmission error and computation speed-up.

The results of the time stepping study confirm that the relative communication step size is a major control parameter for the transmission error (Fig.7a). For relative communication time steps sizes up to 0.2, the transmission error increases independently from the specific load scenario. Larger communication time steps result in an increasing variance of the transmission error and the concurrence of communication time steps with load changes becomes more important. In summary, it can be stated that for communication time steps smaller than 0.2 the transmission error can be estimated quite well, whereas for larger communication time steps, the uncertainty increases. However, increasing the communication time steps leads to a strong improvement of the computational

performance (Fig.7b). Especially, FEFLOW's internal time stepping control can chose larger time steps and thus decrease the simulation time significantly. Tolerating an increase in the relative transmission error from about 1% to 3% allows for an increase in the computational performance by a factor of 4 (Fig.7c).

5. Discussion & conclusion

A TCP/IP interface has been developed, which connects the software package FEFLOW with MATLAB-SIMULINK and facilitates coupled simulations of subsurface processes and HVAC systems. The coupled simulations are particularly advantageous when considering large and complex heating systems, as the mutual interaction of the subsystems can be taken into account. In combination with mathematical optimization algorithms, the high detail of the coupled simulations allows for the appropriate design of system components and the maximization of the overall system performance.

As it is, the approach only provides a loose coupling of the subsystem simulations. This can result in relatively large transmission errors between the respective models and is strongly dependent on the communication time step size. Small communication time steps can limit the transmission error, but they come at a high computational cost. A priori knowledge of the system behavior is critical for the choice of the step size. Future research should focus on the implementation of iteration schemes and an adaptive communication time step control to tighten the coupling between sub-models. This will reduce the transmission errors and make the coupled simulations more robust, even at larger communication time steps that can speed up the simulations significantly.

Nevertheless, in a first example of a BTES system fed by solar thermal collectors, the coupling approach demonstrates its functionality. The coupling interface is, however, not restricted to scenarios considering BHEs, but can easily be applied to any other type of problem linking the subsurface to HVAC, like open-loop systems. This makes the presented approach a versatile tool for detailed simulations of geothermal energy supply systems.

Acknowledgements

References

[1] Schulte, D.O., Rühaak, W., Oladyshkin, S., Welsch, B., Sass, I. (2016) "Optimization of Medium-Deep Borehole Thermal Energy Storage Systems." *Energy Technology* 4.1: 104-113.
[2] Schulte, D.O., Welsch, B., Boockmeyer, A., Rühaak, W., Bär, K., Bauer, S., Sass, I. (2016) "Modeling insulated borehole heat exchangers." *Environmental Earth Sciences* 75.10: 1-12.
[3] Welsch, B., Rühaak, W., Schulte, D.O., Bär, K., Sass, I. (2016) "Characteristics of medium deep borehole thermal energy storage." *International Journal of Energy Research* 40.13: 1855-1868.
[4] Bär, K., Rühaak, W., Welsch, B., Schulte, D., Homuth, S., Sass, I. (2015) "Seasonal High Temperature Heat Storage with Medium Deep Borehole Heat Exchangers." *Energy Procedia* 76: 351-360.
[5] Schulte, D.O., Rühaak, W., Welsch, B., Sass, I. (2016) "BASIMO – Borehole Heat Exchanger Array Simulation and Optimization Tool." *Energy Procedia* 97: 210-217.
[6] Diersch, H.-J.G. (2014) "Feflow - Finite Element Modeling of Flow, Mass and Heat Transport in Porous and Fractured Media." Springer Berlin Heidelberg.
[7] DHI-WASY. (2014) "FEFLOW finite element subsurface flow and transport simulation system - Recent release 6.2."
[8] Diersch, H.-J.G., Bauer, D., Heidemann, W., Rühaak, W., Schätzl, P. (2011) "Finite element modeling of borehole heat exchanger systems: Part 2. Numerical simulation." *Computers & Geosciences* 37.8: 1136-1147.
[9] Eskilson, P., Claesson, J. (1988) "Simulation model for thermally interacting heat extraction boreholes." *Numerical Heat Transfer* 13.2: 149-165.
[10] Solar-Institut Jülich. (2016) "CARNOT 6.0 for MATLAB 2013b.".
[11] The MathWorks Inc. (2016) "MATLAB 2016a."
[12] BBR. (2011) "Updated and enhanced test reference years (TRY) of Germany for medium and extreme weather conditions." in Federal Office for Building and Regional Planning (BBR).
[13] Forsythe, G.E., Malcolm, M.A., Moler, C.B. (1977) "Computer methods for mathematical computations." Prentice-Hall, Englewood Cliffs, NJ pp. XI, 259.

Appendix I – User Manual for the iBHE *FEFLOW* plug-in

The plug-in is capable to consider two different grout sections in the BHE with different thermal conductivities. Furthermore, the plug-in is capable to simulate the following BHE types: Coax with annular inlet (CXA), coax with centered inlet (CXC), u-pipe (1U) and double u-pipe (2U). All material parameters and pipe geometries are defined in the two text files coax.dat and u-pipe.dat. No matter which BHE type you want to simulate, you need both text files located in the import+export folder of your Feflow project. The text files also contain two values for the borehole diameter for the two different grout sections. However, it is not advisable to set different values there: The accuracy of the analytical BHE solution is strongly dependent on the ideal nodal distance (see white papers volume 5) of the FE mesh nodes surrounding the BHE. The nodal distance is determined by the borehole diameter. As the mesh is fixed (at least in Feflow 6.2. and older versions), it cannot be adapted to a change in the borehole diameter.

For the definition of the BHE position in your model, you need to create a nodal reference distribution "BHEnodes". Therefore, you select all nodes that shall belong to the borehole heat exchanger (this should be a vertical line of nodes) and assign the value **"1"** to the reference distribution at the selected nodes. Furthermore, you use the reference distribution to define, at which slice the transition of the upper grout zone to the lower grout zone takes place. The BHE node at the transition slice has to get the value **"2"** (it should already have the value 1, as it must belong to the BHE nodes, overwrite this value).

The operational parameters BHE type, fluid flow rate, and inlet temperature are read from Feflow time series. Theses time series are identified by their unique ID Numbers:

9001:

Here the BHE type is defined. Therefore, the time series must only contain the values

1 (for CXA),
2 (for CXC),
3 (for 1U) or
4 (for 2U).

But, the value may change during simulation. This allows for a change in the operation mode from CXA to CXC and vice versa during the simulation.

9002:

Here you define the volume flow rate of the refrigerant through the BHE in the unit m³/s.

9003:

At this stage, the BHE can only be operated via given inlet temperatures and not via a given heat load. In the time series 9003 you define the inlet temperature in °C.

As there might occur steep temperature gradients at the grout transition zone, the vertical discretization of the FE mesh should be refined in this region.

Appendix J – Digital Supplement

<div style="text-align: right"></div>

CURRICULUM VITAE

WELSCH, BASTIAN
Born on 13.06.1984 in Tübingen, Germany

EDUCATION

SINCE 06/2013
Institute of Applied Geosciences, Geothermal Science and
Technology, Technische Universität Darmstadt &
Darmstadt Graduate School of Excellence Energy Science and
Engineering
Doctorate studies
towards the degree of Doktor-Ingenieur

10/2005 – 10/2012
Technische Universität Darmstadt
Studies of Applied Geosciences
Majors in Geothermal Energy, Engineering Geology, Hydrogeology,
Geotechniques
Degree: Dipl.-Ing.

09/1995 – 06/2004
Quenstedt-Gymnasium, Mössingen
High school
Degree: High school diploma

09/1991 – 07/1995
Oberdorfschule, Mössingen
Primary school

PROFESSIONAL AND OTHER EXPERIENCE

SINCE 02/2013
Institute of Applied Geosciences, Geothermal Science
and Technology, Technische Universität Darmstadt
Research assistant

08/2012 – 01/2013 &
03/2009 – 06/2010
Institute of Applied Geosciences, Geothermal Science
and Technology, Technische Universität Darmstadt
Student research assistant

05/2011 – 07/2011
Fritz Planung GmbH, Geologic division, Bad Urach
Internship

10/2004 – 12/2004
DaimlerChrysler AG, Sindelfingen
Vacation job

SKILLS

Language skills
German (native), English (fluent), French (basics)

Programming and computer skills
MATLAB, Simulink, C++(basics), MS Office, ArcGis, GoCAD, FEFLOW, EED

VOLUNTARY COMMITMENT

SINCE 2015
Active member of the workgroup "Junge Geothermie" of the German Geothermal Association

SINCE 2008
Passive member of the German Geological Society

SINCE 2000
Member in the YMCA Belsen e.V. (2000 – 2004 active member: handball coach, organization of youth camps)

1998 – 2004
Voluntary school activities at the Quenstedt-Gymnasium Mössingen (handball tutor, school council, light and sound technician)